Title
Synthesis of low-valent lanthanide organometallics for photocatalysis and electronic structure studies

Author
Kynman, Amy E

Publication Date
2023

Peer reviewed|Thesis/dissertation

Synthesis of low-valent lanthanide organometallics for photocatalysis and electronic structure studies

By

Amy E Kynman

A dissertation submitted in partial satisfaction of the

requirements for the degree of

Doctor of Philosophy

in

Chemistry

in the

Graduate Division

of the

University of California, Berkeley

Committee in charge:
Professor Polly Arnold
Professor Thomas Maimone
Professor Ramamoorthy Ramesh

Summer 2023

Abstract

Synthesis of low-valent lanthanide organometallics for photocatalysis and electronic structure studies

by
Amy E Kynman
Doctor of Philosophy in Chemistry
University of California, Berkeley
Professor Polly Arnold, Chair

Chapter 1. To date, the exploration of ligands that can support cerium, or any other lanthanide (Ln), in photocatalysis has been limited to halides, pseudohalides, and simple nitrogen donors. No organometallic photocatalyst has yet been reported that combines the photoexcitable cerium cation with strongly binding, multifunctional, tunable ligands. This chapter conveys the synthesis and characterization of a range of cerium photocatalysts, alongside a new family of photoactive Ln(III) compounds (Ln = La, Nd, Sm) supported by a light-absorbing tunable aryloxide-tethered N-heterocyclic carbene (NHC), tetramethylcyclopentadienyl (Cp^{Me4}), and pseudohalide ligands. The synthesis and characterization of the trivalent uranium analogue of these species is also presented, alongside investigation into the photophysical properties of select complexes.

Chapter 2. The complexes described in **Chapter 1** are capable of the rare, selective, photocatalytic C–F bond functionalization of sp^3 hybridized C–F bonds, when used in conjunction with magnesium alkyl reagents. The work described in this chapter is, to the best of our knowledge, the first example of catalytic C–F bond activation and functionalization mediated by a rare-earth metal complex. Ligand light-absorption and redox non-innocence allows for the photocatalysis to be accessed even by typically photo- and redox-inactive metals including lanthanum and magnesium. Through a combination of experiment and theory, this work provides unique insight into the cooperativity between metal and ligand in photocatalysis, and the significance of ligand redox-non innocence in radical mechanisms.

Chapter 3. The studies described in **Chapter 2** of this thesis conclude that specialized, light-absorbing aryloxide ligands are required for the efficient photocatalytic cleavage of strong C–F bonds by Ln complexes. In this chapter, trivalent Ln tetramethylcyclopentadienyl complexes (Ln = La, Ce, Pr, Nd, Sm) are shown to photochemically activate the weaker sp^3 carbon–chlorine bond of chlorinated hydrocarbons via a reactive lanthanide alkyl species. Because light absorption by the Cp^{Me4} ligand is efficient, photocatalytic reactivity is enhanced for cerium and possible for neighboring, normally photoinactive, Ln congeners. Calculations are utilized to further understand the mechanism of this process, and preliminary results in the catalytic dechlorination of polyvinyl chloride (PVC) are presented.

Table of Contents

Acknowledgements

I am so fortunate to be surrounded by a great many people who have helped me throughout my time at graduate school. Their knowledge, support, and guidance has been invaluable.

Firstly, I must thank my supervisor Prof. Polly Arnold for giving me both the opportunity to carry out my graduate studies at Berkeley, and the challenge of working on this project. Moving to California just before a global pandemic was not what I envisioned for my PhD when I first visited the Arnold Group in Edinburgh in 2019, but I have grown more as a person and a researcher than I could ever have imagined over the last four years. I would also like to thank my computational collaborators–Laurent, Yan, and Stella. I appreciate your dedication, expertise, and patience.

My biggest thanks go to the members of the Arnold group past and present–Dr. Amy Price, Dr. Rachel Meyer, Dr. Anthony Wong, Dr. Mikaela Pyrch, Gretchen Brown, Rytė Rutkauskaitė (I wouldn't have made it through the pandemic or graduate school without you), Nick Katzer, David Fiszbein, Matt Hernandez, Jaden Lara, Gabe Herrera, Michael Trinh, Dr. Francis Lam, Dr. Andrea Di Giuseppe, Dr. Addison Desnoyer, Luca Elghanayan. I'm so grateful to have had the chance to work with such outstanding scientists and people, and that the challenges we've faced over the last few years only brought us together. The friendship you've given me has been a highlight of my time at Berkeley.

I must also thank the Arnold group's administrative assistant, Anneke, who deals with more bureaucratic red tape than most, yet always greets us with a smile. Prof. John Arnold and his group took us under their wing when we first arrived in Berkeley and made the fifth floor of Latimer Hall a much more supportive and welcoming place. Elena, Doug, Jihad, Jodie, Mike, Ryan, Laurel and of course Hasan–the department would crumble without you, and I most definitely wouldn't have had a lab to work in or results to write about in this thesis.

I wouldn't be the scientist I am today without Dr. Addison Desnoyer, who worked with me on this project in the depth of the pandemic and coached me back from many a crisis of confidence. Gretchen, my partner in crime and in cerium, thank you for your support, friendship, and constant willingness to do chaotic things with me. Amy, thank you for your patience and guidance, there's no one better to rant about life/drink beers with. Rachel, thank you for believing in me (and introducing me to the American casual dining experience!). Sheridon and Jacob, thank you for Sacramento adventures, pink pineapples, and being my friends.

The hardest part of my time at Berkeley has been the physical distance created between me and my family. Everything I do, I do to make you proud, and none of this would have been possible without your unconditional love and support. Zach, you knew exactly who I was even when I'd lost sight of myself–I love you. (Also, Beans! I definitely have to thank Beans!)

List of Abbreviations

An	Actinide
Ar	Aryl
BDE	Bond Dissociation Energy
Bn	Benzyl
^{n}Bu	Butyl
^{t}Bu	*tert*-Butyl
Cp	Cyclopentadienyl
CV	Cyclic Voltammetry
DFT	Density Functional Theory
Et	Ethyl
FTIR	Fourier-Transform Infrared
GC-MS	Gas Chromatrography-Mass Spectrometry
GPC	Gel Permeation Chromatography
HAT	Hydrogen Atom Transfer
HOMO	Highest Occupied Molecular Orbital
HRMS	High Resolution Mass Spectroscopy
IC	Internal conversion
ISC	Intersystem crossing
LC-MS	Liquid Chromatography-Mass Spectrometry
LED	Light Emitting Diode
LMCT	Ligand-to-Metal Charge Transfer
Ln	Lanthanide
LUMO	Lowest Unoccupied Molecular Orbital
M	Molar
Me	Methyl
Mes	Mesitylene
MLCT	Metal-to-Ligand Charge Transfer
NHC	N-Heterocyclic Carbene
NMR	Nuclear Magnetic Resonance
OTf	Triflate
PE	Poly(ethylene)
Ph	Phenyl
ppm	parts per million
^{i}Pr	*iso*-Propyl
PVC	Poly(vinylchloride)
SET	Single Electron Transfer
SOMO	Singly Occupied Molecular Orbital
THF	Tetrahydrofuran
Tp	Terpyridine
TD-DFT	Time Dependent Density Functional Theory
UV-Vis	Ultraviolet-Visible
X	Halogen atom
XRD	X-ray diffraction
η	Hapticity
μ	Bridging ligand

Research Motivation

Catalytic reactions are crucial in many industrial processes, including the synthesis of valuable feedstock chemicals, and biologically active compounds that are of use in pharmaceuticals. Carbon–carbon bond forming reactions are of particular significance, as they allow for the construction of complex molecules via simple organic building blocks. In many C–C bond forming reactions the first, and often rate-determining, step in the catalytic cycle is the carbon-halide (C–X) bond activation of a substrate in a metal-mediated oxidative addition reaction. Through subsequent reaction of the resulting hydrocarbyl fragment with an appropriate coupling partner, such as an organometallic nucleophile, a target molecule can be accessed. Pioneering works by Stille, Negishi, Heck and Suzuki used this strategy to great success, and as such considerable research effort has been directed at the expansion of coupling partners and accessible organic halide substrates in related reactions. However, despite advances, the coupling of C(sp^3) fragments remains challenging.

Over recent years, the development of metallaphotoredox catalysis has enabled new, useful synthetic methodologies to be accessed. Photoredox catalysis centers on ability of metal complexes or organic dyes to generate reactive intermediates, through their conversion of visible light into chemical energy through engaging in single-electron transfer (SET) reactivity with organic or organometallic substrates. This strategy can provide access to diverse reactive radical species under mild conditions and has consequently aided the development of a wide range of previously inaccessible organic transformations. Significantly, the ability to 'switch on' a catalyst through irradiation with light of a specific wavelength, particularly low energy wavelengths at which common organic molecules do not absorb, is useful in optimizing both the selectivity and energy efficiency of a reaction. However, detailed mechanistic studies of these systems are challenging due to their complexity.

Photoredox reactions using metal complexes has so far primarily focused on the study of cobalt, copper, gold, iridium, nickel, palladium, rhodium, and ruthenium, many of which are expensive and in low supply. Little research has been carried out into photoredox catalysis using *f*-block elements, which are generally understudied relative to transition metals. Lanthanides in particular are cheap, earth-abundant, and generally non-toxic. Their accessibility and unique reactivity provide an opportunity to supplement or even supersede rare and precious metal photosensitizers. Amongst the lanthanides, research into photocatalysis has primarily focused on the study of cerium. Cerium is highly abundant and possesses a unique doublet to doublet $4f \rightarrow 5d$ excitation and emission, which can lead to good energy conservation without losses through spin-state changes. Some cerium photocatalysts have demonstrated photoexcited states with unparalleled reducing power, allowing for the activation of organic substrates that have not otherwise been activated by reported organic or transition-metal photocatalysts.

It is widely accepted that coordinating ligands are capable of drastically changing the reactivity of metal complexes, and large research efforts have been dedicated to understanding the relationship between ligand structure and activity in chemical transformations. The activity of photocatalysts can also be manipulated by oxidation state modulation, and catalyst excitation, both of which can be influenced by ligand design. However, the exploration of ligands that can support cerium, or any other lanthanide-center, in photocatalysis is extremely limited. By conducting investigations into *f*-block metal photocatalysis, their mechanisms, and the effects of ligands in such reactions–particularly C(sp^3)–X bond activations–the capability of rare-earth catalysis can be expanded, and the fundamental knowledge of these elements improved.

Chapter 1

Synthesis and Characterization of Ln and An Organometallic Photocatalysts

1.1 Overview

To date, the exploration of ligands that can support cerium, or any other lanthanide, in photocatalysis has been limited to halides, pseudohalides, and simple N-donors.[1] No organometallic lanthanide photocatalyst has yet been reported that combines the photoexcitable cerium cation with strongly binding, multifunctional, tunable ligands. This chapter conveys the synthesis and characterization of a range of cerium photocatalysts, alongside a new family of photoactive Ln(III) compounds supported by a light-absorbing tunable aryloxide-tethered N-heterocyclic carbene (NHC), tetramethylcyclopentadienyl (Cp^{Me4}), and pseudohalide ligands. The photophysics of a selection of these compounds is also explored to give further insight into their photoreactivity.

The author, in collaboration with Dr. Addison N. Desnoyer, carried out the synthesis and experimental investigation of lanthanide photocatalysts at the University of California, Berkeley. Dr. Andrea Di Giuseppe first synthesized and characterized cerium complex **1-Ce** at the University of Edinburgh, Scotland. Crystallographic data for **3-Ce** was collected by Dr. Rex Handford at beamline 12.2.1 of the Advanced Light Source (ALS) at Lawrence Berkeley National Laboratory. Collection of fluorescence measurements was carried out by the author with assistance from Dr. Leticia Arnedo Sanchez and Dr. Jennifer Wacker at Lawrence Berkeley National Laboratory. TD-DFT studies were carried out by Yan Yang under the supervision of Prof. Laurent Maron at the University of Toulouse. The author and Dr. Addison N. Desnoyer guided these studies and interpreted data. The majority of this work has been published in: *Chem. Sci.*, 2022, **13**, 14090–14100. Additional photophysical data of **1-CeMes, 1-Ce^{t}Bu, 3-Ce** and **4-Ce** are included, alongside the synthesis and characterization of the trivalent uranium complex **1-U**.

1.2 Introduction

Photoredox catalysis has emerged over the last few decades as a powerful synthetic strategy towards the construction of complex organic molecules.[2–4] Recent advances have shown that photocatalysts, which are typically either organic molecules or coordinatively-saturated transition metal complexes, can undergo single electron transfer (SET) reactivity under irradiation with visible light to enable a range of challenging transformations under mild conditions.[5] Examples of such processes include C–H activation,[6–8] radical cross-coupling,[9–12] and the valorization of lignin.[13,14] However, despite their utility, detailed mechanistic studies of photoredox systems are often challenging due to their inherent complexity and the short lifetimes of photoexcited intermediates.

Many lanthanides are more abundant than copper and their salts are less toxic than those of iron, so their potential for applications in catalysis is worthy of exploration.[15–18] In 1990, divalent Sm, Eu, and Yb complexes $Ln(Cp^*)_2$ ($Cp^* = C_5Me_5$), were shown to more effectively cleave vinylic C–F bonds when photolyzed, forming stoichiometric Ln(III) halide complexes and suggesting the increased reducing power of the excited state of Ln(II).[19] Subsequently, analogous reactions to cleave the weaker C–Cl and C–Br bonds could be made catalytic in Ln(II) halide (Ln = Sm, Eu, Yb), under UV-photolysis conditions, by the addition of sacrificial reductant such as Zn or Al.[20,21] The addition of simple donor ligands enabled benzylic C–Cl cleavage by Eu(II) under blue light irradiation.[22] In addition the combination of Lewis acidic LnX_3 salts (X = halide, triflate) and an organic photocatalyst, or a photo-absorbing substrate, has been useful in combining the Lewis acid activation with the enhancement in redox capacity provided by the excited state of the photocatalyst.[23] More efficient light-absorbing ligands such

as porphyrins, phthalocyanins, or porpholactones coordinated to lanthanide centers have been used to stoichiometrically dechlorinate phenols,[24] for certain selective C–H bond oxidations,[25] and as sensitizers to generate singlet oxygen for photodynamic therapy.[26,27]

Although only a few reports of lanthanide photoredox catalysis exist so far, Ce(III) complexes have received the most attention. Cerium possesses both an accessible (III)/(IV) redox couple and a formally allowed excitation from the $4f^1$ ground state to the $5d^1$ excited state, which can give rise to luminescence if appropriate ligands are used. The *d*-character of the excited state is also significant from a synthetic standpoint as it makes the excited state redox potential susceptible to changes in the ligand field. As a result, small modifications to a ligand framework can have substantial effects on the energy of *d*-orbitals and therefore the excited state reduction potential of the complex.[28] As a by-product in rare-earth element (REE) separations, cerium is also the cheapest and most readily isolated of the rare earths, offering a promising alternative to current precious metal photocatalysts.

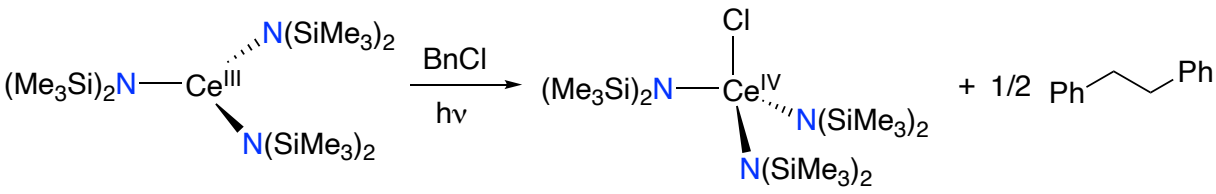

Scheme 1.1. Ce(III) complexes bearing amido ligands as catalysts for halogen atom abstraction of benzyl chloride, as published by Schelter et al.

Building on the pioneering work surrounding stoichiometric photoluminescent cerium chemistry,[29,30] in 2015 Schelter and co-workers demonstrated the first examples of Ce(III) photocatalysis.[31,32] They reported that Ce(III) complexes bearing amido and guanidinate ligands were catalysts for the halogen atom abstraction of benzyl chloride (Scheme 1.1), though the presence of both Na(N{$SiMe_3$}$_2$) and Ce metal were required for catalytic turnover.[35,33]

They presented detailed photophysical studies and proposed an inner-sphere mechanism involving Ce---$ClCR_3$ adduct formation prior to C–Cl bond cleavage, allowing for the activation of substates that would be inaccessible through utilizing redox potentials alone. Typically, electron transfer in redox reactions only progresses if the redox potentials of electron donor and acceptor molecules are well matched, as dictated by the Gibbs free energy of the reaction.[34] However, through the formation of a strong C–X bond (Figure 1.1), additional thermodynamic driving force can be provided to the reaction. Subsequent work from the same group using a more sterically congested Ce(III) tris(guanidinate) complex as catalyst and aryl iodide as substrate was found instead to likely operate *via* an outer-sphere SET mechanism, highlighting the mechanistic diversity that is possible in these systems as a consequence of relatively small changes in reaction type.[35]

Despite this progress, the exploration of ligands that can support cerium, or any other lanthanide-center, in photocatalysis has been limited to halides, pseudohalides, and simple N-donors.[1] No organometallic lanthanide photocatalyst has yet been reported that combines the photoexcitable cerium cation with strongly binding, multifunctional, tunable ligands. We have developed a range of applications of organometallic lanthanide complexes in sustainable

catalysis,[17,18,36,37] and considered that organometallic cerium complexes with light absorption capability and sufficient space to form an inner sphere adduct could achieve efficient C–X bond activation.

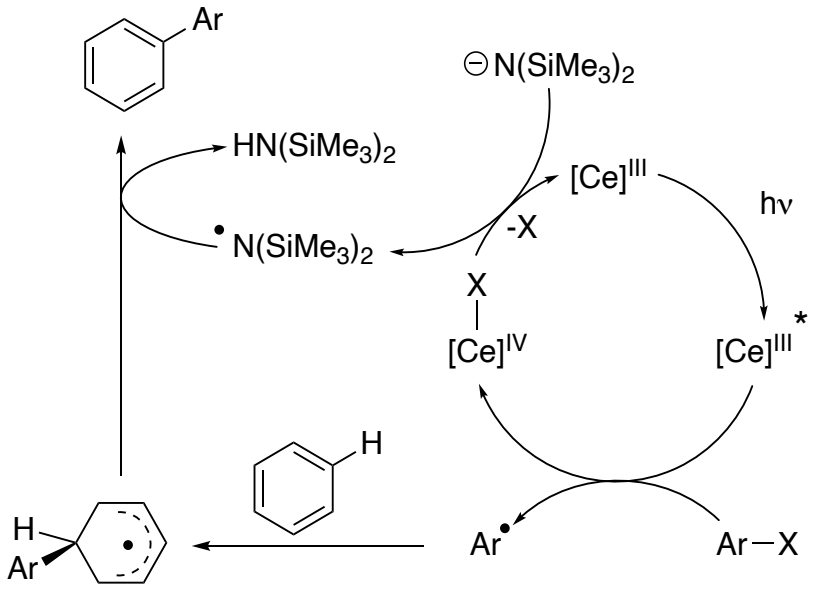

Figure 1.1. Inner sphere mechanism of C–X activation by a cerium photocatalyst proposed by Schelter et al.

To probe this hypothesis and inform on the role of ligands in lanthanide photocatalysis, this chapter presents the synthesis and characterization of a range of organometallic complexes containing cerium, lanthanum, neodymium, samarium, and uranium. These metal candidates were chosen for synthetic ease, and to give a range of ionic radii and redox potentials to study in relation to their effects on *f*-block photocatalysis.

The ionic radii of the lanthanides decreases from lanthanum to samarium due to the lanthanide contraction.[38] Trivalent uranium has a similar ionic radii to trivalent cerium,[39] though the 5*f* orbitals of actinides are more diffuse than the 4*f* orbitals of lanthanides. This is thought to allow actinides to participate in more covalent interactions relative to the lanthanides;[40] the bonding in lanthanide complexes is primarily ionic.[41] Unlike cerium, the other lanthanide ions here do not possess an accessible (III)/(IV) redox couple, though divalent samarium complexes can be readily isolated and exploited in organic synthesis as reductants.[42] Conversely uranium can also be isolated in its (IV), (V) and (VI) oxidation states.[43]

1.3 Results and discussion

1.3.1 Synthesis of lanthanide and actinide complexes

The initial focus of this work was the Ce complex (Cp^{Me4})$_2$Ce(**L**) (**1-Ce**, Cp^{Me4} = C_5Me_4H) where **L** is the bidentate aryloxide- N-heterocyclic carbene (NHC) ligand anion [2-O-3,5-^{t}Bu$_2$-C_6H_2(1-C{N(CH)$_2$N(^{i}Pr)})] previously studied by Arnold et al. for catalytic CO_2 conversions and the transesterification of renewable esters by Ce(**L**)$_3$ (Figure 1.2). In this case, the lability of the NHC ligand is essential for substrate insertion and subsequent catalysis.[17,18]

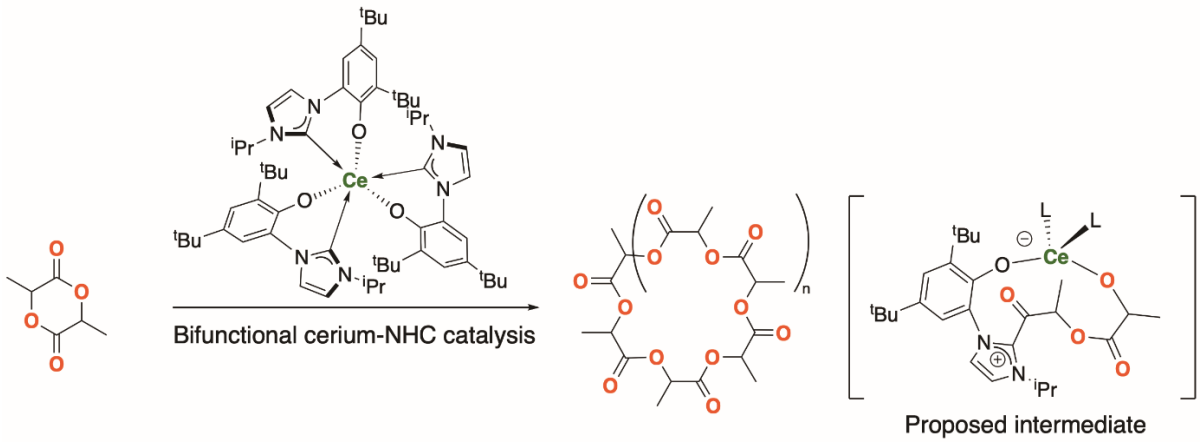

Figure 1.2. Catalytic CO_2 conversion and the transesterification of renewable esters by Ce(**L**)$_3$ reported by Arnold et al. The lability of the NHC ligand is essential for substrate insertion and subsequent catalysis.

The anionic aryloxy-NHC ligand **L** is capable of binding Lewis acidic metal cations via strong M–O bonds. An equimolar protonolysis reaction of $(Cp^{Me4})_3Ce$ (**2-Ce**) and **L** in toluene produced the target complex in 82% yield, and crystals suitable for single crystal X-ray diffraction can be grown from cold hexanes. The solution state ^{1}H NMR spectrum (Figure 1.3) of **1-Ce** in C_6D_6 comprised of resonances with chemical shifts ranging from +22 to -36 ppm, consistent with a paramagnetic Ce(III) $4f^1$ complex.

In the solid state, **1-Ce** crystallizes in the P21/n space group (Figure 1.4). Upon comparison to Ce(**L**)$_3$ which occupies the P21/c space group,[17] **1-Ce** displays shorter Ce–O and Ce–C(NHC) bond lengths (Table 1.1), suggesting a stronger interaction between the ligand and metal center. In addition, the O–Ce–C(NHC) bond angle in **1-Ce** is larger than the average angle in Ce(**L**)$_3$ suggesting less steric bulk surrounding the cerium center.

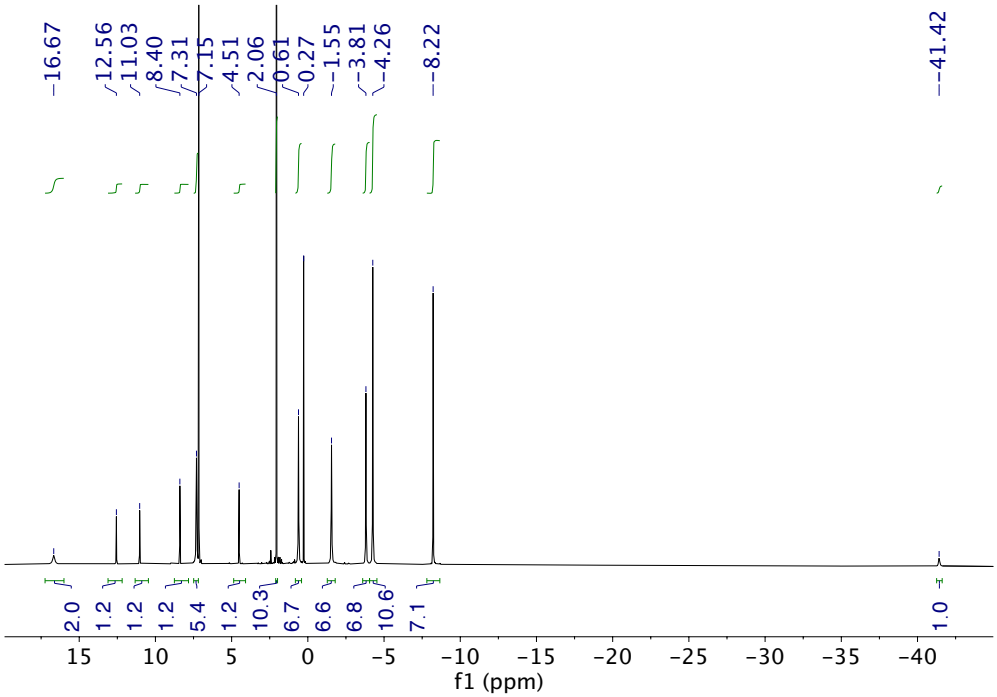

Figure 1.3. ^{1}H NMR Spectrum of **1-Ce** in C_6D_6.

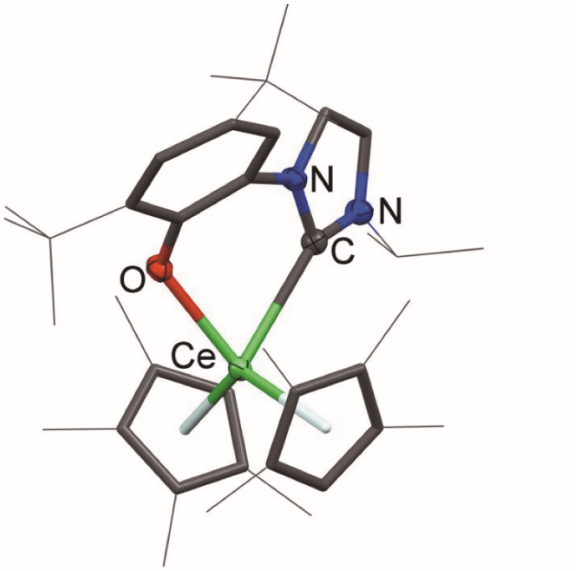

Figure 1.4. Molecular structure of **1-Ce**. Selected ellipsoids shown at 50% probability, peripheral groups drawn as wireframe, hydrogen atoms and lattice solvent molecules have been omitted for clarity. Color code: green – Ce; red – O; grey – C; blue – N.

Table 1.1. Bond metrics for the solid-state structures of **1-Ce** and Ce(**L**)$_3$.

	1-Ce	Ce(**L**)$_3$
Ce–O bond length /Å	2.293(1)	[average] 2.467
Ce–C(NHC) bond length /Å	2.642(2)	[average] 2.742
O–Ce–C(NHC) bond angle /°	72.68(5)	[average] 69.14

It was our intention to use **1-Ce** in light-driven reactions. Therefore, to aid in the understanding of the effects of the ligands in this species on any potential catalytic reactions, a series of Ce(III) complexes were prepared–Ce(Cp^{Me4})$_3$ (**2-Ce**) [(Cp^{Me4})$_2$Ce(μ–Cl)]$_2$[29], (**3-Ce**), (Cp^{Me4})$_2$Ce(OAr) (**4-Ce,** where OAr = O-2,6-^{t}Bu$_2$-4-Me-C$_6$H$_2$),[44] (Cp^{Me4})$_2$Ce(OTf)(THF)[45] (**5-Ce**, OTf = OSO_2CF_3, triflate) and (Cp^{Me4})$_2$Ce(Bn)(THF)[46,47](**6-Ce,** Bn = CH_2Ph, benzyl). The heteroleptic cerium complexes **3-Ce**–**6-Ce** were synthesized in good-to-excellent yield from the same homoleptic starting material **2-Ce** (Scheme 1.2) and characterized fully by standard techniques including single crystal X-ray diffraction (XRD) (Figure 1.6).

The bridging chloride species **3-Ce**, a potential mimic for the envisioned Ce–chloride adduct resulting from a photocatalytic dechlorination reaction,[31] could be synthesized via several routes. The first is reaction of **2-Ce** with chemical oxidant dichloro(phenyl)-λ^3-iodane, $PhICl_2$,[48] in THF at room temperature, and the second is through a comproportionation reaction between **2-Ce** and cerium trichloride ($CeCl_3$) in THF at reflux. The latter was found to be a more efficient synthetic pathway that produced fewer impurities. The former route appeared to generate several unidentified by-products, presumably due to overoxidation, which could be removed by subsequent recrystallization. In addition, it was favorable to use readily available $CeCl_3$ over $PhICl_2$, which is not commercially available and decomposes when exposed to heat and/or light.

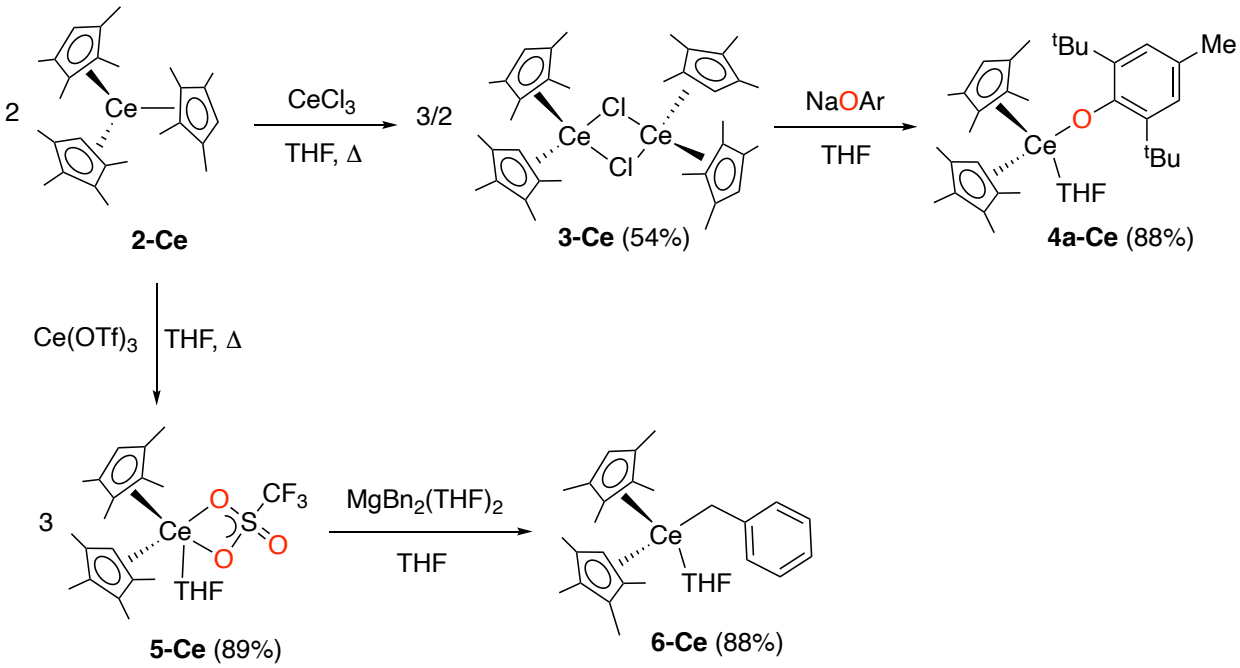

Scheme 1.2. Syntheses of cerium complexes **3-Ce**–**6-Ce**.

3-Ce can be isolated as a bright pink powder, or as yellow crystals which result from layering a THF solution of the complex with hexanes. **3-Ce** has very limited solubility in low polarity organic solvents, being completely insoluble in hexanes, benzene, and toluene. Analysis of the solid-state structure of **3-Ce (**Figure 1.6, top) reveals a dimeric structure, with a Ce–Cl bond distance of 2.842 Å and Ce–Ce bond distance of 4.341 Å. The Ce–Cl–Ce bond angle is 99.72º. Bond metrics consistent with the few analogous complexes reported in the literature, ligated instead with 2,5-di-*tert*-butylcyclopenta-2,4-dien-1-yl or ansa-Cp ligands (CSD-2100439).[49–51] When bulkier Cp* or 2,3,5-tri-*tert*-butylcyclopenta-2,4-dien-1-yl (Cp') ligands are invoked, the bis cyclopentadienyl cerium chloride species can be isolated as a monomeric complex rather than a dimer.[52,53]

Further reaction of **3-Ce** in a salt metathesis reaction with the sodium salt of 2,6-di-*tert*-butyl-4-methylphenol in THF yielded **4a-Ce** in 88% yield as a yellow solid.[44,54–57] The solvent-free analogue of this complex (**4b-Ce**) can also be isolated as a red solid via an otherwise identical route executed in hexanes, though an extended reaction time is needed due to the relative insolubility of the ligand salt in this solvent. This complex is the analogue of **1-Ce** but without the chelating NHC side-arm on the aryloxide ligand. When comparing the solid-state structures of **4a-Ce** and **4b-Ce** (Figure 1.6, middle), the C–Ce–Ce bond angle in **4a-Ce** is 122.6°, smaller than that found in **4b-Ce** (126.2°), consistent with the increased steric hindrance from coordinated THF to **4a-Ce.** The Ce–O(THF) bond length in **4a-Ce** is 2.582 Å, indicating a weak interaction, while the Ce–O(Ar) bond length in both complexes is shorter and stronger at 2.278 Å. In comparison to **1-Ce** the Ce–O bond is also shorter, which could be attributed to the lack of chelating ligand that enforces a rigid coordination geometry.

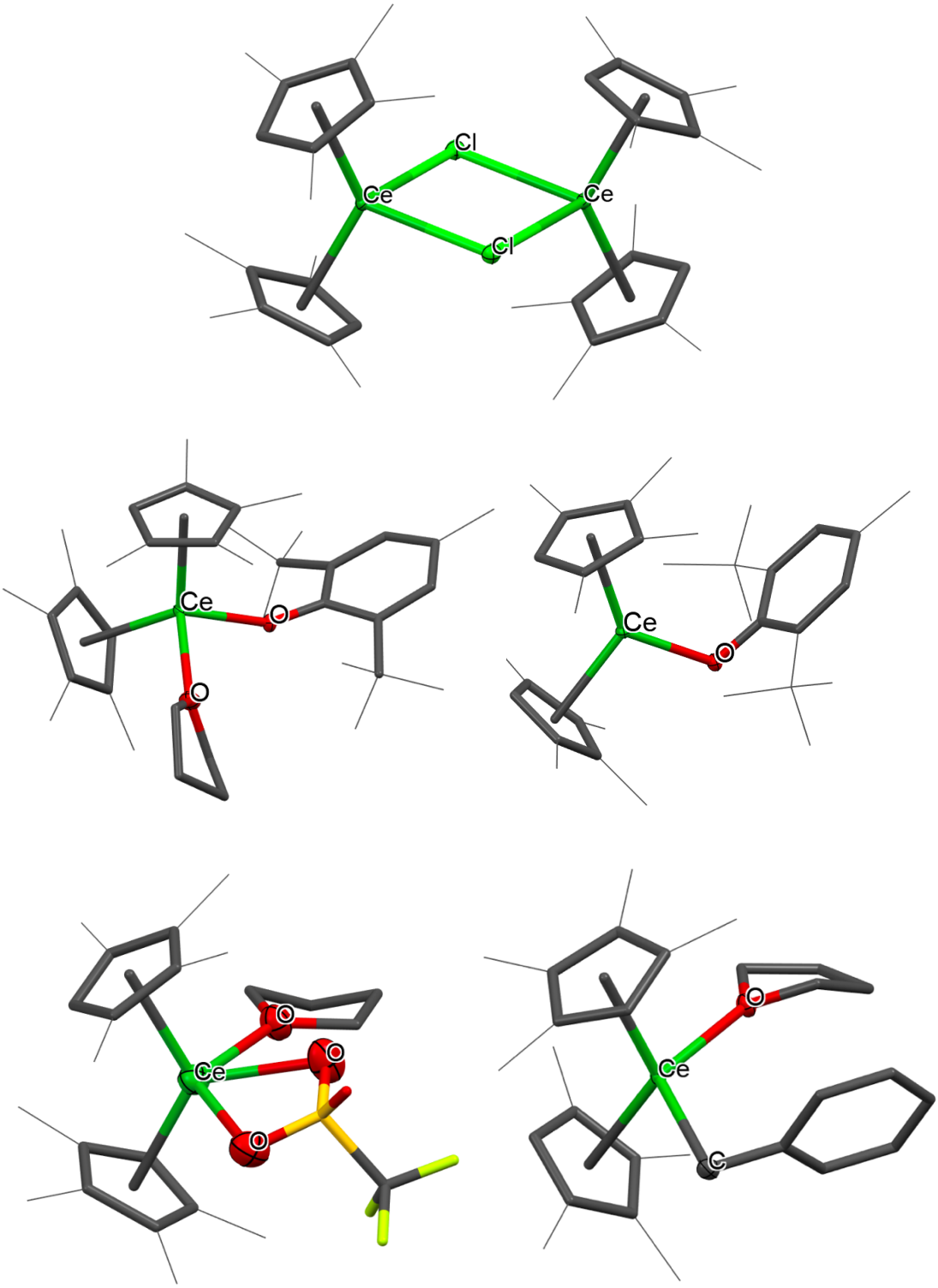

Figure 1.6. Molecular structures of complexes **3-Ce** (top), **4a-Ce** (middle, left), **4b-Ce** (middle, right), **5-Ce** (bottom, left) and **6-Ce** (bottom, right). Ellipsoids shown at 50% probability, peripheral groups drawn as wireframe, hydrogen atoms and lattice solvent molecules have been omitted for clarity. Color code: green – Ce; red – O; grey – C; blue – N; yellow – S, bright green – F.

Complex **5-Ce** was synthesized similarly to **3-Ce**, through a comproportionation reaction of **2-Ce** with cerium triflate ($Ce(OTf)_3$) rather than $CeCl_3$.[58] **5-Ce** is thermochromic, appearing pale yellow when cold (–30 °C) and bright yellow at room temperature in either solution or solid state. The solid state structure of **5-Ce** (Figure 1.6, bottom left) displays the triflate ligand bound η^2 to the metal center.[59] This is unusual for cerium complexes which are primarily observed with triflate binding η^1 to the metal, and could arise in this case due to the relative lack of steric bulk around the metal center and the weak coordination of THF.

Further reaction of **5-Ce** with half an equivalent of dibenzyl magnesium ($MgBn_2(THF)_2$) in THF and subsequent work up yielded benzyl complex **6-Ce** as a yellow microcrystalline powder. The complex is dichroic in solution, appearing green in a dilute (ca. 5 mM) hexane solution and yellow in a more concentrated hexane solution (ca. 50 mM). Recrystallization from cold hexanes yielded a sample suitable for X-ray diffraction studies (Figure 1.6, bottom right). The isolation and crystallographic characterization of lanthanide benzyl complexes is rare due to their instability and synthetic complexity.[60] Indeed, upon prolonged exposure to vacuum **6-Ce** decomposes to a brown oily material, presumably due to irreversible loss of coordinated THF and subsequent decomposition of the benzyl ligand, which could occur via β-hydride elimination.[61] Analogous complexes bearing Cp' ligands can be isolated without a molecule of THF coordinated to the cerium center, which can be attributed to the greater steric bulk of the Cp' ligand relative to Cp^{Me4}.[46,47]

Aryloxy-NHC ligand **L** has two important characteristics that could open up photoredox catalysis to typically redox-innocent lanthanides with other electronic configurations than cerium. Like other planar aromatic heterocycles that fluoresce, the aryloxy-NHC **L** absorbs visible light when coordinated as a rigid bidentate ligand to a lanthanide. The aryloxide group also has the potential to engage in one-electron redox chemistry. The involvement of phenoxy ligand radicals in redox catalysis, including at cerium,[64] have been previously reported.[65,66]

In order to further probe the applicability of the ligand's capacity to contribute light and redox reactivity to other lanthanides, the f^0 lanthanum analogue of **1-Ce,** $(Cp^{Me4})_2La(\mathbf{L})$ (**1-La**), was synthesized, alongside $[(Cp^{Me4})_2La(\mu\text{–}Cl)]_2$ (**3-La**). Smaller lanthanide adducts with different *f*-electron configurations were also prepared; $(Cp^{Me4})_2Nd(\mathbf{L})$ (**1-Nd**) and $(Cp^{Me4})_2Sm(\mathbf{L})$ (**1-Sm**), alongside the uranium adduct $Cp^{Me4})_2U(\mathbf{L})$ and cerium complexes of differently substituted aryloxy-NHC ligands $(Cp^{Me4})_2Ce(\mathbf{L^{Mes}})$ (**1-CeMes**) ($\mathbf{L^{Mes}}$ = 2-O-3,5-^{t}Bu$_2$-C_6H_2(1-C{N(CH)$_2$N(Mes)}) and $(Cp^{Me4})_2Ce(\mathbf{L^{tBu}})$ (**1-Ce^{t}Bu**) ($\mathbf{L^{tBu}}$ = 2-O-3,5-^{t}Bu$_2$-C_6H_2(1-C{N(CH)$_2$N(^{t}Bu)}).

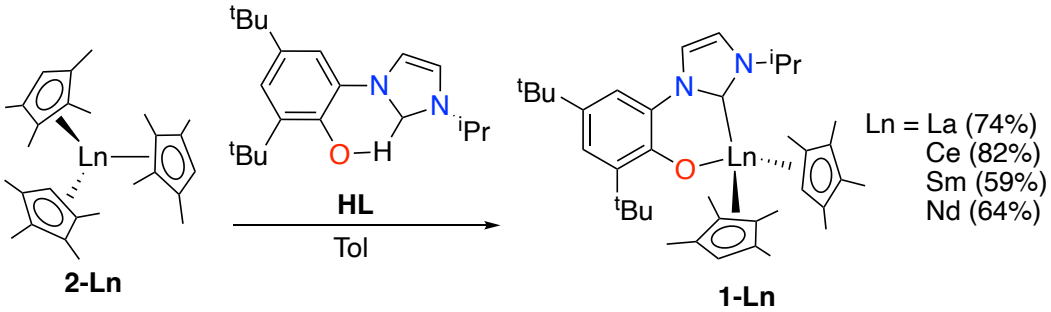

Scheme 1.3. Synthesis of **1-Ln** from **2-Ln**, Ln = La, Ce, Nd, Sm

All complexes **1-Ln** (Ln = La, Ce, Nd, Sm) and **1-U** were synthesized via the same procedure. Reaction of the corresponding tris cyclopentadienyl starting material (**2-Ln**, **2-U**) with **HL** in toluene and subsequent work-up yielded the target complexes in good yields (Scheme 1.3); complex **1-U** was synthesized in 69% yield. Complexes **1-Ln**, **1-U** (Figure 1.7, Figure 1.8), and **2-La** were characterized by single crystal XRD. **1-Ln**, **1-U, 1-CeMes** and **1-Ce^{t}Bu** were characterized by UV-Visible spectroscopy (*vide infra*.).

The complexes **1-Ln** and **1-U** exhibit near identical solid-state bond metrics, (Table 1.2), though a slight contraction in M–O bond length and increase in O–M–C(NHC) bond angle can be observed with decreasing atomic radii. All complexes have bond lengths and angles comparable with similar structures reported in the literature, though limited solid state structures of trivalent, monomeric lanthanum,[5467–69] neodymium[68,70,71] and samarium[72–74] complexes ligated by NHC ligands and/or chelating oxygen donors exist.

Table 1.2. Bond metrics for the solid-state structures of **1-La, 1-Ce, 1-Nd, 1-Sm** and **1-U.**

	1-La	**1-Ce**	**1-Nd**	**1-Sm**	**1-U**
M–O bond length /Å	2.323	2.293	2.262	2.239	2.264
M–C(NHC) bond length /Å	2.647	2.642	2.579	2.568	2.569
O–M–C(NHC) bond angle /°	71.44	72.68	73.14	74.49	72.81
C(Cp^{Me4})–M–C(Cp^{Me4}) bond angle /°	130.8	129.5	130.7	129.8	130.7

A larger number of examples of uranium complexes ligated by chelating alkoxy-NHC ligands can be found in the literature.[75–77]. In particular, (1-(2,6-di-isopropylphenyl)-3-(2-methyl-2-(oxido)propyl)imidazolidin-2-ylidene)-bis(bis(trimethylsilyl)amido)-uranium, published by Arnold et al. in 2010, contains a trivalent uranium center coordinated by the alkoxy-NHC and two bis(trimethylsilyl)amido ligands. The U–O bond distance is shorter in this complex (2.112 Å) relative to **1-U**, while the U–C(NHC) distance (2.693 Å) is longer. In addition, the O–M–C(NHC) bond angle (74.53°) is larger, suggesting the bis(trimethylsilyl)amido ligands are less sterically encumbering than the Cp^{Me4} ligands that ligate **1-U**.

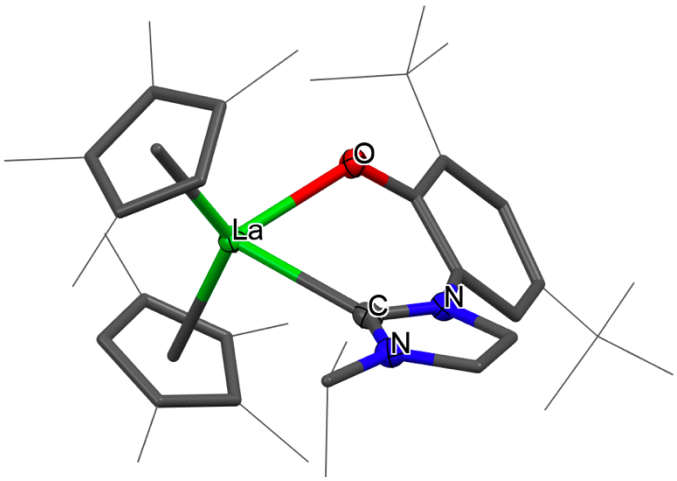

Figure 1.7. Molecular structure of **1-La**. Ellipsoids shown at 50% probability, peripheral groups drawn as wireframe, hydrogen atoms and lattice solvent molecules have been omitted for clarity. Color code: green – Ln/An; red – O; grey – C; blue – N.

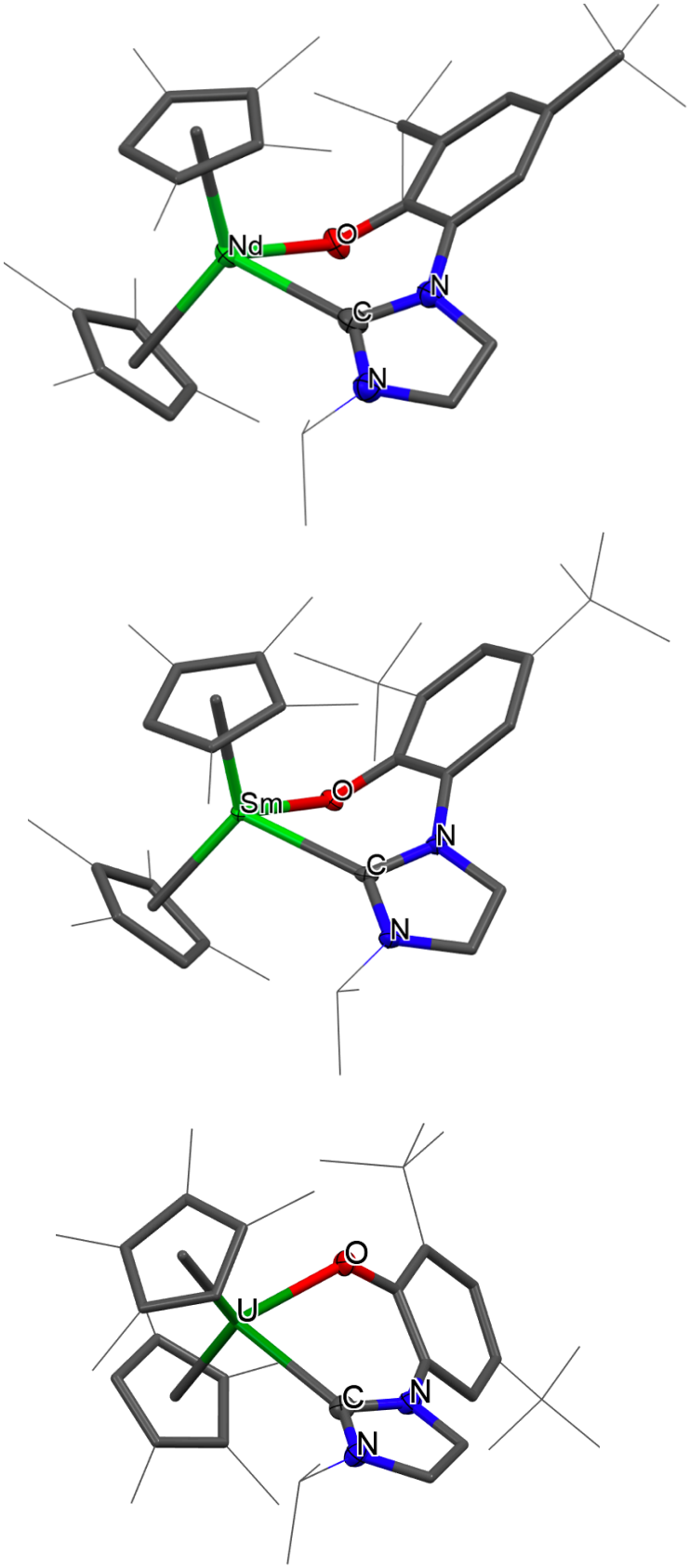

Figure 1.8. Molecular structures of **1-Nd** (top), **1-Sm** (middle) and **1-U** (bottom). Ellipsoids shown at 50% probability, peripheral groups drawn as wireframe, hydrogen atoms and lattice solvent molecules have been omitted for clarity. Color code: green – Ln/An; red – O; grey – C; blue – N.

1.3.2 Photophysical and computational studies

As the aim of this research was to use the previously described complexes in photocatalytic reactions, the light-absorbing and photophysical properties of the complexes were investigated. Further data is presented in **Appendix A** of this thesis.

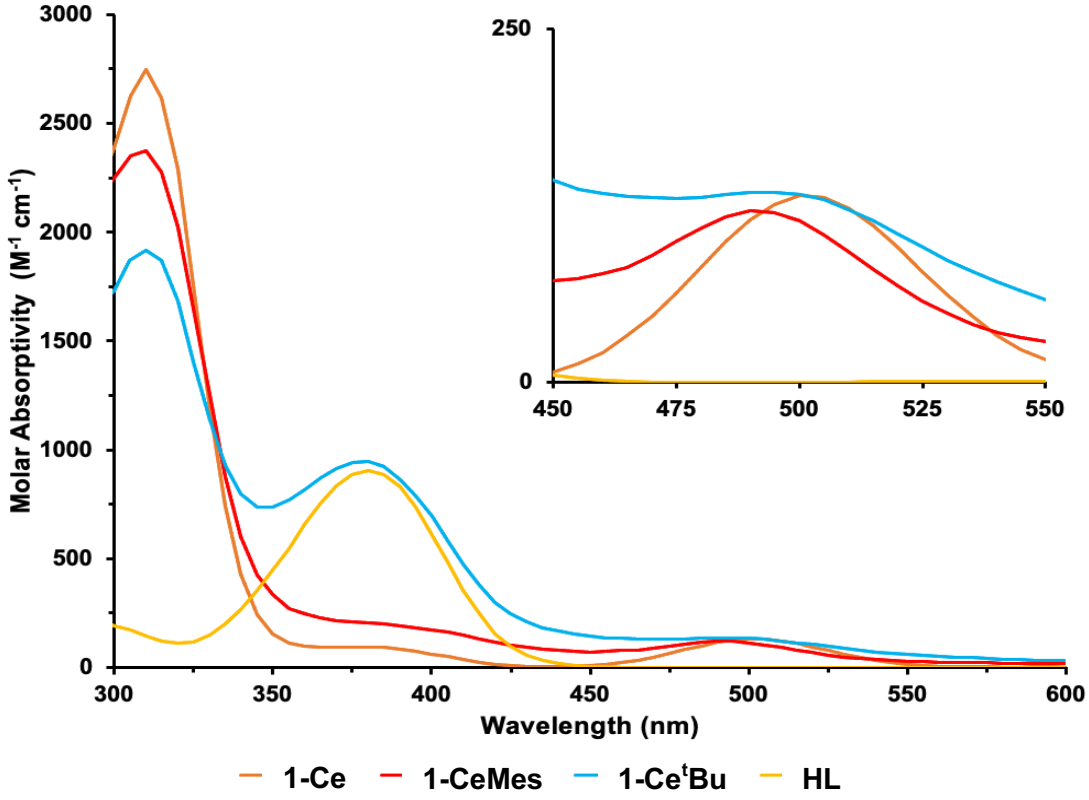

Figure 1.9. The absorption spectra of **1-Ce, 1-CeMes, 1-Ce^{t}Bu**, and proligand **HL**.

Complexes **1-Ce**, **1-CeMes** and **1-Ce^{t}Bu** are bright orange. This is to be expected by trivalent cerium ions coordinated by aromatic ligands; such ligand sets have been shown to red-shift cerium luminescence into the orange wavelength range.[30,78] The UV-Visible spectrum of the f^1 molecule **1-Ce** is shown in Figure 1.9, overlaid with the spectra of **1-CeMes**, **1-Ce^{t}Bu** and proligand **HL** (2-HO-3,5-^{t}Bu$_2$-C$_6$H$_2$(1-C{N(CH)$_2$N(^{i}Pr)})). Through comparison with the absorption spectra of **1-CeMes** and **1-Ce^{t}Bu**, clear metal (ca. 500 nm) and ligand (ca. 380 nm) absorptions can be seen, suggesting the possibility for further catalyst refinement by tuning the positions of these absorbances and optimizing the wavelength of light used. For example, a more electron-donating substituent on the ligand as shown by **1-CeMes** can shift the primarily metal-based excitation to a higher energy, (Table 1.3) due to increased electron density on the metal center.[30] In addition, the intensity of the primarily ligand-based excitation in **1-Ce^{t}Bu** is shown to drastically increase relative to **1-Ce** and **1-CeMes**, perhaps due to increased rigidity in the structure.[49] This suggests the possibility of improving the efficiency of light absorption and quantum yield of the cerium complexes by using ligands that shift the two absorbances closer together. Conversely, separating the two excitations could be used to impart selectivity in chemical transformations.

Table 1.3. Wavelengths of the primarily metal-based absorptions of Ce complexes **1-CeMes, 1-Ce^{t}Bu** and **1-Ce.**

Complex	λ_{max} (nm)
1-CeMes	490
1-Ce^{t}Bu	497
1-Ce	503

The presence of two distinct photoexcitations in **1-Ce** was then corroborated using fluorescence spectroscopy (**Appendix A**). The collection of an emission spectrum at a maximum excitation wavelength of 390 nm, monitored at the maximum emission wavelength of 600 nm, yielded the emission and excitation spectra shown in Figure 1.10. Two clear excitations are observed–a high intensity absorption at approximately 280 nm that can be attributed to a primarily ligand-based excitation and a lower intensity band at approximately 505 nm that can be assigned to a primarily $4f \rightarrow 5d$ metal-based excitation (*vide infra*.). The normalized absorption spectra of **1-Ln** and **1-U** are shown in Figure 1.11, where similar ligand-based excitations can be observed, which suggests the possibility of using these complexes in light-driven reactions despite the lack of $4f \rightarrow 5d$ transition possessed by the trivalent cerium ion.

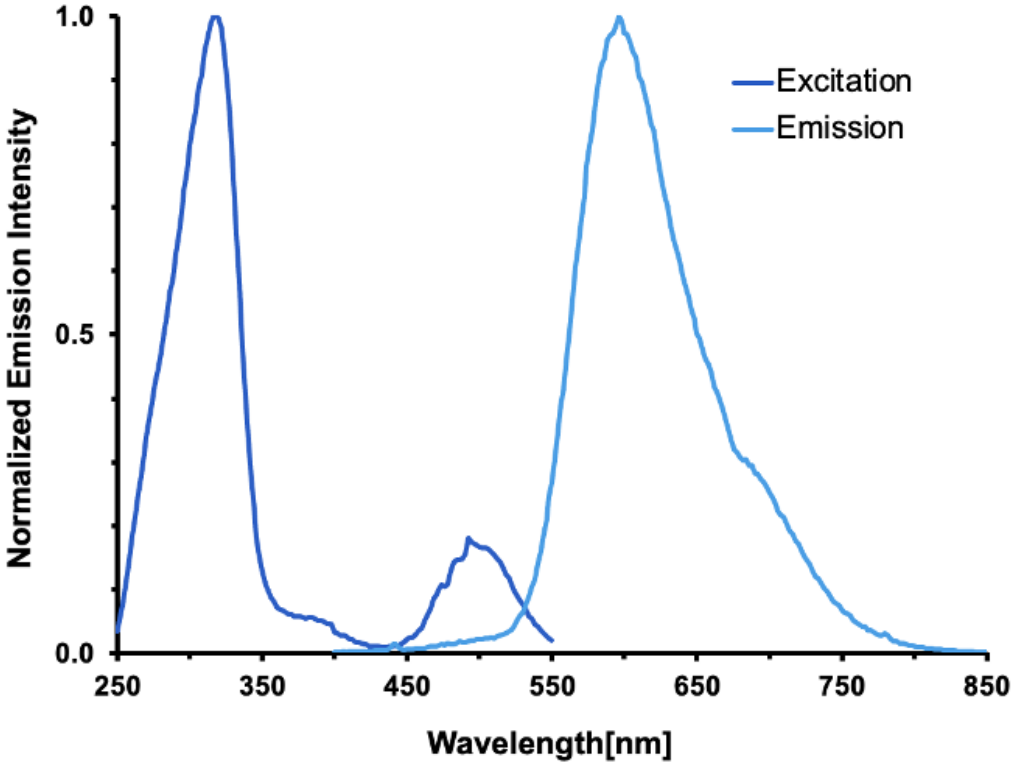

Figure 1.10. Emission and excitation spectra of **1-Ce** recorded in THF. The emission spectrum was collected with an excitation wavelength of 390 nm; the excitation was monitored at an emission wavelength of 600 nm. All data were calibrated to the detector efficiency.

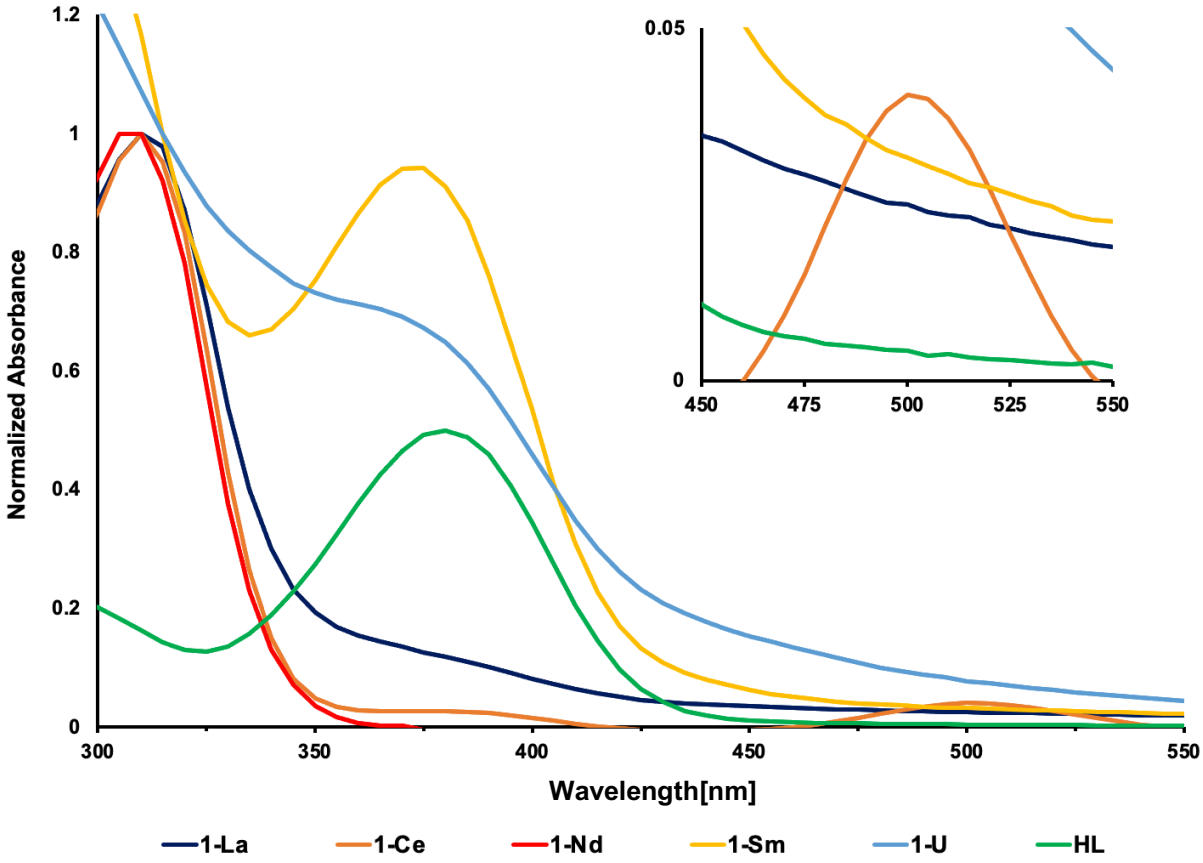

Figure 1.11. UV-Visible spectra of **1-Ln, 1-U** and **HL** recorded in THF.

The Stokes shift of the ligand- and metal-based excitations in **1-Ce** are 325 and 155 nm respectively in THF, and 212 nm and 184 nm in toluene. These values are large compared to the Stokes shift of other cerium complexes reported in the literature (ca. 23–43 nm).[79,80] While a small Stokes shift can be useful for a photoactive complex due to smaller energy losses from the excited state, a large Stokes shift can also be beneficial through the reduction self-quenching arising from molecular self-absorption.[81] This is supported by the long excited state lifetime of **1-Ce,** measured to be 101 ns. Complex **4-Ce** which does not possess a chelating NHC substituent but does have an aryloxy moiety that can absorb light, was shown to also possess excitations at 425 and 530 nm, but with a shorter lifetime of 79 ns. Interestingly the photophysical data of **4-Ce** suggests multiple excited states lying close together in energy (Figure A.7, Figure A.8, **Appendix A**), indicating that small changes to the ligand framework can have large effects on the photoexcitation of cerium complexes due to the *d*-orbital character of the excited state. This is due to strong orbital overlap between ligands and orbitals with *d*-character, despite the poor *f*-orbital extension that typically reduces covalency in lanthanide bonding in the ground state.[30] In addition, it suggests that the encapsulation of the metal center by chelating ligand **L** can reduce vibrations and unwanted interactions with solvent in order to extend the lifetime of the excited state.

To study the potential light-absorbance by cerium complexes without an aryloxy group, fluorescence and lifetime measurements of **3-Ce** were collected. Lanthanide Cp complexes have been shown to have some capacity for light absorption,[82] and **3-Ce** displays excitation and emission spectra consistent with both a ligand and metal based excitation, albeit at a higher energy (ca. 300 and 450 nm). The excited state lifetime of **3-Ce** is 175 ns, which is among the

longest excited state lifetimes of a cerium complex shown in the literature. Only two reported cerium complexes possess longer excited state lifetimes– $[(Me_3Si)_2NC(N^iPr)_2]_2Ce(N(SiMe_3)^tBu)$ and $[(C_8H_8)Ce(\mu–O_3SCF_3)(THF)_2]_2$ published by Schelter et al. display lifetimes of 221 ns and 205 ns respectively.[74,79,83] Interestingly $[(C_8H_8)Ce(\mu–O_3SCF_3)(THF)_2]_2$, like **3-Ce**, is a dimeric complex, which could provide additional shielding to the metal center and reduce energy losses through non-radiative pathways. Indeed, $[(C_8H_8)Ce(\mu–Cl)(THF)_2]_2$, a complex analogous to **3-Ce** which bears cyclooctatetraene (COT) rather than Cp ligands, also has a long excited state lifetime of 145 ns.[79]

Quantum yield measurements could not be collected for the complexes previously described, as the spectrophotometer used was not equipped with an integrating sphere.[84] However, related dimeric cerium chloride complex $[(Cp^{tBu2})_2Ce(\mu–Cl)]_2$ (Cp^{tBu2} =1,3-di(*tert*-butyl)cyclopentadienyl) displays a high quantum yield of 61(±2)%. This was thought to be related to a low vibrational coupling strength and consequent inefficient thermal quenching.[85] Notably, the interaction between the two cerium centers through the Cl ligands enhanced the photoluminescence intensity through a potential self-absorption effect between the ions. In addition, high quantum yields have been reported for sterically encumbered complexes such as $[Eu(Cp^{BIG})_2]$ (Cp^{BIG} = (4-^{n}Bu-$C_6H_4)_5$-cyclopentadienyl)),[86] implying that the coordination of bulky ligands such as **L, L^{Mes} and L^{tBu}** and further substituted analogues to lanthanides could lead to improved quantum yields for these ions.

While photophysical data of **1-La** could not be acquired as only the ligand-based excitation could be observed within the accessible wavelength range of the instrument, time-dependent density functional theory (TD-DFT; B3PW91) calculations were performed on both **1-Ce** and **1-La** to explore and compare the orbitals involved in the photoexcitation for a metal with (cerium) and without (lanthanum) an accessible 4*f* →5*d* transition. The calculated and experimental absorption spectra agreed well for **1-Ce** (Figure 1.12) and **1-La** (Figure 1.13). As expected, the SOMO of **1-Ce** is comprised predominately of 4*f* character with minor orbital contributions from the aryloxide ligand (Figure 1.14).

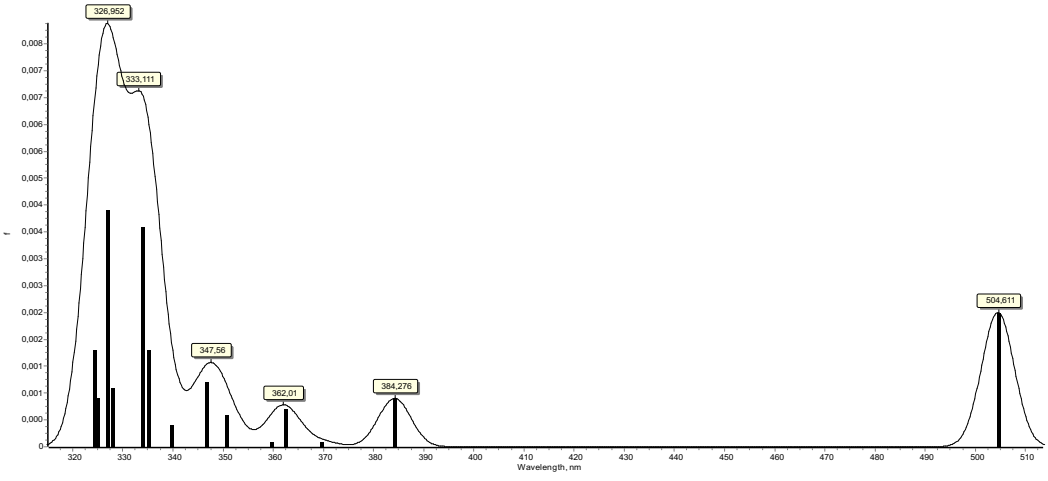

Figure 1.9. Computed UV-Visible spectrum of **1-Ce** using TD-DFT.

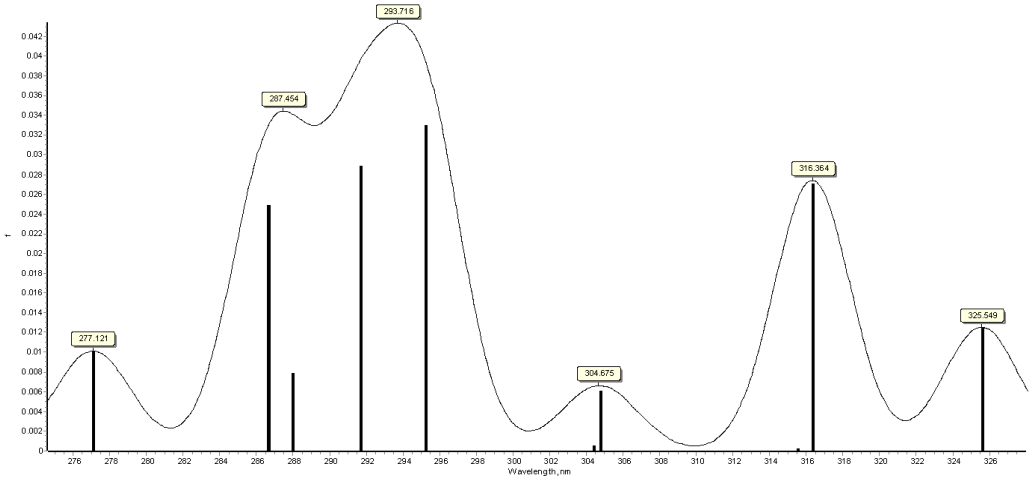

Figure 1.13. Computed UV-Visible spectrum of **1-La** using TD-DFT.

The visible absorption found at 504 nm corresponds mainly to the SOMO-LUMO and SOMO-LUMO+1 transitions. This is an excitation from an *f*-orbital onto either the Ce–NHC or Ce–Cp^{Me4} orbitals. The LUMO+1 is calculated to be a Ce-based (89%) hybrid of *f*- and *d*-orbitals (54% 5*d* and 46% 4*f* mixture) with no significant contributions from the ligands (11%). Notably, the LUMO, which also contributes to the calculated absorbance bands at 504 and 384 nm, is calculated to be primarily of *p*-character and delocalized over both the aromatic ring and NHC moiety of the ligand **L**.

In the case of **1-La**, the HOMO was calculated to be composed of significant π-orbital contributions from both the Cp^{Me4} and **L** ligands, Figure 1.15. As expected, given its formal f^0 electron configuration, there is no appreciable contribution from any La-based orbital to the HOMO. Interestingly, it was found that the LUMO+1 is composed of predominately *d*-character (63% 5*d* and 23% 4*f*). TD-DFT predicts that the transition from HOMO to LUMO+1 results in a band at 325 nm. For both complexes, transitions are calculated in the higher energy region (between 320 and 390 nm) that involve π-type orbitals (Ln–Cp^{Me4}, Ln–NHC). Although UV-Visible spectroscopy confirms that **1-La** does absorb light in the visible region, it does not display the same distinct features as **1-Ce** (Figure 1.14).

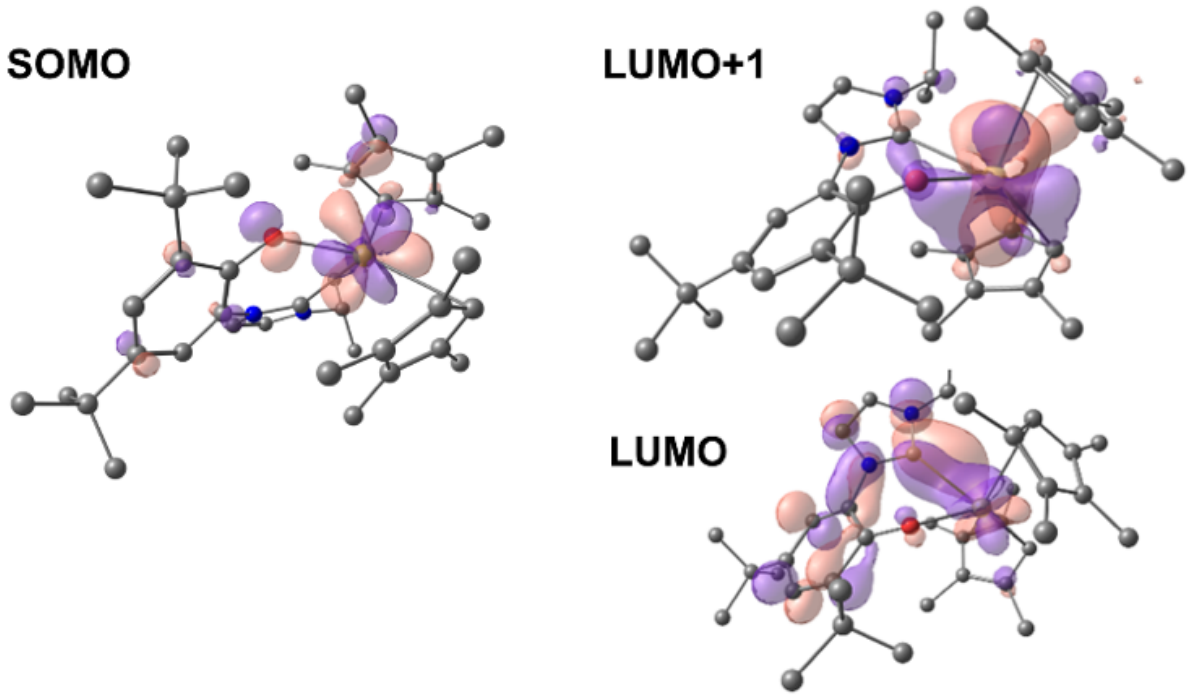

Figure 1.14. Depictions of the TD-DFT-calculated SOMO (left) and LUMO (right, upper) and LUMO+1 (right, lower) orbitals of **1-Ce**.

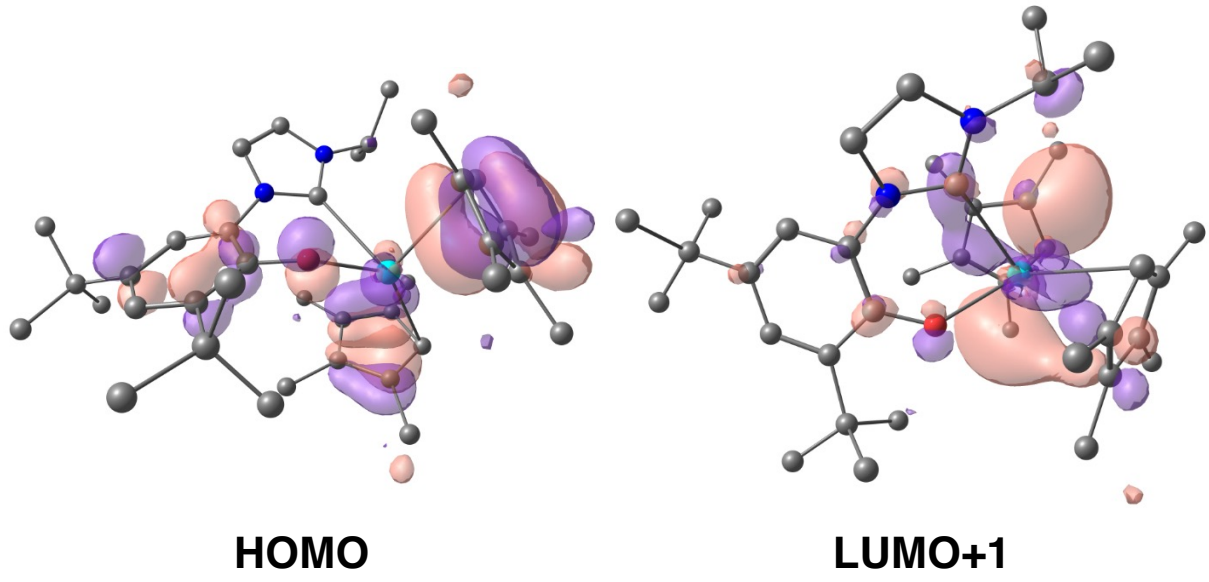

Figure 1.15. Depictions of the TD-DFT-calculated HOMO (left) and LUMO+1 (right) for **1-La**.

1.4 Conclusions

In conclusion, this chapter presents the synthesis of a new family of Ln(III) compounds supported by a light-absorbing aryloxide-tethered N-heterocyclic carbene, Cp^{Me4}, and pseudohalide ligands, alongside the synthesis and characterization of a trivalent uranium complex also supported by Cp^{Me4} and chelating aryloxy NHC ligands.

All complexes have been fully characterized, and the photophysics of key complexes evaluated. UV-Visible and fluorescence spectroscopies suggest that a distinct ligand-based photoexcitation is possible for metals that do not possess the $4f \rightarrow 5d$ excitation, as well as for cerium. Computational experiments also highlight the synergy between ligand-based and metal-based orbitals in the photoexcitation process. This indicates that not only could the chosen ligand framework allow for the generation of an efficient cerium photocatalyst by exploiting two possible routes for photoexcitation,[62] but also allow photoredox catalysis to be extended to other typically photoinactive metals.

1.5 Experimental

General details. All moisture and air sensitive materials were manipulated using standard high-vacuum Schlenk-line techniques and MBraun gloveboxes and stored under an atmosphere of dried and deoxygenated dinitrogen. All glassware items, cannulae and Fisherbrand 1.2 μm retention glass microfiber filters were dried in a 160 °C oven overnight before use.

Solvents and reagents. Hexanes, tetrahydrofuran (THF), diethyl ether (Et_2O) and toluene for use with moisture and air sensitive compounds were dried using an MBraun SPS 800 Manual solvent purification system and stored over activated 3 Å molecular sieves. Benzene-D_6, pyridine-D_5 were purchased from Cambridge Isotope Laboratories and were refluxed over potassium metal for 24 hours, freeze-pump-thaw degassed and purified by trap-to-trap distillation prior to use. THF-D_8 was purchased from Cambridge Isotope Laboratories and dried over sodium/benzophenone before being freeze-pump-thaw degassed and purified by trap-to-trap distillation prior to use. All solvents were purchased from Sigma-Aldrich or Fisher Scientific and stored over 3 Å molecular sieves for 4 hours before being used.

$PhICl_2$ was prepared according to the literature procedure[87] and stored at –30 °C. Dihydrocarbyl magnesium reagents,[88] **HL**, $\mathbf{HL^{Mes}}$ and $\mathbf{HL^{tBu}}$,[89] KC_5Me_4H,[90] lanthanide triiodides (Ln = La, Ce, Nd, Sm),[91,92] lanthanide tris(tetramethylcyclopentadienyl) complexes (Ln = La, Ce, Nd, Sm),[92,93], $UI_3(dioxane)_2$ and $UCp^{Me4}{}_3$,[90] were all prepared using published methods. All other chemicals were purchased from commercial suppliers and degassed and/or dried under vacuum or over 3 Å molecular sieves for 12 hours before use.

Characterization. NMR spectra were recorded on Bruker Avance 400, 500 and 600 MHz spectrometers and are referenced to residual protio solvent (3.58 and 1.72 ppm for THF-D_8, 7.16 ppm for C_6D_6) for ^1H NMR spectroscopy. THF was used as solvents for No Deuterium (NoD) NMR experiments,[10] and was referenced to added tetramethylsilane (0.00 ppm for both ^1H and $^{13}C\{^1H\}$ NMR spectroscopic experiments). Quantitative ^1H NMR data were acquired with a minimum of eight scans, with the delay time set to 5 x the longest T_1 value present. Chemical shifts are quoted in ppm and coupling constants in Hz. Tetrakis(trimethylsilyl)silane (TMS*) was used as internal standards for quantitative ^1H NMR spectroscopy. NMR spectra were taken at 25°C unless otherwise noted. Structural assignments were performed using HSQC and HMBC NMR spectroscopic experiments when necessary. Elemental analyses were

carried out by the microanalytic services in the College of Chemistry at the University of California, Berkeley. Multiple attempts to collect data have been made but poor carbon combustion has been a problem.

Photophysical data. Quartz cells with a 10 mm pathlength equipped with a J-Young valve were used to contain samples prepared under a dinitrogen atmosphere for electronic absorption spectra (UV-Visible) and fluorescence measurements. UV-Visible measurements were collected on an Agilent Varian Cary 50 UV-Visible spectrophotometer. Emission and excitation spectra were collected on Fluorolog®-3 spectrofluorometer.

Crystallography. Single crystal X-ray diffraction data of **1-Ce** were collected using an Excalibur Eos diffractometer, fitted with a CCD area detector and using MoKα radiation (λ = 0.71073 Å) at 170 K. X-ray diffraction data for **3-Ce** were collected at beamline 12.2.1 of the Advanced Light Source (ALS) at Lawrence Berkeley National Lab, using a Bruker D8 diffractometer coupled to a Bruker PhotonII CPAD detector with Si(111)-monochromated synchrotron radiation (17 keV radiation). Single crystal X-ray diffraction data of all other compounds were collected using a Rigaku XtaLAB Synergy-S diffractometer fitted with a HyPix-6000HE photon counting detector using MoKα (λ = 0.71073 Å) or CuKα (λ = 1.5418Å) radiation. All structures were solved using SHELXT in Olex2 and refined using SHELXL in Olex2.[89,9094,95]Absorption corrections were completed using CrysAlis PRO (Rigaku Oxford Diffraction) software. Analytical numeric absorption corrections used a multifaceted crystal model based on expressions derived by Clark and Reid.[96] Numerical absorption correction was based on a Gaussian integration over a multifaceted crystal model.

Computational details. All the structures reported in this study were fully optimized with the Becke's 3-parameter hybrid functional[97] combined with the non-local correlation functional provided by Perdew/Wang (denoted as B3PW91).[98] The basis set used for lanthanum and cerium atom were the Stuttgart-Dresden small core ECP in combination with its adapted basis set.[99,100] For the Mg atom a 6-311++G(d,p) basis set was used whereas for all the other atoms a 6-31G(d,p) basis set was set.[101,102] In all computations no constraints were imposed on the geometry. All stationary points have been identified for minimum (number of imaginary frequencies Nimag=0). The vibrational modes and the corresponding frequencies are based on a harmonic force field. Gibbs free energies were obtained at T=298.15K within the harmonic approximation. GAUSSIAN09 program suite was used in all calculations.[103] The UV-Visible spectra were simulated at the TD-DFT level using the same functional.

Synthesis of $(Cp^{Me4})_2Ce(L)$ (1-Ce). In a glovebox, to a magnetically stirred green solution of $(Cp^{Me4})_3Ce$ (**2-Ce**) (1.21 g, 2.40 mmol, 1.00 equiv.) in toluene (50 mL), was added **HL** (0.756 g, 2.40 mmol, 1.00 equiv.) and the solution stirred overnight. After this time, volatiles were removed under reduced pressure and the orange solid washed with cold (–30°C) hexane (2 x 5 mL) to afford $(Cp^{Me4})_2Ce(\mathbf{L})$. Yield: 1.34 g, 82%. Diffraction quality crystals were grown from a concentrated hexane solution at –30°C.

^{1}H NMR (500 MHz, C_6D_6, 298 K): δ 16.66 (s, 2H, CH_{Cp}), 12.59 (s, 1H, CH_{Im}), 11.03 (s, 1H, CH_{Ph}), 7.29 (s, 6H, CH_{3Cp}), 4.53 (s, 1H, CH_{Im}), 2.05 (s, 9H, CH_{3tBu}), 1.57 (s, 6H, CH_{3Cp}), 0.59 (s, 6H, CH_{3Cp}), -3.84 (s, 6H, CH_{3Cp}), -4.27 (s, 9H, CH_{3tBu}), -8.23 (d, J_{H-H} = 6.7, 6H, CH_{3iPr}), -41.41 (s, 1H, CH_{iPr}). ^{13}C NMR (125.8 MHz, C_6D_6, 300 K), 186.1 (s, C-O), 157.20 (s, Cq_{Cp}), 155.8 (s, C_{Ph}), 149.6 (s, C_{Ph}), 142.8 (s, Cq_{Cp}), 141.0 (s, C_{Ph}), 138.9 (s, Cq_{Cp}), 137.1 (s, CH_{Im}), 135.6 (s, Cq_{Cp}), 124.2 (s, CH_{Ph}), 123.1 (s, CH_{Ph}), 121.3 (s, CH_{Im}), 34.8 (s, C_{tBu}), 33.7 (s, C_{tBu}), 32.8 (s, CH_{3tBu}), 24.7 (s, CH_{3tBu}), 13.31 (s, CH_{3Cp}), 0.61 (s, CH_{3Cp}), 0.15 (s, CH_{3Cp}), -5.69 (s,

CH_{3Cp}). Anal. Calcd for $C_{38}H_{55}CeN_2O$: C, 65.58, H, 7.97, N, 4.03. Found: C, 64.11; H; 7.82; N, 4.03.

Synthesis of $(Cp^{Me4})_2Ce(L^{Mes})$ (1-CeMes). In a glovebox, to a magnetically stirred green solution of **2-Ce** (38.4 mg, 0.0760 mmol, 1.00 equiv.) in toluene (5 mL), $\mathbf{HL^{Mes}}$ (30.0 mg, 0.0760 mmol, 1.00 equiv.) was added and the solution stirred overnight. After this time, volatiles were removed by vacuum evaporation and the orange solid washed with cold (– 30°C) hexane (2 x 2 mL) to afford $(Cp^{Me4})_2Ce(\mathbf{L^{Mes}})$. Yield: 45.2 mg, 77%.

^{1}H NMR (400 MHz, C_6D_6, 298 K): δ 17.69 (br s, 2H, CH_{Cp}), 13.33 (s, 1H, CH_{Im}), 11.49 (s, 1H, CH_{Ph}), 8.46 (s, 1H, CH_{Ph}), 8.34(s, 6H, CH_{3Cp}), 5.50 (s, 1H, CH_{Im}), 3.62 (s, 6H, CH_{3Mes}) 2.07 (s, 9H, CH_{3tBu}), 0.36 (s, 2H, CH_{Mes}), -1.54 (s, 3H, CH_{3Mes}), -3.14 (s, 6H, CH_{3Cp}), -3.36 (s, 6H, CH_{3Cp}), -4.31 (s, 9H, CH_{3tBu}), -7.53 (br s, 6H, CH_{3Cp}). Anal. Calcd for $C_{44}H_{61}CeN_2O$: C, 68.27, H, 7.94, N, 3.62. Found: C, 63.83; H, 7.85; N, 3.92.

Synthesis of $(Cp^{Me4})_2Ce(L^{tBu})$ (1-Ce^{t}Bu). In a glovebox, to a magnetically stirred green solution of **2-Ce** (125 mg, 0.254 mmol, 1.00 equiv.) in toluene (50 mL), $\mathbf{HL^{tBu}}$ (83.9 mg, 0.254 mmol, 1.00 equiv.) was added and the solution stirred overnight. After this time, volatiles were removed by vacuum evaporation and the orange solid washed with cold (– 30°C) hexane (2 x 2 mL) to afford $(Cp^{Me4})_2Ce(\mathbf{L^{tBu}})$. Yield: 142 mg, 78%.

^{1}H NMR (400 MHz, C_6D_6) δ 17.58 (br s, 2H, CH_{Cp}), 13.06 (s, 1H, CH_{Im}), 11.31 (s, 1H, CH_{Ph}), 8.49 (s, 1H, CH_{Ph}), 7.97 (s, 6H, CH_{3Cp}), 4.51 (s, 1H, CH_{Im}), 2.15 (s, 9H, $CH_{3tBu(Ph)}$), 0.46 (s, 9H, CH_{3tBu}), -1.65 (s, 6H, CH_{3Cp}), -4.28 (s, 6H, CH_{3Cp}), -4.51 (s, 9H, $CH_{3tBu(Ph)}$), -8.67 (s, 6H, CH_{3Cp}). Anal. Calcd for $C_{39}H_{58}CeN_2O$: C, 65.88, H, 8.22, N, 3.94. Found: C, 65.75; H,8.43; N, 4.14.

Synthesis of $[(Cp^{Me4})_2Ce(\mu–Cl)]_2$ (3-Ce). Method A: In a glovebox a vial was charged with **2-Ce** (47.0 mg, 0.0933 mmol, 1.00 equiv.) in THF (5 mL), resulting in a green solution. With stirring, a colorless solution of $PhICl_2$ (13.5 mg, 0.0484 mmol, 0.520 equiv.) in THF (1 mL) was added dropwise. Upon addition, the color of the solution quickly changed from green to orange-yellow. After stirring for two hours at room temperature, the volatiles were removed under vacuum, resulting in a pink-orange powder which was subsequently washed with hexanes (2 x 0.5 mL). The powder was redissolved in a minimum of THF (1 mL), and the bright orange-yellow solution was filtered through glass fiber into a 1 mL vial, layered with hexanes (3 mL) and stored at –30 °C for three days to yield large orange blocks of $[(Cp^{Me4})_2Ce(\mu–Cl)]_2$ that were dried in vacuo. Yield: 21.5 mg 54%. Crystals grown via this method were suitable for X-ray diffraction studies.

Method B: A Teflon-stoppered ampoule was charged with $CeCl_3$ (11.5 mg, 0.0467 mmol, 1.00 equiv.) **2-Ce** (47.0 mg, 0.0933 mmol, 2.00 equiv.) and THF (5 mL), resulting in a green slurry. The ampoule was sealed and heated to 70°C for 24 hours, resulting in a color change from green to yellow. The volatiles were removed under vacuum, resulting in a pink-orange powder, which was subsequently washed with hexanes (2 x 0.5 mL). The powder was redissolved in a minimum of THF (1 mL), and the bright orange-yellow solution was filtered through glass fiber into a 1 mL vial, layered with hexanes (3 mL) and stored at –30 °C for 3 days to yield large orange blocks of $[(Cp^{Me4})_2Ce(\mu–Cl)]_2$ that were dried under vacuum. Yield: 28.0 mg,

70% Note: $[(Cp^{Me4})_2Ce(\mu–Cl)]_2$ is dichroic, appearing as a pink solid when isolated as a powder and orange-yellow in THF solution.

^{1}H NMR (500 MHz, THF-D_8) δ 8.79 (br. s, 6H, CH_{3Cp}), 6.83 (br. s, 1H, H_{Cp}), –0.93 (br. s, 6H, CH_{3Cp}). Anal. Calcd for: $C_{36}H_{52}Ce_2Cl_2$: C, 51.72; H, 6.27. Found: C, 51.28; H, 6.09.

Synthesis of $(Cp^{Me4})_2Ce(OAr)$ (4-Ce) (OAr = 1-O-2,6-tBu_2-4-Me-C_6H_2). In a glovebox, a vial was charged with $[(Cp^{Me4})_2Ce(\mu–Cl)]_2$ (**3-Ce**) (31.5 mg, 0.0377 mmol, 1.00 equiv.), sodium 2,6-di-tert-butyl-4-methylphenolate (18.3 mg, 0.0754 mmol, 2.00 equiv.) and hexanes (5 mL). The reaction was stirred at room temperature for 48 hours and following a gradual color change from yellow to deep red, volatiles were removed under vacuum. The red residue was extracted into hexane before being dried to give a red powder identified as $(Cp^{Me4})_2Ce(OAr)$ by ^{1}H NMR spectroscopy. Yield: 18.4 mg, 80%. Diffraction quality crystals of **$(Cp^{Me4})_2Ce(OAr)(THF)$ (4a-Ce)** were grown from a THF solution layered with hexanes at –30°C, crystals of **$(Cp^{Me4})_2Ce(OAr)$** (**4b-Ce)** were grown from a concentrated hexane solution at –30°C.

^{1}H NMR (400 MHz, C_6D_6): δ 28.01 (br. s, 2H, H_{Cp}), 6.57 (s, 2H, $H_{m\text{-}Ph}$), 3.18 (br. s, 12H, CH_{3Cp}), 2.18 (s, 3H, $3H_{p\text{-}Ph}$), -4.18 (br. s, 12H, CH_{3Cp}), -6.26 (br. s, 18H, CH_{3tBu}). Anal. Calcd for: $C_{33}H_{49}CeO$: C, 65.86; H, 8.21. Found: C, 66.00; H, 8.03.

Synthesis of $(Cp^{Me4})_2Ce(OTf)(THF)$ (5-Ce). In a glovebox, a teflon-stoppered ampoule was charged with **2-Ce** (1.04 g, 2.07 mmol, 2.01 equiv.), $Ce(OTf)_3$ (0.607 g, 1.03 mmol, 1.00 equiv.) and THF (30 mL), resulting in a dark green slurry. The ampoule was sealed and placed in a 70 ºC oil bath with stirring for 20 hours, during which time the color changed from dark green to a bright yellow. The reaction mixture was then cooled to room temperature before being filtered through glass fiber. The yellow filtrate was dried under vacuum to yield a pale-yellow powder which was washed with hexanes (2 x 4 mL) before drying under vacuum again, yielding 5-Ce. Yield: 1.13 g, 89%. X-ray quality crystals of **5-Ce** were grown by layering a concentrated THF solution with hexanes and storing at –30 °C for 3 days. Note: **5-Ce** is thermochromic, appearing pale yellow when cold (–30 °C) and bright yellow at room temperature in either solution or solid state.

^{1}H NMR (500 MHz, THF-D_8) δ 11.68 (br. s, 12H), 10.78 (br. s, 2H), –4.50 (br. s, 12H).^{19}F NMR (471 MHz, THF-D_8) δ –96.2 (s). Anal. Calcd for: $C_{23}H_{43}CeO_4F_3S$: C, 45.76; H, 5.68. Found: C, 42.26; H, 4.68.

Synthesis of $(Cp^{Me4})_2Ce(Bn)(THF)$ (6-Ce). In a glovebox, a 20 mL vial was charged with $(Cp^{Me4})_2Ce(OTf)(THF)$ (**5-Ce**) (262 mg, 0.435 mmol, 1.00 equiv.) dissolved in THF (8 mL), yielding a bright yellow solution. With stirring, a THF solution (2 mL) of $MgBn_2(THF)_2$ (80.6 mg, 0.230 mmol, 0.530 equiv.) was added dropwise, resulting in a darkening of the color to a golden yellow. The solution was stirred at room temperature for 1 hour before being dried under vacuum to yield a bright yellow residue, which was extracted with hexanes (20 mL). The yellow solution was filtered and concentrated, then stored at –30 ºC overnight to yield a bright yellow microcrystalline solid. After decanting the supernatant, the solid was dried under vacuum to yield $(Cp^{Me4})_2Ce(Bn)(THF)$. Yield: 212 mg, 88%. X-ray quality crystals were grown by cooling a hexanes solution to –30 °C for 3 days. The complex is dichroic in solution, appearing yellow when concentrated but green when dilute in hexane solution.

Note: In this case, **6-Ce** was found to decompose to a dark brown material upon prolonged exposure to vacuum (i.e. >3 hours), presumably due to irreversible loss of coordinated THF.

^{1}H NMR (500 MHz, C_6D_6) δ 15.62 (br. s, 2H), 5.14 (br. s, 12H), 3.04 (br. s, 12H), 0.14 (br. s, 2H), –1.20 (br. s, 4H), –2.65 (t, J = 6.8 Hz, 1H, $H_{p\text{-}Ar}$), –4.33 (br. s, 4H), –4.67 (br. s, 2H), –11.27 (br. s, 2H). Anal. Calcd for: $C_{29}H_{42}CeO$: C, 63.7; H, 7.74. Found: C, 58.02; H, 6.79. [Multiple Attempts]

Synthesis of $(Cp^{Me4})_2La(L)$ (1-La). In a glovebox, to a magnetically stirred solution of $(Cp^{Me4})_3La$ (**2-La**) (1.21 g, 2.40 mmol, 1.00 equiv.) in toluene (50 mL), **HL** (0.756 g, 2.40 mmol, 1.00 equiv). was added and the solution stirred overnight. After this time, volatiles were removed by vacuum evaporation and the cream solid washed with cold (–30°C) hexane (2 x 5 ml) to afford $(Cp^{Me4})_2La(\mathbf{L})$. Yield: 1.24 g, 74%. Diffraction quality crystals were grown from a concentrated toluene solution at –30°C.

^{1}H NMR (500 MHz, C_6D_6, 298 K) : δ 7.50 (1H, d, $J_{H\text{-}H}$ = 2.4, CH_{Im}), 7.10 (1H, d, $J_{H\text{-}H}$ = 2.5, CH_{Im}), 6.73 (1H, d, $J_{H\text{-}H}$ = 1.7, CH_{Ph}), 6.26 (1H, d, $J_{H\text{-}H}$ = 1.8, CH_{Ph}), 5.77 (2H, s, CH_{Cp}), 4.41 (1H, sept, $J_{H\text{-}H}$ = 6.8, H_{iPr}), 2.23 (6H, s, CH_{3Cp}), 2.21 (6H, s, CH_{3Cp}), 2.11 (6H, s, CH_{3Cp}), 1.97 (6H, s, CH_{3Cp}), 1.87 (9H, s, CH_{3tBu}), 1.69 (9H, s, CH_{3tBu}), 1.39 (9H, s, CH_{3tBu}), 1.17 (6H, d, $J_{H\text{-}H}$ = 6.8, CH_{iPr}). ^{13}C NMR (125 MHz, C_6D_6, 298 K): δ 154.1 (s, C-O), 138.9 (s, C_{Ph}), 136.5 (s, C_{Ph}), 128.4 (s, NCN), 123.4 (s, C_{PhH}), 122.5 (s, C_{im}), 121.8 (s, Cp), 120.7 (s, Cp), 119.8 (s, Cp), 118.8 (s, Cp), 118.5 (s, C_{im}), 114.7 (s, C_{PhH}), 111.9 (s, CpH), 52.9 (s, iPrCH), 36.2 (s, C_{CH3}), 34.3 (s, C_{CH3}), 32.1 (s, C_{tBu}), 30.6 (s, C_{tBu}), 24.0 (s, iPr_{CH3}), 13.0 (s, CpMe), 12.9 (s, CpMe), 11.4 (s, CpMe), 10.07 (s, CpMe). Anal. Calcd for: $C_{38}H_{55}LaN_2O$: C, 65.58, H, 7.97, N, 4.03. Found: C, 66.07 H; 8.03; N, 3.67.

Synthesis of $[(Cp^{Me4})_2La(\mu\text{–}Cl)]_2$ (3-La) Method A: In a glovebox, to a magnetically stirred solution of **2-La** (40.0 mg, 0.0575 mmol, 1.00 equiv.) in toluene (2 mL), benzyl chloride (6.66 µL, 0.0579 mmol, 1.00 equiv.). was added and the solution stirred overnight. After this time, volatiles were removed by vacuum evaporation and the white solid washed with cold (-20°C) hexane (2 x 5 ml) to afford **$[(Cp^{Me4})_2La(\mu\text{–}Cl)]_2$**. Yield: 19.3 mg, 79%. Diffraction quality crystals (Figure 1.16) were grown from a concentrated toluene solution at –30°C.

Method B: In a glovebox a vial was charged with **2-La** (40.0 mg, 0.0575 mmol, 1.00 equiv.) in THF (5 mL). With stirring, a colorless solution of $PhICl_2$ (7.92 mg, 0.0288 mmol, 0.520 equiv.) in THF (1 mL) was added dropwise. After stirring for 2 hours at room temperature, the volatiles were removed under vacuum, resulting in a cream powder which was subsequently washed with hexanes (2 x 0.5 mL). The powder was redissolved in a minimum of THF (1 mL), and the colorless solution was filtered through glass fiber into a 4 mL vial, layered with hexanes (3 mL) and stored at –30 °C for 3 days to yield large colorless blocks of **$[(Cp^{Me4})_2La(\mu\text{–}Cl)]_2$** that were dried *in vacuo*. Yield: 15.4 mg, 63%.

^{1}H NMR (400 MHz, THF-H_8, 298 K): δ 5.51 (2H, s, CH_{3Cp}), 1.99 (6H, s, CH_{3Cp}), 1.90 (6H, s, C_5Me_4H). ^{13}C NMR (125 MHz, THF-H_8, 298 K): δ 122.0 (s, C_{Cp}), 122.0 (s, C_{Cp}), 112.9 (s, C_{HCp}), 12.5 (s, C_{H3Cp}). Anal. Calcd for $C_{36}Cl_2H_{52}La_2$: C, 51.88; H, 6.29; Found: C, 49.03; H, 5.69.

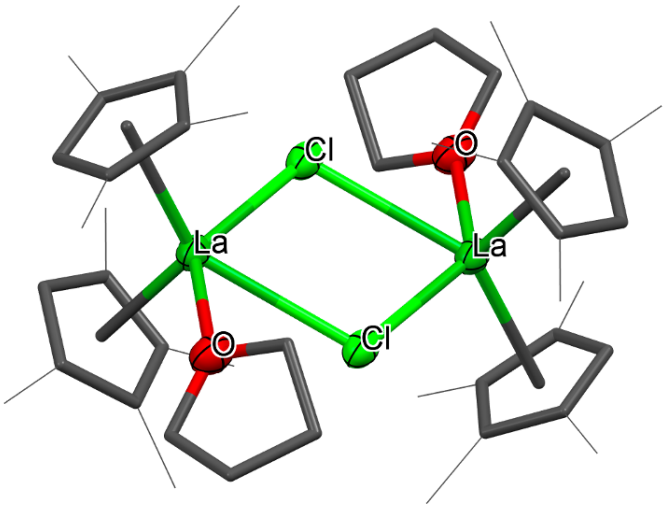

Figure 1.16. Molecular structure of $[(Cp^{Me4})_2La(\mu–Cl)]_2$ (**3-La**). Ellipsoids shown at 50% probability, peripheral groups drawn as wireframe, hydrogen atoms and lattice solvent molecules have been omitted for clarity. Color code: green – La; grey – C; bright green – Cl.

Synthesis of $(Cp^{Me4})_2Nd(L)$ (1-Nd). In a glovebox, to a magnetically stirred solution of $(Cp^{Me4})_3Nd$ (**2-Nd**) (54.9 mg, 0.108 mmol, 1.00 equiv.) in toluene (5 mL), **HL** (34.1 mg, 0.108 mmol, 1.00 equiv). was added and the blue solution stirred overnight. After this time a color change to green was observed, volatiles were removed by vacuum evaporation and the resulting blue solid washed with cold (–30°C) hexane (2 x 2 mL) to afford $(Cp^{Me4})_2Nd$(**L**). Yield: 50.0 mg, 64%. Diffraction quality crystals were grown from a concentrated toluene solution at –30 °C. Anal. Calcd for: $C_{38}H_{55}N_2ONd$: C, 65.19; H, 7.92; N, 4.00. Found: C, 65.47; H, 7.73; N, 3.82.

Synthesis of $(Cp^{Me4})_2Sm(L)$ (1-Sm). In a glovebox, to a magnetically stirred solution of $(Cp^{Me4})_3Sm$ (**2-Sm**) (24.0 mg, 0.0460 mmol, 1.00 equiv.) in toluene (2 mL), **HL** (14.7 mg, 0.0460 mmol, 1.00 equiv). was added and the red solution stirred overnight. After this time, volatiles were removed by vacuum evaporation and the yellow solid washed with cold (–30°C) hexane (2 x 2 mL) to afford $(Cp^{Me4})_2Sm$(**L**). Yield: 59%. Diffraction quality crystals were grown from a concentrated toluene solution at –30°C. Anal. Calcd for: $C_{38}H_{55}N_2OSm$: C, 64.63; H, 7.85; N, 3.97. Found: C, 62.05; H, 7.41; N, 3.19.

Synthesis of $(Cp^{Me4})_2U(L)$ (1-U). In a glovebox, to a magnetically stirred solution of $(Cp^{Me4})_3U$ (**2-U**) (61.0 mg, 0.102 mmol, 1.00 equiv.) in toluene (2 mL), **HL** (31.9 mg, 0.102 mmol, 1.00 equiv). was added and the red solution stirred overnight. After this time, volatiles were removed by vacuum evaporation and the black solid washed with cold (–30°C) hexane (2 x 2 mL) to afford $(Cp^{Me4})_2U$(**L**). Yield: 51.3 mg, 69%. Diffraction quality crystals were grown from a concentrated toluene solution at –30°C. Anal. Calcd for: $C_{38}H_{55}N_2OU$: C, 56.91; H, 7.92; N, 3.49. Found: C, 52.36; H, 6.31; N, 2.85. [Multiple attempts]

Table 1.4. Crystal data and structure refinement for **1-Ce, 3-Ce,** and **4a-Ce.**

	1-Ce	**3-Ce**	**4a-Ce**
Empirical formula	$C_{38}H_{55}CeN_2O$	$C_{36}H_{52}Ce_2Cl_2$	$C_{33}H_{49}CeO$
Formula weight	1391.91	417.96	601.84
Temperature/K	293(2)	100	100.00(10)
Crystal system	monoclinic	monoclinic	triclinic
Space group	$P2_1/n$	$P2_1/n$	P-1
a/Å	10.66730(10)	8.5165(4)	9.63360(10)
b/Å	17.46410(10)	10.4652(4)	10.07670(10)
c/Å	19.30400(10)	19.4321(8)	16.3047(2)
α/°	90	90	93.2430(10)
β/°	89.9070(10)	92.0320(10)	90.3960(10)
γ/°	90	90	107.6780(10)
Volume/Å^3	3596.23(4)	1730.83(13)	1505.14(3)
Z	4	2	2
ρ_{calc}g/cm^3	1.285	1.604	1.328
μ/mm^{-1}	1.295	2.943	1.534
F(000)	1452.0	836.0	626.0
Crystal size/mm^3	0.351 × 0.251 × 0.164	0.07 × 0.055 × 0.03	0.21 × 0.1 × 0.07
Radiation	Mo Kα (λ = 0.71073)	synchrotron (λ = 0.7288)	Mo Kα (λ = 0.71073)
2Θ range for data collection/°	6.748 to 52.744	4.302 to 55.738	4.25 to 62.182
Index ranges	$-13 \le h \le 13$, $-21 \le k \le 21$, $-24 \le l \le 24$	$-10 \le h \le 10$, $-13 \le k \le 13$, $-24 \le l \le 24$	$-13 \le h \le 13$, $-14 \le k \le 14$, $-22 \le l \le 23$
Reflections collected	72839	22581	67296
Independent reflections	7352 [R_{int} = 0.0362, R_{sigma} = 0.0180]	3819 [R_{int} = 0.1107, R_{sigma} = 0.0729]	8291 [R_{int} = 0.0451, R_{sigma} = 0.0277]
Data/restraints/parameters	7352/0/395	3819/0/190	8291/0/331
Goodness-of-fit on F^2	1.061	1.068	1.052
Final R indexes [I>=2σ (I)]	R_1 = 0.0190, wR_2 = 0.0434	R_1 = 0.0490, wR_2 = 0.1212	R_1 = 0.0205, wR_2 = 0.0438
Final R indexes [all data]	R_1 = 0.0232, wR_2 = 0.0453	R_1 = 0.0514, wR_2 = 0.1239	R_1 = 0.0240, wR_2 = 0.0447
Largest diff. peak/hole / e Å^{-3}	0.34/-0.34	1.16/-1.38	0.91/-0.50

Table 1.5. Crystal data and structure refinement for **4b-Ce**, **5-Ce,** and **6-Ce.**

	4b-Ce	**5-Ce**	**6-Ce**
Empirical formula	$C_{37}H_{57}CeO_2$	$C_{23}H_{34}CeF_3OS$	$C_{29}H_{41}CeO$
Formula weight	673.94	150.92	545.74
Temperature/K	100.00(11)	99.99(11)	293(2)
Crystal system	monoclinic	monoclinic	monoclinic
Space group	$P2_1$	Ia	$P2_1/c$
a/Å	10.4698(2)	17.5622(3)	16.2557(2)
b/Å	12.0899(3)	9.40990(10)	8.82900(10)
c/Å	13.9747(3)	16.2878(3)	18.3743(2)
α/°	90	90	90
β/°	107.666(2)	108.821(2)	105.1410(10)
γ/°	90	90	90
Volume/Å^3	1685.48(7)	2547.78(8)	2545.56(5)
Z	2	4	4
ρ_{calc}g/cm^3	1.328	1.574	1.424
μ/mm^{-1}	1.380	1.916	1.806
F(000)	706.0	1220.0	1124.0
Crystal size/mm^3	0.272 × 0.26 × 0.206	0.374 × 0.263 × 0.203	0.306 × 0.217 × 0.096
Radiation	Mo Kα (λ = 0.71073)	Mo Kα (λ = 0.71073)	MoKα (λ = 0.71073)
2Θ range for data collection/°	4.082 to 61.938	4.9 to 61.74	4.594 to 61.904
Index ranges	$-14 \le h \le 14$, $-16 \le k \le 15$, $-20 \le l \le 19$	$-22 \le h \le 24$, $-13 \le k \le 13$, $-23 \le l \le 22$	$-22 \le h \le 22$, $-12 \le k \le 12$, $-24 \le l \le 26$
Reflections collected	39085	28412	57712
Independent reflections	8812 [R_{int} = 0.0419, R_{sigma} = 0.0359]	6338 [R_{int} = 0.0752, R_{sigma} = 0.0465]	7165 [R_{int} = 0.0350, R_{sigma} = 0.0217]
Data/restraints/parameters	8812/1/376	6338/2/297	7165/0/288
Goodness-of-fit on F^2	1.055	0.928	1.057
Final R indexes [I>=2σ (I)]	R_1 = 0.0226, wR_2 = 0.0464	R_1 = 0.0413, wR_2 = 0.1179	R_1 = 0.0183, wR_2 = 0.0399
Final R indexes [all data]	R_1 = 0.0270, wR_2 = 0.0474	R_1 = 0.0432, wR_2 = 0.1200	R_1 = 0.0216, wR_2 = 0.0407
Largest diff. peak/hole / e Å^{-3}	0.69/-0.39	0.91/-1.34	0.49/-0.36

Table 1.6. Crystal data and structure refinement for **1-La**, **3-La**, and **1-Nd.**

	1-La	**3-La**	**1-Nd**
Empirical formula	$C_{45}H_{63}LaN_2O$	$C_{44}H_{68}Cl_2LaO_2$	$C_{45}H_{63}N_2NdO$
Formula weight	786.88	244.42	792.21
Temperature/K	100.01(10)	99.99(14)	100.00(13)
Crystal system	monoclinic	monoclinic	monoclinic
Space group	$P2_1/c$	$P2_1/n$	$P2_1/c$
a/Å	13.30050(10)	11.3760(4)	13.1816(2)
b/Å	22.02780(10)	15.3980(7)	22.1050(2)
c/Å	15.63480(10)	12.4103(4)	15.5529(2)
α/°	90	90	90
β/°	113.5670(10)	91.155(3)	112.9380(10)
γ/°	90	90	90
Volume/Å^3	4198.63(5)	2173.44(14)	4173.45(10)
Z	4	2	4
ρ_{calc}g/cm^3	1.245	1.494	1.261
μ/mm^{-1}	8.101	16.351	9.732
F(000)	1648.0	992.0	1660.0
Crystal size/mm^3	0.154 × 0.133 × 0.093	0.104 × 0.07 × 0.031	0.096 × 0.08 × 0.027
Radiation	Cu Kα (λ = 1.54184)	Cu Kα (λ = 1.54184)	Cu Kα (λ = 1.54184)
2Θ range for data collection/°	7.252 to 154.87	9.154 to 148.996	7.282 to 155.594
Index ranges	$-16 \le h \le 15$, $-27 \le k \le 27$, $-19 \le l \le 19$	$-14 \le h \le 14$, $-19 \le k \le 18$, $-15 \le l \le 15$	$-16 \le h \le 16$, $-27 \le k \le 26$, $-18 \le l \le 19$
Reflections collected	163711	40521	85278
Independent reflections	8870 [R_{int} = 0.0535, R_{sigma} = 0.0171]	4453 [R_{int} = 0.1585, R_{sigma} = 0.0559]	8821 [R_{int} = 0.0540, R_{sigma} = 0.0253]
Data/restraints/parameters	8870/289/524	4453/0/234	8821/105/524
Goodness-of-fit on F^2	1.069	1.131	1.103
Final R indexes [I>=2σ (I)]	R_1 = 0.0214, wR_2 = 0.0545	R_1 = 0.0559, wR_2 = 0.1350	R_1 = 0.0334, wR_2 = 0.0779
Final R indexes [all data]	R_1 = 0.0226, wR_2 = 0.0551	R_1 = 0.0712, wR_2 = 0.1428	R_1 = 0.0369, wR_2 = 0.0795
Largest diff. peak/hole / e Å^{-3}	0.43/-0.53	1.06/-1.55	0.59/-1.31

Table 1.7. Crystal data and structure refinement for **1-Sm** and **1-U**.

	1-Sm	**1-U**
Empirical formula	$C_{38}H_{55}N_2OSm$	$C_{45}H_{63}N_2OU$
Formula weight	706.19	886.00
Temperature/K	100.00(11)	99.99(10)
Crystal system	monoclinic	monoclinic
Space group	$P2_1/n$	$P2_1/c$
a/Å	10.68690(5)	13.1962(2)
b/Å	17.26346(8)	22.0800(2)
c/Å	19.16251(8)	15.5224(2)
α/°	90	90
β/°	90.4636(4)	112.936(2)
γ/°	90	90
Volume/Å^3	3535.23(3)	4165.22(11)
Z	4	4
ρ_{calc}g/cm^3	1.327	1.413
μ/mm^{-1}	12.684	11.211
F(000)	1468.0	1788.0
Crystal size/mm^3	0.2 × 0.11 × 0.07	0.123 × 0.115 × 0.059
Radiation	Cu Kα (λ = 1.54184)	Cu Kα (λ = 1.54184)
2Θ range for data collection/°	6.892 to 148.996	7.274 to 154.978
Index ranges	$-13 \le h \le 13$, $-21 \le k \le 20$, $-23 \le l \le 23$	$-16 \le h \le 16$, $-27 \le k \le 26$, $-19 \le l \le 19$
Reflections collected	136174	85158
Independent reflections	7240 [R_{int} = 0.0781, R_{sigma} = 0.0211]	8791 [R_{int} = 0.0654, R_{sigma} = 0.0280]
Data/restraints/parameters	7240/0/395	8791/244/524
Goodness-of-fit on F^2	1.055	1.072
Final R indexes [I>=2σ (I)]	R_1 = 0.0225, wR_2 = 0.0559	R_1 = 0.0311, wR_2 = 0.0762
Final R indexes [all data]	R_1 = 0.0232, wR_2 = 0.0563	R_1 = 0.0345, wR_2 = 0.0780
Largest diff. peak/hole / e Å^{-3}	0.53/-0.96	1.60/-1.57

1.6 References

(1) Prieto, A.; Jaroschik, F. Recent Applications of Rare Earth Complexes in Photoredox Catalysis for Organic Synthesis. *Current Organic Chemistry* **2021**, *26* (1), 6–41. https://doi.org/10.2174/1385272825666211126123928.

(2) Crisenza, G. E. M.; Melchiorre, P. Chemistry Glows Green with Photoredox Catalysis. *Nature Communications* **2020**, *11* (1). https://doi.org/10.1038/s41467-019-13887-8.

(3) Tucker, J. W.; Stephenson, C. R. J. Shining Light on Photoredox Catalysis: Theory and Synthetic Applications. *Journal of Organic Chemistry* **2012**, *77* (4), 1617–1622. https://doi.org/10.1021/jo202538x.

(4) Twilton, J.; Le, C.; Zhang, P.; Shaw, M. H.; Evans, R. W.; MacMillan, D. W. C. The Merger of Transition Metal and Photocatalysis. *Nature Reviews Chemistry* **2017**, *1* (7), 0052. https://doi.org/10.1038/s41570-017-0052.

(5) Cheung, K. P. S.; Sarkar, S.; Gevorgyan, V. Visible Light-Induced Transition Metal Catalysis. *Chem. Rev.* **2022**, *122* (2), 1543–1625. https://doi.org/10.1021/acs.chemrev.1c00403.

(6) Mazzarella, D.; Crisenza, G. E. M.; Melchiorre, P. Asymmetric Photocatalytic C-H Functionalization of Toluene and Derivatives. *J. Am. Chem. Soc.* **2018**, *140* (27), 8439–8443. https://doi.org/10.1021/jacs.8b05240.

(7) Ahneman, D. T.; Doyle, A. G. C-H Functionalization of Amines with Aryl Halides by Nickel-Photoredox Catalysis. *Chem. Sci.* **2016**, *7* (12), 7002–7006. https://doi.org/10.1039/c6sc02815b.

(8) Hu, A.; Guo, J. J.; Pan, H.; Zuo, Z. Selective Functionalization of Methane, Ethane, and Higher Alkanes by Cerium Photocatalysis. *Science* **2018**, *361* (6403), 668–672. https://doi.org/10.1126/science.aat9750.

(9) Zuo, Z.; Ahneman, D. T.; Chu, L.; Terrett, J. A.; Doyle, A. G.; Macmillan, D. W. C. Merging Photoredox with Nickel Catalysis : The Coupling of Sp3-Carbons with Aryl Halides Using Feedstock Chemicals. *Science* **2014**, *345* (6195), 437–440.

(10) Schweitzer-Chaput, B.; Horwitz, M. A.; de Pedro Beato, E.; Melchiorre, P. Photochemical Generation of Radicals from Alkyl Electrophiles Using a Nucleophilic Organic Catalyst. *Nature Chemistry* **2019**, *11* (2), 129–135. https://doi.org/10.1038/s41557-018-0173-x.

(11) Goti, G.; Bieszczad, B.; Vega-Peñaloza, A.; Melchiorre, P. Stereocontrolled Synthesis of 1,4-Dicarbonyl Compounds by Photochemical Organocatalytic Acyl Radical Addition to Enals. *Angewandte Chemie* **2019**, *131* (4), 1226–1230. https://doi.org/10.1002/ange.201810798.

(12) Le, C.; Chen, T. Q.; Liang, T.; Zhang, P.; MacMillan, D. W. C. A Radical Approach to the Copper Oxidative Addition Problem: Trifluoromethylation of Bromoarenes. *Science* **2018**, *360* (6392), 1010–1014. https://doi.org/10.1126/science.aat4133.

(13) Nguyen, S. T.; Murray, P. R. D.; Knowles, R. R. Light-Driven Depolymerization of Native Lignin Enabled by Proton-Coupled Electron Transfer. *ACS Catal.* **2020**, *10* (1), 800–805. https://doi.org/10.1021/acscatal.9b04813.

(14) Zhou, Y.; Hu, D.; Li, D.; Jiang, X. Uranyl-Photocatalyzed Hydrolysis of Diaryl Ethers at Ambient Environment for the Directional Degradation of 4-O-5 Lignin. *JACS Au* **2021**, *1* (8), 1141–1146. https://doi.org/10.1021/jacsau.1c00168.

(15) Guo, J.-J.; Hu, A.; Chen, Y.; Sun, J.; Tang, H.; Zuo, Z. Photocatalytic C−C Bond Cleavage and Amination of Cycloalkanols by Cerium(III) Chloride Complex. *Angew. Chem. Int. Ed.* **2016**, *128* (49), 15545–15548. https://doi.org/10.1002/ange.201609035.

(16) Cheisson, T.; Schelter, E. J. Rare Earth Elements: Mendeleev's Bane, Modern Marvels. *Science* **2019**, *363* (6426), 489–493. https://doi.org/10.1126/science.aau7628.

(17) Arnold, P. L.; Kerr, R. W. F.; Weetman, C.; Docherty, S. R.; Rieb, J.; Cruickshank, F. L.; Wang, K.; Jandl, C.; McMullon, M. W.; Pöthig, A.; Kühn, F. E.; Smith, A. D. Selective and Catalytic Carbon Dioxide and Heteroallene Activation Mediated by Cerium N-Heterocyclic Carbene Complexes. *Chem. Sci.* **2018**, *9* (42), 8035–8045. https://doi.org/10.1039/c8sc03312a.
(18) Kerr, R. W. F.; Ewing, P. M. D. A.; Raman, S. K.; Smith, A. D.; Williams, C. K.; Arnold, P. L. Ultrarapid Cerium(III)-NHC Catalysts for High Molar Mass Cyclic Polylactide. *ACS Catal.* **2021**, *11* (3), 1563–1569. https://doi.org/10.1021/acscatal.0c04858.
(19) Watson, P. L.; Tulip, T. H.; Williams, I. Defluorination of Perfluoroolefins by Divalent Lanthanoid Reagents: Activating C–F Bonds. *Organometallics* **1990**, *9* (7), 1999–2009. https://doi.org/10.1021/om00157a006.
(20) Kondo, T.; Akazome, M.; Watanabe, Y. Lanthanide(II) Iodide Catalysed Photochemical Allylation of Aldehydes with Allylic Halides. *J. Chem. Soc. Chem. Commun.* **1991**, No. 11, 757–758. https://doi.org/10.1039/C39910000757.
(21) Ogawa, A.; Ohya, S.; Sumino, Y.; Sonoda, N.; Hirao, T. Novel Enhancement of the Reducing Ability of Ytterbium Diiodide by Irradiation with Near-UV Light. *Tetrahedron Lett.* **1997**, *38* (52), 9017–9018. https://doi.org/10.1016/S0040-4039(97)10409-9.
(22) Jenks, T. C.; Bailey, M. D.; Hovey, J. L.; Fernando, S.; Basnayake, G.; Cross, M. E.; Li, W.; Allen, M. J. First Use of a Divalent Lanthanide for Visible-Light-Promoted Photoredox Catalysis. *Chem. Sci.* **2018**, *9* (5), 1273–1278. https://doi.org/10.1039/c7sc02479g.
(23) Ma, J.; Schäfers, F.; Daniliuc, C.; Bergander, K.; Strassert, C. A.; Glorius, F. Gadolinium Photocatalysis: Dearomative [2+2] Cycloaddition/Ring-Expansion Sequence with Indoles. *Angewandte Chemie - International Edition* **2020**, *59* (24), 9639–9645. https://doi.org/10.1002/anie.202001200.
(24) Nensala, N.; Nyokong, T. Photosensitization Reactions of Neodymium, Dysprosium and Lutetium Diphthalocyanine. *Polyhedron* **1997**, *16* (17), 2971–2978. https://doi.org/10.1016/s0277-5387(97)00045-4.
(25) Ke, X. S.; Ning, Y.; Tang, J.; Hu, J. Y.; Yin, H. Y.; Wang, G. X.; Yang, Z. S.; Jie, J.; Liu, K.; Meng, Z. S.; Zhang, Z.; Su, H.; Shu, C.; Zhang, J. L. Gadolinium(III) Porpholactones as Efficient and Robust Singlet Oxygen Photosensitizers. *Chem. Eur. J.* **2016**, *22* (28), 9676–9686. https://doi.org/10.1002/chem.201601517.
(26) Zhang, T.; Lan, R.; Chan, C. F.; Law, G. L.; Wong, W. K.; Wong, K. L. In Vivo Selective Cancer-Tracking Gadolinium Eradicator as New-Generation Photodynamic Therapy Agent. *Proceedings of the National Academy of Sciences of the United States of America* **2014**, *111* (51), E5492–E5497. https://doi.org/10.1073/pnas.1414499111.
(27) Lammer, A. D.; Thiabaud, G.; Brewster, J. T.; Alaniz, J.; Bender, J. A.; Sessler, J. L. Lanthanide Texaphyrins as Photocatalysts. *Inorganic Chemistry* **2018**, *57* (6), 3458–3464. https://doi.org/10.1021/acs.inorgchem.8b00248.
(28) Qiao, Y.; Yin, H.; Moreau, L. M.; Feng, R.; Higgins, R. F.; Manor, B. C.; Carroll, P. J.; Booth, C. H.; Autschbach, J.; Schelter, E. J. Cerium(IV) Complexes with Guanidinate Ligands: Intense Colors and Anomalous Electronic Structures. *Chem. Sci.* **2021**, *12* (10), 3558–3567. https://doi.org/10.1039/D0SC05193D.
(29) Rausch, M. D.; Moriarty, K. J.; Atwood, J. L.; Weeks, J. A.; Hunter, W. E.; Brittain, H. G. Synthetic, X-Ray Structural, and Photolumlnescence Studies on Pentamethylcyclopentadienyl Derivatives of Lanthanum, Cerium, and Praseodymium. *Organometallics* **1986**, *5* (6), 1281–1283. https://doi.org/10.1021/om00137a048.
(30) Hazin, P. N.; Bruno, J. W.; Brittain, H. G. Luminescence Spectra of a Series of Cerium(III) Halides and Organometallics: Probes of Bonding Properties Using 4f-5d Excited States. *Organometallics* **1987**, *6* (5), 913–918. https://doi.org/10.1021/om00148a002.

(31) Yin, H.; Carroll, P. J.; Anna, J. M.; Schelter, E. J. Luminescent Ce(III) Complexes as Stoichiometric and Catalytic Photoreductants for Halogen Atom Abstraction Reactions. *J. Am. Chem. Soc.* **2015**, *137* (29), 9234–9237. https://doi.org/10.1021/jacs.5b05411.
(32) Qiao, Y.; Schelter, E. J. Lanthanide Photocatalysis. *Acc. Chem. Res.* **2018**, *51* (11), 2926–2936. https://doi.org/10.1021/acs.accounts.8b00336.
(33) Yin, H.; Carroll, P. J.; Manor, B. C.; Anna, J. M.; Schelter, E. J. Cerium Photosensitizers: Structure-Function Relationships and Applications in Photocatalytic Aryl Coupling Reactions. *Journal of the American Chemical Society* **2016**, *138* (18), 5984–5993. https://doi.org/10.1021/jacs.6b02248.
(34) Lee, Y.-M.; Nam, W.; Fukuzumi, S. Redox Catalysis *via* Photoinduced Electron Transfer. *Chem. Sci.* **2023**, *14* (16), 4205–4218. https://doi.org/10.1039/D2SC07101K.
(35) Yin, H.; Jin, Y.; Hertzog, J. E.; Mullane, K. C.; Carroll, P. J.; Manor, B. C.; Anna, J. M.; Schelter, E. J. The Hexachlorocerate(III) Anion: A Potent, Benchtop Stable, and Readily Available Ultraviolet A Photosensitizer for Aryl Chlorides. *J. Am. Chem. Soc.* **2016**, *138* (50), 16266–16273. https://doi.org/10.1021/jacs.6b05712.
(36) Gray, S. J.; Brown, K.; Lam, F. Y. T.; Garden, J. A.; Arnold, P. L. Dinuclear Ce(IV) Aryloxides: Highly Active Catalysts for Anhydride/Epoxide Ring-Opening Copolymerization. *Organometallics* **2021**, *40* (7), 948–958. https://doi.org/10.1021/acs.organomet.1c00055.
(37) Sinclair, F.; Hlina, J. A.; Wells, J. A. L.; Shaver, M. P.; Arnold, P. L. Ring Opening Polymerisation of Lactide with Uranium(IV) and Cerium(IV) Phosphinoaryloxide Complexes. *Dalton Transactions* **2017**, *46* (33), 10786–10790. https://doi.org/10.1039/c7dt02167d.
(38) Pyykko, P. Relativistic Effects in Structural Chemistry. *Chem. Rev.* **1988**, *88* (3), 563–594. https://doi.org/10.1021/cr00085a006.
(39) Shannon, R. D. Revised Effective Ionic Radii and Systematic Studies of Interatomic Distances in Halides and Chalcogenides. *Acta Crystallographica Section A* **1976**, *32* (5), 751–767. https://doi.org/10.1107/S0567739476001551.
(40) Pace, K. A.; Klepov, V. V.; Berseneva, A. A.; Loye, H. Covalency in Actinide Compounds. *Chem. Eur. J.* **2021**, *27* (19), 5835–5841. https://doi.org/10.1002/chem.202004632.
(41) Vitova, T.; Roesky, P. W.; Dehnen, S. Open Questions on Bonding Involving Lanthanide Atoms. *Commun Chem* **2022**, *5* (1), 12. https://doi.org/10.1038/s42004-022-00630-6.
(42) Girard, P.; Namy, J. L.; Kagan, H. B. Divalent Lanthanide Derivatives in Organic Synthesis. 1. Mild Preparation of Samarium Iodide and Ytterbium Iodide and Their Use as Reducing or Coupling Agents. *J. Am. Chem. Soc.* **1980**, *102* (8), 2693–2698. https://doi.org/10.1021/ja00528a029.
(43) Arnold, P. L.; Love, J. B.; Patel, D. Pentavalent Uranyl Complexes. *Coordination Chemistry Reviews* **2009**, *253* (15–16), 1973–1978. https://doi.org/10.1016/j.ccr.2009.03.014.
(44) Norambuena, V. F. Q.; Heeres, A.; Heeres, H. J.; Meetsma, A.; Teuben, J. H.; Hessen, B. Synthesis, Structure, and Reactivity of Rare-Earth Metallocene H3-Propargyl/Allenyl Complexes. *Organometallics* **2008**, *27* (21), 5672–5683. https://doi.org/10.1021/om800547n.
(45) Werkema, E. L.; Castro, L.; Maron, L.; Eisenstein, O.; Andersen, R. A. Cleaving Bonds in CH3OSO2CF3 with [1,2,4-(Me3C)3C5H2]2CeH; An Experimental and Computational Study. *New J. Chem.* **2013**, *37* (1), 132–142. https://doi.org/10.1039/c2nj40624a.
(46) Werkema, E. L.; Andersen, R. A.; Maron, L.; Eisenstein, O. The Reaction of Bis(1,2,4-Tri-t-Butylcyclopentadienyl)Ceriumbenzyl, Cp′2CeCH2Ph, with Methylhalides: A Metathesis Reaction That Does Not Proceed by a Metathesis Transition State. *Dalton Transactions* **2010**, *39* (29), 6648–6660. https://doi.org/10.1039/b918103b.
(47) Maron, L.; Werkema, E. L.; Perrin, L.; Eisenstein, O.; Andersen, R. A. Hydrogen for Fluorine Exchange in C6F6 and C 6F5H by Monomeric [1,3,4-(Me3C) 3C5H2]2CeH:

Experimental and Computational Studies. *Journal of the American Chemical Society* **2005**, *127* (1), 279–292. https://doi.org/10.1021/ja0451012.
(48) Knight, D. W.; Russell, G. A. Phenyliodine(III) Dichloride. In *Encyclopedia of Reagents for Organic Synthesis*; John Wiley & Sons, Ltd, Ed.; John Wiley & Sons, Ltd: Chichester, UK, 2001; p rp071. https://doi.org/10.1002/047084289X.rp071.
(49) Pinter, P.; Schüßlbauer, C. M.; Watt, F. A.; Dickmann, N.; Herbst-Irmer, R.; Morgenstern, B.; Grünwald, A.; Ullrich, T.; Zimmer, M.; Hohloch, S.; Guldi, D. M.; Munz, D. Bright Luminescent Lithium and Magnesium Carbene Complexes. *Chem. Sci.* **2021**, *12* (21), 7401–7410. https://doi.org/10.1039/d1sc00846c.
(50) Lobkovsky, E. B.; Gun'ko, Yu. K.; Bulychev, B. M.; Belsky, V. K.; Soloveichik, G. L.; Antipin, M. Yu. Crystal and Molecular Structures of Bis(1,3-Di-Tert-Butylcyclopentadienyl)Cerium Chloride and Borohydride. First Example of the Bridging Tetradentate BH4-Group with Two M3-Hydrogens: M : H4-[(M3-H)2B(M2-H)2]. *Journal of Organometallic Chemistry* **1991**, *406* (3), 343–352. https://doi.org/10.1016/0022-328X(91)83122-K.
(51) Groom, C. R.; Bruno, I. J.; Lightfoot, M. P.; Ward, S. C. The Cambridge Structural Database. *Acta Crystallogr B Struct Sci Cryst Eng Mater* **2016**, *72* (2), 171–179. https://doi.org/10.1107/S2052520616003954.
(52) Liu, J.; Reta, D.; Cleghorn, J. A.; Yeoh, Y. X.; Ortu, F.; Goodwin, C. A. P.; Chilton, N. F.; Mills, D. P. Light Lanthanide Metallocenium Cations Exhibiting Weak Equatorial Anion Interactions. *Chem. Eur. J.* **2019**, *25* (32), 7749–7758. https://doi.org/10.1002/chem.201901167.
(53) Evans, W. J.; Olofson, J. M.; Zhang, H.; Atwood, J. L. Synthesis and X-Ray Crystal Structure of an Unusual Oligomeric Bis(Pentamethylcyclopentadienyl) Halide Complex of Cerium: [(C5Me5)2CeCl2K(THF)]n. *Organometallics* **1988**, *7* (3), 629–633. https://doi.org/10.1021/om00093a009.
(54) Gun'ko, Y. K.; Hitchcock, P. B.; Lappert, M. F. Activation of a C□O Bond by Reaction of a Tris(Cyclopentadienyl)Lanthanide Complex with an Alkali Metal in Dimethoxyethane (DME); Crystal Structures of [Ndη-C5H3(SiMe3)2-1,32(μ-OMe)2Li(DME)] and [{Ce(η-C5H3tBu2-1,3)2(μ-OMe)2]. *Journal of Organometallic Chemistry* **1995**, *499* (1–2), 213–219. https://doi.org/10.1016/0022-328X(95)00330-S.
(55) Werkema, E. L.; Yahia, A.; Maron, L.; Eisenstein, O.; Andersen, R. A. Bridging Silyl Groups in σ-Bond Metathesis and [1,2]-Shifts. Experimental and Computational Study of the Reaction between Cerium Metallocenes and MeOSiMe $_3$. *Organometallics* **2010**, *29* (21), 5103–5110. https://doi.org/10.1021/om1003286.
(56) Wedal, J. C.; Ziller, J. W.; Furche, F.; Evans, W. J. Synthesis and Reduction of Heteroleptic Bis(Cyclopentadienyl) Uranium(III) Complexes. *Inorg. Chem.* **2022**, *61* (19), 7365–7376. https://doi.org/10.1021/acs.inorgchem.2c00322.
(57) Palumbo, C. T.; Darago, L. E.; Windorff, C. J.; Ziller, J. W.; Evans, W. J. Trimethylsilyl versus Bis(Trimethylsilyl) Substitution in Tris(Cyclopentadienyl) Complexes of La, Ce, and Pr: Comparison of Structure, Magnetic Properties, and Reactivity. *Organometallics* **2018**, *37* (6), 900–905. https://doi.org/10.1021/acs.organomet.7b00881.
(58) Maynadié, J.; Berthet, J.-C.; Thuéry, P.; Ephritikhine, M. Cyanide Metallocenes of Trivalent F-Elements. *Organometallics* **2007**, *26* (10), 2623–2629. https://doi.org/10.1021/om061131x.
(59) Berthet, J.-C.; Onno, J.-M.; Gupta, F.; Rivière, C.; Thuéry, P.; Nierlich, M.; Madic, C.; Ephritikhine, M. Coordination of 1,10-Phenanthroline, 3,4,7,8-Tetramethyl-1,10-Phenanthroline and 2,4,6-Tris(2-Pyridyl)-1,3,5-Triazine to MX3 (M=Ce, U; X=I, OSO2CF3) in Pyridine and Acetonitrile. *Polyhedron* **2012**, *45* (1), 107–125. https://doi.org/10.1016/j.poly.2012.07.040.

(60) Wooles, A. J.; Mills, D. P.; Lewis, W.; Blake, A. J.; Liddle, S. T. Lanthanide Tri-Benzyl Complexes: Structural Variations and Useful Precursors to Phosphorus-Stabilised Lanthanide Carbenes. *Dalton Trans.* **2010**, *39* (2), 500–510. https://doi.org/10.1039/B911717B.
(61) Wayda, A. L.; Evans, W. J. Synthesis and Thermal Decomposition of Homoleptic Tert-Butyl Lanthanide Complexes. *J. Am. Chem. Soc.* **1978**, *100* (22), 7119–7121. https://doi.org/10.1021/ja00490a081.
(62) Li, J.; Huang, C.-Y.; Li, C.-J. Two-in-One Metallaphotoredox Cross-Couplings Enabled by a Photoactive Ligand. *Chem* **2022**, S2451929422002650. https://doi.org/10.1016/j.chempr.2022.05.011.
(63) Yamashita, H.; Ikezawa, T.; Kobayashi, Y.; Abe, J. Photochromic Phenoxyl-Imidazolyl Radical Complexes with Decoloration Rates from Tens of Nanoseconds to Seconds. *Journal of the American Chemical Society* **2015**, *137* (15), 4952–4955. https://doi.org/10.1021/jacs.5b02353.
(64) Shirase, S.; Shinohara, K.; Tsurugi, H.; Mashima, K. Oxidation of Alcohols to Carbonyl Compounds Catalyzed by Oxo-Bridged Dinuclear Cerium Complexes with Pentadentate Schiff-Base Ligands under a Dioxygen Atmosphere. *ACS Catal.* **2018**, *8* (8), 6939–6947. https://doi.org/10.1021/acscatal.8b01718.
(65) Ringenberg, M. R.; Kokatam, S. L.; Heiden, Z. M.; Rauchfuss, T. B. Redox-Switched Oxidation of Dihydrogen Using a Non-Innocent Ligand. *Journal of the American Chemical Society* **2008**, *130* (3), 788–789. https://doi.org/10.1021/ja076801k.
(66) Benisvy, L.; Blake, A. J.; Collison, D.; Davies, E. S.; Garner, C. D.; McInnes, E. J. L.; McMaster, J.; Whittaker, G.; Wilson, C. A Phenol-Imidazole pro-Ligand That Can Exist as a Phenoxyl Radical, Alone and When Complexed to Copper(II) and Zinc(II). *Dalton Transactions* **2003**, No. 10, 1975–1985. https://doi.org/10.1039/b212209j.
(67) Chapman, A. M.; Haddow, M. F.; Wass, D. F. Frustrated Lewis Pairs beyond the Main Group: Synthesis, Reactivity, and Small Molecule Activation with Cationic Zirconocene–Phosphinoaryloxide Complexes. *J. Am. Chem. Soc.* **2011**, *133* (45), 18463–18478. https://doi.org/10.1021/ja207936p.
(68) Zhang, M.; Ni, X.; Shen, Z. Synthesis of Bimetallic Bis(Phenolate) N-Heterocyclic Carbene Lanthanide Complexes and Their Applications in the Ring-Opening Polymerization of L -Lactide. *Organometallics* **2014**, *33* (23), 6861–6867. https://doi.org/10.1021/om500930m.
(69) Yi, C.; Wu, L.; Chen, L.; Ren, W. Reactivity Studies on Lanthanum and Cerium Hydrido Metallocenes. *Dalton Trans.* **2022**, *51* (24), 9241–9246. https://doi.org/10.1039/D2DT00996J.
(70) Qian, C.; Zou, G.; Sun, J. Chiral Lanthanocene Complexes with an Ether-Functionalized Indene Ligand: Synthesis and Structure of Bis{1-(2-Methoxyethyl)Indenyl}lanthanocene Chlorides. *Journal of Organometallic Chemistry* **1998**, *566* (1–2), 21–28. https://doi.org/10.1016/S0022-328X(98)00635-4.
(71) Deacon, G. B.; Nickel, S.; Tiekink, E. R. T. The Preparation and Crystal Structure of Bis(Cyclopentadienyl)(2,6-Diphenylphenoxo)Bis(Tetrahydrofuran)Neodymium(III); an Unexpected Example of Formal Nine Coordination. *Journal of Organometallic Chemistry* **1991**, *409* (1–2), C1–C4. https://doi.org/10.1016/0022-328X(91)86156-K.
(72) Rabe, G. W.; Riederer, F. A.; Zhang-Presse, M.; Rheingold, A. L. Flexible Coordination Mode of a Donor-Functionalized Terphenyl Ligand in Monomeric Cp-Based Lanthanocenes. *Organometallics* **2009**, *28* (17), 5277–5280. https://doi.org/10.1021/om900465c.
(73) Qian, C.; Zou, G.; Jiang, W.; Chen, Y.; Sun, J.; Li, N. Selective Synthesis, Structure, and Catalytic Behavior of *m Eso* -Divalent 1,1‘-(3-Oxapentamethylene)-Bridged

Bis(Indenyl)Lanthanidocenes. *Organometallics* **2004**, *23* (21), 4980–4986. https://doi.org/10.1021/om049753a.
(74) Evans, W. J.; Miller, K. A.; Ziller, J. W. Synthesis of ($O_2CEPh)^{1-}$ Ligands (E = S, Se) by CO_2 Insertion into Lanthanide Chalcogen Bonds and Their Utility in Forming Crystallographically Characterizable Organoaluminum Complexes $[Me_2Al(\mu\text{-}O_2CEPh)]_2$. *Inorg. Chem.* **2006**, *45* (1), 424–429. https://doi.org/10.1021/ic0515610.
(75) Turner, Z. R.; Bellabarba, R.; Tooze, R. P.; Arnold, P. L. Addition-Elimination Reactions across the M-C Bond of Metal N-Heterocyclic Carbenes. *Journal of the American Chemical Society* **2010**, *132* (12), 4050–4051. https://doi.org/10.1021/ja910673q.
(76) Arnold, P. L.; Turner, Z. R.; Kaltsoyannis, N.; Pelekanaki, P.; Bellabarba, R. M.; Tooze, R. P. Covalency in CeIV and UIV Halide and N-Heterocyclic Carbene Bonds. *Chem. Eur. J.* **2010**, *16* (31), 9623–9629. https://doi.org/10.1002/chem.201001471.
(77) Arnold, P. L.; Turner, Z. R.; Germeroth, A. I.; Casely, I. J.; Bellabarba, R.; Tooze, R. P. Lanthanide/Actinide Differentiation with Sterically Encumbered N-Heterocyclic Carbene Ligands. *Dalton Trans.* **2010**, *39* (29), 6808. https://doi.org/10.1039/c001584a.
(78) Hazin, P. N.; Lakshminarayan, C.; Brinen, L. S.; Knee, J. L.; Bruno, J. W.; Streib, W. E.; Folting, K. Luminescence Spectra and Lifetimes of Cerium(III) Compounds as Indicators of Solution Behavior and Radiative Efficiency. *Inorg. Chem.* **1988**, *27* (8), 1393–1400. https://doi.org/10.1021/ic00281a019.
(79) Pandey, P.; Yang, Q.; Gau, M. R.; Schelter, E. J. Evaluating the Photophysical and Photochemical Characteristics of Green-Emitting Cerium(III) Mono-Cyclooctatetraenide Complexes. *Dalton Trans.* **2023**, *52* (18), 5909–5917. https://doi.org/10.1039/D3DT00351E.
(80) Qiao, Y.; Sergentu, D.-C.; Yin, H.; Zabula, A. V.; Cheisson, T.; McSkimming, A.; Manor, B. C.; Carroll, P. J.; Anna, J. M.; Autschbach, J.; Schelter, E. J. Understanding and Controlling the Emission Brightness and Color of Molecular Cerium Luminophores. *J. Am. Chem. Soc.* **2018**, *140* (13), 4588–4595. https://doi.org/10.1021/jacs.7b13339.
(81) Gao, Z.; Hao, Y.; Zheng, M.; Chen, Y. A Fluorescent Dye with Large Stokes Shift and High Stability: Synthesis and Application to Live Cell Imaging. *RSC Adv.* **2017**, *7* (13), 7604–7609. https://doi.org/10.1039/C6RA27547H.
(82) Fieser, M. E.; Johnson, C. W.; Bates, J. E.; Ziller, J. W.; Furche, F.; Evans, W. J. Dinitrogen Reduction, Sulfur Reduction, and Isoprene Polymerization via Photochemical Activation of Trivalent Bis(Cyclopentadienyl) Rare-Earth-Metal Allyl Complexes. *Organometallics* **2015**, *34* (17), 4387–4393. https://doi.org/10.1021/acs.organomet.5b00613.
(83) Qiao, Y.; Cheisson, T.; Manor, B. C.; Carroll, P. J.; Schelter, E. J. A Strategy to Improve the Performance of Cerium(III) Photocatalysts. *Chem. Commun.* **2019**, *55* (28), 4067–4070. https://doi.org/10.1039/C9CC00282K.
(84) Gaigalas, A. K.; Wang, L. Measurement of the Fluorescence Quantum Yield Using a Spectrometer with an Integrating Sphere Detector. *J. Res. Natl. Inst. Stand. Technol.* **2008**, *113* (1), 17. https://doi.org/10.6028/jres.113.004.
(85) Suta, M.; Harmgarth, N.; Kühling, M.; Liebing, P.; Edelmann, F. T.; Wickleder, C. Bright Photoluminescence of $[\{(CptBu2)_2Ce(\mu\text{-}Cl)\}_2]$: A Valuable Technique for the Determination of the Oxidation State of Cerium. *Chem. Asian J.* **2018**, *13* (8), 1038–1044. https://doi.org/10.1002/asia.201701818.
(86) Harder, S.; Naglav, D.; Ruspic, C.; Wickleder, C.; Adlung, M.; Hermes, W.; Eul, M.; Pöttgen, R.; Rego, D. B.; Poineau, F.; Czerwinski, K. R.; Herber, R. H.; Nowik, I. Physical Properties of Superbulky Lanthanide Metallocenes: Synthesis and Extraordinary Luminescence of $[Eu^{II}(Cp^{BIG})_2]$ (Cp^{BIG} =(4-*n*Bu-$C_6H_4)_5$-Cyclopentadienyl). *Chem. Eur. J.* **2013**, *19* (37), 12272–12280. https://doi.org/10.1002/chem.201302021.

(87) Canestrari, D.; Lancianesi, S.; Badiola, E.; Strinna, C.; Ibrahim, H.; Adamo, M. F. A. Desulfurative Chlorination of Alkyl Phenyl Sulfides. *Org. Lett.* **2017**, *19* (4), 918–921. https://doi.org/10.1021/acs.orglett.7b00077.
(88) Sandoval, J. J.; Palma, P.; Álvarez, E.; Cámpora, J.; Rodríguez-Delgado, A. Mechanism of Alkyl Migration in Diorganomagnesium 2,6-Bis(Imino)Pyridine Complexes: Formation of Grignard-Type Complexes with Square-Planar Mg(II) Centers. *Organometallics* **2016**, *35* (18), 3197–3204. https://doi.org/10.1021/acs.organomet.6b00528.
(89) Kong, Y.; Ren, H.; Xu, S.; Song, H.; Liu, B.; Wang, B. Synthesis, Structures, and Norbornene Polymerization Behavior of Bis(Aryloxide-N-Heterocyclic Carbene) Palladium Complexes. *Organometallics* **2009**, *28* (20), 5934–5940. https://doi.org/10.1021/om900625r.
(90) Evans, W. J.; Kozimor, S. A.; Ziller, J. W.; Fagin, A. A.; Bochkarev, M. N. Facile Syntheses of Unsolvated UI $_3$ and Tetramethylcyclopentadienyl Uranium Halides. *Inorg. Chem.* **2005**, *44* (11), 3993–4000. https://doi.org/10.1021/ic0482685.
(91) Gompa, T. P.; Rice, N. T.; Russo, D. R.; Aguirre Quintana, L. M.; Yik, B. J.; Bacsa, J.; La Pierre, H. S. Diethyl Ether Adducts of Trivalent Lanthanide Iodides. *Dalton Trans.* **2019**, *48* (23), 8030–8033. https://doi.org/10.1039/C9DT00775J.
(92) Windorff, C. J.; Dumas, M. T.; Ziller, J. W.; Gaunt, A. J.; Kozimor, S. A.; Evans, W. J. Small-Scale Metal-Based Syntheses of Lanthanide Iodide, Amide, and Cyclopentadienyl Complexes as Analogues for Transuranic Reactions. *Inorg. Chem.* **2017**, *56* (19), 11981–11989. https://doi.org/10.1021/acs.inorgchem.7b01968.
(93) Scherg, T.; Schneider, S.; Frey, G.; Schwarz, J.; Herdtweck, E.; Herrmann, W. Bridged Imidazolium Salts Used as Precursors for Chelating Carbene Complexes of Palladium in the Mizoroki-Heck Reaction. *Synlett* **2006**, *2006* (18), 2894–2907. https://doi.org/10.1055/s-2006-951539.
(94) Dolomanov, O. V.; Bourhis, L. J.; Gildea, R. J.; Howard, J. A. K.; Puschmann, H. *OLEX2* : A Complete Structure Solution, Refinement and Analysis Program. *J. Appl. Crystallogr.* **2009**, *42* (2), 339–341. https://doi.org/10.1107/S0021889808042726.
(95) Sheldrick, G. M. *SHELXT* – Integrated Space-Group and Crystal-Structure Determination. *Acta Crystallogr. A* **2015**, *71* (1), 3–8. https://doi.org/10.1107/S2053273314026370.
(96) Clark, R. C.; Reid, J. S. The Analytical Calculation of Absorption in Multifaceted Crystals. *Acta Crystallographica Section A* **1995**, *51*, 887–897.
(97) Becke, A. D. Density-functional Thermochemistry. III. The Role of Exact Exchange. *J. Chem. Phys* **1993**, *98* (7), 5648–5652. https://doi.org/10.1063/1.464913.
(98) Perdew, J. P.; Wang, Y. Accurate and Simple Analytic Representation of the Electron-Gas Correlation Energy. *Phys. Rev. B* **1992**, *45* (23), 13244–13249. https://doi.org/10.1103/PhysRevB.45.13244.
(99) Cao, X.; Dolg, M.; Stoll, H. Valence Basis Sets for Relativistic Energy-Consistent Small-Core Actinide Pseudopotentials. *J. Chem. Phys* **2003**, *118* (2), 487–496. https://doi.org/10.1063/1.1521431.
(100) Küchle, W.; Dolg, M.; Stoll, H.; Preuss, H. Energy-adjusted Pseudopotentials for the Actinides. Parameter Sets and Test Calculations for Thorium and Thorium Monoxide. *J. Chem. Phys* **1994**, *100* (10), 7535–7542. https://doi.org/10.1063/1.466847.
(101) Hariharan, P. C.; Pople, J. A. The Influence of Polarization Functions on Molecular Orbital Hydrogenation Energies. *Theoret. Chim. Acta* **1973**, *28* (3), 213–222. https://doi.org/10.1007/BF00533485.
(102) Hehre, W. J.; Ditchfield, R.; Pople, J. A. Self—Consistent Molecular Orbital Methods. XII. Further Extensions of Gaussian—Type Basis Sets for Use in Molecular Orbital Studies of Organic Molecules. *J. Chem. Phys* **1972**, *56* (5), 2257–2261. https://doi.org/10.1063/1.1677527.

(103) M. J. Frisch, G. W. Trucks, H. B. Schlegel, G. E. Scuseria, M. A. Robb, J. R.; Cheeseman, G. Scalmani, V. Barone, B. Mennucci, G. A. Petersson, H. Nakatsuji, M. Caricato, X. Li, H.; P. Hratchian, A. F. Izmaylov, J. Bloino, G. Zheng, J. L. Sonnenberg, M. Hada, M. Ehara, K. Toyota, R.; Fukuda, J. Hasegawa, M. Ishida, T. Nakajima, Y. Honda, O. Kitao, H. Nakai, T. Vreven, J. A.; Montgomery, Jr., J. E. Peralta, F. Ogliaro, M. Bearpark, J. J. Heyd, E. Brothers, K. N. Kudin, V. N.; Staroverov, R. Kobayashi, J. Normand, K. Raghavachari, A. Rendell, J. C. Burant, S. S. Iyengar, J.; Tomasi, M. Cossi, N. Rega, J. M. Millam, M. Klene, J. E. Knox, J. B. Cross, V. Bakken, C. Adamo, J.; Jaramillo, R. Gomperts, R. E. Stratmann, O. Yazyev, A. J. Austin, R. Cammi, C. Pomelli, J. W. Ochterski,; R. L. Martin, K. Morokuma, V. G. Zakrzewski, G. A. Voth, P. Salvador, J. J. Dannenberg, S. Dapprich, A.; D. Daniels, O. Farkas, J. B. Foresman, J. V. Ortiz, J. Cioslowski, D. J. Fox, Gaussian, Inc., Wallingford CT, 2013. Gaussian 09, Revision D.01.

Chapter 2

Controlled Monodefluorination and Alkylation of C(sp^3)–F Bonds by Lanthanide Photocatalysts

2.1 Overview

The complexes previously described in **Chapter 1** are capable of the rare, selective, photocatalytic C–F bond functionalization of sp^3 hybridized C–F bonds, when used in conjunction with magnesium alkyl reagents. The work described in this chapter is, to the best of our knowledge, the first example of photocatalytic C–F bond activation and functionalization mediated by a rare-earth metal complex. This work also provides unique insight into the cooperativity between metal and ligand in photocatalysis, and the significance of ligand redox non-innocence in radical mechanisms.

The author, in collaboration with Dr. Addison N. Desnoyer, carried out the synthesis and experimental investigation of lanthanide photocatalysts at the University of California, Berkeley. Electrochemical studies were carried out by Dr. Laurent Sévery at the University of California, Berkeley. Mechanistic calculations were carried out by Yan Yang under the supervision of Prof. Laurent Maron at the University of Toulouse. The author and Dr. Addison N. Desnoyer guided these studies and interpreted data. Most of this work has been published in: *Chem. Sci.*, 2022, **13**, 14090–14100.

2.2 Introduction

Carbon–halide (C–X) bond activation reactions are of great significance in catalysis as they provide a facile route to the formation of new carbon–carbon bonds and consequently new complex organic molecules.[1] Despite advances, the coupling of C(sp^3) fragments in such reactions is challenging. Over recent decades however, photoredox catalysis has been used extensively as a strategy to activate a C–X bonds in a variety of organic halides.

In 1984, Tanaka and Fukuzumi published the C–Br bond activation of benzyl bromide in the presence of 1-benzyl-1,4-dihydronicotinamide (BNAH) and the now widely used ruthenium photocatalyst, Ru(II)$(bpy)_3^{2+}$(bpy = bipyridine) (Scheme 2.1).[2] Reactions of this type follow a reductive quenching cycle, which involves the excitation of $Ru(bpy)_3^{2+}$ prior to a single electron transfer (SET) with BNAH. This transformation results in the formation of $Ru(I)(bpy)_3^{+}$ which is a powerful reductant, capable of the reduction of benzyl bromide. The resulting benzyl radical is long-lived through conjugation with the aromatic ring,[3] and so homocoupling of the radical can occur and bibenzyl is produced.

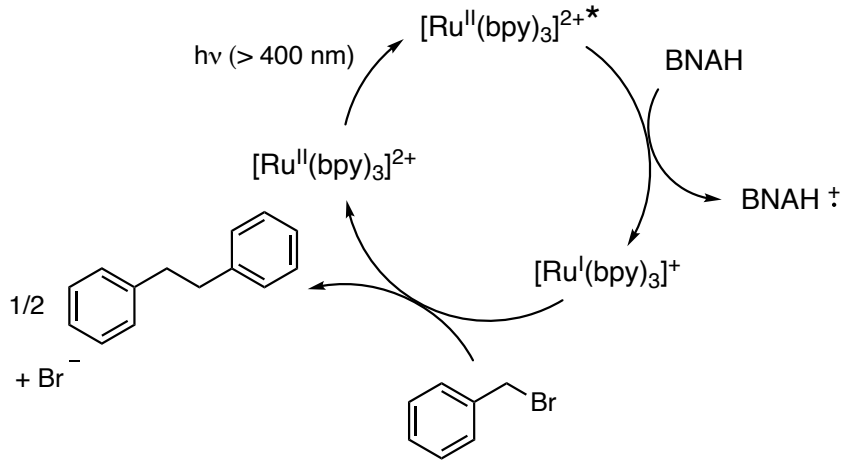

Scheme 2.1. Photochemical C–Br bond activation of benzyl bromide by Ru(II)$(bpy)_3^{2+}$.

Stephenson and co-workers have also researched extensively in this field. In 2012 they published the C–I bond activation of unactivated alkyl, alkenyl and aryl iodides, facilitated by the highly reducing photocatalyst $Ir(ppy)_3$ in the presence of blue light irradiation.[4] It was hypothesized such reactions occur through oxidative quenching between the excited photocatalyst and substrate. The oxidized photocatalyst subsequently generates ground state $Ir(ppy)_3$ (ppy = 2-phenylpyridine) and the reduced product by SET with sacrificial electron donors. However, even with well-explored catalysts such as $Ir(ppy)_3$, there is still much discussion surrounding their mechanism of reactivity.[5] In general, detailed mechanistic studies of photoredox systems are rare due to their complexity.

Until recently, photoredox catalysts have primarily been transition metal complexes or organic dyes.[6,7] Little research into photoredox catalysis using lanthanides has been carried out despite their high earth-abundance and low toxicity.[8–11] As previously described in **Chapter 1**, Schelter and co-workers published the first examples of photocatalysis using cerium, demonstrating the light-driven C–Cl bond activation of benzyl chloride and activated chlorobenzenes, by exploiting the halophilicity of the cerium cation in an inner sphere mechanism. However, the activation of stronger C–X bonds was not attempted with this system.

Fluorine forms the strongest single bond to carbon and the C–F bond is *ca.* 25 $kcalmol^{-1}$ stronger than the C–Cl bond in monohaloalkanes, and the C–H bond in alkanes.[12] The selective activation and functionalization of C–F bonds is important, both due to the high bioaccumulation and toxicity of many perfluorinated compounds, and the promise shown by fluorinated pharmaceuticals.[9] In fact, it has been estimated that 20% of new drugs contain one or multiple C–F bonds in their structure.[13] In contrast to stoichiometric $C(sp^2)$–F bond activation, which has been well-documented with *d*-block and a small number of *f*-block complexes, examples of even stoichiometric $C(sp^3)$–F bond activations are much rarer.[14–16]

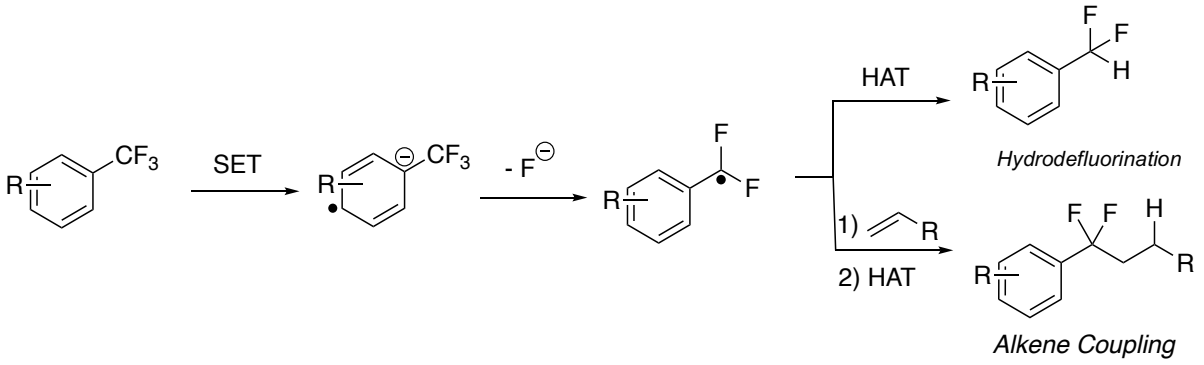

Scheme 2.2. Hydrodefluorination and defluoroalkylation of trifluoromethylarenes published by Jui et al.

Aryldifluoromethyl species of the form $ArCF_2R$ (R = alkyl, aryl) in particular are important building blocks in many bioactive compounds.[17] The straightforward synthesis of $ArCF_2R$ derivatives from easily available trifluoromethylarenes ($ArCF_3$) via selective single $C(sp^3)$–F bond cleavage is therefore desirable as it allows for structural diversification by a range of coupling partners while benzylic fluorination is retained. As no preactivation of the starting material is needed and byproducts, i.e. F^-, are minimal, this transformation is highly atom- and step-economical, albeit synthetically difficult. The aliphatic C–F bond strength decreases as the degree of fluorination at the carbon decreases and the C–F bond length lengthens,

decreasing steric crowding. As a result, typical hydrodefluorination protocols for trifluoromethylarenes result in complete defluorination of all three C–F bonds.[18]

Recent efforts from several groups have focused on addressing this synthetic challenge using both photochemical[19,20] and non-photochemical methods.[21–23] Radical methodologies are attractive here because they allow access to partially defluorinated products which are otherwise challenging to prepare. For instance, in 2017 Jui and co-workers have demonstrated that the organic photosenstizer *N*-phenylphenothiazine (PTH), first introduced by Read de Alaniz and Hawker,[24] can facilitate the selective single C(sp^3)–F bond activation of trifluoromethylarenes including 1,3-bistrifluoromethylbenzene.

Following irradiation with light, SET from the highly reducing excited state of PTH to 1,3-bistrifluoromethylbenzene produced the corresponding radical anion alongside the oxidized ground state species PTH^+. It was then hypothesized that the radical anion could undergo mesolytic clevage, producing fluoride and a putative electrophilic $ArCF_2$ radical capable of being quenched directly via hydrogen atom transfer (HAT) or participating in intermolecular radical addition with alkene acceptor molecules (Scheme 2.2). The nucleophilic radical arising from this reaction could then be quenched via HAT with cyclohexanethiol, producing the defluoroalkylated product and the corresponding thiyl species. Both catalysts could be regenerated by reaction with sodium formate, producing carbon dioxide and sodium fluoride as by-products.

However, this system was unable to defluoroalkyate unactivated trifluoromethylarenes, and only substrates bearing stronger electron-withdrawing substituents, such as additional trifluoromethyl or alkyl groups, were shown to undergo alkene coupling and further reduction to give the corresponding alkylaromatics. Subsequent work using a range of commonly used photocatalysts however allowed for the defluoroalkylation of unactivated trifluoromethylarenes, though heating to 100 °C was required alongside irradiation for optimum reactivity.[25,26] The most effective catalyst in this case, 3,7-di([1,1'-biphenyl]-4-yl)-10-(naphthalen-1-yl)-10H-phenoxazine**,** originally developed by Miyake for organic atom-transfer radical polymerization[27] was reported to be highly absorbent in the visible wavelength range with high intersystem crossing (ISC) efficiency to a long-lived, triplet, highly reducing excited state. Notably, for the organic SET catalysts used in this system, reaction progress was shown to be more highly dependent on the excited state lifetime of the catalyst rather than its reduction potential.

In 2021, Zhang and co-workers reported the first example of selective carbofunctionalization of the C(sp^3)–F bond in the CF_3 moiety of trifluoromethylarenes through a transition-metal-catalyzed cross-coupling.[20] An excited-state palladium complex was shown to facilitate the C(sp^3)–F bond oxidative addition via a SET pathway to generate a α,α-difluororobenzylic palladium complex. Transmetallation of the resulting of $ArCF_2Pd(L_n)$–F species with arylboronic acids through formation of a strong B–F bond and subsequent reductive elimination yielded the desired cross-coupled product under mild reaction conditions (Scheme 2.3).

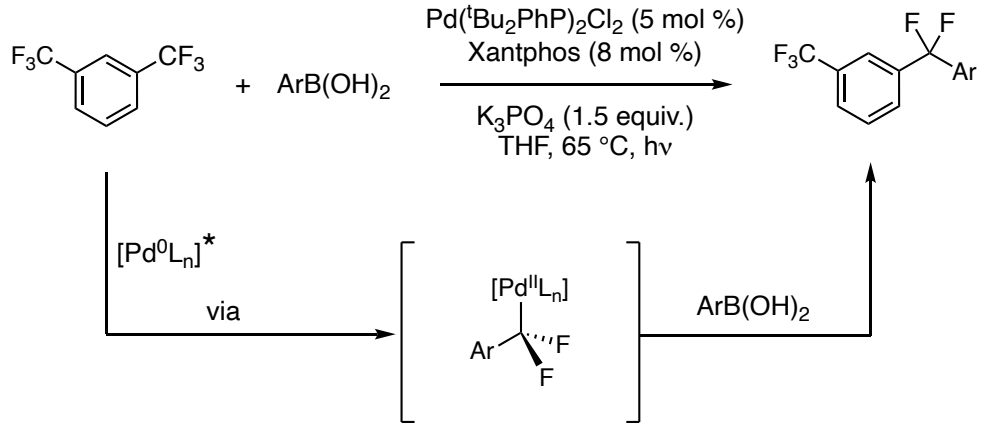

Scheme 2.3. Visible-light-induced palladium-catalyzed selective defluoroarylation of trifluoromethylarenes with arylboronic acids as reported by Zhang et al. (Xantphos = (9,9-Dimethyl-9H-xanthene-4,5-diyl)bis(diphenylphosphane)).

In related work, König has shown the functionalization of electron-poor trifluoromethylarenes using photochemical methods, with *fac*-Ir(ppy)$_3$ as the photocatalyst and *N*-methyl-*N*-phenylmethacrylamide as the trapping reagent and proton source.[28] By irradiating this system under blue light, the selective single C(sp^3)–F bond cleavage of 4-trifluoromethylbenzonitrile in 1,2-dichloroethane was observed. The authors hypothesised that ArCF$_3$ is converted into the corresponding radical anion via photocatalytic SET reduction, and subsequently releases F$^-$ to form the aryldifluoromethyl radical (ArCF$_2$·). The use of a Lewis acidic fluoride scavenger is thought to accelerate radical generation and suppress electron transfer,[29,30] while the aryldifluoromethyl radical is captured by the trapping reagent to give the desired ArCF$_2$R product. Very recently, Nishimoto and Yasuda have described related C–F coupling protocols of perfluoroalkylarenes using tin reagents and Ir(ppy)$_3$.[31] Allyltributylstannane was shown to be necessary for efficent defluoroalkylation. as the authors reported that neither the Jui or König systems previously described were able to facilitate the C(sp^3)–F bond activation of 4-(1,1,4,4,4,4,4,4,4-nonafluoro-4λ^8-but-2-yn-1-yl)benzonitrile.

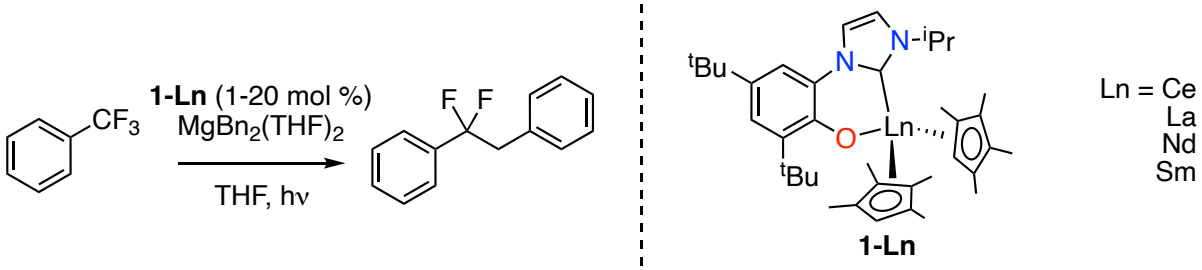

Figure 2.1. Photocatalytic defluoroalkylation of trifluorotoluene by lanthanide organometallic complexes.

We have developed a range of applications of organometallic lanthanide complexes in sustainable catalysis,[10,11,32,33] and considered that organometallic cerium complexes with light absorption capability and sufficient space to form an inner sphere adduct (**Chapter 1**) could achieve the rare and difficult, selective catalytic conversion of sp^3 C–F bonds. In this chapter it is shown how selective, catalytic C–F bond functionalization can be achieved using a new family of Ln(III) compounds supported by a light-absorbing aryloxide-tethered N-heterocyclic carbene, tetramethylcyclopentadienyl (Cp^{Me4}), and pseudohalide ligands. We show that visible

light-irradiated cerium complexes can selectively abstract a single fluoride from trifluorotoluene ($PhCF_3$) and catalyze its alkylation by MgR_2 to afford $PhCF_2R$ (Figure 2.1). The $PhCF_2$ radical can also be quenched to selectively form difluorotoluene ($PhCF_2H$) or further alkylated via coupling with an alkene or other metal alkyls. Combined experiment and theory show the importance of coordination of the fluorinated substrate to the Lewis acidic metal in C–F activation, and the utility of the ligand in enabling photoredox catalysis for other lanthanide congeners.

2.3 Results and discussion

2.3.1 Stoichiometric C–F Activation of $PhCF_3$ to afford $PhCF_2H$

2.3.1.1 General procedures and reactivity of cerium complexes

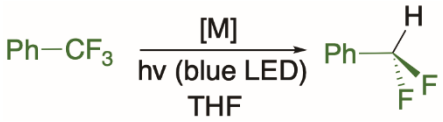

Scheme 2.4. General reaction scheme for C–F activation and hydrodefluorination of trifluorotoluene.

Stoichiometric reactions of $PhCF_3$ with the lanthanide organometallics described previously, denoted [M] in Scheme 2.4, were conducted to assess capability in photoinduced C–F bond cleavage. The reaction is expected to proceed by homolytic C–F bond scission, with the $PhCF_2$ radical subsequently abstracting a H atom from the solvent THF, a good H atom donor (Scheme 2.5.

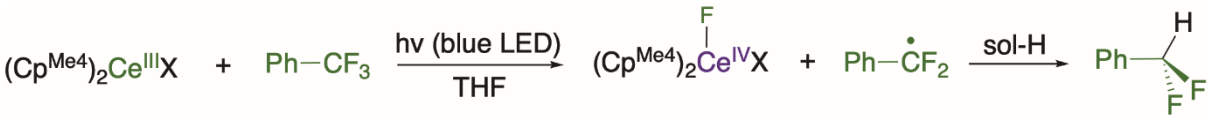

Scheme 2.5. General reaction scheme for C–F activation and hydrodefluorination the Ce photocatalysts **1-Ce**–**6-Ce** with $PhCF_3$ (X = the monoanionic ligand Cp^{Me4}, Cl, OAr, OTf, Bn)

In preliminary experiments, complexes **1-Ce**–**6-Ce** were separately dissolved in THF, $PhCF_3$ added (1.00 equiv.). The samples were then irradiated with a 40 W Kessil A160WE Tuna Blue lamp (Figure 2.2) in Young's tap-valved NMR tubes for 48 hours. Little conversion was seen in these reactions, hypothesized to be due to binding competition between $PhCF_3$ and THF solvent. Therefore, optimized reactions with five equivalents of $PhCF_3$ in THF solution were irradiated under identical conditions. Reaction progress was monitored by ^{19}F NMR spectroscopy. Prior to irradiation, the solution of **1-Ce** and $PhCF_3$ produced a ^{19}F resonance 0.09 ppm relative to a $PhCF_3$ capillary (Figure 2.3) indicating a difference in fluorine environment created by solution interactions. This should provide an additional Lewis acid activation that should facilitate the cleavage of the C–F bond in the excited state complex.[34]

All Ce complexes **1-Ce**–**6-Ce** are capable of the conversion of $PhCF_3$ to $PhCF_2H$ to varying degrees, with irradiation required for any reactivity. The sole fluorinated product of this reaction, $PhCF_2H$, can be observed and quantified by ^{19}F NMR spectroscopy, as a doublet

arising from the CF_2 group coupling to a single proton at -111.5 ppm. The proton source is the THF solvent, *vide infra*.

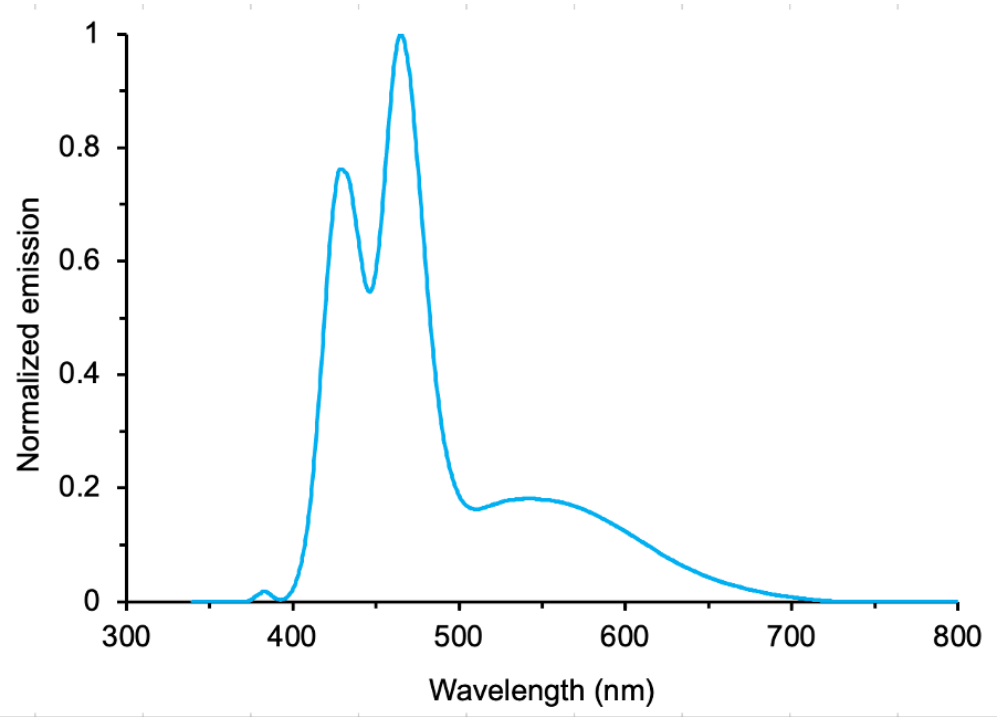

Figure 2.2. Emission spectrum of a 40 W Kessil A160WE Tuna Blue lamp.

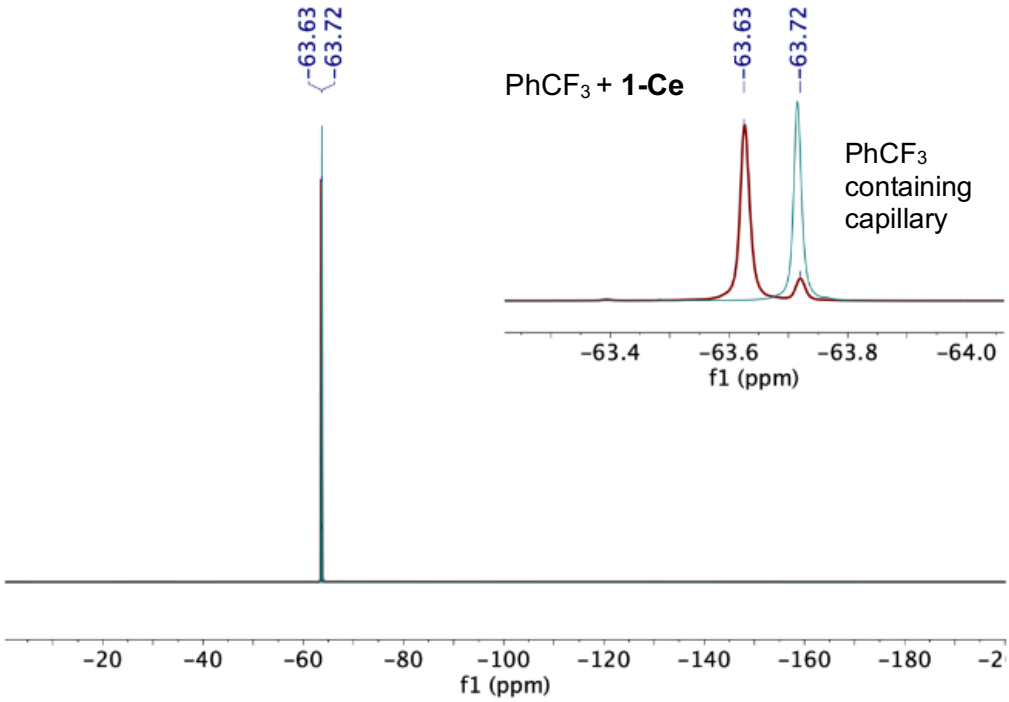

Figure 2.3. ^{19}F NMR spectrum of a 325 μM solution of $PhCF_3$ in THF-H_8 in a Young-tapped NMR tube with a capillary containing the same 325 μM solution of $PhCF_3$ in THF-H_8 before (green trace) and after (red trace) the addition of 0.01 mmol **1-Ce**. A shift is seen between $PhCF_3$ inside and outside the capillary which could be attributed to an interaction between $PhCF_3$ and **1-Ce**.

Complex **1-Ce** formed the product $PhCF_2H$ in approximately 75% yield under optimized conditions of 120 hours of irradiation at room temperature with five equivalents of $PhCF_3$. The $(Cp^{Me4})_3Ce$ complex **2-Ce** produces $PhCF_2H$ in just 5% yield under the same conditions, underlining the utility of the aryloxy ligand in creating a useful excited state. Complex **4a-Ce** is less effective than **1-Ce** at carrying out this transformation, yielding approximately 25% yield of $PhCF_2H$, despite also having an aryloxide ligand capable of absorbing light. This could be attributed to the shorter excited state lifetime of this complex relative to **1-Ce**, and improved light absorbance by **L** due to rigidity imparted by the chelating NHC.[35] Rigid ligand scaffolds have been shown to disfavor nonradiative deactivation pathways of light emitting organometallic complexes (see **Chapter 1**).[36]

Though limited, investigation in the substrate scope of defluorination mediated by **1-Ce** was also carried out. Five equivalents of the fluorinated substrates hexafluorobenzene, 1,3-bis(trifluoromethyl)benzene and (trifluoromethoxy)benzene were irradiated with **1-Ce** for 20 hours but yielded only trace dehydrofluorinated product in all cases. Irradiation of five equivalents of pentafluoro(trifluoromethyl)benzene with **1-Ce** for two days resulted in the generation of a red-brown solution and the complete consumption of **1-Ce**, alongside the formation of at least one new, paramagnetic Ce-containing product. ^{19}F NMR spectroscopy showed several products arising from C–F activation of the aryl C–F bonds, with no activation of the CF_3 moiety. Two of the new products were identified as 2,3,5,6-tetrafluorobenzotrifluoride and the perfluorinated biphenyl product, both of which are likely derived from the radical formed from activation of the para-fluoride of the pentafluoro(trifluoromethyl)benzene starting material. While product yields could not be accurately determined due to the generation of other fluorine-containing by-products, and the new cerium species could not be isolated or characterized, we can infer that **1-Ce** preferentially reacts with $C(sp^2)$–F bonds over $C(sp^3)$–F bonds. This in line with the increased radical stabilization in the radical arising from the activation of $C(sp^2)$–F bonds relative to $C(sp^3)$–F bonds.[37]

2.3.1.2 Reactivity of La complexes

The La congener **1-La** is also able to convert $PhCF_3$ to $PhCF_2H$, although less effectively than **1-Ce**. $PhCF_2H$ is formed in just 10% yield following 120 hours of irradiation of five equivalents of $PhCF_3$ with **1-La** at room temperature. Like **1-Ce**, a solution interaction between **1-La** and $PhCF_3$ can also be readily seen by ^{19}F NMR spectroscopy. In this case the resonance resulting from the solution interaction is shifted 0.03 ppm from the $PhCF_3$ capillary, suggesting that the change in resonance is not solely due to a paramagnetic shift in the case of **1-Ce**. In addition, **1-La** absorbs light at 310 nm, as shown in **Chapter 1**, which allows it to be photoactive.[38] This is attributed to a ligand to metal charge transfer that places an electron in a dz^2 orbital. For many cerium photocatalysts reported in the literature, the metal based $4f \rightarrow 5d$ transition is also thought to result in an excited state with $5dz^2$ character.[39]

While rare, the photoinduced homolysis of Ln–C bonds have been reported,[40,41] and the hydrodefluorination reactivity is attributed to the ability of one of the La–ligand bonds to be homolyzed under irradiation, forming a radical La fragment that can formally abstract F• from the La–coordinated substrate (*vide infra*.). $(Cp^{Me4})_3La$ (**2-La**) is also able to convert $PhCF_3$ to form trace $PhCF_2H$, although multiple other unidentified fluorine-containing products are also generated. Control reactions showed that **2-La** thermally decomposes upon introduction of $PhCF_3$ even without blue light irradiation, which could be responsible for the lack of defluorination selectivity when using this complex.

2.3.1.3 Experimental and Computational analysis of $PhCF_3$ binding and C–F bond homolysis

To elucidate the mechanism of C–F bond activation of $PhCF_3$ by **1-Ce** and **1-La**, experimental and computational studies were carried out. First, the Rehm-Weller formalism was used to estimate the excited state reduction potential ($E_{1/2}$*) of photocatalyst **1-Ce** (Equation 2.1).[42]

$$E^*_{\frac{1}{2}red} = E_{\frac{1}{2}red} - E_{0,0} + \omega \quad (2.1)$$

$E_{\frac{1}{2}red}$ is the ground state reduction potential between the Ce(III) /Ce(IV) redox couple. $E_{0,0}$ is the energy difference between 0th vibrational states of ground state and excited states which can be approximated by the emission energy. ω is the work function which describes electrostatic interactions due to the separation of charges upon the redox event. The work function is relatively small and is generally omitted.
As demonstrated in **Chapter 1**, excitation of a solution of **1-Ce** in THF with a 390 nm laser produces an emission band at 600 nm. Moreover, cyclic voltammetry experiments (*vide infra*.) on **1-Ce** displays a quasireversible $Ce^{III/IV}$ redox couple at –0.15 V vs. $Fc^{0/+}$. Together, these data indicate that the estimated $E_{1/2}$* of **1-Ce** is approximately –2.20 V (Equations 2.2–2.4).

$$E^*_{\frac{1}{2}red} = E_{\frac{1}{2}red} - E_{0,0} \quad (2.2)$$

$$E^*_{\frac{1}{2}red} = -0.15\ V\ - 2.05\ V \quad (2.3)$$

$$E^*_{\frac{1}{2}red} = -2.2\ V \quad (2.4)$$

This value is similar to those calculated for related Ce(III) amido and guanidinate complexes, and more positive than the literature $E_{1/2}$ of $PhCF_3$ (–3.23 V vs. $Fc^{0/+}$ in THF).[43] This result supports an inner-sphere mechanism[44] of photoreduction of $PhCF_3$ as drawn in (Scheme 2.5), in which the fluorophilicity of the lanthanide cation is essential in enabling the strong bond cleavage.[38,44] Unfortunately, similar calculations for **1-La**, as well as Stern-Volmer quenching experiments to aid this research, could not be carried out due to the high energy absorption of this complex and the limitations of the spectrophotometer used in this wavelength range.

Computational approaches (DFT, B3PW91 functional) were then used to gain insight into a plausible reaction mechanism for the C–F bond activation of trifluorotoluene facilitated by **1-Ce** (Figure 2.4). The reaction begins by the photoexcitation of the **1-Ce** ground state to **1-Ce***, a transition which is calculated to be 81.3 kcal.mol^{-1} since the $PhCF_3$ coordination is very weak. This would correspond to absorption of a photon at 350 nm. From this intermediate, a transition state (TS1) was located on the Potential Energy Surface (PES) that corresponds to C–F activation of the $PhCF_3$ substrate. The associated barrier from **1-Ce** is high (125.7 kcal.mol^{-1}); that is, 44.4 kcal.mol^{-1} from the photoexcited Ce^{III} state, **1-Ce***. The TS was located on the doublet spin state surface, with the electron shared between the Ce and the $PhCF_3$ molecule evenly so that the oxidation state of Ce is neither +(III) nor +(IV) at the TS.

Following the intrinsic reaction coordinate (IRC) leads to the formation of a Ce(IV)–F complex (**INT1**) and a free $PhCF_2$ radical which is endothermic by 28.2 kcal.mol^{-1} from the photoexcited **1-Ce*** state. The formation of the product $PhCF_2H$ via hydrogen atom abstraction from the solvent THF is computed to be athermic. This mechanism is distinct from the associative interchange process previously calculated for the reaction of $(Cp')_2CeCH_2Ph$ (Cp' = 1,2,4-tri-*tert*-butylcyclopentadienyl) with methyl halides.[45]

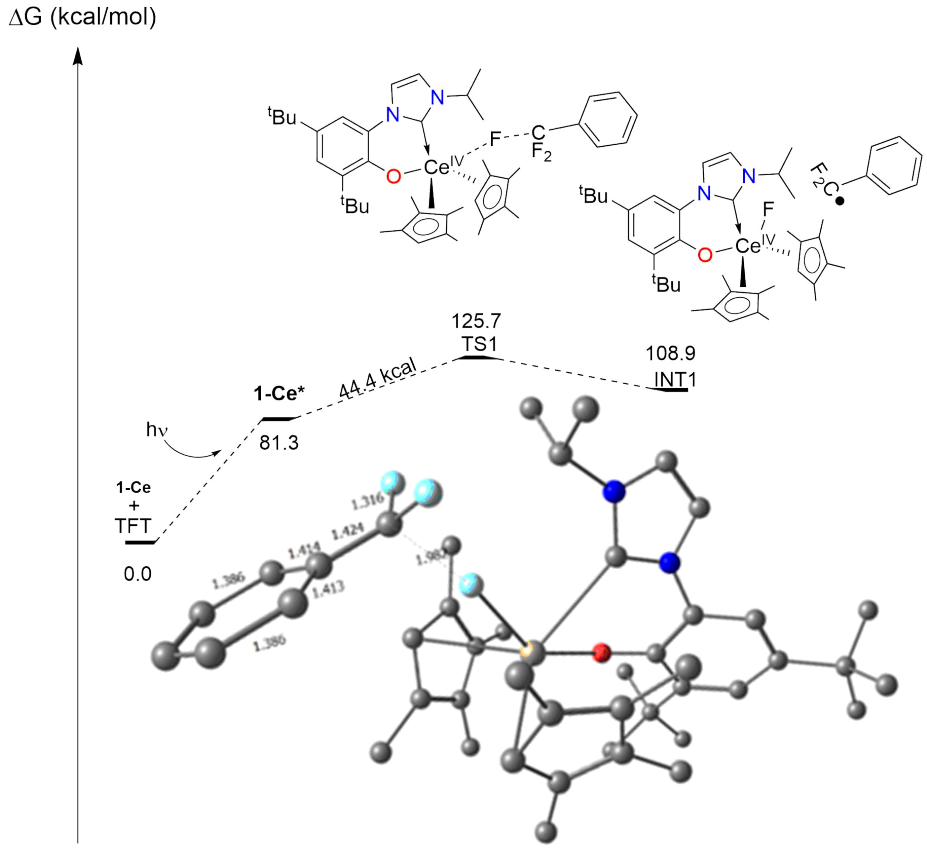

Figure 2.4. Computed C–F bond activation pathway from **1-Ce**, as well as representation of **TS1**.

Conversely, the triplet transition state TS1 computed for the d^0f^0 **1-La** analogue, was calculated to be just 7.9 kcal above the **1-La*** excited state energy. The low barrier calculated for the **1-La** reaction corresponds less well to the observed reactivity, so it may be that the light absorption probability for **1-La** is lower, since it involves a form of ligand-to-ligand charge transfer that may well be dipole forbidden.

2.3.1.4 Experimental evidence for the formation of an $ArCF_2^{\cdot}$ radical intermediate

Seeking experimental support for the formation of a discrete $ArCF_2$ radical intermediate, we prepared *ortho*-substituted benzotrifluoride 1-allyl-2-(trifluoromethyl)benzene (**7**),[43] hypothesizing that the pendant alkene group would serve as an intramolecular radical trap. Indeed, irradiating a mixture of **1-Ce** and **7** in THF at 70°C for six days results in the slow formation of a major new product in 50% yield, assigned based on its ^{19}F NMR spectroscopic data as the ring-closed species **8** (Scheme 2.6). Particularly distinctive are the ^{19}F NMR resonances, which display large $^2J_{F,F}$ coupling constants of 250 Hz. The reaction of **1-Ce** with

7 is significantly slower than the corresponding reaction with $PhCF_3$, which we attribute to the increased steric hindrance about the activated CF_3 group caused by the *ortho* substituent of **7**. Reaction of **7** with **1-La** under irradiation at 70°C results in the decomposition of **1-La.** Analogous reaction at room temperature also generates the same product, albeit in a lower yield of 20%.

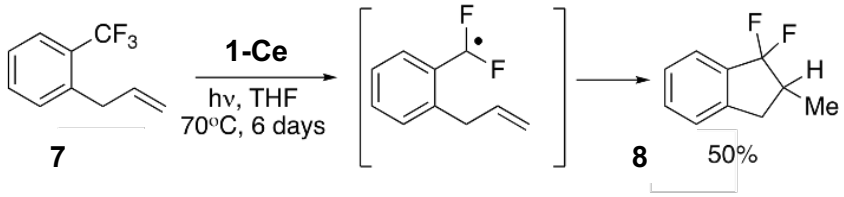

Scheme 2.6. The C–F bond activation of **7** mediated by **1-Ce**.

A second radical trap, 1-(allyloxy)-2-(trifluoromethyl)benzene, was also tested in conjunction with **1-Ce**. However, irradiation of the reaction mixture for six days resulted in just trace new product, shown to contain a difluoromethylene moiety by ^{19}F NMR. Reaction between **1-Ce** and 1-(allyloxy)-2-(trifluoromethyl)benzene is much slower than that between **1-Ce** and **7**, which could support the assignment of the five-membered ring-closed product rather than the six-membered ring-closed product.

To further support the conclusion that reaction of **7** with **1-Ce** and **1-La** generated the five-membered ring **8**, the independent synthesis of **8** was carried out via the fluorination of 2-methyl-2,3-dihydro-1*H*-inden-1-one with the commonly used fluorinating agent diethylaminosulfur trifluoride (DAST).[46] Following reflux of 2-methyl-2,3-dihydro-1H-inden-1-one with an excess of DAST in THF and subsequent work-up, ^{19}F NMR spectroscopy of the crude product displayed chemical shifts and J-values that matched exactly with those of the product of the reaction of **7** with **1-Ce** (Figure 2.5). However, the yield of this reaction was extremely low, making full purification and characterization of this species difficult. Further attempts to improve the yield of the synthesis failed due to the generation of additional fluorine containing species when more forcing conditions were used. Attempts to purify the product by column chromatography and preparative TLC using a range of conditions were also unsuccessful due to the low yield of product, the similar polarities of product and 2-methyl-2,3-dihydro-1*H*-inden-1-one starting material, and the decomposition of product on silica.

Nevertheless, the six-membered ring (1,1-difluoro-1,2,3,4-tetrahydronaphthalene) proposed as an alternate product from reaction of **7** with **1-Ce** and **1-La** would not be possible via this synthetic route. The ring expansion of a five-membered species in the DAST-mediated fluorination would instead be expected to yield known compound,1-fluoro-1,2,3,4-tetrahydronaphthalene, which is not observed in the resulting ^{19}F NMR spectra of this reaction.[47]

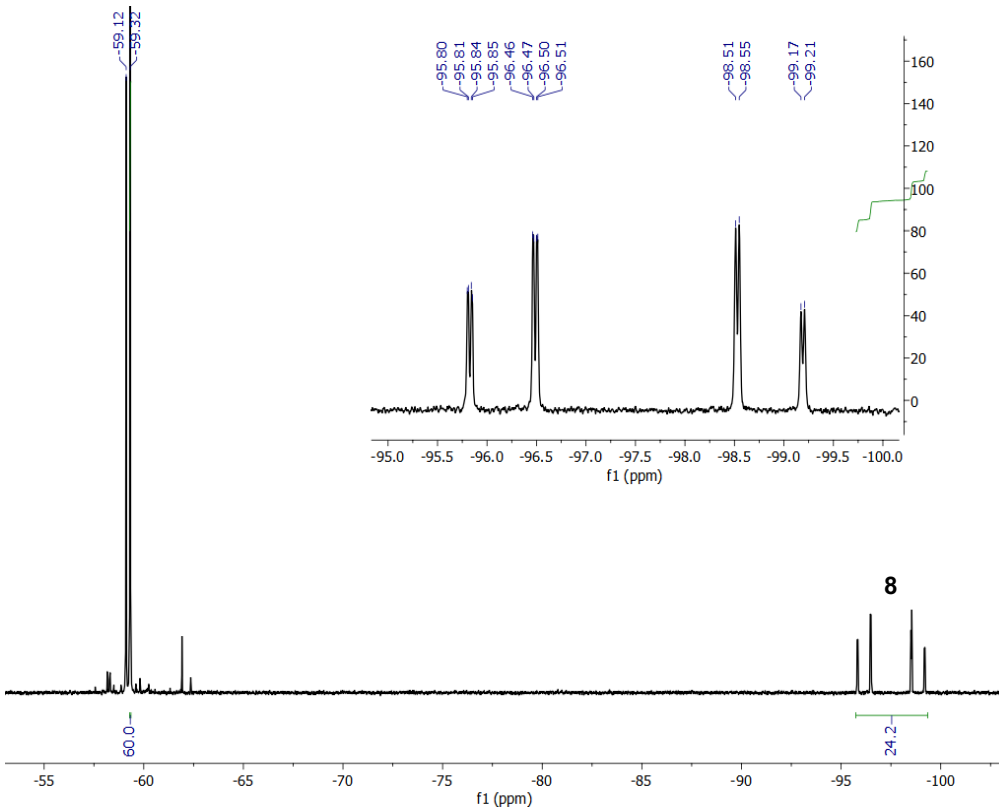

Figure 2.5. ^{19}F NMR in THF-H_8 of **1-Ce** with 5 equiv. **7**, following 6 days irradiation with a 40 W Kessil A160WE Tuna Blue lamp at 70 ° C.

2.3.2. Stoichiometric and catalytic defluoroalkylation of C(sp3)–F bonds: Conversion of $PhCF_3$ to $PhCF_2CH_2R$

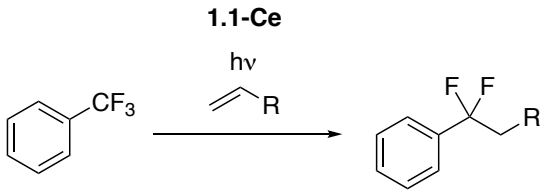

Scheme 2.7. Stoichiometric defluoroalkylation of $PhCF_3$ with **1-Ce** and CH_2CHR (R = ^{t}Bu, $SiMe_3$, $Si(OMe)_3$).

Complex **1-Ce** can facilitate defluoroalkylation stoichiometrically using alkenes (Scheme 2.7). The light-driven reactions between **1-Ce** and 5 equivalents of $PhCF_3$ with a series of alkenes–3,3-dimethylbut-1-ene, trimethyl(vinyl)silane and trimethoxy(vinyl)silane–in THF yields the dehydrofluorinated product $PhCF_2H$ alongside the corresponding defluoroalkylated molecule $PhCF_2CH_2R$. The products were identified by GC-MS and ^{19}F NMR spectroscopy. Analogous reactions with **1-La** gave just trace product. The ratio between the two products fluorinated products varied depending on the substrate, and the defluoralkylation of trimethyl(vinyl)silane by 1-Ce is most selective for $PhCF_2CH_2R$ (Table 2.1).

However ultimately, long reaction times, consistently low yields, and side-reactions between **1-Ce** and trimethyoxy(vinyl)silane halted our studies. We hypothesize that these side reactions involved the σ-bond metathesis and [1,2]-shift of the silyoxy- substituent in a silyl-Wittig rearrangement which has been observed for Ce metallocene complexes in the literature.[48] Furthermore, attempts to induce catalytic turnover with external reductants (Zn, Ce) were also unsuccessful, though further investigation into a wider range of reductants and substrates may yield more promising results.

Table 2.1. Stoichiometric defluoroalkylation of $PhCF_3$ with **1-Ce** and CH_2CHR in THF followed by 110 hours irradiation with a 40 W Kessil A160WE Tuna Blue lamp.

Entry	Alkene R Identity	Yield of $PhCF_2CH_2R$ (%)	Yield of $PhCF_2H$ (%)
1	^{t}Bu	13	8
2	$SiMe_3$	27	6
3	$Si(OMe)_3$	19	7

With these results in hand, we then sought to access catalytic defluoralkylation instead using metal alkyl reagents, which could act as both a coupling partner for the difluorotoluene radical and as a sacrificial reductant to enable the turnover of catalyst. Complexes **1-Ce**–**6-Ce** can defluoroalkylate $PhCF_3$ catalytically using Mg dialkyl reagents. $MgBn_2(THF)_2$[21] was the most efficacious reagent (Scheme 2.8), and is therefore described in the reactions shown here, though the alkylation is also possible using $Mg(allyl)_2$, $MgPh_2(THF)_2$, and ^{n}Bu_3Sn(allyl) in poorer yields. Bulkier metal alkyl reagents such as $Mg(Mes)_2$ do not result in defluoroalkylative coupling, and only difluorotoluene is observed as a product.

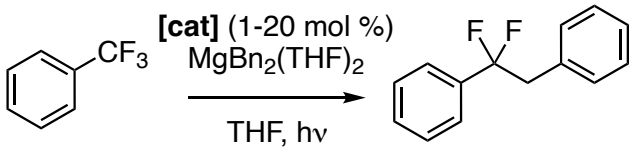

Scheme 2.8. Photocatalytic defluoroalkylation of $PhCF_3$ with catalyst and $MgBn_2(THF)_2$. **[cat] = 1-Ce–6-Ce, 1-Ln, 2-La.**

Standard reaction conditions consisted of 20 mol % catalyst loading, with one equivalent of $MgBn_2(THF)_2$ and $PhCF_3$ respectively in THF-H_8, with samples irradiated with a 40 W Kessil A160WE Tuna Blue lamp at room temperature for 48 hours. Products were identified as $PhCF_2R$ (R = H, Bn) by GC-MS and ^{19}F NMR spectroscopy (
Figure 2.6 2.6), with minor amounts of the by-product $PhCF_2H$ and bibenzyl observed, presumably formed via homocoupling of benzyl radical.[44]

Notably, the subsequent C–F bond activation of difluorotoluene is not possible for this system under these conditions, demonstrated by the independent irradiation of difluorotoluene with **1-Ce** and $MgBn_2(THF)_2$ for 110 hours. Over this extended period 47% yield of the defluoroalkylated product (1-fluoroethane-1,2-diyl)dibenzene ($PhCFH_2CH_2Ph$) was generated. The negligible amount of this compound observed in the photocatalytic defluoroalklyation of $PhCF_3$ by **1-Ce** indicate that a second defluorination is not favorable.

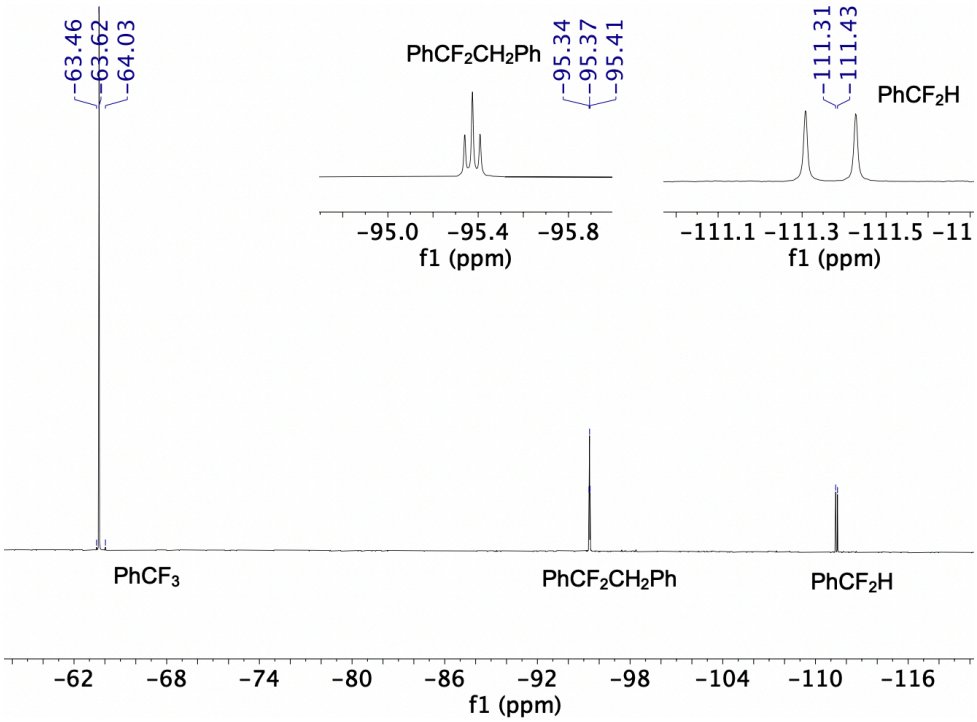

Figure 2.6. Example ^{19}F NMR spectrum collected in THF-H_8 of the defluoroalkyation of $PhCF_3$ by **1-Ce** in the presence of $MgBn_2(THF)_2$ following irradiation under a 40 W Kessil A160WE Tuna Blue lamp.

Of the Ce(III) photocatalysts, **1-Ce** was again most effective at the photocatalytic defluoroalkylation of $PhCF_3$ (Table 2.2). The combined yield of the two C–F activation products can be improved to 91% after 80 hours irradiation using 20 mol % **1-Ce**, although sequential addition of $MgBn_2(THF)_2$ during the reaction is required. Control reactions involving irradiation of a mixture of $MgBn_2(THF)_2$ and $PhCF_3$ produce bibenzyl and a $PhCF_3$ conversion of just 22% after a significantly longer period of irradiation (260 hours); the products are a mixture of $PhCF_2CH_2Ph$ and $PhCF_2H$ in a 2:1 ratio.

Table 2.2. Defluoroalkylative coupling of $PhCF_3$ with dibenzyl magnesium mediated by 20 mol % catalyst loading of **1-Ce**–**6-Ce** followed by 48 hours irradiation with a 40 W Kessil A160WE Tuna Blue lamp.

Catalyst [20 mol %]	Conversion to $PhCF_2CH_2Ph$ and $PhCF_2H$ (%)
1-Ce	51
2-Ce	6
3-Ce	18
4-Ce	41
5-Ce	18
6-Ce	33

The product yield is highly dependent on the irradiation wavelength, as expected for a light-driven reaction. Best results are observed using the Kessil Tuna Blue lamp (Figure 2.2) which has a broad irradiation wavelength spanning 400–600 nm, with an intense emission peak at approximately 460 nm. We hypothesize that this is due to strong emission bands overlapping with both the metal and ligand-based absorptions of **1-Ce**. Lowest yields are observed when using a lower energy light source (505 nm) despite its good overlap with the metal-based absorption of **1-Ce**, highlighting the utility of the higher energy ligand-based excitation in this photochemical transformation. This further suggests that metals lacking and accessible metal-based $4f^1 \rightarrow 5d^1$ excitation could be capable of facilitating photocatalytic reactions when ligated by **HL** due to this transition.

Table 2.3. Defluoroalkylative coupling of $PhCF_3$ with dibenzyl magnesium mediated by 20 mol % catalyst loading of **1-Ce** followed by 11 days irradiation with a variety of wavelength of light, with yields determined by ^{19}F NMR spectroscopy.

Irradiation wavelength (nm)	Conversion to $PhCF_2CH_2Ph$ and $PhCF_2H$ (%)
390	46
467	35
505	25

For the potential photocatalyst series **1-Ln** (Ln = La, Ce, Nd, Sm), and **1-U**, the same reaction procedure was followed, and product yield and purity monitored after 48 hours irradiation. Gratifyingly, photocatalytic defluoroalkylation is observed for all lanthanide complexes. Again, we attribute this reactivity to light absorption through **L** in a ligand to metal charge transfer (LMCT) (**Chapter 1**).

The yield decreases with decreasing atomic radius of the lanthanide, from 67% for La to 13 % for Sm, again emphasizing the importance of substrate binding through an inner sphere mechanism. **1-Nd** generates the defluorinated products in a combined yield of 32% following 48 hours irradiation, and an 87% yield is observed following 140 hours total irradiation. While trace formation of $PhCF_2H$ was observed in stoichiometric reactions between **1-U** and $PhCF_3$, defluoroalkylation was not possible using $MgBn_2(THF)_2$ due to extensive thermally driven reaction between the two complexes and subsequent catalyst degradation. This could be attributed to the increased covalent interactions possible for actinides and the larger number of accessible oxidation states possessed by uranium.[49,50]

Significantly, **1-La** can defluoroalkylate $PhCF_3$ faster than **1-Ce** despite lacking the accessible metal-based $4f^1 \rightarrow 5d^1$ excitation or (III)/(IV) redox couple. However, **1-Ce** is more selective in this transformation, capable of giving higher ratio of $PhCF_2CH_2Ph$ to $PhCF_2H$ (5:1) than **1-La** (2:1) at lower catalyst loadings (*vide infra*).

The formation of a small amount of diamagnetic, **L**-containing compound during catalysis with **1-Ce** was attributed to ligand transfer to the Mg alkyl.[51] The major by-product was identified as $[Mg(Bn)(\mathbf{L})]_2$ (**9-Mg**) by X-ray diffraction and ^1H NMR spectroscopy. The ligand exchange between $MgBn_2(THF)_2$ and **1-La** (30% conversion to **9-Mg** observed over 24 hours) is greater than between **1-Ce,** (less than 1% conversion to **9-Mg** observed over 24 hours). This is consistent with the larger ionic radii of lanthanum relative to cerium, and the greater accessibility of La to the magnesium reagent.

Ligand exchange between catalyst Mg alkyl can also be seen with complexes **2-Ce**–**5-Ce** by ^{1}H NMR spectroscopy during photocatalytic reactions, with each gradually converting into **6-Ce** as the reaction progresses. This is not observed for **1-Ce** due to presence of chelating ligand **L**. **6-Ce** is highly reactive but relatively unstable and degrades to **2-Ce** and bibenzyl under prolonged light irradiation. This could explain the increased reactivity of **1-Ce** relative to the other cerium photocatalysts, as chelating ligand **L** provides both the capacity for additional light absorption and also enhanced protection from ligand exchange that may lead to catalyst decomposition. Preliminary reactions with the simple cerium amide Ce(N{SiMe$_3$}$_2$)$_3$ as a defluorination catalyst and MgBn$_2$(THF)$_2$ also led to the isolation of species Mg(N{SiMe$_3$}$_2$)$_2$(THF)$_2$ through ligand redistribution, identified by XRD,[52] highlighting the inherent complexity of radical reactions and the potential difficulties in elucidating their mechanisms.

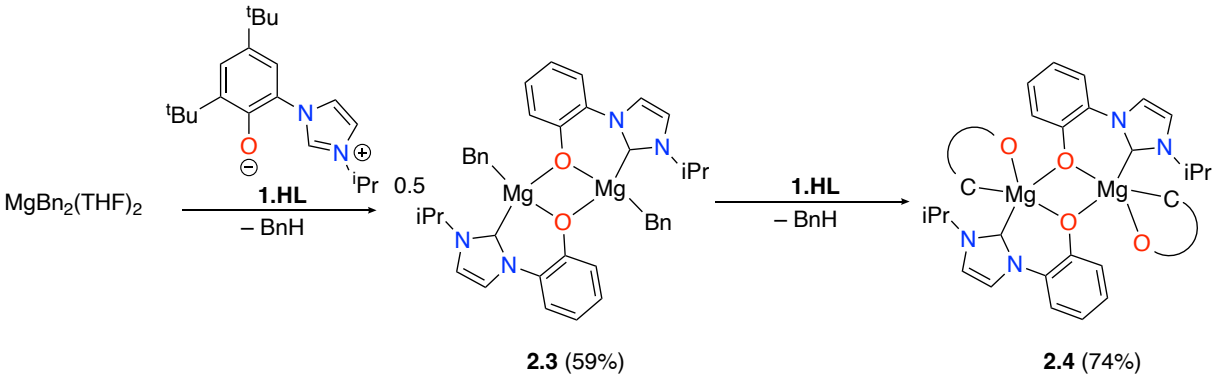

Scheme 2.9. Synthesis of Mg complexes to test as catalysts for C–F bond functionalization.

Pure [Mg(Bn)(**L**)]$_2$ (**9-Mg**) and [Mg(**L**)$_2$]$_2$ (**10-Mg**) were prepared (Scheme 2.9) to independently test their C–F bond activation reactivity. **9-Mg** can be isolated in 59% yield following the slow addition of one equivalent of **HL** to a cold, stirred solution of MgBn$_2$(THF)$_2$. **10-Mg** can be generated in 74% yield through the addition of a further two equivalents of ligand to **9-Mg**, or the addition of 2.1 equivalents of **HL** to a room temperature solution MgBn$_2$(THF)$_2$. Both complexes were characterized through standard techniques including single crystal XRD (Figure 2.7 and Figure 2.8).

Mg complexes bearing NHC ligands are relatively underexplored,[53,54] in particular Mg–NHC complexes with chelating anionic functional groups are extremely rare.[55–58] In 2004 Arnold et al. reported the first amido N-heterocyclic carbene Mg(II) complex, Mg(^{t}Bu-N-CH$_2$CH$_2$-C$_3$N$_2$H$_2$-^{t}Bu)$_2$],[57] and in 2006 Kawaguchi and Zhang published the first Mg complex of an aryloxy-bound NHC ligand. [Mg(**L**$^{\mathbf{Me}}$)(Mes)]$_2$ (where **L**$^{\mathbf{Me}}$ = 2-O-3,5-^{t}Bu$_2$-C$_6$H$_2$(1-C{N(CH)$_2$N(Me)}), Mes = mesityl) was synthesized through treatment of Na**L**$^{\mathbf{Me}}$ with one equivalent mesitylmagnesium bromide. In this complex, as in **9-Mg** and **10-Mg**, a magnesium dimer is formed via the bridging aryloxy group. In the case of [Mg(**L**$^{\mathbf{Me}}$)(Mes)]$_2$ the open coordination site is occupied by a mesityl group, analogous to the benzyl substituent in **9-Mg**. In all complexes the two bridged oxygen and two carbon atoms in the NHC coordinate to magnesium in a tetrahedral geometry. **9-Mg** and **10-Mg** contain a Mg–C(NHC) bond distance of 2.179 and 2.228 Å respectively, in line with the 2.224 Å Mg–C(NHC) bond distance in [Mg(**L**$^{\mathbf{Me}}$)(Mes)]$_2$[55] The relatively shorter Mg–C distance in **9-Mg** could be attributed to the decreased steric hindrance imparted by the benzyl substituent relative to Mes.

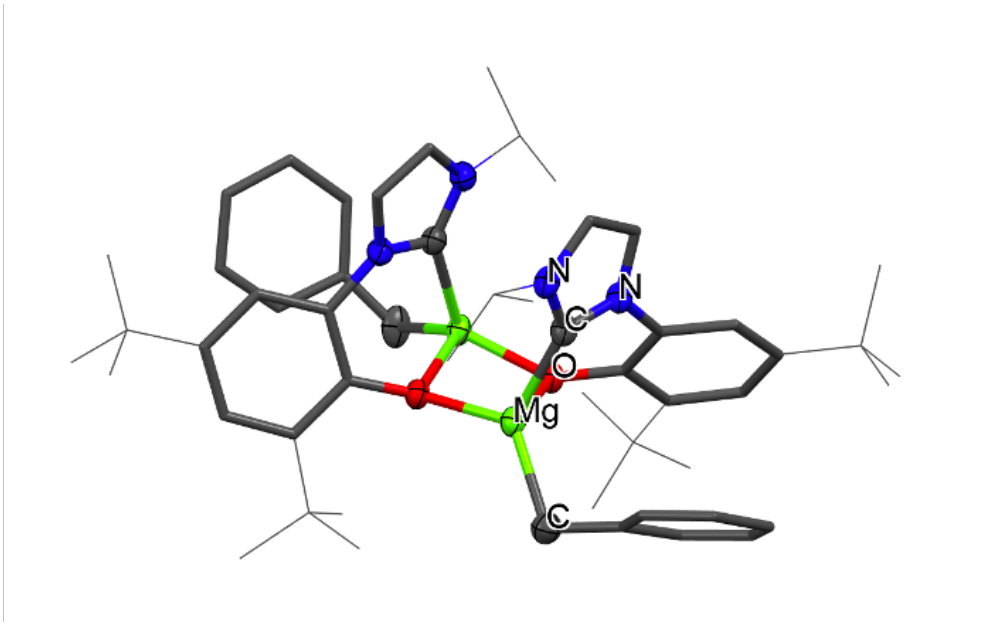

Figure 2.7. Molecular structure of **9-Mg.** Ellipsoids shown at 50% probability, peripheral groups shown in wireframe, hydrogen atoms and lattice solvent molecules have been omitted for clarity. Color code: green – Mg; red – O; grey – C; blue – N.

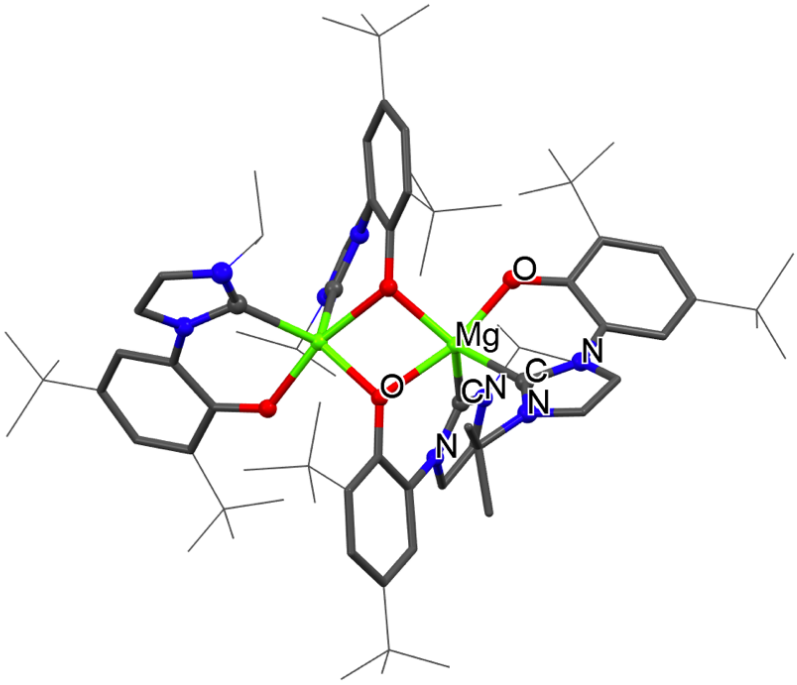

Figure 2.8. Molecular structure of **10-Mg**. Ellipsoids shown at 50% probability, peripheral groups shown in wireframe, hydrogen atoms and lattice solvent molecules have been omitted for clarity. Color code: green – Mg; red – O; grey – C; blue – N.

Under standard catalytic conditions for the conversion of $PhCF_3$ to $PhCF_2CH_2Ph$, the aryloxy-NHC complex **9-Mg** cleaves the $PhCF_3$ C–F bond under irradiation, forming a mixture of products in total 24% yield. The bis(ligand) complex **10-Mg** is less active for either $PhCF_2H$ or $PhCF_2CH_2Ph$ formation. We propose that this is due to both the increased steric crowding of **9-Mg** relative to **10-Mg** which could hinder the interaction of substrate with the metal center in an inner sphere mechanism, as well as slow ligand exchange between **10-Mg** and additional $MgBn_2(THF)_2$. In addition, **10-Mg** lacks the of alkyl group required to necessitate C–C bond formation (*vide infra*). Furthermore, computational approaches (DFT, B3PW91 functional) indicate the barrier for the excited state of the Mg(II) complex **9-Mg***, is around 35 kcal mol^{-1}, supporting the experimental observation that the reaction can occur but is relatively slow, especially since the overall reaction is endothermic by 11.4 kcal mol^{-1}.

The group 2 analogue $[CaBn\mathbf{L}]_x$ was also targeted since Ca(II) has a similar ionic radius to Ln(III) ($r_{cov\ 6\ coordinate}$ Ce = 1.15; Ca = 1.14; Nd = 1.123 Å) and would provide a catalyst with similar Lewis acidity but much less accessible *d*-orbitals at the metal. $CaBn_2(THF)_4$ was synthesized via a literature procedure involving the reaction of calcium iodide with two equivalents of benzyl potassium in THF.[59] $[CaBnL]_x$ was then targeted through the addition of a cold solution of $CaBn_2(THF)_4$ in THF to a cold solution of **HL** in an analogous procedure to the synthesis of **9-Mg**. However, Schlenk equilibria prevented the isolation of a pure complex that could inform the mechanistic studies.

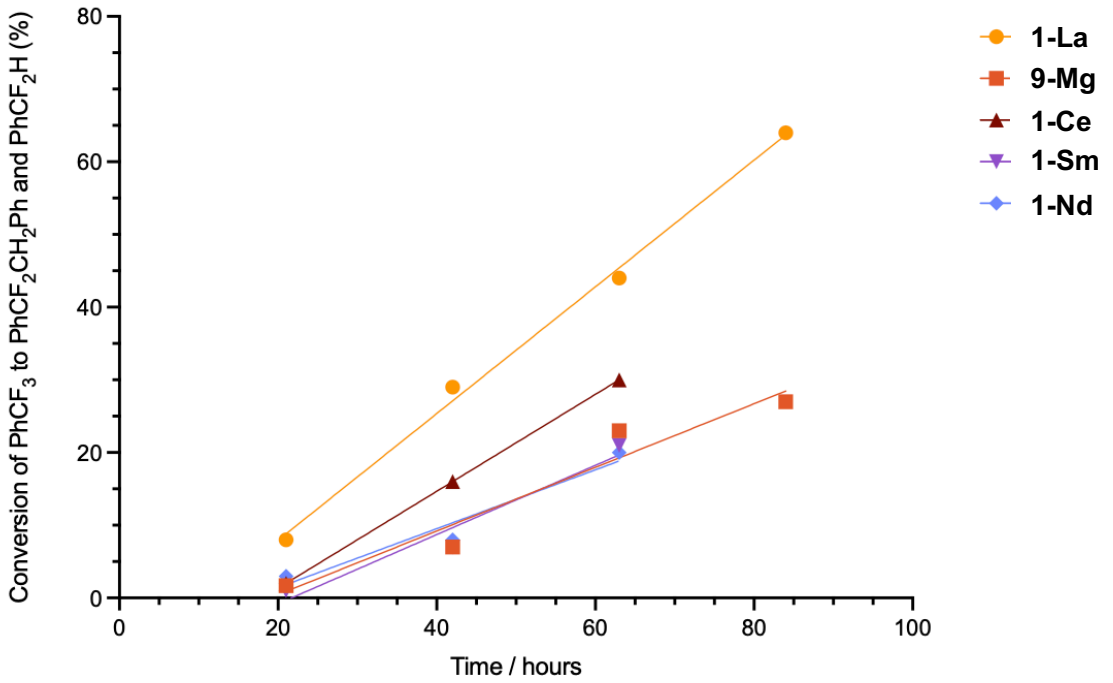

Figure 2.9. Graph of the conversion of $PhCF_3$ to $PhCF_2CH_2Ph$ and $PhCF_2H$ mediated by 1 mol % loading of **1-La, 1-Ce, 1-Nd, 1-Sm** and **9-Mg**,

The conversion of $PhCF_3$ to $PhCF_2CH_2Ph$ can be catalyzed at loadings as low as 1 mol %. Figure 2.9 shows the data for the catalyzed conversion of $PhCF_3$ to $PhCF_2CH_2Ph$ in THF-H_8, mediated by 1 mol % loading of **1-Ce**, **1-La**, **1-Nd**, **1-Sm** or **9-Mg**. There appears to be a significant kinetic isotope effect in these reactions as the formation of $PhCF_2D$ as a side-product is suppressed in THF-D_8, leading to an improved $PhCF_2CH_2Ph$:$PhCF_2H$ ration of 12:1, though overall product yield is much reduced. An average ratio of 3:1 is observed when the corresponding reaction is performed in THF-H_8.

2.3.3 Mechanistic studies and discussion

2.3.3.1 Oxidation of metal and/or ligand

The interesting ability of supposedly redox-inert **1-Ln** and **9-Mg** to perform catalytic C–F activation indeed implicates the ligands in enabling the redox part of the catalytic cycle. The formation of the $ArCF_2$• catalyzed by **1-Ln** should lead to an oxidized F-containing intermediate, [**1-Ln**–F**]**. The redox active and innocent metals can achieve this in different ways, shown in Scheme **2.10** 2.10. For **1-Ce** we expect the Ce(III)/(IV) redox couple to be involved, forming the fluoride intermediate Ce(IV) $[(Cp^{Me4})_2Ce(\mathbf{L})(F)]$ **1-Ce–F**, although we recognize that oxidation of **L** or Cp^{Me4} ligand is also possible. For **1-La** and the other lanthanides which must remain Ln(III) we expect either $[(Cp^{Me4})_2Ln(\mathbf{L}•)(F)]$ or $[(Cp^{Me4}•)(Cp^{Me4})Ln(F)(\mathbf{L})]$. We assume **9-Mg** will form [Mg(F)(**L**•)(Bn)] or [Mg(F)(**L**)] and •Bn.

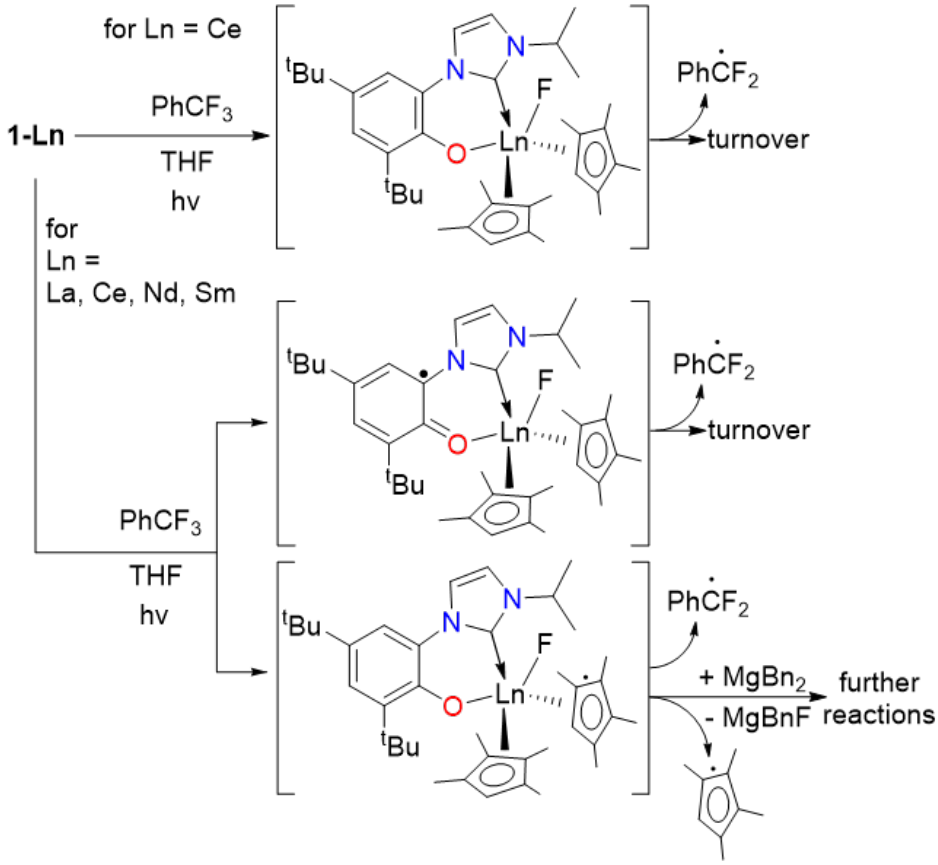

Scheme 2.10. The proposed pathways of oxidation of **1-Ln** that lead to turnover or catalyst degradation.

In order to implicate either the oxidation of **L** or Cp^{Me4} in the mechanism of defluoroalkyation, we targeted the [**1-Ln**–F] intermediate independently of catalysis. As cerium(IV) fluorides are uncommon and difficult to work with, and if a fluoride was formed in the catalytic cycle, we did not expect it would be isolable.[60] We had hoped, however, that potential oxidation products would be distinct enough to identify through in situ characterization techniques. For example, the C=O–Ln intermediate arising from the potential oxidation of **L** should distinct stretches observed by FT-IR.[61] Conversely, the oxidation and potential homolysis of Cp^{Me4} may result in the formation of HCp^{Me4} or the dimer $[Cp^{Me4}]_2$ which could be characterized by ^{1}H NMR spectroscopy.[62] In both cases, the addition of fluoride to any potential ligand radical produced by oxidation could also provide an informative ^{19}F NMR handle.

Accordingly, the chemical oxidations of **1-Ce** and **1-La** were targeted. However, no [Ln–F] or otherwise informative species from oxidation of **1-Ce** using N-fluorobenzenesulfonimide (NFSI) or 1-(Chloromethyl)-4-fluoro-1,4-diazabicyclo[2.2.2]octane-1,4-diium ditetrafluoroborate (Selectfluor), or oxidation of **1-La** using xenon difluoride (XeF_2) could be unambiguously characterized by ^{1}H NMR, ^{19}F NMR or FT-IR spectroscopy, or separated by fractional crystallization. Furthermore, the independent synthesis of Ce(IV)–F species was attempted, through the generation of a Ce(III)–F complex and its subsequent oxidation. However, reaction of CeF_3 with two equivalents of KCp^{Me4} generated an insoluble solid that could not be characterized, while treatment of **6-Ce** with $BF_3(OEt)_2$ instead yielded $[(Cp^{Me4})_2Ce(BF_4)]_2$ (Figure 2.15).

The hypervalent iodine reagent $PhICl_2$ was then used, to instead access the chloride analogue of the [Ln–F] intermediate that could form from F atom abstraction from $PhCF_3$. This reagent has also previously been used with success in organometallic Ce^{IV} chemistry.[63,64] Upon addition of $PhICl_2$ to **1-Ce**, an immediate color change from orange-pink to a purple characteristic of tetravalent cerium occurred, which was subsequently followed by a bleaching of the solution to a pale pink color. Unfortunately, ^{1}H NMR spectroscopic analysis of the crude mixture showed multiple products and attempts to separate these by crystallization resulted only in the recovery of some unreacted **1-Ce**. **1-La** reacts with 0.5 equiv. of $PhICl_2$ to form some unidentified material tentatively assigned as the La^{III} compound $[(Cp^{Me4})La(\mathbf{L})(Cl)]$ since spectra indicate the loss of a Cp^{Me4} ligand radical, though again, no species could be confidently assigned by ^{1}H NMR or FT-IR spectroscopy. Interestingly, **9-Mg** does not react with $PhICl_2$, which could be attributed to the relative Lewis acidity of Mg vs Ln, and suggests a further reason for the decreased reactivity of **9-Mg** in defluoroalkylation compared to **1-La**.

As experimental results could not give conclusive evidence for the preferential oxidation of Cp^{Me4} or **L**, computational approaches (DFT, B3PW91 functional) were instead used to provide more insight into the oxidation step of defluoroalkyation reaction facilitated by **1-La**. Calculations show that Cp^{Me4} is spontaneously released as a radical from the La center upon oxidation and provides a possible reason for the instability of **1-La** in catalysis particularly when using higher energy lamps; catalysis is not possible with **1-La** using a 390 nm lamp, only decomposition is seen. There is also precedent for the homolysis of Ln–Cp bonds.[65]

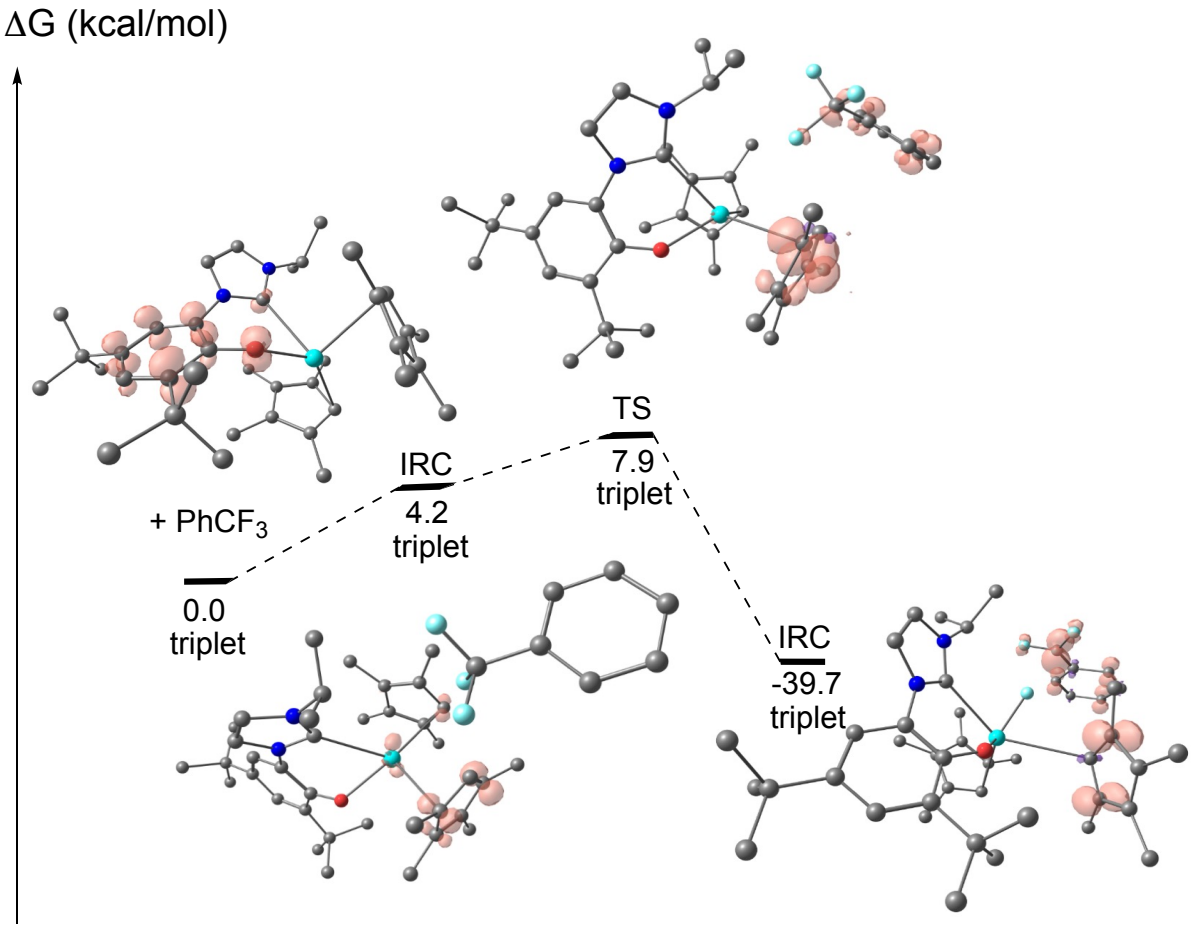

Figure 2.10. Computed C–F bond activation pathway from **1-La**.

Figure 2.10 shows how for photoexcited **1-La*** the unpaired spin density is mainly located at the aryloxy-NHC ligand but localizes on the Cp^{Me4} ring and develops on the coordinated $PhCF_3$ approaching the C–F activation step, finishing with unpaired spin density on both the $PhCF_2$• radical and the Cp^{Me4} ligand. Therefore, Cp^{Me4} oxidation is likely to lead to La–Cp^{Me4} homolysis alongside the release of further radicals (i.e. Cp^{Me4}•, (**L**)(Cp^{Me4})La•) that could also facilitate reactivity. In addition, the capacity for the pseudo-reversible oxidation (*vide infra*.) of phenoxy-NHC ligand **L** could enable a non-oxidizable Ln^{III} complex (Ln = La, Sm, Nd) to turnover in the proposed catalytic cycle via a modified mechanism to **1-Ce** where the redox process can also occur at the metal.

Cyclic voltammetry (CV) measurements were also carried out to analyze the redox potentials and reversibility of the oxidations of complexes **1-Ce**, **2-Ce**, **1-La** and **2-La** as well as of the ligand **HL**, to provide further information of the process of oxidation in catalysis (**Appendix B**). Measurements were performed in tetrabutylammonium tetraphenylborate ($TBABPh_4$) (Figure 2.11, Table 2.4), or in tetrabutylammonium hexafluorophosphate ($TBAPF_6$) electrolyte solutions. The $TBAPh_4$ electrolyte has a narrower potential window (up to 0.25 V vs Fc/Fc^+) but it avoids the potential for abstraction of F by the lanthanide complex.

Table 2.4. Onset of oxidation in volts for **1-Ce, 1-La, 2-Ce, 2-La** and **HL** observed upon scanning oxidatively at 500 mV/s. The calculated excited state reduction potential of **1-Ce** is shown in brackets adjacent to the ground state reduction potential.

Molecule	Redox potential (vs Fc/Fc+) / V
1-Ce	–0.15 (–2.2)
1-La	0.15
2-Ce	–0.3
2-La	–0.05
HL	0

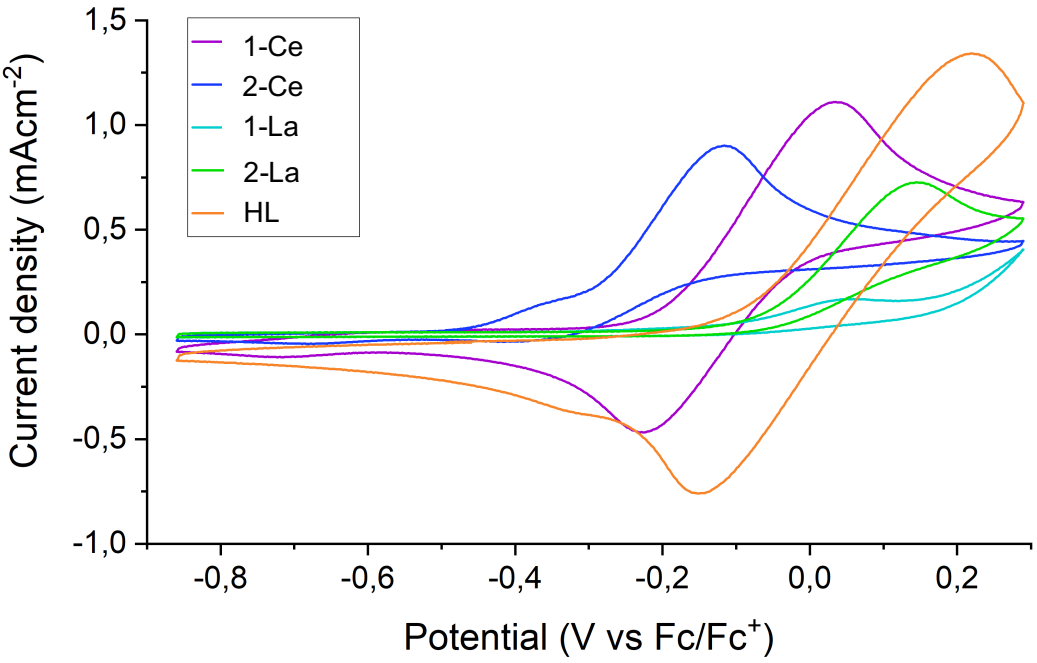

Figure 2.11 Cyclic voltammograms of **1-Ce** (purple), **2-Ce** (dark blue), **1-La** (light blue), **2-La** (green) and **HL** (orange) in THF with 0.085 M [^{n}Bu$_4$N][BPh$_4$] supporting electrolyte. [analyte] = ca. 5 mM; ν = 0.5 V/sec.

In the case of **HL**, a redox peak around 0 V (vs Fc/Fc+) was observed upon scanning oxidatively, displaying partial reversibility upon increasing the scan speed. This can be explained by a slow, irreversible reaction of the oxidized ligand. A similar redox feature around –0.15 V is observed for **1-Ce**; the position of the oxidation at a more negative potential than that of free ligand implies a contribution from both the ligand and the metal center to this oxidation. This agrees with our observation that electrons can be photoexcited from both metal and ligand.

In comparison, **1-La** shows an onset of oxidation current of similar amplitude only close to the electrolyte potential window (onset around 0.15 V), There is also a smaller feature at –0.15 V, attributed to small amounts of free ligand that are released after the first oxidative scan of the bulk solution. **2-Ce** and **2-La** both display fully irreversible oxidations with onsets around –0.3 and –0.05 V, respectively. The presence of additional redox features may indicate the formation of electrochemically active degradation products of the oxidation, consistent with

our hypothesis. The voltammograms of **2-La** and **2-Ce** have recently been reported and show that the oxidation of lanthanide tris(Cp^{Me4}) complexes leads to decomposition at most standard scan rates.[66] Here in contrast, the oxidation of **2-Ce** is partially reversible at a scan rate of 500 mV/sec.

2.3.3.2 The C–C bond forming step

We were interested in examining in more detail the C–C bond forming step of this coupling reaction. Conventional organometallic Ce(IV) species are documented to be unstable.[67,68] In line with our experimental observations, DFT calculations indicate that the formation of a discrete [Ce(IV)]–Bn is energetically unfavorable.

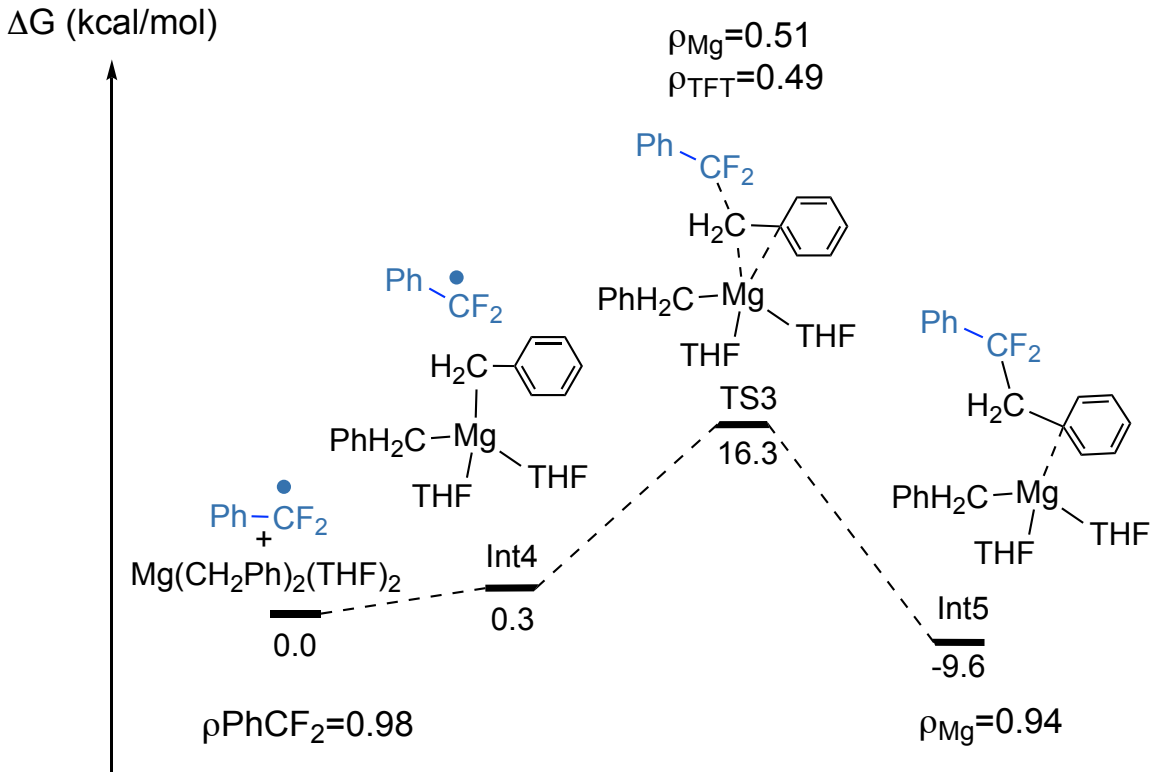

Figure 2.12. Computed C–C coupling pathway at $MgBn_2(THF)_2$.

We examined whether the C–C bond was formed by coupling of the $PhCF_2$ radical directly with the reagent $MgBn_2(THF)_2$, and also with **9-Mg**, since we observe this as a by-product in catalysis involving **1-Ln**. Intrinsic reaction coordinate (IRC) calculations on the coupling of the $PhCF_2$ radical with $MgBn_2(THF)_2$ (Figure 2.12) identify a transition state with a barrier that is 3.5 kcal/mol lower than that calculated for **9-Mg*** (a computational model wherein the dimeric structure of **9-Mg** observed by XRD has been broken up by donor THF solvent). The formation of **9-Mg*** (THF solvate) from **9-Mg** (the unsolvated dimer) is computed to be almost athermic (2.1 kcal/mol) making **9-Mg*** a viable model for this reaction. The transition state for the latter is 19.8 kcal/mol above the energy of **9-Mg*** and the $PhCF_2$ radical (Figure 2.13). These results indicate that C–C bond formation is likely occurring at $MgBn_2(THF)_2$, which is also at significantly higher concentrations than **9-Mg** in solution during catalysis.

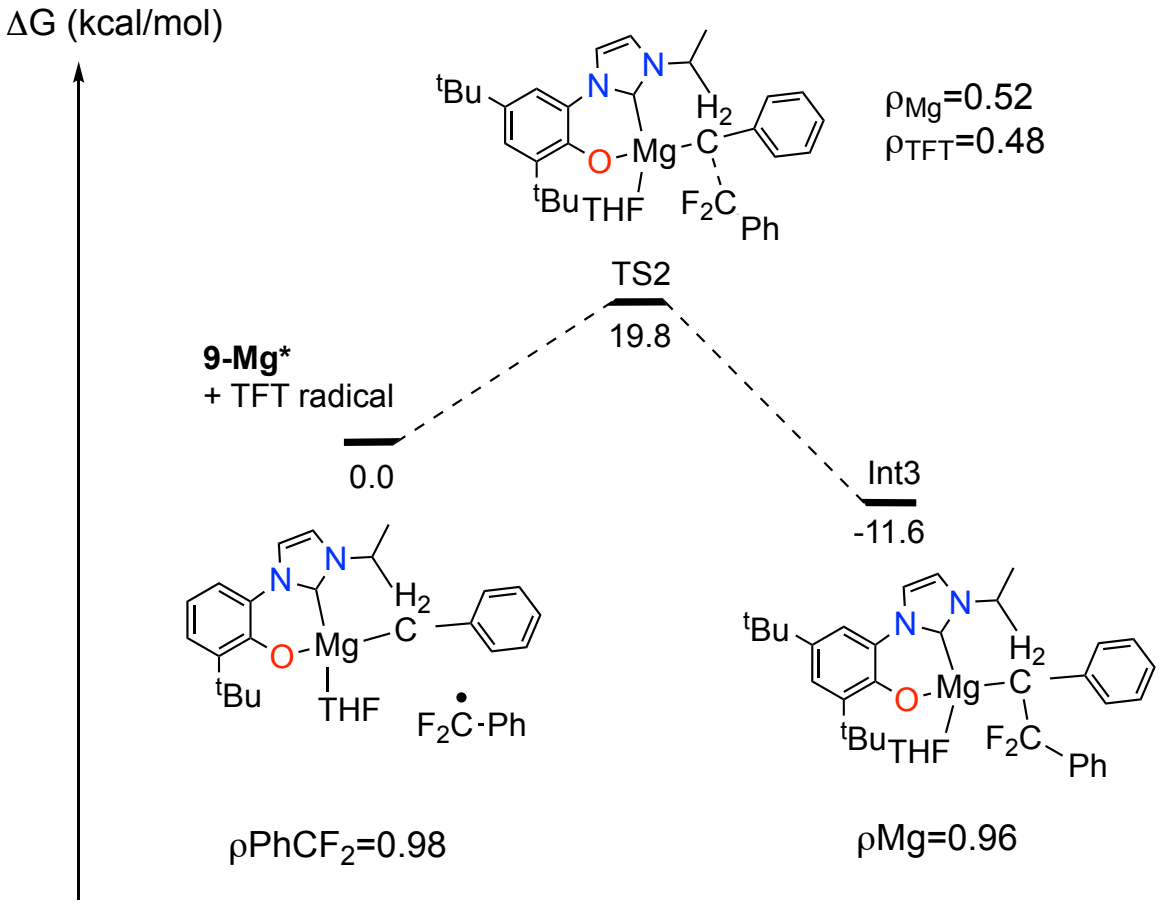

Figure 2.13. Computed C–C coupling pathway at **9-Mg**.

2.3.3.3 Mechanistic summary

The reactivity described here is notable in that it is not limited to Ce, which is the only rare earth with a readily accessible (III)/(IV) redox couple and *f* → *d*-orbital transition. It is these properties that have led to the recent and widespread interest in photoredox catalysis with Ce complexes. Of all the complexes that are capable catalysts described here, the **1-Ce** congener shows the longest catalyst life, and cleanest product formations. This may be because for the photoactivated Ce(III)/(IV) system there is a simple, metal-based process for redox shuttling that enables the F atom to be captured and removed, as well as the opportunity for both ligand and metal orbitals to contribute to the light absorption and bonding of the complex. For La and other metals, the redox part of the cycle relies on the redox reactivity of an ancillary ligand. The involvement of phenoxy ligand radicals in redox reactions has been previously documented,[69–71] and cyclic voltammetry experiments show that **HL** possesses a pseudo-reversible redox event.

Calculations suggest that the ease of M–Cp^{Me4} bond homolysis is greater for La versus Ce, and CV experiments imply that loss of a Cp^{Me4} ligand from **1-La** may lead to a cascading degradation process where the release of radical fragments accelerate decomposition. This supports the observation that complex **1-Ce** is more effective for C–F activation while complex **1-La** is faster for the coupling of the radical to form benzylated product, acting as a source of

radicals that can facilitate C–F bond cleavage at the Lewis-acid coordinated substrate. Moreover, **1-Ce** has been found to be the most thermally robust during catalysis of the **1-Ln** family described herein, able to operate at elevated temperatures (*i.e.* 70 °C).

The proposed mechanism is outlined in Scheme 2.11. First, a weak but observable interaction between a fluoride of $PhCF_3$ and the Ln metal, as observed in ^{19}F NMR experiments for both Ce and La, serves to bring the substrate into the active site. C–F→Ln(III) (Ln = La, Sm, Yb) interactions have previously been hypothesized in the functionalization of C–F bonds mediated by lanthanide complexes.[14–16]

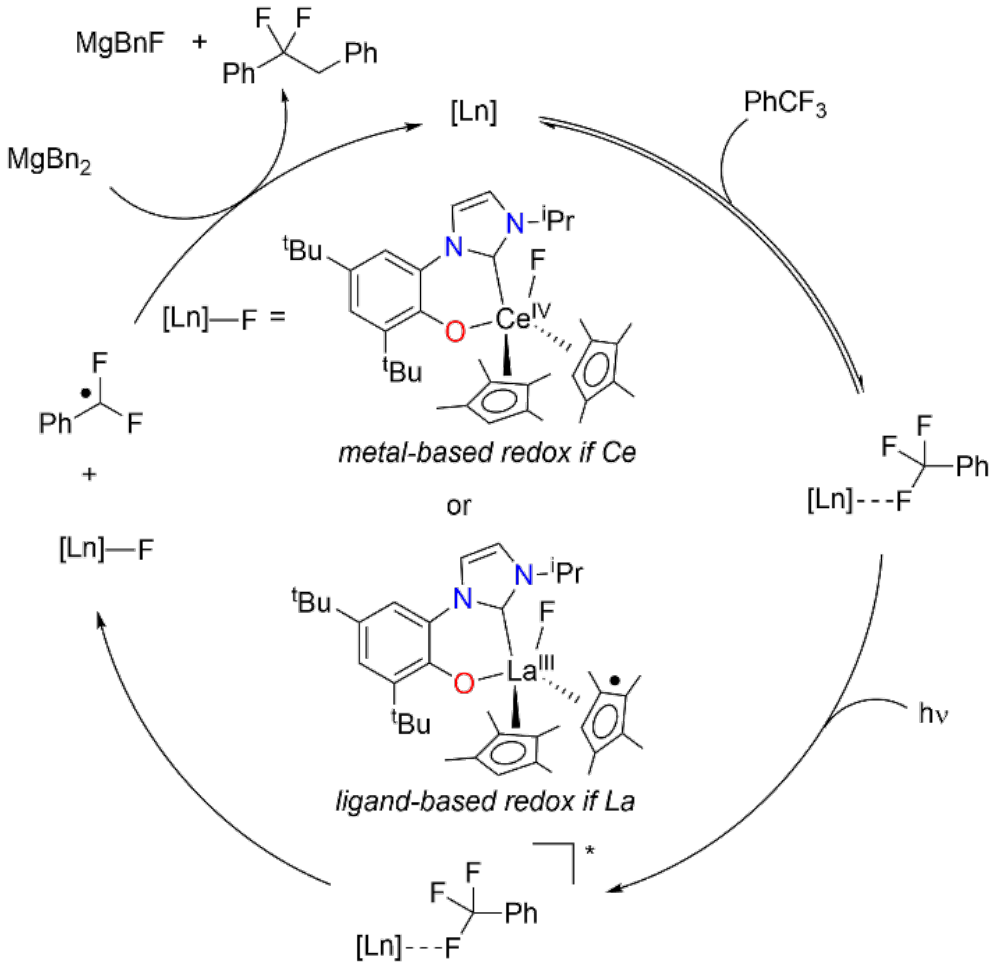

Scheme 2.11 Proposed mechanism of photocatalytic C–C coupling.

Photoexcitation to a more reducing excited state[72] follows, which leads to C–F cleavage and the generation of an $ArCF_2$ radical, as supported by experiments with a radical trapping substrate. The nature of the resulting putative Ln–F species depends on the identity of the rare earth element. For Ce, the formation of a discrete Ce(IV) species is the most likely intermediate. As this higher oxidation state is inaccessible for La, the ligands (either **L** or Cp^{Me4}) can serve as the electron source through ligand-based redox non-innocence. Reduction likely occurs when the generated $PhCF_2$ radical couples with $MgBn_2$ to form the C–C bond, with the resulting transient Mg(I) complex serving to reduce either the metal (in the case of Ce) or the ligand (in the case of La) back to the initial catalytic species.

This generates the defluoroalkylated product alongside a proposed magnesium fluoride species, MgBnF, which would likely disproportionate to form $MgBn_2(THF)_2$ and magnesium fluoride. The presence of a fluoride containing species in these reactions can be supported through the addition of one equivalent of chlorotrimethylsilane with respect to the fluorinated substrate following the completion of a reaction, which results in the formation of fluorotrimethylsilane that can be observed by ^{19}F NMR spectroscopy.[73]

Calculations support the proposed mechanism, agreeing with the need for inner-sphere complexation between the Lewis acidic metal and the substrate to provide sufficient weaking of the C–X bond to enable photochemical cleavage. They also show how the ligands can contribute to light absorption to generate the reactive excited state (**Chapter 1**), and how oxidation of the complex can be localized on the metal (for Ce) or ligand (for the other metals) to enable turnover.

Trends in reactivity also support the proposed mechanism. Reactivity decreases along the lanthanide series, consistent with the larger lanthanides providing greater access for substrate binding and a consequent inner sphere mechanism. Another contributing factor to this trend could be the relative energies between the ligand orbitals and *d*-character orbitals on the metal. Energy matching of these orbitals could lead to more efficient LMCT and enhanced photoactivity. The energy of the *d*-orbitals in the lanthanides decrease along the series due to the lanthanide contraction, which could make their energy match with the ligand poorer for later lanthanides relative to lanthanum. However, further computational, and spectroscopic data for **1-La**, **1-Sm** and **1-Nd** would be needed to validate this hypothesis. The study of fluorophilic Group 3 metals such as gallium or indium which do not have an accessible 5*d* orbital could also provide insight into this claim,[74,75] as could the synthesis and catalysis of the calcium analogue of **9-Mg** previously discussed.

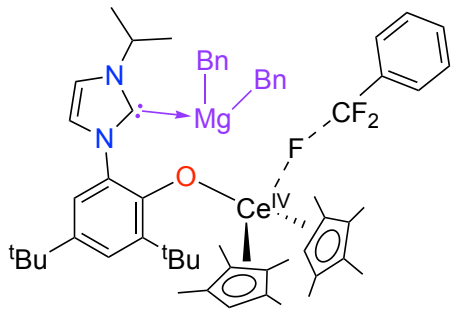

Figure 2.14. Envisioned intermediate arising from the interaction between **1-Ce** and $MgBn_2(THF)_2$ if NHC substituent of **L** was labile.

To the best of our knowledge the NHC in ligand **L** is not labile, and all computed barriers increase in energy in systems where the NHC is unbound or binds to a Mg (or other) reagent. This is supported by experimental data, as variable temperature ^1H NMR spectroscopy experiments do not show any interactions between **1-Ce** and $MgBn_2(THF)_2$ in THF solutions (**Error! Not a valid bookmark self-reference.**Figure 2.14). This result is in contrast to related Ce systems examined by us previously, which display hemilability of the NHC moiety of the **L** ligand as a key reactivity feature in the ring opening of lactide to form polylactide. [10,76,77] Unsurprisingly, the calculations do not support the presence of a [Ce^{IV}–Bn] complex at any point.

2.4 Conclusions

Cleavage and functionalization of the strong and inert sp^3 C–F bond of $PhCF_3$ can be readily achieved using single component, earth-abundant organometallic photocatalysts, requiring both the Lewis acidity of the metal to bind the substrate, and the visible light-absorbing capabilities of the rigid aromatic ligands. The reactivity described here is notable in that it is not limited to Ce, which has been the focus of a recent surge of interest in earth-abundant metal photocatalysts.

The photochemical hydrodefluorination and defluoroalkylation of $PhCF_3$ is feasible for typically photoinactive metals including La and Mg because the rigid aryloxy-NHC ligand facilitates visible light absorption. Experiments with a radical-trapping substrate support the formation of $ArCF_2$ radicals after C–F bond activation, and catalytic turnover in C–C bond forming reactions is most readily achieved using reagents such as $MgBn_2(THF)_2$ which can provide both the alkyl group and reduction of the catalyst intermediate. Ligand non-innocence allows for the redox part of the catalytic cycle to occur for metals without a readily accessible tetravalent oxidation state. The propensity of the reported complexes to facilitate C–F bond activation also suggests the ability to cleave other C–X bonds.

2.5 Experimental

General details. All moisture and air sensitive materials were manipulated using standard high-vacuum Schlenk-line techniques and MBraun gloveboxes and stored under an atmosphere of dried and deoxygenated dinitrogen. All glassware items, cannulae and Fisherbrand 1.2 μm retention glass microfibre filters were dried in a 160 °C oven overnight before use.

Solvents and reagents. Hexanes, tetrahydrofuran (THF), diethyl ether (Et_2O) and toluene for use with moisture and air sensitive compounds were dried using an MBRAUN SPS 800 Manual solvent purification system and stored over activated 3 Å molecular sieves. Benzene-D_6, pyridine-D_5 were purchased from Cambridge Isotope Laboratories and were refluxed over potassium metal for 24 hours, freeze-pump-thaw degassed and purified by trap-to-trap distillation prior to use. THF-D_8 was purchased from Cambridge Isotope Laboratories and dried over sodium/benzophenone before being freeze-pump-thaw degassed and purified by trap-to-trap distillation prior to use. All solvents were purchased from Sigma-Aldrich or Fisher Scientific and stored over 3 Å molecular sieves for 4 hours before being used.

$PhICl_2$ was prepared according to the literature procedure[78] and stored at –30 °C. Dihydrocarbyl magnesium reagents,[79] $CaBn_2(THF)_4$,[59] **HL**,[80] KC_5Me_4H,[81] lanthanide triiodides (Ln = La, Ce, Nd, Sm),[82,83] lanthanide tris(tetramethylcyclopentadienyl) complexes (Ln = La, Ce, Nd, Sm),[83,84], $UI_3(dioxane)_2$ and UCp^{Me4}_3,[81] were all prepared using published methods. Complexes **1-Ce**–**6-Ce**, **1-Ln**, and **1-U** were synthesized as previously described in **Chapter 1**. The radical traps **7**, and 1-(allyloxy)-2-(trifluoromethyl)benzene, were synthesized according to the literature procedure.[85] All other chemicals were purchased from commercial suppliers and degassed and/or dried under vacuum or over 3 Å molecular sieves for 12 hours before use.

Characterization. NMR spectra were recorded on Bruker Avance 400, 500 and 600 MHz spectrometers and are referenced to residual protio solvent (3.58 and 1.72 ppm for THF-D_8, 7.16 ppm for C_6D_6) for ^1H NMR spectroscopy. THF was used as solvents for No Deuterium

(NoD) NMR experiments,[10] and was referenced to added tetramethylsilane (0.00 ppm for both ^{1}H and $^{13}C\{^{1}H\}$ NMR spectroscopic experiments). Quantitative ^{1}H NMR data were acquired with a minimum of eight scans, with the delay time set to 5 x the longest T_1 value present. Chemical shifts are quoted in ppm and coupling constants in Hz. Tetrakis(trimethylsilyl)silane (TMS*) was used as internal standards for quantitative ^{1}H NMR spectroscopy. NMR spectra were taken at 25°C unless otherwise noted. Structural assignments were performed using HSQC and HMBC NMR spectroscopic experiments when necessary. Elemental analyses were carried out by the microanalytic services in the College of Chemistry at the University of California, Berkeley. Multiple attempts to collect data have been made but poor carbon combustion has been a problem. GC-MS measurements were acquired using an Agilent 7890B GC-MS system; LC-MS data was collected with the ACQUITY™ UPLC™ H-Class PLUS System; HRMS data was collected using a PerkinElmer HRMS. ATR-FTIR spectra were recorded on a Shimadzu IRSpirit FTIR spectrometer on neat powders.

Photochemical reactions. The station for photochemical reactions was equipped with a fan to maintain constant temperature, and unless otherwise stated, a single 40 W Kessil A160WE Tuna Blue lamp. The reactions were conducted in J-Young valved NMR tubes fixed at a distance of 7.5 cm from the light source unless otherwise stated.

Photophysical data. Quartz cells with a 10 mm pathlength equipped with a J-Young valve were used to contain samples prepared under a dinitrogen atmosphere for electronic absorption spectra (UV-Visible) and fluorescence measurements. UV-Visible measurements were collected on an Agilent Varian Cary 50 UV-Visible spectrophotometer. Emission and excitation spectra were collected on Fluorolog®-3 spectrofluorometer.

Crystallography. Single crystal X-ray diffraction data of **1-Ce** were collected using an Excalibur Eos diffractometer, fitted with a CCD area detector and using MoKα radiation (λ = 0.71073 Å) at 170 K. X-ray diffraction data for **3-Ce** were collected at beamline 12.2.1 of the Advanced Light Source (ALS) at Lawrence Berkeley National Lab, using a Bruker D8 diffractometer coupled to a Bruker PhotonII CPAD detector with Si(111)-monochromated synchrotron radiation (17 keV radiation). Single crystal X-ray diffraction data of all other compounds were collected using a Rigaku Xtalab Synergy-S diffractometer fitted with a HyPix-6000HE photon counting detector using MoKα (λ = 0.71073 Å) or CuKα (λ = 1.5418Å) radiation. All structures were solved using SHELXT in Olex2 and refined using SHELXL in Olex2.[86,87]Absorption corrections were completed using CrysAlis PRO (Rigaku Oxford Diffraction) software. Analytical numeric absorption corrections used a multifaceted crystal model based on expressions derived by Clark and Reid.[88] Numerical absorption correction was based on a Gaussian integration over a multifaceted crystal model.

Computational details. All the structures reported in this study were fully optimized with the Becke's 3-parameter hybrid functional[89] combined with the non-local correlation functional provided by Perdew/Wang (denoted as B3PW91).[90] The basis set used for lanthanum and cerium atom were the Stuttgart-Dresden small core ECP in combination with its adapted basis set.[91,92] For the Mg atom a 6-311++G(d,p) basis set was used whereas for all the other atoms a 6-31G(d,p) basis set was set.[93,94] In all computations no constraints were imposed on the geometry. All stationary points have been identified for minimum (number of imaginary frequencies Nimag=0). The vibrational modes and the corresponding frequencies are based on a harmonic force field. Gibbs Free energies were obtained at T=298.15K within the harmonic approximation. GAUSSIAN09 program suite was used in all calculations.[95] The UV-Visibleible spectra were simulated at the TDDFT level using the same functional.

Cyclic Voltammetry. Cyclic voltammetry (CV) was performed inside a glovebox under nitrogen atmosphere, using an EC Epsilon (BASi) potentiostat. The working electrodes were glassy carbon with an area of 0.071 cm^2 that were polished with Al_2O_3 (1 um, 0.3 um, 0.05 um) and rinsed with ultrapure water and acetone before the measurements. The counter electrode was a platinum wire. The reference electrode (Ag/Ag^+) consisted of a silver wire in a reservoir of the electrolyte solution to which a small amount of $AgBF_4$ was added, connected to the sample solution by a frit. Potentials were calibrated to the Fc/Fc^+ redox couple in each electrolyte solution. Experiments were performed in $TBAPF_6$ in THF (0.1 M) or in $TBABPh_4$ in THF (0.085 M, close to saturation) at room temperature. Analyte concentrations were kept at around 5 mM for the measurements.

Synthesis of 8. Method A: In a glovebox, an ampoule was charged with **1-Ce** (16.4 mg, 0.0236 mmol, 1.00 equiv.), **7** (6.5 mg, 0.0349 mmol, 28.6, 1.5 equiv.) and THF (1 mL). The ampoule was then heated to 70 °C and irradiated in front of a 40 W Kessil A160WE Tuna Blue lamp for 6 days. The reaction was then analyzed by ^{19}F NMR spectroscopy, and the product assigned as **8** in 50% yield in situ.

^{19}F NMR (376 MHz, THF-H_8) δ -95.8 (dd, *J* = 15.3, 4.4 Hz), -96.5 (dd, *J* = 14.9, 4.6 Hz), -98.5 (d, *J* = 14.1 Hz), -99.2 (d, *J* = 13.9 Hz).

Method B: Under nitrogen, diethylaminosulfur trifluoride (2.70 mL, 0.0205 mol, 3.00 equiv.), was added dropwise to an ice-cold solution of 2-methyl-2,3-dihydro-1*H*-inden-1-one (0.940 mL, 0.0680, 1.00 equiv.) in dichloromethane (20 mL). The reaction mixture was warmed to room temperature and then heated to reflux for 36 hours. The solution was cooled and added dropwise to a saturated aqueous sodium hydrogencarbonate, extracted with dichloromethane (3 x 10 mL), washed with brine, and dried over magnesium sulfate. Volatiles were removed under vacuum to yield trace of the crude product, identified by ^{19}F NMR, LCMS and HRMS.

^{19}F NMR (470 MHz, THF-H_8) δ -96.1 (dd, *J* = 15.2, 4.4 Hz), -96.6 (dd, *J* = 15.3, 4.4 Hz), -98.8 (d, *J* = 14.3 Hz), -99.3 (d, *J* = 14.2 Hz). m/z=168. HRMS Calcd $[2M+MeCN+H]^+$ 378.1942; found $[2M+MeCN+H]^+$ 378.1948. Residual = 1.586 ppm.

Synthesis of $[Mg(Bn)(L)]_2$ (9-Mg). To a cold (–78 °C) solution of **HL** (31.4 mg, 0.100 mmol, 1.00 equiv.) in THF (2 mL) was added a cold solution of $MgBn_2(THF)_2$ (35.0 mg, 0.100 mmol, 1.00 equiv.) dropwise over ten minutes. The mixture was allowed to warm to room temperature, with stirring, overnight. After this period, volatiles were removed by vacuum evaporation, and the cream powder washed with cold hexanes. Yield: 37.5 mg, 59%. Diffraction quality crystals were grown from a concentrated toluene solution at –30°C.

^1H NMR (500 MHz, C_6D_6, 298 K) : δ 7.59 (1H, d, J_{H-H} = 2.6, CH_{im}), 6.94 (d, J_{H-H} = 2.4, 1H, CH_{im}), 6.86 (2H, t, J_{H-H} = 7.5, CH_{Bn}), 6.69 (2H, d, J_{H-H} = 7.6, CH_{Bn}), 6.56 (1H, d, J_{H-H} = 1.7, CH_{Ph}), 6.53 (1H, J_{H-H} =7.2, CH_{Bn}), 5.82 (1H, d, J_{H-H} = 1.7, CH_{Ph}), 3.13 (1H, h, J_{H-H} = 6.6, CH_{iPr}), 2.00 (2H, dd, J_{H-H} = 8.9, CH_{2Bn}), 1.83 (9H, s, CH_{3tBu}), 1.35 (9H, s, CH_{3tBu}), 0.71 (3H, d, J_{H-H} = 6.6, CH_{3iPr}), 0.62 (3H, d, J_{H-H} = 6.6, CH_{3iPr}). ^{13}C NMR (125 MHz, C_6D_6, 298 K): δ 156.3 (s, C-O), 142.7 (s, C_{Ph}), 140.8 (s, C_{Ph}), 130.7 (s, NCN), 124.1 (s, C_{Bn}), 123.8 (s, C_{Bn}) 123.7 (s, C_{im}), 119.7 (s, C_{Ph}), 118.9 (s, C_{im}), 117.7 (s, C_{PhH}), 116.5 (s, C_{PhH}), 116.3 (s, C_{Bn}), 51.9 (s, C_{HiPr}), 36.2 (s, C_{CH3}), 34.5 (s, C_{CH3}), 31.8 (s, C_{tBu}), 32.6 (s, C_{tBu}), 25.1 (s, C_{H2Bn}), 23.8 (s, C_{iPr}), 23.3 (s, C_{iPr}). Anal. Calcd for: $C_{54}H_{74}Mg_2N_4O_2$: C, 75.43; H, 8.68; N, 6.52. Found: C, 71.67; H, 8.26; N,6.35.

Synthesis of $[Mg(L)]_2$ (10-Mg). Method A: To a solution of **HL** (62.8 mg, 0.200 mmol, 2 equiv.) in THF (2 mL) was added a solution of $MgBn_2(THF)_2$ (35.0 mg, 0.100 mmol, 1.00 equiv.). The mixture was stirred overnight. After this period, volatiles were removed by vacuum evaporation, and the cream powder washed with cold hexanes. Yield: 63.6 mg, 74% Diffraction quality crystals were grown from a concentrated toluene solution at –30°C.

Method B: To a solution of **HL** (6.28 mg, 0.0200 mmol, 1.00 equiv.) in THF (2 mL) was added a solution of **9-Mg** (6.36 mg, 0.004 mmol, 0.500 equiv.). The mixture was stirred overnight. After this period, **10-Mg** was observed by ^{1}H NMR spectroscopy.

^{1}H NMR (500 MHz, C_6D_6, 298 K) : δ 7.57 (2H, d, J_{H-H} = 2.5, CH_{im}), 7.2 (2H, d, J_{H-H} = 2.5, CH_{im}), 7.00 (2H, d, J_{H-H} = 1.8, CH_{Ph}), 6.22 (2H, d, J_{H-H} = 2.0, CH_{Ph}), 4.18 (2H, br s, CH_{iPr}), 1.78 (18H, s, CH_{3tBu}), 1.43 (18H, s, CH_{3tBu}), 1.01 (6H, d, J_{H-H} = 6.7, CH_{3iPr}), 0.90 (6H, d, J_{H-H} = 6.8, CH_{3iPr}). ^{13}C NMR (125 MHz, C_6D_6, 298 K): δ 156.8 (s, C_O), 141.7 (C_{Ph}), 134.4 (s, NCN), 129.3 (s, C_{Ph}), 128.6 (s, C_{Ph}), 125.7 (s, C_{Ph}), 122.3 (s, C_{Ph}), 120.6 (s, CH_{im}), 116.5 (s, CH_{im}), 115.5 (s, C_{Ph}), 52.5 (s,CH_{iPr}), 36.4 (s, C_{tBu}), 34.3 (s, C_{tBu}), 32.2 (s, $C_{(CH3)3}$), 30.2 (s, $C_{(CH3)3}$), 23.9 (s, C_{iPr}), 23.4 (C_{iPr}). Anal. Calcd for: $C_{40}H_{58}N_4O_2Mg$: C,73.77; H, 8.98; N, 8.60. Found: C, 71.45; H, 9.22; N, 7.27.

Targeting the synthesis of $[Ca(Bn)(L)]_x$. To a cold (–78 °C) solution of **HL** (31.4 mg, 0.100 mmol, 1.00 equiv.) in THF (2 mL) was added a cold solution of $CaBn_2(THF)_4$ (51.1 mg, 0.100 mmol, 1.00 equiv.) dropwise over ten minutes. The mixture was allowed to warm to room temperature, with stirring, overnight. After this period, volatiles were removed by vacuum evaporation, and the red powder washed with cold hexanes. The solid could not be characterized by ^{1}H NMR spectroscopy. Red crystals could be grown from layering a THF solution of the product with hexanes at –30 °C, but they were not suitable for characterization by XRD. Anal. Calcd for: $C_{27}H_{36}N_2OCa$: C,72.93; H, 8.16; N, 6.30. Found: C, 65.21; H, 7.68; N, 4.71.

Targeting the synthesis of $(Cp^{Me4})_2Ce(F)$. Method A: A Teflon-stoppered ampoule was charged with anhydrous cerium trifluoride (CeF_3) (43.3 mg, 0.219 mmol, 1.00 equiv.), KCp^{Me4} (71.4 mg, 0.445 mmol, 2.03 equiv.) and THF (5 mL), resulting in a pale yellow slurry. The ampoule was sealed and heated to 70°C for 24 hours, which resulted in no change to the reaction mixture.

Method B: In a glovebox $(Cp^{Me4})_2Ce(Bn)(THF)$ (**6-Ce**) (89.4 mg, 0.164 mmol, 1.00 equiv.) was dissolved in THF (5 mL), resulting in a yellow-green solution. With stirring, a solution of $BF_3(OEt)_2$ (47.8 mg, 0.337 mmol, 2.06 equiv.) in THF (2 mL) was added dropwise, resulting in a rapid color change to orange-yellow. The solution was stirred at room temperature for 1 hour, during which time the reaction mixture became turbid. The volatiles were then removed under vacuum, resulting in a pale, off-white residue. After washing with hexanes (2 x 3 mL), the residue was extracted with a minimum volume of toluene (4 mL) and filtered through glass fiber to yield a bright yellow solution. After layering with hexanes (16 mL), the solution was left to crystallize overnight, yielding large white blocks that were identified as $[(Cp^{Me4})_2Ce(\mu\text{–}BF_4)]_2$ (Figure 2.15).

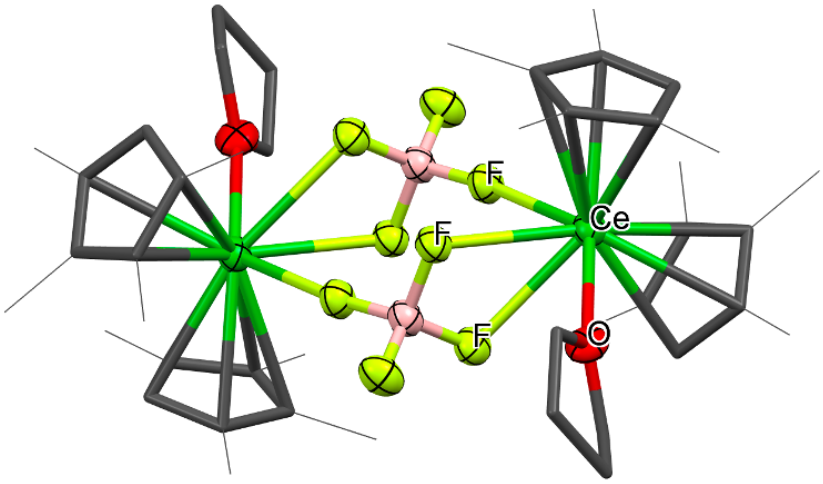

Figure 2.15. Molecular structure of $[(Cp^{Me4})_2Ce(\mu–BF_4)]_2$. Ellipsoids shown at 50% probability, peripheral groups drawn as wireframe, hydrogen atoms and lattice solvent molecules have been omitted for clarity. Color code: green – Ce; red – O; grey – C; bright green – F; pink – B.

Method C: To a 20 mL vial was added **6-Ce** (61.1 mg, 0.112 mmol, 1.00 equiv.) dissolved in THF (5 mL), resulting in a yellow-green solution. This solution was chilled in a freezer (–30 ºC) for 15 minutes. With stirring, a similarly chilled solution of BF_3OEt_2 (5.1 mg, 0.0359 mmol, 0.320 equiv.) in THF (2 mL) was added dropwise, resulting in a rapid color change to bright yellow. The solution was warmed to room temperature with stirring for 1 hour, during which time the reaction mixture became turbid, then lightened to a brighter yellow and became homogeneous. The volatiles were then removed *in vacuo*, resulting in a yellow-green residue. Extracting with hexanes (2 x 3 mL) gave a bright green solution, which ^{1}H NMR spectroscopy revealed to be $(Cp^{Me4})_3Ce$. The remaining yellow-orange residue was extracted with toluene and filtered to give a yellow-orange filtrate, which was analyzed by ^{1}H NMR spectroscopy and shown to contain either $CeBn_3(THF)_3$[96] or $(Cp^{Me4})CeBn_2$.

Reaction to target the chemical oxidation of 1-Ce and synthesis of $(Cp^{Me4})_2Ce(L)(Cl)$. In a glovebox, a vial was charged with **1-Ce** (22.0 mg, 0.0316 mmol, 1.00 equiv.) and toluene (2 mL) $PhICl_2$ (4.6 mg, 0.0167 mmol, 0.530 equiv.) in toluene (2 mL) was added dropwise resulting in a dark purple solution that bleached to pale purple within seconds. Only unreacted **1-Ce** could be recovered and characterized by ^{1}H NMR spectroscopy and single crystal X-ray diffraction.

Reactions to target the chemical oxidation of 1-La and synthesis of $(Cp^{Me4})_2La(L)(Cl)$. In a glovebox, a Young's valve-equipped NMR tube was charged with **1-La** (13.1 mg, 0.0189 mmol, 1.00 equiv.), $PhICl_2$ (3.0 mg, 0.0109 mmol, 0.580 equiv.) and THF (0.6 mL), resulting in a pale yellow solution. The tube was sealed and monitored by ^{1}H NMR spectroscopy. After 20 minutes a color change to dark yellow-brown was observed. ^{1}H NMR analysis showed only trace amounts of **1-La** remaining in solution, as well as the formation of a new, diamagnetic species that has a 1:1 ratio of Cp^{Me4} to **L** ligand, which could not be characterized by ^{1}H NMR spectroscopy, fractional crystallization or FT-IR.

Reaction to target the chemical oxidation of 9-Mg. In a glovebox, a Young's valve-equipped NMR tube was charged with **9-Mg** (11.1 mg, 0.0129 mmol, 1.00 equiv.), $PhICl_2$ (1.6 mg, 0.00582 mmol, 0.450 equiv.) and THF (0.6 mL), resulting in a very pale yellow solution. The

tube was sealed and monitored by ^{1}H NMR spectroscopy. After 4 hours, ^{1}H NMR analysis showed no reaction between **9-Mg** and $PhICl_2$.

Targeting the synthesis of $(Cp^{Me4})_2Ce(L)(F)$. Method A: In a glovebox a vial was charged with **1-Ce** (19.5 mg, 0.0280 mmol, 1.00 equiv.) and toluene (5 mL). 1-(Chloromethyl)-4-fluoro-1,4-diazabicyclo[2.2.2]octane-1,4-diium ditetrafluoroborate (Selectfluor) (9.8 mg, 0.0280 mmol, 1.00 equiv.) was added, and the orange solution stirred at room temperature. Following 16 hours stirring, no reaction was observed.

Method B: In a glovebox a vial was charged with **1-Ce** (20.5 mg, 0.0294 mmol, 1.00 equiv.) and toluene (2 mL). A solution of N-fluorobenzenesulfonimide (NFSI) (14.2 mg, 0.0450 mmol, 1.50 equiv.) in toluene (2 mL) was added, and the orange solution quickly darkened to purple characteristic of Ce(IV). Following 15 minutes stirring the color had changed to black, and no material could be characterized by ^{1}H NMR spectroscopy or crystallization.

Targeting the synthesis of $(Cp^{Me4})_2La(L)(F)$. Method A**:** In a glovebox a Young's valve-equipped NMR tube was charged with **1-La** (6.95 mg, 0.0100 mmol, 1.00 equiv.) and THF (0.5 mL). Xenon difluoride (XeF_2) (1.9 mg, 0.0110 mmol, 1.10 equiv.) was added, and the tube sealed and monitored by ^{1}H NMR and ^{19}F spectroscopy. Following 20 minutes the complete consumption of **1-La** and **XeF_2** was observed, and no peaks seen in ^{19}F NMR spectra. Volatiles were removed under vacuum, and the resulting pale-yellow solid was unable to be characterized by X-ray diffraction or FT-IR.

General procedure for the unoptimized stoichiometric C–F activation of $PhCF_3$. In a glovebox, a Young's valve-equipped NMR tube was charged with metal complex (0.0100 mmol, 1.00 equiv.) and THF (0.5 mL). $PhCF_3$ (1.23 μL, 0.0100 mmol, 1.00 equiv.) was then added using a micropipette. The sample was then irradiated with light and monitored periodically by ^{1}H and ^{19}F NMR spectroscopy. Final time point measurements were collected after 48 hours.

General procedure for the optimized stoichiometric C–F activation of $PhCF_3$. In a glovebox, a Young's valve-equipped NMR tube was charged with metal complex (0.0100 mmol, 1.00 equiv.) and THF (0.5 mL). $PhCF_3$ (6.13 μL, 0.0500 mmol, 5.00 equiv.) was then added using a micropipette. The sample was then irradiated with light at 70°C and monitored periodically by ^{1}H and ^{19}F NMR spectroscopy. Final time point measurements were collected after 120 hours.

Evidence for fluoride generation in defluoroalkyation mechanism. The general procedure for 1 mol % catalytic defluoroalkylative coupling of $PhCF_3$ with $MgBn_2(THF)_2$ in THF-H_8 was followed. Following the completion of the reaction, the sample tube was taken into a glovebox, opened, and a drop of trimethylsilyl chloride (ca. 0.05 mL, 0.393 mmol) added. The sample was then sonicated to ensure thorough mixing and analyzed by ^{19}F NMR spectroscopy. The generation of fluorotrimethylsilane was observed.[98]

General procedure for stoichiometric C–F activation substrate scope with 1-Ce. In a glovebox, a Young's valve-equipped NMR tube was charged with **1-Ce** (7.0 mg, 0.0100 mmol, 1.00 equiv.) and THF (0.5 mL). Fluorinated substrate (0.0500 mmol, 5.00 equiv.) was then added using a micropipette. The sample was then irradiated with light and analyzed by ^{1}H and ^{19}F NMR spectroscopy after 20 hours. Substrates: trifluoromethoxybenzene; 1,3-bis(trifluoromethyl)benzene; 1 ,4-bis(trifluoromethyl)benzene, hexafluorobenzene.

C–F activation of pentafluoro(trifluoromethyl)benzene with 1-Ce. In a glovebox, a Young's valve-equipped NMR tube was charged with **1-Ce** (10.6 mg, 0.0152 mmol, 1.00 equiv.), pentafluoro(trifluoromethyl)benzene (18.1 mg, 0.0767 mmol, 5.04 equiv.) and THF (0.5 mL), resulting in an orange-pink solution. The tube was sealed, placed in front of a 427 nm lamp and monitored periodically by ^{1}H and ^{19}F NMR spectroscopy. After 2 days of irradiation, the solution had changed color to dark red-brown, and ^{19}F NMR spectroscopy several products of C–F activation of the aryl C–F bonds, with no activation of the CF_3 moiety. Two of the new products were identified as 2,3,5,6-tetrafluorobenzotrifluoride and 2,2',3,3',5,5',6,6'-octafluoro-4,4'-bis(trifluoromethyl)-1,1'-biphenyl.

Reaction of 1-Ce with 7. In a glovebox, a cuvette fitted with a Young's tap was charged with **1-Ce** (20.0 mg, 0.0287 mmol, 1.00 equiv.) and THF (2 mL). **7** (26.8 mg, 0.144 mmol, 5.00 equiv.) was then added, and the cuvette sealed. The sample was then irradiated with a 40 W Kessil A160WE Tuna Blue lamp at 70°C. Following 6 days irradiation **8** was observed in 50% by ^{19}F NMR spectroscopy.

Reaction of 1-La with 7. Method A: In a glovebox, a cuvette fitted with a Young's tap was charged with **1-La** (19.9 mg, 0.0287 mmol, 1.00 equiv.) and THF (2 mL). **7** (26.8 mg, 0.144 mmol, 5.00 equiv.) was then added, and the cuvette sealed. The sample was then irradiated with a 40 W Kessil A160WE Tuna Blue lamp at room temperature. Following 6 days irradiation only the decomposition of **1-La** and unreacted **7** could be observed by NMR spectroscopy.

Method B: In a glovebox, a cuvette fitted with a Young tap was charged with **1-La** (19.9 mg, 0.0287 mmol, 1.00 equiv.) and THF (2 mL). **7** (26.8 mg, 0.144 mmol, 5.00 equiv.) was then added, and the cuvette sealed. The sample was then irradiated with a 40 W Kessil A160WE Tuna Blue lamp at room temperature. Following 6 days irradiation **8** was observed in 20% by ^{19}F NMR spectroscopy.

Reaction of 1-Ce with 1-(allyloxy)-2-(trifluoromethyl)benzene. In a glovebox, a Young's valve-equipped NMR tube was charged with **1-Ce** (14.8 mg, 0.0213 mmol, 1.00 equiv.), 1-(allyloxy)-2-(trifluoromethyl)benzene (6.6 mg, 0.0326 mmol, 1.53 equiv.), and THF (0.6 mL). The tube was sealed, placed in front of a 40 W Kessil A160WE Tuna Blue lamp and monitored periodically by ^{1}H and ^{19}F NMR spectroscopy. After 16 hours of irradiation, ^{1}H NMR showed mostly unreacted **1-Ce**, and ^{19}F NMR showed only trace formation of a new difluoromethylene-containing product, as well as unreacted starting material. Further irradiation for several days did not result in a significant increase in the amount of new product.

General procedure for stoichiometric defluoroalkylative coupling of $PhCF_3$ with alkenes. In a glovebox, a Young's valve-equipped NMR tube was charged with catalyst (0.0500 mmol, 5.00 equiv.) and THF (0.5 mL). Alkene (0.0500 mmol, 5.00 equiv.) was then added using a micropipette. The sample was then irradiated with light and monitored periodically by ^{1}H and ^{19}F NMR spectroscopy, with a final time point being taken after 110 hours irradiation.

General procedure for 20 mol % catalytic defluoroalkylative coupling of $PhCF_3$ with $MgBn_2(THF)_2$ in THF-H_8. In a glovebox, a vial was charged with $MgBn_2(THF)_2$, (17.5 mg, 0.0500 mmol, 1.00 equiv.) $PhCF_3$ (6.13 μL, 0.0500 mmol, 1.00 equiv.) and THF (0.5 mL). The solution was then used to dissolve the metal complex (0.0100 mmol, 0.200 equiv.), and the reaction mixture transferred to a Young's valve-equipped NMR tube. The sample was

irradiated with a 40 W Kessil A160WE Tuna Blue lamp and monitored periodically by ^{1}H and ^{19}F NMR spectroscopy, with a time point for all reactions measured after 48 hours.

20 mol % catalytic defluoroalkylative coupling of $PhCF_3$ with $Mg(allyl)_2(THF)_2$ in THF-H_8. In a glovebox, a vial was charged with $Mg(allyl)_2(THF)_2$, (12.5 mg, 0.0500 mmol, 1.00 equiv.) $PhCF_3$ (6.13 μL, 0.0500 mmol, 1.00 equiv.) and THF (0.5 mL). The solution was then used to dissolve **1-Ce** (7.0 mg, 0.0100 mmol, 0.200 equiv.), and the reaction mixture transferred to a Young's valve-equipped NMR tube. The sample was irradiated with a 40 W Kessil A160WE Tuna Blue lamp for 48 hours at room temperature, before being analyzed by ^{1}H and ^{19}F NMR spectroscopy. (1,1-difluorobut-3-en-1-yl)benzene was observed in 2% yield.

20 mol % catalytic defluoroalkylative coupling of $PhCF_3$ with $Mg(Ph)_2(THF)_2$ in THF-H_8. In a glovebox, a vial was charged with $Mg(Ph)_2(THF)_2$, (16.1 mg, 0.0500 mmol, 1.00 equiv.) $PhCF_3$ (6.13 μL , 0.0500 mmol, 1.00 equiv.) and THF (0.5 mL). The solution was then used to dissolve **1-Ce** (7.0 mg, 0.0100 mmol, 0.200 equiv.), and the reaction mixture transferred to a Young's valve-equipped NMR tube. The sample was irradiated with a 40 W Kessil A160WE Tuna Blue lamp for 48 hours at room temperature, before being analyzed by ^{1}H and ^{19}F NMR spectroscopy. Difluorodiphenylmethane and $PhCF_2H$ were observed in a combined 31 % yield.

20 mol % catalytic defluoroalkylative coupling of $PhCF_3$ with $Bu_3Sn(allyl)$ in THF-H_8. In a glovebox, a vial was charged with $Bu_3Sn(allyl)$ (16.6 mg, 0.0500 mmol, 1.00 equiv.) $PhCF_3$ (6.13 μL , 0.0500 mmol, 1.00 equiv.) and THF (0.5 mL). The solution was then used to dissolve **1-Ce** (7.0 mg, 0.0100 mmol, 0.2 equiv.), and the reaction mixture transferred to a Young's valve-equipped NMR tube. The sample was irradiated with a 40 W Kessil A160WE Tuna Blue lamp for 48 hours at room temperature, before being analyzed by ^{1}H and ^{19}F NMR spectroscopy. (1,1-difluorobut-3-en-1-yl)benzene and $PhCF_2H$ were observed in combined 7% yield.

Reaction to target the 20 mol % catalytic defluoroalkylative coupling of $PhCF_3$ with $Mg(Mes)_2(THF)_2$ in THF-H_8. In a glovebox, a vial was charged with $Mg(Mes)_2(THF)_2$ (20.2 mg, 0.0500 mmol, 1.00 equiv.) $PhCF_3$ (6.13 μL , 0.0500 mmol, 1.00 equiv.) and THF (0.5 mL). The solution was then used to dissolve **1-Ce** (7.0 mg, 0.0100 mmol, 0.200 equiv.), and the reaction mixture transferred to a Young's valve-equipped NMR tube. The sample was irradiated with a 40 W Kessil A160WE Tuna Blue lamp for 5 days at room temperature, before being analyzed by ^{1}H and ^{19}F NMR spectroscopy. Difluorotoluene was observed in 70% yield by ^{19}F NMR spectroscopy.

General procedure for 20 mol % catalytic defluoroalkylative coupling of $PhCF_3$ with $MgBn_2(THF)_2$ in THF-H_8 by 1-Ce under different irradiation wavelengths. In a glovebox, a vial was charged with $MgBn_2(THF)_2$, (17.5 mg, 0.0500 mmol, 1.00 equiv.) $PhCF_3$ (6.13 μL , 0.0500 mmol, 1.00 equiv.) and THF (0.5 mL). The solution was then used to dissolve **1-Ce** (7.0 mg, 0.0100 mmol, 0.200 equiv.), and the reaction mixture transferred to a Young's valve-equipped NMR tube. Each sample was irradiated with a different wavelength Kessil lamp at maximum power (390, 467, 505 nm) and analyzed by ^{1}H and ^{19}F NMR spectroscopy, with a time point for all reactions measured after 42 hours.

General procedure for 1 mol % catalytic defluoroalkylative coupling of $PhCF_3$ with $MgBn_2(THF)_2$ in THF-H_8. In a glovebox, a vial was charged with $MgBn_2(THF)_2$ (87.7 mg, 2.50 mmol, 1.00 equiv.) in THF (0.5 mL) and $PhCF_3$ (30.7 μL, 2.50 mmol, 1.00 equiv.). The

solution was then used to dissolve the catalyst (0.0025 mmol, 0.0100 equiv.), and the reaction mixture transferred to a Young's valve-equipped NMR tube with a capillary containing 1,2-difluorobenzene as internal standard. The sample was irradiated with a 40 W Kessil A160WE Tuna Blue lamp and monitored periodically by ^{1}H and ^{19}F NMR spectroscopy every 21 hours for a maximum of 84 hours.

General procedure for 1 mol % catalytic defluoroalkylative coupling of $PhCF_3$ with $MgBn_2(THF)_2$ in THF-D_8. In a glovebox, a vial was charged with $MgBn_2(THF)_2$ (87.7 mg, 2.50 mmol, 1.00 equiv.) in THF-D_8 (0.5 mL) and $PhCF_3$ (30.7 μL, 2.50 mmol, 1.00 equiv.). The solution was then used to dissolve the catalyst, and the reaction mixture transferred to a Young's valve-equipped NMR tube with a capillary containing 1,2-difluorobenzene. The sample was irradiated with a 40 W Kessil A160WE Tuna Blue lamp and monitored by ^{1}H and ^{19}F NMR spectroscopy after 42 hours.

Control experiments for the defluoralkylative coupling of $PhCF_3$ with $MgBn_2(THF)_2$ in THF-H_8 in the absence of light. In a glovebox, a vial was charged with $MgBn_2(THF)_2$, (1.00 equiv.) $PhCF_3$ (1.00 equiv.) and THF (0.5 mL). The solution was then used to dissolve the metal complex (0.200—0.0100 equiv.), and the reaction mixture transferred to a Young's valve-equipped NMR tube. The sample was wrapped in aluminum foil, stored in the dark and monitored periodically by ^{1}H and ^{19}F NMR spectroscopy; no product formation was observed.

Control experiment between $PhCF_3$ and $MgBn_2(THF)_2$ in the absence of catalyst. In a glovebox, a vial was charged with $MgBn_2(THF)_2$, (35.5 mg, 1.0 mmol, 1.00 equiv.) $PhCF_3$ (61.4 μL, 5.0 mmol, 5.00 equiv.) and THF (0.5 mL). The solution was then transferred to a Young's valve-equipped NMR tube. The sample was irradiated with a 40 W Kessil A160WE Tuna Blue lamp and monitored by ^{1}H and ^{19}F NMR spectroscopy until final measurements were recorded after 260 hours.

Experiment to show solution interactions between 1-Ce and $PhCF_3$. In a glovebox, 0.5 mL of a 325 μM solution of $PhCF_3$ in THF-H_8 was added to a Young-tapped NMR tube with a capillary containing the same 325 μM solution of $PhCF_3$ in THF-H_8. The sample was analyzed by ^{1}H and ^{19}F NMR spectroscopy before the addition of **1-Ce** (7.0 mg, 0.0100 mmol). A second ^{1}H and ^{19}F spectrum was then recorded, and shift of 0.09 ppm observed between the ^{19}F resonance of $PhCF_3$ inside and outside the capillary which could be attributed to an interaction between $PhCF_3$ and **1-Ce**.

Experiment to show solution interactions between 1-La and $PhCF_3$. In a glovebox, 0.5 mL of a 325 μM solution of $PhCF_3$ in THF-H_8 was added to a Young-tapped NMR tube with a capillary containing the same 325 μM solution of $PhCF_3$ in THF-H_8. The sample was analyzed by ^{1}H and ^{19}F NMR spectroscopy before the addition of **1-La** (6.9 mg, 0.0100 mmol)**.** A second ^{1}H and ^{19}F spectrum was then recorded, and shift of 0.03 ppm observed between the ^{19}F resonance of $PhCF_3$ inside and outside the capillary which could be attributed to an interaction between $PhCF_3$ and **1-La**.

Formation of 9-Mg via addition of $MgBn_2(THF)_2$ to 1-Ce. In a glovebox, a Young's valve-equipped NMR tube was charged with **1-Ce** (12.0 mg, 0.0172 mmol, 1.00 equiv.), $MgBn_2(THF)_2$ (30.1 mg, 0.0860 mmol, 5.00 equiv.), THF (0.5 mL) and an internal standard. The tube was then sealed and monitored by ^{1}H NMR spectroscopy for a total of 24 hours. Less than 1% conversion to **9-Mg** was observed over this time.

Formation of 9-Mg via addition of $MgBn_2(THF)_2$ to 1-La. In a glovebox, a Young's valve-equipped NMR tube was charged with **1-La** (11.9 mg, 0.0172 mmol, 1.00 equiv.), $MgBn_2(THF)_2$ (30.1 mg, 0.0860 mmol, 5.00 equiv.), THF (0.5 mL) and an internal standard. The tube was then sealed and monitored by ^1H NMR spectroscopy for a total of 24 hours. Over this time 30% conversion to **9-Mg** was observed.

Formation of 6-Ce from 4-Ce in the presence of $MgBn_2(THF)_2$ under irradiation. In a glovebox, a vial was charged with $MgBn_2(THF)_2$, (17.5 mg, 0.0500 mmol, 1.00 equiv.) $PhCF_3$ (6.13 μL, 0.0500 mmol, 1.00 equiv.) and THF (0.5 mL). The solution was then used to dissolve **4a-Ce** (6.8 mg, 0.0100 mmol, 0.200 equiv.), and the reaction mixture transferred to a Young's valve-equipped NMR tube. The tube was then sealed, placed in front of a 40 W Kessil A160WE Tuna Blue lamp and monitored and irradiated for 72 hours. Following this time, the complete conversion of **4-Ce** to **6-Ce** and 2,6-di-*tert*-butyl-4-methylphenol was observed.

Formation of $Mg(N\{SiMe_3\}_2)_2(THF)_2$ from $Ce(N\{SiMe_3\}_2)_3$ in the presence of $MgBn_2(THF)_2$ under irradiation. In a glovebox, a vial was charged with $MgBn_2(THF)_2$, (17.5 mg, 0.0500 mmol, 1.00 equiv.) $PhCF_3$ (6.13 μL , 0.0500 mmol, 1.00 equiv.) and THF (0.5 mL). The solution was then used to dissolve $Ce(N\{SiMe_3\}_2)_3$ (6.2 mg, 0.0100 mmol, 0.200 equiv.), and the reaction mixture transferred to a Young's valve-equipped NMR tube. The tube was then sealed, placed in front of a 40 W Kessil A160WE Tuna Blue lamp and monitored and irradiated for 72 hours. Following this time, a color change from bright yellow to golden yellow was observed. The solution was decanted into a vial in a glovebox, and cooled to –30°C, yielding yellow needles that were identified by single crystal X-ray diffraction as $Mg(N\{SiMe_3\}_2)_2(THF)_2$.

Formation of 2-Ce from 6-Ce under irradiation. In a glovebox, a Young's valve-equipped NMR tube was charged with **6-Ce** (10.1 mg, 0.0185 mmol, 1.00 equiv.), THF (0.5 mL) and an internal standard. The tube was then sealed, placed in front of a 40 W Kessil A160WE Tuna Blue lamp and monitored and irradiated for 72 hours. Following this time, the complete decomposition of **6-Ce** to **2-Ce**, bibenzyl, and an unidentified cerium-containing by product was observed by ^1H NMR spectroscopy.

Catalytic defluoroalkylative coupling of $PhCF_3$ with $MgBn_2(THF)_2$ in THF-H_8 by 1-La under 390 nm light irradiation. In a glovebox, a vial was charged with $MgBn_2(THF)_2$, (17.5 mg, 0.0500 mmol, 1.00 equiv.) $PhCF_3$ (6.13 μL, 0.0500 mmol, 1.00 equiv.) and THF (0.5 mL). The solution was then used to dissolve **1-La** (6.9 mg, 0.001 mmol, 0.200 equiv.), and the reaction mixture transferred to a Young's valve-equipped NMR tube. The sample was irradiated with a different 390 nm Kessil lamp at maximum power and analyzed by ^1H and ^{19}F NMR spectroscopy for 48 hours. Following this time, the decomposition of **1-La**, and numerous unidentified fluorinated products, were observed, with 1% conversion to $PhCF_2H$ and no conversion to $PhCF_2CH_2Ph$ seen by ^{19}F NMR spectroscopy.

Testing for NHC lability using variable temperature (VT) NMR spectroscopy. In a glovebox, a Young's valve-equipped NMR tube was charged with **1-Ce** (20.0 mg, 0.0287 mmol, 1.00 equiv.), $MgBn_2(THF)_2$ (10.1 mg, 0.0287 mmol, 5.00 equiv.) and THF (0.5 mL) The tube was then sealed and monitored by VT ^1H NMR spectroscopy. No evidence of NHC lability was observed (Figure 2.16).

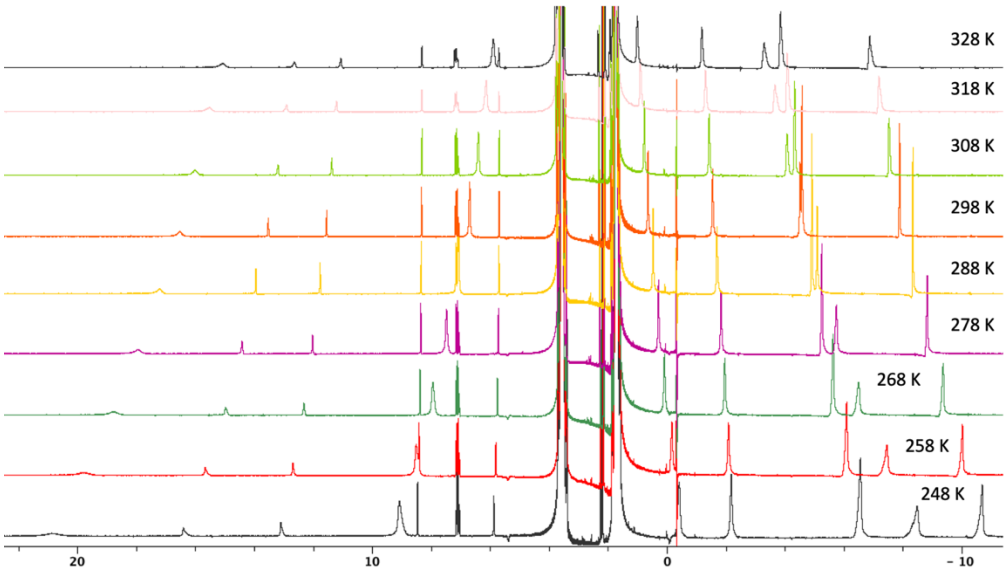

Figure 2.16. Variable temperature NoD ^{1}H NMR of **1-Ce** in THF-H_8 with one equivalent $MgBn_2(THF)_2$.

Table 2.5. Crystal data and structure refinement for **9-Mg**, **10-Mg** and $[(Cp^{Me4})_2Ce(\mu–BF_4)]_2$.

	9-Mg	**10-Mg**	**$[(Cp^{Me4})_2Ce(\mu–BF_4)]_2$**
Empirical formula	$C_{57.5}H_{76}Mg_2N_4O_2$	$C_{92}H_{142}Mg_2N_8O_4$	$C_{51}H_{76}B_2Ce_2F_8O_2$
Formula weight	903.84	1472.75	1174.94
Temperature/K	99.99(13)	100.00(11)	100.00(11)
Crystal system	monoclinic	triclinic	triclinic
Space group	$P2_1/n$	P-1	P-1
a/Å	13.1713(2)	13.91760(10)	8.8809(2)
b/Å	18.0503(2)	17.0140(3)	10.2164(2)
c/Å	23.2076(4)	19.2571(3)	15.0376(3)
α/°	90	99.0740(10)	94.808(2)
β/°	104.996(2)	98.3570(10)	103.253(2)
γ/°	90	91.4750(10)	105.252(2)
Volume/Å^3	5329.61(14)	4449.56(11)	1266.08(5)
Z	4	2	1
ρ_{calc}g/cm^3	1.126	1.099	1.541
μ/mm^{-1}	0.731	0.638	1.842
F(000)	1956	1612	596
Crystal size/mm^3	0.2 × 0.18 × 0.14	0.164 × 0.149 × 0.09	0.312 × 0.209 × 0.
Radiation	Cu Kα (λ = 1.54184)	Cu Kα (λ = 1.54184)	Mo Kα (λ = 0.71073)
2Θ range for data collection/°	6.286 to 154.828	5.266 to 148.996	4.182 to 62.112
Index ranges	-16 ≤ h ≤ 16, -22 ≤ k ≤ 15, -29 ≤ l ≤ 29	-17 ≤ h ≤ 15, -21 ≤ k ≤ 21, -23 ≤ l ≤ 24	-12 ≤ h ≤ 12, -13 ≤ k ≤ 14, -19 ≤ l ≤ 20
Reflections collected	104258	91809	268653
Independent reflections	11176 [R_{int} = 0.0709, R_{sigma} = 0.0316]	18131 [R_{int} = 0.0443, R_{sigma} = 0.0330]	6635 [Rint = 0.0920, Rsigma = 0.0632]
Data/restraints/parameters	11176/524/699	18131/284/1077	6635/646/454
Goodness-of-fit on F^2	1.022	1.045	0.978
Final R indexes [I>=2σ (I)]	R_1 = 0.0598, wR_2 = 0.1611	R_1 = 0.0494, wR_2 = 0.1188	R1 = 0.0337, wR2 = 0.0712
Final R indexes [all data]	R_1 = 0.0708, wR_2 = 0.1696	R_1 = 0.0585, wR_2 = 0.1238	R_1 = 0.0396, wR_2 = 0.0746
Largest diff. peak/hole / e Å^{-3}	0.84/-0.41	0.50/-0.34	0.60/-1.01

2.6 References

(1) Van Leeuwen, P. W. N. M. *Homogeneous Catalysis: Understanding the Art*; Springer Netherlands: Dordrecht, 2004. https://doi.org/10.1007/1-4020-2000-7.

(2) Hironaka, K.; Fukuzumi, S.; Tanaka, T. Tris(Bipyridyl)Ruthenium(II)-Photosensitized Reaction of 1-Benzyl-1,4-Dihydronicotinamide with Benzyl Bromide. *J. Chem. Soc., Perkin Trans. 2* **1984**, No. 10, 1705. https://doi.org/10.1039/p29840001705.

(3) Van Hoomissen, D. J.; Vyas, S. Impact of Conjugation and Hyperconjugation on the Radical Stability of Allylic and Benzylic Systems: A Theoretical Study. *J. Org. Chem.* **2017**, *82* (11), 5731–5742. https://doi.org/10.1021/acs.joc.7b00549.

(4) Nguyen, J. D.; D'Amato, E. M.; Narayanam, J. M. R.; Stephenson, C. R. J. Engaging Unactivated Alkyl, Alkenyl and Aryl Iodides in Visible-Light-Mediated Free Radical Reactions. *Nature Chem* **2012**, *4* (10), 854–859. https://doi.org/10.1038/nchem.1452.

(5) Shen, Y.; Cornella, J.; Juliá-Hernández, F.; Martin, R. Visible-Light-Promoted Atom Transfer Radical Cyclization of Unactivated Alkyl Iodides. *ACS Catal.* **2017**, *7* (1), 409–412. https://doi.org/10.1021/acscatal.6b03205.

(6) Nicewicz, D. A.; Nguyen, T. M. Recent Applications of Organic Dyes as Photoredox Catalysts in Organic Synthesis. *ACS Catal.* **2014**, *4* (1), 355–360. https://doi.org/10.1021/cs400956a.

(7) Prier, C. K.; Rankic, D. A.; MacMillan, D. W. C. Visible Light Photoredox Catalysis with Transition Metal Complexes: Applications in Organic Synthesis. *Chem. Rev.* **2013**, *113* (7), 5322–5363. https://doi.org/10.1021/cr300503r.

(8) Guo, J.-J.; Hu, A.; Chen, Y.; Sun, J.; Tang, H.; Zuo, Z. Photocatalytic C−C Bond Cleavage and Amination of Cycloalkanols by Cerium(III) Chloride Complex. *Angew. Chem. Int. Ed.* **2016**, *128* (49), 15545–15548. https://doi.org/10.1002/ange.201609035.

(9) Cheisson, T.; Schelter, E. J. Rare Earth Elements: Mendeleev's Bane, Modern Marvels. *Science* **2019**, *363* (6426), 489–493. https://doi.org/10.1126/science.aau7628.

(10) Arnold, P. L.; Kerr, R. W. F.; Weetman, C.; Docherty, S. R.; Rieb, J.; Cruickshank, F. L.; Wang, K.; Jandl, C.; McMullon, M. W.; Pöthig, A.; Kühn, F. E.; Smith, A. D. Selective and Catalytic Carbon Dioxide and Heteroallene Activation Mediated by Cerium N-Heterocyclic Carbene Complexes. *Chem. Sci.* **2018**, *9* (42), 8035–8045. https://doi.org/10.1039/c8sc03312a.

(11) Kerr, R. W. F.; Ewing, P. M. D. A.; Raman, S. K.; Smith, A. D.; Williams, C. K.; Arnold, P. L. Ultrarapid Cerium(III)-NHC Catalysts for High Molar Mass Cyclic Polylactide. *ACS Catal.* **2021**, *11* (3), 1563–1569. https://doi.org/10.1021/acscatal.0c04858.

(12) Smart, B. E. Characteristics of C-F Systems BT - Organofluorine Chemistry: Principles and Commercial Applications. **1994**, 57–88.

(13) Müller, K.; Faeh, C.; Diederich, F. Fluorine in Pharmaceuticals: Looking Beyond Intuition. *Science* **2007**, *317* (5846), 1881–1886. https://doi.org/10.1126/science.1131943.

(14) Janjetovic, M.; Träff, A. M.; Ankner, T.; Wettergrena, J.; Hilmersson, G. Solvent Dependent Reductive Defluorination of Aliphatic C–F Bonds Employing Sm(HMDS)2. *Chem. Commun.* **2013**, *49* (18), 1826–1828. https://doi.org/10.1039/c3cc37828d.

(15) Träff, A. M.; Janjetovic, M.; Ta, L.; Hilmersson, G. Selective C-F Bond Activation: Substitution of Unactivated Alkyl Fluorides Using YbI3. *Angewandte Chemie - International Edition* **2013**, *52* (46), 12073–12076. https://doi.org/10.1002/anie.201306104.

(16) Janjetovic, M.; Träff, A. M.; Hilmersson, G. Mild and Selective Activation and Substitution of Strong Aliphatic C-F Bonds. *Chemistry - A European Journal* **2015**, *21* (9), 3772–3777. https://doi.org/10.1002/chem.201406097.

(17) Meanwell, N. A. Synopsis of Some Recent Tactical Application of Bioisosteres in Drug Design. *J. Med. Chem.* **2011**, *54* (8), 2529–2591. https://doi.org/10.1021/jm1013693.

(18) Iwamoto, H.; Imiya, H.; Ohashi, M.; Ogoshi, S. Cleavage of C(Sp3)-F Bonds in Trifluoromethylarenes Using a Bis(NHC)Nickel(0) Complex. *J. Am. Chem. Soc.* **2020**, *142* (45), 19360–19367. https://doi.org/10.1021/jacs.0c09639.
(19) Sap, J. B. I.; Straathof, N. J. W.; Knauber, T.; Meyer, C. F.; Meyer, C. F.; Médebielle, M.; Buglioni, L.; Genicot, C.; Trabanco, A. A.; Noël, T.; Am Ende, C. W.; Gouverneur, V. Organophotoredox Hydrodefluorination of Trifluoromethylarenes with Translational Applicability to Drug Discovery. *Journal of the American Chemical Society* **2020**, *142* (20), 9181–9187. https://doi.org/10.1021/jacs.0c03881.
(20) Luo, Y. C.; Tong, F. F.; Zhang, Y.; He, C. Y.; Zhang, X. Visible-Light-Induced Palladium-Catalyzed Selective Defluoroarylation of Trifluoromethylarenes with Arylboronic Acids. *J. Am. Chem. Soc.* **2021**, *143* (34), 13971–13979. https://doi.org/10.1021/jacs.1c07459.
(21) Luo, C.; Bandar, J. S. Selective Defluoroallylation of Trifluoromethylarenes. *Journal of the American Chemical Society* **2019**, *141* (36), 14120–14125. https://doi.org/10.1021/jacs.9b07766.
(22) Mandal, D.; Gupta, R.; Jaiswal, A. K.; Young, R. D. Frustrated Lewis-Pair-Meditated Selective Single Fluoride Substitution in Trifluoromethyl Groups. *Journal of the American Chemical Society* **2020**, *142* (5), 2572–2578. https://doi.org/10.1021/jacs.9b12167.
(23) Yoshida, S.; Shimomori, K.; Kim, Y.; Hosoya, T. Single C−F Bond Cleavage of Trifluoromethylarenes with an *Ortho* -Silyl Group. *Angew. Chem. Int. Ed.* **2016**, *55* (35), 10406–10409. https://doi.org/10.1002/anie.201604776.
(24) Discekici, E. H.; Treat, N. J.; Poelma, S. O.; Mattson, K. M.; Hudson, Z. M.; Luo, Y.; Hawker, C. J.; De Alaniz, J. R. A Highly Reducing Metal-Free Photoredox Catalyst: Design and Application in Radical Dehalogenations. *Chem. Commun.* **2015**, *51* (58), 11705–11708. https://doi.org/10.1039/C5CC04677G.
(25) Vogt, D. B.; Seath, C. P.; Wang, H.; Jui, N. T. Selective C-F Functionalization of Unactivated Trifluoromethylarenes. *Journal of the American Chemical Society* **2019**, *141* (33), 13203–13211. https://doi.org/10.1021/jacs.9b06004.
(26) Wang, H.; Jui, N. T. Catalytic Defluoroalkylation of Trifluoromethylaromatics with Unactivated Alkenes. *J. Am. Chem. Soc.* **2018**, *140* (1), 163–166. https://doi.org/10.1021/jacs.7b12590.
(27) Pearson, R. M.; Lim, C.-H.; McCarthy, B. G.; Musgrave, C. B.; Miyake, G. M. Organocatalyzed Atom Transfer Radical Polymerization Using *N* -Aryl Phenoxazines as Photoredox Catalysts. *J. Am. Chem. Soc.* **2016**, *138* (35), 11399–11407. https://doi.org/10.1021/jacs.6b08068.
(28) Chen, K.; Berg, N.; Gschwind, R.; König, B. Selective Single C(Sp3)-F Bond Cleavage in Trifluoromethylarenes: Merging Visible-Light Catalysis with Lewis Acid Activation. *J. Am. Chem. Soc.* **2017**, *139* (51), 18444–18447. https://doi.org/10.1021/jacs.7b10755.
(29) Skubi, K. L.; Blum, T. R.; Yoon, T. P. Dual Catalysis Strategies in Photochemical Synthesis. *Chem. Rev.* **2016**, *116* (17), 10035–10074. https://doi.org/10.1021/acs.chemrev.6b00018.
(30) Fuchibe, K.; Hatta, H.; Oh, K.; Oki, R.; Ichikawa, J. Lewis Acid Promoted Single C-F Bond Activation of the CF_3 Group: S_N1'-Type 3,3-Difluoroallylation of Arenes with 2-Trifluoromethyl-1-Alkenes. *Angew. Chem. Int. Ed.* **2017**, *56* (21), 5890–5893. https://doi.org/10.1002/anie.201701985.
(31) Sugihara, N.; Suzuki, K.; Nishimoto, Y.; Yasuda, M. Photoredox-Catalyzed C-F Bond Allylation of Perfluoroalkylarenes at the Benzylic Position. *J. Am. Chem. Soc.* **2021**, *143* (25), 9308–9313. https://doi.org/10.1021/jacs.1c03760.
(32) Gray, S. J.; Brown, K.; Lam, F. Y. T.; Garden, J. A.; Arnold, P. L. Dinuclear Ce(IV) Aryloxides: Highly Active Catalysts for Anhydride/Epoxide Ring-Opening Copolymerization. *Organometallics* **2021**, *40* (7), 948–958. https://doi.org/10.1021/acs.organomet.1c00055.

(33) Sinclair, F.; Hlina, J. A.; Wells, J. A. L.; Shaver, M. P.; Arnold, P. L. Ring Opening Polymerisation of Lactide with Uranium(IV) and Cerium(IV) Phosphinoaryloxide Complexes. *Dalton Transactions* **2017**, *46* (33), 10786–10790. https://doi.org/10.1039/c7dt02167d.
(34) Corma, A.; García, H. Lewis Acids: From Conventional Homogeneous to Green Homogeneous and Heterogeneous Catalysis. *Chem. Rev.* **2003**, *103* (11), 4307–4366. https://doi.org/10.1021/cr030680z.
(35) Pinter, P.; Schüßlbauer, C. M.; Watt, F. A.; Dickmann, N.; Herbst-Irmer, R.; Morgenstern, B.; Grünwald, A.; Ullrich, T.; Zimmer, M.; Hohloch, S.; Guldi, D. M.; Munz, D. Bright Luminescent Lithium and Magnesium Carbene Complexes. *Chem. Sci.* **2021**, *12* (21), 7401–7410. https://doi.org/10.1039/d1sc00846c.
(36) Wei, F.; Lai, S.-L.; Zhao, S.; Ng, M.; Chan, M.-Y.; Yam, V. W.-W.; Wong, K. M.-C. Ligand Mediated Luminescence Enhancement in Cyclometalated Rhodium(III) Complexes and Their Applications in Efficient Organic Light-Emitting Devices. *J. Am. Chem. Soc.* **2019**, *141* (32), 12863–12871. https://doi.org/10.1021/jacs.9b06308.
(37) Li, S.; Shu, W. Recent Advances in Radical Enabled Selective C_{sp^3}–F Bond Activation of Multifluorinated Compounds. *Chem. Commun.* **2022**, *58* (8), 1066–1077. https://doi.org/10.1039/D1CC06446K.
(38) Yin, H.; Zabula, A. V.; Schelter, E. J. C-F→Ln/An Interactions in Synthetic f-Element Chemistry. *Dalton Trans.* **2016**, *45* (15), 6313–6323. https://doi.org/10.1039/c6dt00108d.
(39) Qiao, Y.; Cheisson, T.; Manor, B. C.; Carroll, P. J.; Schelter, E. J. A Strategy to Improve the Performance of Cerium(III) Photocatalysts. *Chem. Commun.* **2019**, *55* (28), 4067–4070. https://doi.org/10.1039/C9CC00282K.
(40) Watson, P. L.; Tulip, T. H.; Williams, I. Defluorination of Perfluoroolefins by Divalent Lanthanoid Reagents: Activating C–F Bonds. *Organometallics* **1990**, *9* (7), 1999–2009. https://doi.org/10.1021/om00157a006.
(41) Fieser, M. E.; Johnson, C. W.; Bates, J. E.; Ziller, J. W.; Furche, F.; Evans, W. J. Dinitrogen Reduction, Sulfur Reduction, and Isoprene Polymerization via Photochemical Activation of Trivalent Bis(Cyclopentadienyl) Rare-Earth-Metal Allyl Complexes. *Organometallics* **2015**, *34* (17), 4387–4393. https://doi.org/10.1021/acs.organomet.5b00613.
(42) Tucker, J. W.; Stephenson, C. R. J. Shining Light on Photoredox Catalysis: Theory and Synthetic Applications. *Journal of Organic Chemistry* **2012**, *77* (4), 1617–1622. https://doi.org/10.1021/jo202538x.
(43) Clavel, P.; Lessene, G.; Biran, C.; Bordeau, M.; Roques, N.; Trévin, S.; de Montauzon, D. Selective Electrochemical Synthesis and Reactivity of Functional Benzylic Fluorosilylsynthons. *Journal of Fluorine Chemistry* **2001**, *107* (2), 301–310. https://doi.org/10.1016/S0022-1139(00)00373-0.
(44) Yin, H.; Carroll, P. J.; Manor, B. C.; Anna, J. M.; Schelter, E. J. Cerium Photosensitizers: Structure-Function Relationships and Applications in Photocatalytic Aryl Coupling Reactions. *Journal of the American Chemical Society* **2016**, *138* (18), 5984–5993. https://doi.org/10.1021/jacs.6b02248.
(45) Werkema, E. L.; Andersen, R. A.; Maron, L.; Eisenstein, O. The Reaction of Bis(1,2,4-Tri-t-Butylcyclopentadienyl)Ceriumbenzyl, Cp′2CeCH2Ph, with Methylhalides: A Metathesis Reaction That Does Not Proceed by a Metathesis Transition State. *Dalton Transactions* **2010**, *39* (29), 6648–6660. https://doi.org/10.1039/b918103b.
(46) Middleton, W. J. New Fluorinating Reagents. Dialkylaminosulfur Fluorides. *J. Org. Chem.* **1975**, *40* (5), 574–578. https://doi.org/10.1021/jo00893a007.
(47) Vasilopoulos, A.; Golden, D. L.; Buss, J. A.; Stahl, S. S. Copper-Catalyzed C–H Fluorination/Functionalization Sequence Enabling Benzylic C–H Cross Coupling with Diverse Nucleophiles. *Org. Lett.* **2020**, *22* (15), 5753–5757. https://doi.org/10.1021/acs.orglett.0c02238.

(48) Werkema, E. L.; Yahia, A.; Maron, L.; Eisenstein, O.; Andersen, R. A. Bridging Silyl Groups in σ-Bond Metathesis and [1,2]-Shifts. Experimental and Computational Study of the Reaction between Cerium Metallocenes and MeOSiMe $_3$. *Organometallics* **2010**, *29* (21), 5103–5110. https://doi.org/10.1021/om1003286.
(49) Arnold, P. L.; Turner, Z. R.; Kaltsoyannis, N.; Pelekanaki, P.; Bellabarba, R. M.; Tooze, R. P. Covalency in CeIV and UIV Halide and N-Heterocyclic Carbene Bonds. *Chem. Eur. J.* **2010**, *16* (31), 9623–9629. https://doi.org/10.1002/chem.201001471.
(50) Romanchuk, A. Yu.; Vlasova, I. E.; Kalmykov, S. N. Speciation of Uranium and Plutonium From Nuclear Legacy Sites to the Environment: A Mini Review. *Front. Chem.* **2020**, *8*, 630. https://doi.org/10.3389/fchem.2020.00630.
(51) Waters, J. B.; Goicoechea, J. M. Alkali Metal Salts of Ditopic Carbanionic Carbenes as Reagents for the Synthesis of Novel Complexes of Group 12 and 14 Metals. *Dalton Transactions* **2014**, *43* (38), 14239–14248. https://doi.org/10.1039/c4dt00954a.
(52) Bradley, D. C.; Hursthouse, M. B.; Ibrahim, A. A.; Malik, K. M. A.; Motevalli, M.; Möseler, R.; Powell, H.; Runnacles, J. D.; Sullivan, A. C. Synthesis and Chemistry of the Bis(Trimethylsilyl)Amido Bis-Tetrahydrofuranates of the Group 2 Metals Magnesium, Calcium, Strontium and Barium. X-Ray Crystal Structures of Mg[N(SiMe3)2]2·2THF and Related Mn[N(SiMe3)2]2·2THF. *Polyhedron* **1990**, *9* (24), 2959–2964. https://doi.org/10.1016/S0277-5387(00)84207-2.
(53) Bellemin-Laponnaz, S.; Dagorne, S. Group 1 and 2 and Early Transition Metal Complexes Bearing N-Heterocyclic Carbene Ligands: Coordination Chemistry, Reactivity, and Applications. *Chem. Rev.* **2014**, *114* (18), 8747–8774. https://doi.org/10.1021/cr500227y.
(54) Bruyere, J.-C.; Gourlaouen, C.; Karmazin, L.; Bailly, C.; Boudon, C.; Ruhlmann, L.; De Frémont, P.; Dagorne, S. Synthesis and Characterization of Neutral and Cationic Magnesium Complexes Supported by NHC Ligands. *Organometallics* **2019**, *38* (14), 2748–2757. https://doi.org/10.1021/acs.organomet.9b00304.
(55) Zhang, D.; Kawaguchi, H. Deprotonation Attempts on Imidazolium Salt Tethered by Substituted Phenol and Construction of Its Magnesium Complex by Transmetalation. *Organometallics* **2006**, *25* (22), 5506–5509. https://doi.org/10.1021/om060691t.
(56) Arnold, P. L.; Mungur, S. A.; Blake, A. J.; Wilson, C. Anionic Amido N-Heterocyclic Carbenes: Synthesis of Covalently Tethered Lanthanide–Carbene Complexes. *Angew. Chem. Int. Ed.* **2003**, *42* (48), 5981–5984. https://doi.org/10.1002/anie.200352710.
(57) Mungur, S. A.; Liddle, S. T.; Wilson, C.; Sarsfield, M. J.; Arnold, P. L. Bent Metal Carbene Geometries in Amido N-Heterocyclic Carbene Complexes. *Chem. Commun.* **2004**, No. 23, 2738. https://doi.org/10.1039/b410074c.
(58) Arnold, P. L.; Rodden, M.; Wilson, C. Thermally Stable Potassium N-Heterocyclic Carbene Complexes with Alkoxide Ligands, and a Polymeric Crystal Structure with Distorted, Bridging Carbenes. *Chem. Commun.* **2005**, No. 13, 1743. https://doi.org/10.1039/b418302a.
(59) Harder, S.; Müller, S.; Hübner, E. Syntheses and Crystal Structures of Simple Dibenzylcalcium Complexes: Useful Reagents in the Preparation of Calcium Compounds. *Organometallics* **2004**, *23* (2), 178–183. https://doi.org/10.1021/om0341350.
(60) Williams, U. J.; Robinson, J. R.; Lewis, A. J.; Carroll, P. J.; Walsh, P. J.; Schelter, E. J. Synthesis, Bonding, and Reactivity of a Cerium(IV) Fluoride Complex. *Inorganic Chemistry* **2014**, *53* (1), 27–29. https://doi.org/10.1021/ic402769u.
(61) Plečnik, C. E.; Liu, S.; Liu, J.; Chen, X.; Meyers, E. A.; Shore, S. G. Lanthanide−Transition-Metal Carbonyl Complexes. 1. Syntheses and Structures of Ytterbium(II) Solvent-Separated Ion Pairs and Isocarbonyl Polymeric Arrays of Tetracarbonylcobaltate. *Inorg. Chem.* **2002**, *41* (19), 4936–4943. https://doi.org/10.1021/ic020254g.

(62) Cole, B. E.; Cheisson, T.; Higgins, R. F.; Nakamaru-Ogiso, E.; Manor, B. C.; Carroll, P. J.; Schelter, E. J. Redox-Driven Chelation and Kinetic Separation of Select Rare Earths Using a Tripodal Nitroxide Proligand. *Inorg. Chem.* **2020**, *59* (1), 172–178. https://doi.org/10.1021/acs.inorgchem.9b00975.
(63) Dröse, P.; Crozier, A. R.; Lashkari, S.; Gottfriedsen, J.; Blaurock, S.; Hrib, C. G.; Maichle-Mössmer, C.; Schädle, C.; Anwander, R.; Edelmann, F. T. Facile Access to Tetravalent Cerium Compounds: One-Electron Oxidation Using Iodine(III) Reagents. *Journal of the American Chemical Society* **2010**, *132* (40), 14046–14047. https://doi.org/10.1021/ja107494h.
(64) Schneider, D.; Harmgarth, N.; Edelmann, F. T.; Anwander, R. Ceric Cyclopentadienides Bearing Alkoxy, Aryloxy, Chlorido, or Iodido Co-Ligands. *Chem. Eur. J.* **2017**, *23* (50), 12243–12252. https://doi.org/10.1002/chem.201700743.
(65) Mueller, T. J.; Fieser, M. E.; Ziller, J. W.; Evans, W. J. (C5Me4H)1--Based Reduction of Dinitrogen by the Mixed Ligand Tris(Polyalkylcyclopentadienyl) Lutetium and Yttrium Complexes, (C5Me5)3-x(C5Me 4H)XLn. *Chemical Science* **2011**, *2* (10), 1992–1996. https://doi.org/10.1039/c1sc00139f.
(66) Trinh, M. T.; Wedal, J. C.; Evans, W. J. Evaluating Electrochemical Accessibility of 4fn5d1and 4fn+1Ln(Ii) Ions in (C5H4SiMe3)3Ln and (C5Me4H)3Ln Complexes. *Dalton Transactions* **2021**, *50* (40), 14384–14389. https://doi.org/10.1039/d1dt02427b.
(67) Schweitzer-Chaput, B.; Horwitz, M. A.; de Pedro Beato, E.; Melchiorre, P. Photochemical Generation of Radicals from Alkyl Electrophiles Using a Nucleophilic Organic Catalyst. *Nature Chemistry* **2019**, *11* (2), 129–135. https://doi.org/10.1038/s41557-018-0173-x.
(68) Anwander, R.; Dolg, M.; Edelmann, F. T. The Difficult Search for Organocerium(Iv) Compounds. *Chemical Society Reviews* **2017**, *46* (22), 6697–6709. https://doi.org/10.1039/c7cs00147a.
(69) Shirase, S.; Shinohara, K.; Tsurugi, H.; Mashima, K. Oxidation of Alcohols to Carbonyl Compounds Catalyzed by Oxo-Bridged Dinuclear Cerium Complexes with Pentadentate Schiff-Base Ligands under a Dioxygen Atmosphere. *ACS Catal.* **2018**, *8* (8), 6939–6947. https://doi.org/10.1021/acscatal.8b01718.
(70) Ringenberg, M. R.; Kokatam, S. L.; Heiden, Z. M.; Rauchfuss, T. B. Redox-Switched Oxidation of Dihydrogen Using a Non-Innocent Ligand. *Journal of the American Chemical Society* **2008**, *130* (3), 788–789. https://doi.org/10.1021/ja076801k.
(71) Benisvy, L.; Blake, A. J.; Collison, D.; Davies, E. S.; Garner, C. D.; McInnes, E. J. L.; McMaster, J.; Whittaker, G.; Wilson, C. A Phenol-Imidazole pro-Ligand That Can Exist as a Phenoxyl Radical, Alone and When Complexed to Copper(II) and Zinc(II). *Dalton Transactions* **2003**, No. 10, 1975–1985. https://doi.org/10.1039/b212209j.
(72) Twilton, J.; Le, C.; Zhang, P.; Shaw, M. H.; Evans, R. W.; MacMillan, D. W. C. The Merger of Transition Metal and Photocatalysis. *Nature Reviews Chemistry* **2017**, *1* (7), 0052. https://doi.org/10.1038/s41570-017-0052.
(73) Frankiss, S. G. Fluorine Magnetic Resonance Spectra of Methylfluorosilanes. *J. Phys. Chem.* **1967**, *71* (11), 3418–3421. https://doi.org/10.1021/j100870a010.
(74) Hidaka, H.; Tsukamoto, T.; Oyama, T.; Mitsutsuka, Y.; Takamura, T.; Serpone, N. Photoassisted Defluorination of Fluorinated Substrates and Pharmaceuticals by a Wide Bandgap Metal Oxide in Aqueous Media. *Photochem Photobiol Sci* **2013**, *12* (5), 751–759. https://doi.org/10.1039/c2pp25358e.
(75) Friedmann, D.; Caruso, R. A. Indium Oxides and Related Indium-based Photocatalysts for Water Treatment: Materials Studied, Photocatalytic Performance, and Special Highlights. *Solar RRL* **2021**, *5* (7), 2100086. https://doi.org/10.1002/solr.202100086.

(76) Casely, I. J.; Liddle, S. T.; Blake, A. J.; Wilson, C.; Arnold, P. L. Tetravalent Cerium Carbene Complexes. *Chemical Communications* **2007**, No. 47, 5037–5039. https://doi.org/10.1039/b713041d.
(77) Turner, Z. R.; Bellabarba, R.; Tooze, R. P.; Arnold, P. L. Addition-Elimination Reactions across the M-C Bond of Metal N-Heterocyclic Carbenes. *Journal of the American Chemical Society* **2010**, *132* (12), 4050–4051. https://doi.org/10.1021/ja910673q.
(78) Canestrari, D.; Lancianesi, S.; Badiola, E.; Strinna, C.; Ibrahim, H.; Adamo, M. F. A. Desulfurative Chlorination of Alkyl Phenyl Sulfides. *Org. Lett.* **2017**, *19* (4), 918–921. https://doi.org/10.1021/acs.orglett.7b00077.
(79) Sandoval, J. J.; Palma, P.; Álvarez, E.; Cámpora, J.; Rodríguez-Delgado, A. Mechanism of Alkyl Migration in Diorganomagnesium 2,6-Bis(Imino)Pyridine Complexes: Formation of Grignard-Type Complexes with Square-Planar Mg(II) Centers. *Organometallics* **2016**, *35* (18), 3197–3204. https://doi.org/10.1021/acs.organomet.6b00528.
(80) Kong, Y.; Ren, H.; Xu, S.; Song, H.; Liu, B.; Wang, B. Synthesis, Structures, and Norbornene Polymerization Behavior of Bis(Aryloxide-N-Heterocyclic Carbene) Palladium Complexes. *Organometallics* **2009**, *28* (20), 5934–5940. https://doi.org/10.1021/om900625r.
(81) Evans, W. J.; Kozimor, S. A.; Ziller, J. W.; Fagin, A. A.; Bochkarev, M. N. Facile Syntheses of Unsolvated UI $_3$ and Tetramethylcyclopentadienyl Uranium Halides. *Inorg. Chem.* **2005**, *44* (11), 3993–4000. https://doi.org/10.1021/ic0482685.
(82) Gompa, T. P.; Rice, N. T.; Russo, D. R.; Aguirre Quintana, L. M.; Yik, B. J.; Bacsa, J.; La Pierre, H. S. Diethyl Ether Adducts of Trivalent Lanthanide Iodides. *Dalton Trans.* **2019**, *48* (23), 8030–8033. https://doi.org/10.1039/C9DT00775J.
(83) Windorff, C. J.; Dumas, M. T.; Ziller, J. W.; Gaunt, A. J.; Kozimor, S. A.; Evans, W. J. Small-Scale Metal-Based Syntheses of Lanthanide Iodide, Amide, and Cyclopentadienyl Complexes as Analogues for Transuranic Reactions. *Inorg. Chem.* **2017**, *56* (19), 11981–11989. https://doi.org/10.1021/acs.inorgchem.7b01968.
(84) Scherg, T.; Schneider, S.; Frey, G.; Schwarz, J.; Herdtweck, E.; Herrmann, W. Bridged Imidazolium Salts Used as Precursors for Chelating Carbene Complexes of Palladium in the Mizoroki-Heck Reaction. *Synlett* **2006**, *2006* (18), 2894–2907. https://doi.org/10.1055/s-2006-951539.
(85) Fang, S.; Wang, X.; Yin, F.; Cai, P.; Yang, H.; Kong, L. Palladium-Catalyzed *Meta* -C–H Olefination of Arene-Tethered Diols Directed by Well-Designed Pyrimidine-Based Group. *Org. Lett.* **2019**, *21* (6), 1841–1844. https://doi.org/10.1021/acs.orglett.9b00433.
(86) Dolomanov, O. V.; Bourhis, L. J.; Gildea, R. J.; Howard, J. A. K.; Puschmann, H. *OLEX2* : A Complete Structure Solution, Refinement and Analysis Program. *J. Appl. Crystallogr.* **2009**, *42* (2), 339–341. https://doi.org/10.1107/S0021889808042726.
(87) Sheldrick, G. M. *SHELXT* – Integrated Space-Group and Crystal-Structure Determination. *Acta Crystallogr. A* **2015**, *71* (1), 3–8. https://doi.org/10.1107/S2053273314026370.
(88) Clark, R. C.; Reid, J. S. The Analytical Calculation of Absorption in Multifaceted Crystals. *Acta Crystallographica Section A* **1995**, *51*, 887–897.
(89) Becke, A. D. Density-functional Thermochemistry. III. The Role of Exact Exchange. *J. Chem. Phys* **1993**, *98* (7), 5648–5652. https://doi.org/10.1063/1.464913.
(90) Perdew, J. P.; Wang, Y. Accurate and Simple Analytic Representation of the Electron-Gas Correlation Energy. *Phys. Rev. B* **1992**, *45* (23), 13244–13249. https://doi.org/10.1103/PhysRevB.45.13244.
(91) Cao, X.; Dolg, M.; Stoll, H. Valence Basis Sets for Relativistic Energy-Consistent Small-Core Actinide Pseudopotentials. *J. Chem. Phys* **2003**, *118* (2), 487–496. https://doi.org/10.1063/1.1521431.

(92) Küchle, W.; Dolg, M.; Stoll, H.; Preuss, H. Energy-adjusted Pseudopotentials for the Actinides. Parameter Sets and Test Calculations for Thorium and Thorium Monoxide. *J. Chem. Phys* **1994**, *100* (10), 7535–7542. https://doi.org/10.1063/1.466847.
(93) Hariharan, P. C.; Pople, J. A. The Influence of Polarization Functions on Molecular Orbital Hydrogenation Energies. *Theoret. Chim. Acta* **1973**, *28* (3), 213–222. https://doi.org/10.1007/BF00533485.
(94) Hehre, W. J.; Ditchfield, R.; Pople, J. A. Self—Consistent Molecular Orbital Methods. XII. Further Extensions of Gaussian—Type Basis Sets for Use in Molecular Orbital Studies of Organic Molecules. *J. Chem. Phys* **1972**, *56* (5), 2257–2261. https://doi.org/10.1063/1.1677527.
(95) M. J. Frisch, G. W. Trucks, H. B. Schlegel, G. E. Scuseria, M. A. Robb, J. R.; Cheeseman, G. Scalmani, V. Barone, B. Mennucci, G. A. Petersson, H. Nakatsuji, M. Caricato, X. Li, H.; P. Hratchian, A. F. Izmaylov, J. Bloino, G. Zheng, J. L. Sonnenberg, M. Hada, M. Ehara, K. Toyota, R.; Fukuda, J. Hasegawa, M. Ishida, T. Nakajima, Y. Honda, O. Kitao, H. Nakai, T. Vreven, J. A.; Montgomery, Jr., J. E. Peralta, F. Ogliaro, M. Bearpark, J. J. Heyd, E. Brothers, K. N. Kudin, V. N.; Staroverov, R. Kobayashi, J. Normand, K. Raghavachari, A. Rendell, J. C. Burant, S. S. Iyengar, J.; Tomasi, M. Cossi, N. Rega, J. M. Millam, M. Klene, J. E. Knox, J. B. Cross, V. Bakken, C. Adamo, J.; Jaramillo, R. Gomperts, R. E. Stratmann, O. Yazyev, A. J. Austin, R. Cammi, C. Pomelli, J. W. Ochterski,; R. L. Martin, K. Morokuma, V. G. Zakrzewski, G. A. Voth, P. Salvador, J. J. Dannenberg, S. Dapprich, A.; D. Daniels, O. Farkas, J. B. Foresman, J. V. Ortiz, J. Cioslowski, D. J. Fox, Gaussian, Inc., Wallingford CT, 2013. Gaussian 09, Revision D.01.
(96) Wooles, A. J.; Mills, D. P.; Lewis, W.; Blake, A. J.; Liddle, S. T. Lanthanide Tri-Benzyl Complexes: Structural Variations and Useful Precursors to Phosphorus-Stabilised Lanthanide Carbenes. *Dalton Trans.* **2010**, *39* (2), 500–510. https://doi.org/10.1039/B911717B.
(97) Engelhardt, G.; Licht, K. 19F-NMR- Und IR-Spektroskopische Untersuchungen an Organofluor-Silanen Und -Germanen. *Z. Chem.* **2010**, *10* (7), 266–267. https://doi.org/10.1002/zfch.19700100707.

Chapter 3

Photocatalytic Dechlorination of Chlorinated Hydrocarbons Using Organolanthanide Complexes

3.1 Overview

The ability of the aforementioned lanthanide catalysts (**Chapter 1**) to cleave carbon–fluorine bonds (**Chapter 2**) suggested the capability of these complexes in activating weaker carbon–chlorine bonds. In this chapter we show that simple lanthanide tetramethylcyclopentadienyl (Cp^{Me4}) complexes can photochemically cleave the sp^3 carbon–chlorine bond of unactivated chlorinated hydrocarbons including polyvinyl chloride (PVC) via a reactive lanthanide alkyl intermediate. Because light absorption by the Cp^{Me4} ligand is efficient, photocatalytic reactivity is enhanced for cerium and made possible for neighboring, normally photoinactive, lanthanide congeners.

The author carried out the synthesis and experimental investigation of lanthanide photocatalysts at the University of California, Berkeley. Mechanistic calculations were carried out by Stella Christodoulou under the supervision of Prof. Laurent Maron at the University of Toulouse. Crystallographic data of **3-Nd** and **3-Sm** was collected by Erik T. Ouellette, Dr. Appie Peterson, and Sheridon Kelly at beamline 12.2.1 of the Advanced Light Source (ALS) at Lawrence Berkeley National Laboratory and solved by Erik T. Ouellette. Dr. Jeremy Demarteau and Dr. Brett Helms aided with polymer characterization by Gel Permeation Chromatography (GPC). Much of the work presented in this chapter has been published in the peer-reviewed Royal Society of Chemistry (RSC) journal Chemical Communications.[1]

3.2 Introduction

Photoredox catalysis provides versatile and energy-efficient routes for the synthesis of complex molecules.[2–4] Modern photocatalysts can undergo single electron transfer (SET) processes following irradiation with UV or, more desirably, visible light, enabling challenging chemical transformations to be accessed under milder conditions than thermally driven reactions.[5] The use of lanthanides in catalysis is favourable due to the relative abundance of many and their low toxicity.[6–9] Their halophilicity has led us and others to explore their potential for catalytic carbon–halogen functionalization reactions. In general, the strong $C(sp^3)$–Cl bond is weakened by coordination to a lanthanide center, and early work showed that under light irradiation at 40 °C, SmI_2 can reductively dechlorinate 1-chlorodocecane stoichiometrically.[10] Divalent lanthanide complexes, $Ln(Cp^*)_2$ (Ln = Sm, Eu, and Yb, $Cp^* = C_5Me_5$), were also shown to activate C–Cl bonds forming the Ln^{III} halide, and the reaction could be made catalytic under higher energy (near UV) irradiation in the presence of sacrificial reductant.[11–13]

The strong Ln–Cl bond can provide an additional thermodynamic driving force to a reaction with a substrate that would otherwise be unreactive according to the redox potentials of the photoexcited metal and halocarbon. However, photoredox catalysis by lanthanide complexes, especially using low energy, visible light remains underexploited, and simple Ce(III) coordination complexes dominate the studies.[14,15] Cerium possesses both an accessible (III)(/IV) redox couple and a formally allowed excitation from the $4f^1$ ground state to the $5d^1$ excited state, which can give rise to luminescence. It is also the cheapest and most readily isolated of the rare earths, offering a promising alternative to current precious metal photocatalysts.

Chapters 1 and **2** of this thesis have described a cerium photocatalyst (Cp^{Me4})$_2$Ce(**L**) (**1-Ce**, Cp^{Me4} = C_5Me_4H, **L**= [2-O-3,5-^{t}Bu$_2$-C_6H_2(1-C{N(CH)$_2$N(^{i}Pr)})]) that combines the photoexcitable Ce(III) ion with multifunctional, tunable ligands, to cleave and functionalize the strong and inert sp^3 C–F bond of $PhCF_3$ through an inner sphere mechanism (Figure 3.1,

top).[16] Notably, the redox non-innocent ligand framework allowed this reactivity to also be facilitated by typically photo- and redox-inactive Lewis-acidic metals, including lanthanum and magnesium. The aryloxy-NHC, **L**, allows for additional light absorption and photoexcitation, while the oxidation of **L** or, more likely, a Cp^{Me4} ligand allows for turnover with metals that lack a metal-based redox event. Importantly, in order to cleave the strong C–F bond, **L** is required, and little reactivity is observed when using $(Cp^{Me4})_3Ce$ (**2-Ce**) rather than **1-Ce** as a defluorination catalyst.[16]

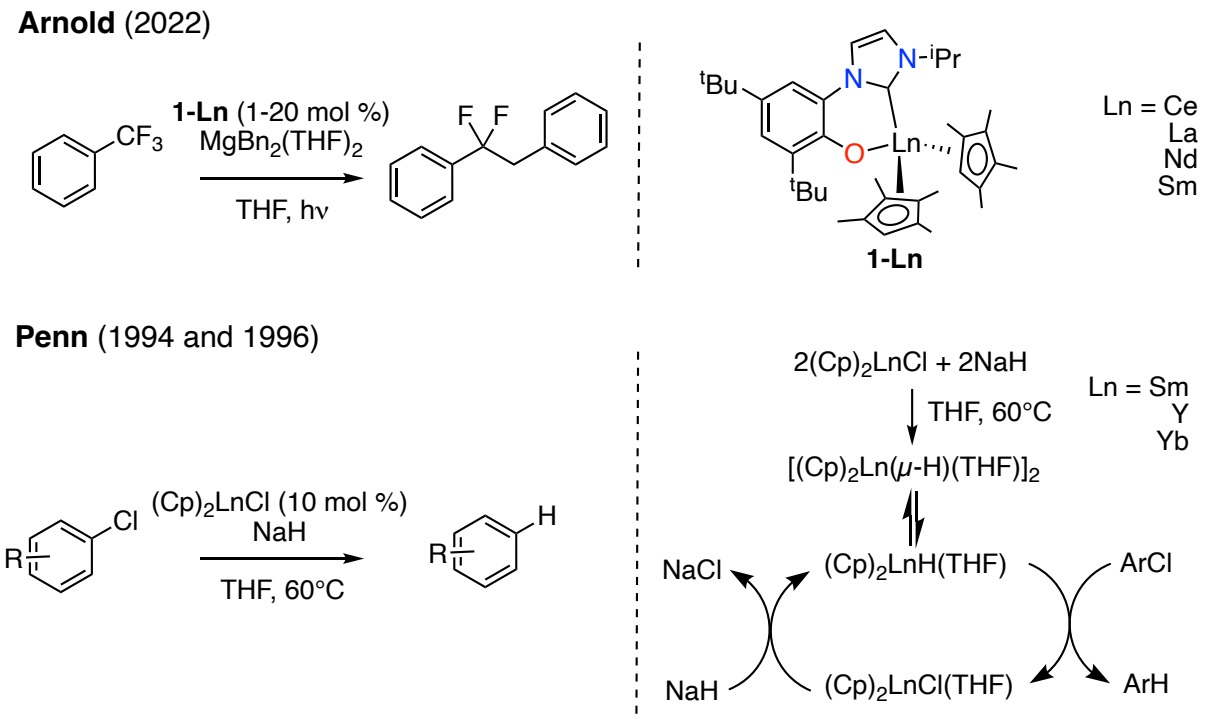

Figure 3.1. Photocatalytic C-F bond functionalization by complexes **1-Ln** (Ln = Ce, La, Nd, Sm) (top), and the dechlorination of aromatic chlorides by Cp_2LnCl complexes (Cp = C_5H_5, Ln = Y, Yb, Sm) carried out by Penn et al. (bottom).

We were interested in Penn and co-workers' report that Cp_2LnCl complexes (Cp = C_5H_5 Ln = Y, Yb, Sm) could catalyze the dechlorination of activated aromatic chlorides with sodium hydride (NaH) (suspension in THF) at 60°C. They proposed a lanthanide hydride species as the active catalyst (Figure 3.1, bottom), which is capable of cleaving a C–Cl bond, thus regenerating the lanthanide chloride species.[17,18] This, and the ability of our complexes to cleave C–F bonds encouraged us to target functionalization of unactivated alkyl C–Cl bonds that have so far been outside the reach of other lanthanide-based visible light photocatalysts. This could be of utility in the chemical upcycling of polyvinyl chloride (PVC).[19,20]

Globally, approximately 40 million tons of PVC are produced a year, yet a low percentage is recycled and the majority is through mechanical recycling in spite of its high energy demands.[21,22] Incineration or thermal degradation of PVC can release toxic by-products; low-energy dechlorination routes that would facilitate its conversion to valuable products are desirable.[23] Hydrodechlorination is an appealing option to remove Cl from PVC, resulting in polyethylene (PE)-like products. This strategy could also have useful applications in the purification of PE prior to recycling if waste streams contain small amounts of PVC. However, the hydrodechlorination of PVC under mild, chemical conditions is rare.[24–30]

In 2022 Fieser and co-workers reported the reaction of PVC with five equivalents of triethyl silane in the presence of an in situ-generated (Xantphos)RhCl catalyst (Xantphos = (9,9-dimethyl-9H-xanthene-4,5-diyl)bis(diphenylphosphane)).[31] The partial reduction of PVC to poly(vinyl chloride-co-ethylene) was observed. Analogous reaction with two equivalents of sodium formate in place of triethyl silane instead led to complete dechlorination of PVC and the generation of PE. Variation of catalyst loading, solvent, and co-reagent influenced the selectivity of hydrodechlorination relative to dehydrochlorination. More recent work from the same group presented tandem hydrodechlorination/Friedel–Crafts alkylation of PVC facilitated by silylium ion cataylsts.[32] Products were new styrenic copolymers of polyethylene, with the conversion of PVC being complete within minutes even at low catalyst loadings.

Previous work has implicated both cyclopentadienyl and chlorine radicals in photocatalytic bond activation.[15,16,33,34,35] We also recognize from our work and others that the Cp ligand has some capacity for light absorbance.[36] In 2005, Evans at co-workers demonstrated that dinitrogen can be reduced by photochemical activation of Ln(III) mixed-ligand tris(cyclopentadienyl) rare-earth complexes of the form $(\eta^5\text{-}C_5Me_5)_{3-x}(C_5Me_4H)_xLn$ (Ln = Y, Lu, Dy; x = 1, 2).[36] Dinitrogen complexes $[(C_5Me_4R)_2Ln]_2(\mu\text{-}\eta^2\text{:}\eta^2\text{-}N_2)$ (R = H, Me) were formed in reactions in which N_2 was reduced to $(N{=}N)^{2-}$ and $(C_5Me_4H)^-$ was oxidized to $(C_5Me_4H)_2$ (Figure 3.2). The reducing power of these complexes was rationalized by absorptions involving the $(\eta^3\text{-}C_5Me_4H)^-$ ligand, as the complexes were shown to possess low energy LMCT bands. DFT studies showed that irradiation of these bands could lead to formation of an $(\eta^3\text{-}C_5Me_4H)$ radical and an excited d^1 metal fragment reactive enough to reduce N_2. Subsequent work showed that the photolytic activation of $(C_5Me_5)_2Ln(\eta^3\text{-}C_3H_5)$ (Ln = Y, Lu) in the presence of isoprene results in the generation of polyisoprene, and that sulfur can also be reduced through photolysis of these complexes.[37]

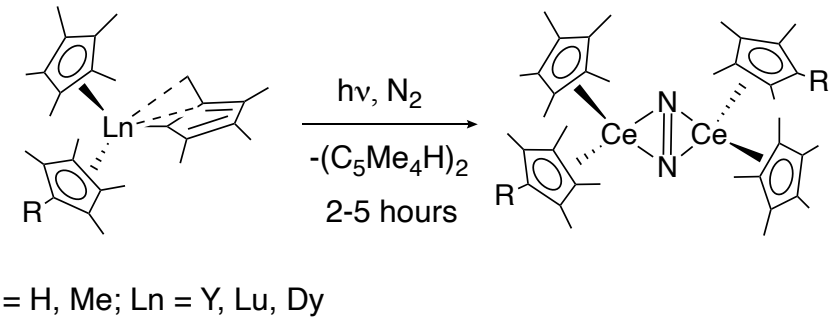

Figure 3.2. Reduction of N_2 under Photolytic Conditions by Ln–Cp complexes (Ln = Y, Lu, Dy), reported by Evans et al.

In recent years there has been extensive discussion surrounding the role of Cl radicals in the C–H bond activation of alkanes targeted using $CeCl_3$ and an alcohol co-catalyst.[15,34] Previous work by Zuo et al. reported a photoinduced alkane oxidation reaction using $CeCl_3$ in conjunction with catalytic 2,2,2-trichloroethanol and tetrabutylammonium chloride (TBACl) (Figure 3.3). Following oxidation of the cerium center by the alcohol co-catalyst, LMCT was thought to regenerate Ce(III) and produce an alkoxy radical that was capable of C–H bond activation of methane, ethane, and other higher alkanes. The resulting alkyl radical could then be quenched with a number of organic molecules, including di-*tert*-butyl azodicarboxylate (DIAD) to produce hydrazines.[15] A trapping study using styrene implicated alkoxy radicals as an active species, with methoxy, trichloroethoxy and trifluoroethoxy radicals generating 1,2-alkoxyamination products in fair yield (Scheme 3.1).

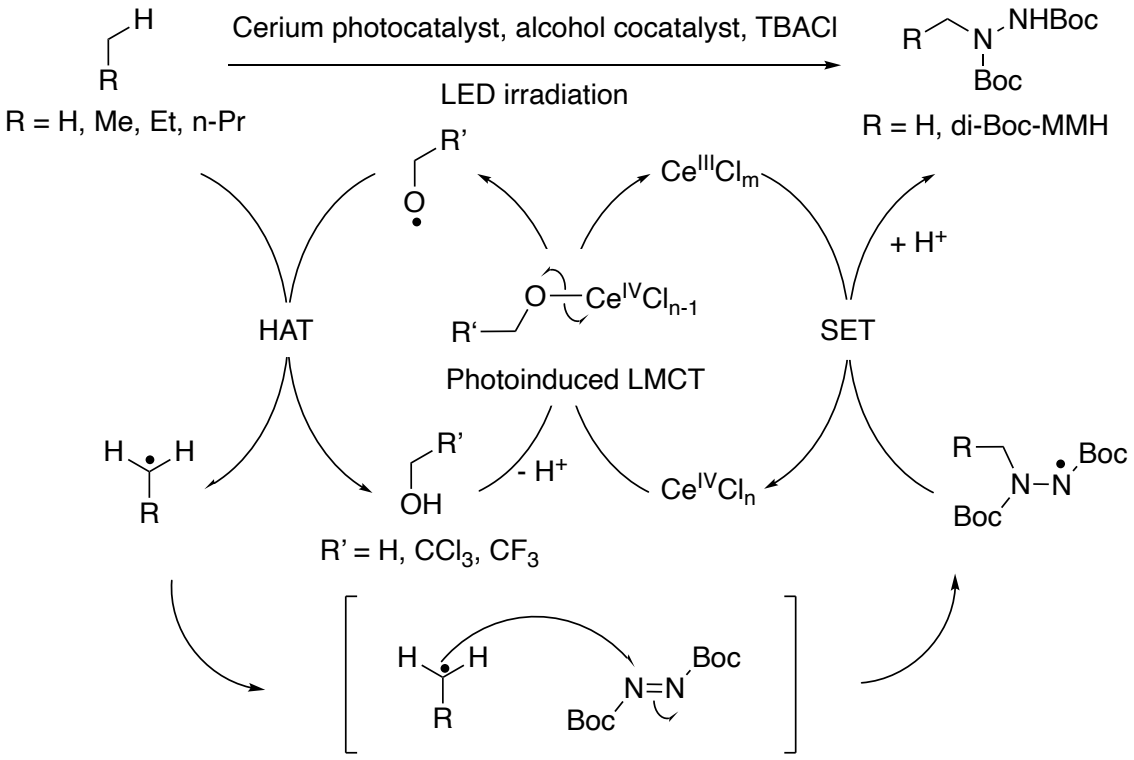

Figure 3.3. C-H bond activation of methane and higher alkanes by cerium photocatalysts in conjunction with an alcohol co-catalyst, reported by Zuo et al.

However subsequent spectroscopic, kinetic, and isotopic labeling studies by Schelter and Walsh et. al. suggested that chlorine radicals, rather than alkoxy, were the key radical intermediate, and that the prior trapping results instead resulted from the complexation of chlorine with alcohols.[34] They suggested that the cerium complex $[NEt_4]_2[CeCl_6]$ (NEt_4^+ = tetraethylammonium) instead mediates the reaction, and releases chlorine radicals upon irradiation. Chlorine radicals have been shown interact with organic solvents including alcohols,[38] and to form charge transfer complexes.[39] Spectroscopic analyses and kinetics studies implicated chlorine radical generation as the rate-limiting step in catalysis, and computational studies supported the generation of [Cl–OHR]• intermediates that could be trapped by styrene to the yield the same 1,2-alkoxyaminated products previously characterized by Zuo, alongside the elimination of HCl.

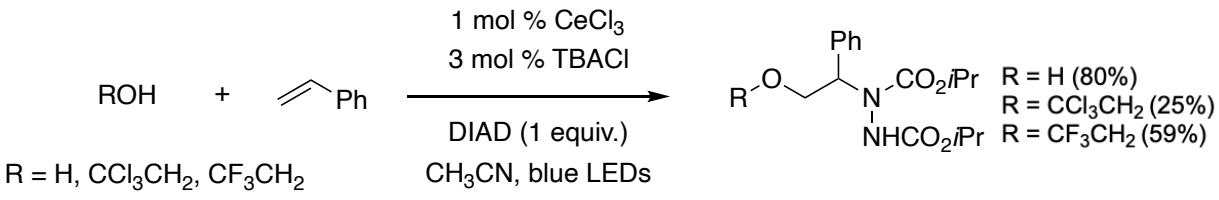

Scheme 3.1. Alkoxy radical trapping experiments carried out by Zuo et al.

Recent work from Zuo however sought to confirm the importance of alkoxy radicals in the cerium-catalyzed C–H functionalization. Operando electron paramagnetic resonance and transient absorption spectroscopy experiments on isolated pentachloro Ce(IV) alkoxide species were used to identify alkoxy radicals as the sole heteroatom-centered radical species generated via LMCT excitation, and analogous reactions under strictly chloride-free conditions were found to be successful.[35] Nevertheless, the potential impact of chlorine radicals in bond cleavage activation reactions should not be discounted, as they have been implicated as reactive species and key intermediates in a number of thermal[40–44] and light-driven reactions.[45–54]

Figure 3.4. Photocatalytic dechlorination of chlorocyclohexane by lanthanide organometallic complexes described in this chapter.

Due to this literature precedent, we hypothesized that sp^2 and sp^3 C–Cl bond activation could even be possible for other lanthanide Cp complexes, especially since the bond dissociation energy for the C(sp^3)–Cl bond (ca. 350 $kJmol^{-1}$) is approximately 140 $kJmol^{-1}$ weaker than the C–F bond.[55] Here, we show that lanthanide tetramethylcyclopentadienyl complexes are efficient photocatalysts for the dechlorination of unactivated sp^2 C–Cl and sp^3 C–Cl bonds in chlorohydrocarbons (Figure 3.4), including those in PVC. Through experiment and theory, we demonstrate that light absorption by the Cp^{Me4} ligand enhances photocatalytic reactivity for cerium and allows for photocatalysis to be facilitated by normally photoinactive lanthanide congeners.

3.3 Results and discussion

3.3.1 Preliminary dechlorination reactions with 1-Ce and 1-La

3.3.1.1 Dechlorination and homocoupling of benzyl chloride

As previously discussed, the first examples of Ce(III) photocatalysis were presented by Schelter et. al.[14,56] They reported photocatalytic C–Cl activation of benzyl chloride using Ce(III) complexes bearing amido and guanidinate ligands, though sodium bis(trimethylsilyl)amide (Na(N{$SiMe_3$}$_2$)) and Ce^0 metal were required for catalytic turnover. The C–X (X = Cl, Br, I) bond cleavage of activated aryl halides were also presented.[56,57] Given the propensity of **1-Ce** and **1-La** to cleave strong C–F bonds, we expected them to also perform well in dechlorination reactions. We decided to test both complexes in the dechlorination of benzyl chloride as reported by Schelter, which we used as a benchmark for our reactivity studies.

Preliminary reactions displayed the ability of **1-Ce** to dechlorinate benzyl chloride. A loading of 10 mol % **1-Ce**, benzyl chloride and sacrificial reductant potassium bis(trimethylsilyl)amide (K(N{$SiMe_3$}$_2$)) in C_6D_6 resulted in 80% yield of bibenzyl after 48 hours irradiation. This product presumably arises via the homocoupling of the generated benzyl radical, as previously

reported.[56] The ability of **1-Ce** to catalytically reduce benzyl chloride is superior to the reactivity observed for other Ce(III) photocatalysts published in the literature, which gave a maximum yield of 68% when Ce metal was also used as an external reductant and radical scavenger.[57]

In contrast, **1-La** gave just 8% conversion to bibenzyl under stoichiometric conditions, and no catalytic activity was observed in the presence of K(N{SiMe$_3$}$_2$). We attribute this to unwanted side reactions between benzyl chloride, K(N{SiMe$_3$}$_2$) and **1-La** due to the increased ionic radius of La. Our previous studies have indicated the reduced stability of **1-La** relative to **1-Ce** for this reason.

3.3.1.2 Stoichiometric dechlorination of chlorocyclohexane by 1-Ce

Given the ability of **1-Ce** to cleave stabilized C(sp^3)–Cl bonds, we sought to target complexes lacking the radical stabilization of benzyl chloride. Chlorocyclohexane was first selected as a simple, easily identifiable mimic for PVC. Photochemical dechlorination of this substrate was expected to generate cyclohexane, the product arising from the generation of the cyclohexyl radical, which then abstracts an H atom from the THF solvent (*vide infra*.). Cyclohexane can be observed as a singlet by ^{1}H NMR; simple integration of this peak relative to an in internal standard gives an in-situ yield.

Irradiation of a THF solution containing **1-Ce** and five equivalents of chlorocyclohexane for 48 hours with a 40 W Kessil Tuna Blue lamp gave 40% conversion to cyclohexane, as observed by ^{1}H NMR spectroscopy. Trace cyclohexene, formed through an elimination reaction, was also observed as a reaction product. Upon completion of this reaction, **1-Ce** is consumed, and the solution has changed color from the orange that is characteristic of **1-Ce**, to yellow. Analysis by ^{1}H NMR spectroscopy shows that multiple paramagnetic species with broad resonances between +16 and -6 ppm are formed alongside the generation of two equivalents of HCp^{Me4}, likely through loss of ligand radical and abstraction of a H atom from the THF solvent. This suggests that in a stoichiometric reaction, each Cl abstraction from chlorocyclohexane results in a Ce–Cl bond that displaces a Cp^{Me4} ligand,[58] allowing for the dechlorination of two molecules of substrate for each molecule of **1-Ce**. The new paramagnetic species was therefore tentatively assigned as (**L**)CeCl$_2$ (**11-Ce)**, with amounts of (**L**)CeCp^{Me4}Cl likely also present (Scheme 3.2).

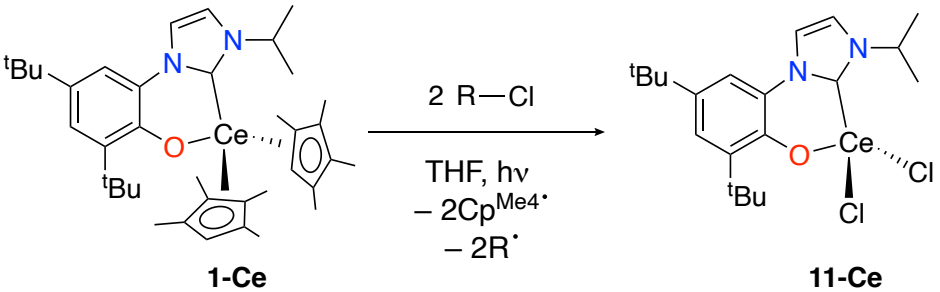

1-Ce **11-Ce**

Scheme 3.2. Generation of proposed species **11-Ce** from **1-Ce**.

The presence of **11-Ce** was further suggested by targeting its independent synthesis and comparison of its crude ^{1}H NMR spectrum with that of completed reaction mixtures. Treatment of CeCl$_3$ with one equivalent of **KL** in THF and subsequent work up resulted in a yellow solid, shown to be mixture of paramagnetic species by ^{1}H NMR. The crude sample matches the

chemical shifts of the species observed in situ following 24 hours irradiation of **1-Ce** in the presence of chlorocyclohexane, though the complex could not be fully purified or characterized. This was in part due to the decreased solubility of **11-Ce** in organic solvents once a number of organic ligands had been displaced, which hindered its purification.[59] The complex was also found to be extremely air- and moisture- sensitive, perhaps due to poor shielding of the metal center from oxygen and water by the chloride ligands.

3.3.1.3 Stoichiometric dechlorination of chlorocyclohexane by 1-Ce and 1-Ce^{t}Bu

Alongside this work, we aimed to further study the role of the light- absorbing aryloxy-NHC ligand **L** in simple dechlorination reactions. As reported in **Chapter 1**, analogues of **L** can be synthesized with a variety of substituents on the 3-position of the NHC (Figure 3.5). The ligand- and metal-based absorptions in these complexes shift according to the nature of the ligand, and interestingly, the intensity of the ligand-based absorption in **1-Ce^{t}Bu** is much larger than that found in **1-Ce** or **1-CeMe**. We hypothesized that this was due to increased rigidity of the complex imparted by the ^{t}Bu substituent. We were interested in investigating whether this would lead to an improved performance of **1-Ce^{t}Bu** relative to **1-Ce** in light-driven dechlorination reactions.

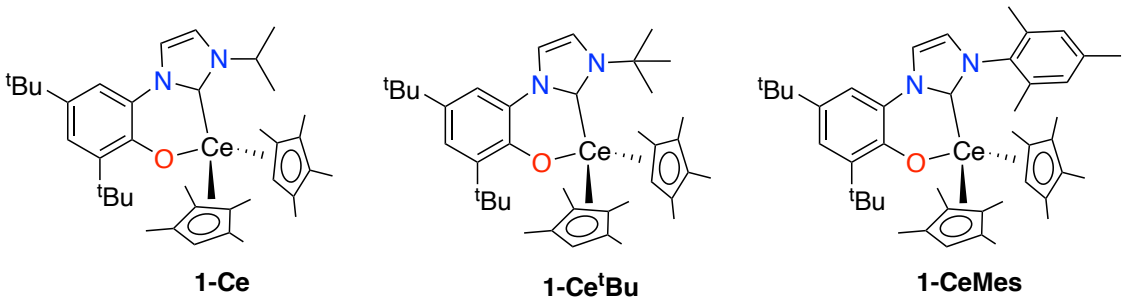

Figure 3.5. Complexes **1-Ce**, **1-Ce^{t}Bu**, **1-CeMes**. The synthesis and characterization of these complexes are described in **Chapter 1** of this thesis.

Indeed, when THF solutions containing **1-Ce** or **1-Ce^{t}Bu** and five equivalents of chlorocyclohexane were irradiated for 24 hours by a variety of Kessil lamps, improved yields were seen for **1-Ce^{t}Bu** at all wavelengths (Table 3.1). Varying amounts of cyclohexene were also produced, but a clear trend could not be elucidated. While experimental investigation and spectroscopic data is needed to support these preliminary results, they provide further promising evidence that simple tuning of the ligand on a lanthanide photocatalyst can improve its light absorbance and consequent reactivity. Due to these results, the 440 nm lamp was then used in place of the 40 W Tuna Blue lamp in subsequent reactions.

Table 3.1. Dechlorination of chlorocyclohexane to form cyclohexane and cyclohexene mediated by **1-Ce** or **1-Ce^{t}Bu**, followed by 24 hours irradiation with a variety of wavelength of light, with yields determined by ^{1}H NMR spectroscopy. Yield of cyclohexene shown in parentheses.

Irradiation wavelength (nm)	Conversion to cyclohexane (%) by **1-Ce**	Conversion to cyclohexane (%) by **1-Ce^{t}Bu**
390	24 (7)	28 (10)
427	29 (12)	40
440	34 (6)	40
467	29 (8)	36 (3)
Tuna Blue	18 (8)	32 (4)

3.3.1.4 Targeting the catalytic dechlorination of chlorocyclohexane by 1-Ln

Given that C–Cl bond activation using complex **1-Ce** appeared to lead to eventual deactivation via **11-Ce** we sought turnover reagents that could abstract Cl prior to Cp^{Me4} loss and impart catalytic activity. The use of cerium or zinc metal, Group 1 bis(trimethylsilyl)amides and pyrazines were not successful. In general, many turnover reagents were difficult to use due to their incompatibility with the pendant NHC substituent of **L**, insertion into the Ce–C(NHC) bond, or displacement of a Cp^{Me4} ligand.[60]

The addition of five equivalents of KCp^{Me4} into a mixture of **1-Ce** and five equivalents of chlorocyclohexane in 0.5 mL THF solvent and subsequent irradiation yielded 35% cyclohexane alongside 19% yield of cyclohexene after 24 hours, with no **1-Ce** consumed over this time. While the lack of formation of **11-Ce** by ^{1}H NMR spectroscopy appeared promising, the basicity of the potassium salt increased the yield of cyclohexene through an elimination pathway. Stoichiometric control reactions using KCp^{Me4} to dechlorinate chlorocyclohexane without **1-Ce** present yielded 8% cyclohexane and 7% cyclohexene, alongside the generation of a white precipitate thought to be potassium chloride.

We then instead sought to test NaH as a turnover reagent which had been used with success by Penn et al. and others in related reactions previously.[17,18] However dechlorination of chlorocyclohexane using 20 mol % loading **1-Ce**, **1-Nd** or **1-Sm** in conjunction with NaH were not catalytic. Reaction with **1-Ce** yielded 20% cyclohexane, while the analogous reactions with **1-Nd** and **1-Sm** yielded just 3% and 2% cyclohexane respectively. Poorer reactivity with the smaller lanthanide congeners could be due to the smaller ionic radii hindering both substrate binding and reactivity with sodium hydride. Results could also be attributed to the lack of solubility of NaH in THF, and so we instead turned to magnesium alkyl reagents to attempt to turn over the catalysis. Many dialkyl magnesium reagents are highly THF-soluble and efficient as a reductant and coupling partner, as observed by us in photocatalytic functionalization.[16] When using a metal alkyl reductant in this reaction instead of NaH, we anticipated a lanthanide alkyl intermediate in place of the metal hydride proposed by Penn.

Dissolution of **1-Ce** in THF with five equivalents of chlorohydrocarbon and $MgPh_2(THF)_2$, internal standard, and exposure to 440 nm light for 24 hours produced cyclohexane in 23% yield; no cyclohexene was observed. However, using $MgBn_2(THF)_2$ yielded 96% cyclohexane in a catalytic reaction. Analogous control reactions using $MgBn_2(THF)_2$, $MgPh_2(THF)_2$ and

$MgCl_2$ to dechlorinate chlorocyclohexane without any **1-Ln** present resulted in just trace cyclohexane generation.

Following catalysis, **1-Ce** was completely consumed to form a new paramagnetic species identified as $[(Cp^{Me4})_2Ce(\mu–Cl)]_2$ (**3-Ce**) by ^1H NMR spectroscopy. This species is presumably formed through ligand exchange between **1-Ce** and $MgBn_2(THF)_2$ and coordination by a Cl produced by C–Cl bond activation. Given this result and the capability of Cp_2LnCl (Ln = Y, Yb, Sm) complexes to thermally cleave $C(sp^2)$–Cl bonds in conjunction with NaH, we chose to shift our efforts to studying the robust, and soluble $(Cp^{Me4})_3Ln$ (**2-Ln** (Ln = La, Ce, Pr, Nd, Sm, Dy) and $[(Cp^{Me4})_2LnCl]_2$ **3-Ln** (Ln = Ce,[16] Nd, Sm).

3.3.2 Catalytic dechlorination reactions with 2-Ln and 3-Ln

3.3.2.1 Synthesis and characterization of new complexes 3-Ln (Ln = Pr, Nd, Sm)

The later lanthanide congeners $[(Cp^{Me4})_2Pr(\mu–Cl)]_2$ (**3-Pr**), $[(Cp^{Me4})_2Nd(\mu–Cl)]_2$ (**3-Nd**) and $[(Cp^{Me4})_2Sm(\mu–Cl)]_2$ (**3-Sm**) of the bridging chloride species **3-Ce**, described in **Chapter 1**, were synthesized. Anhydrous lanthanide trichloride species $LnCl_3$ (Ln = Pr, Nd, Sm) needed to access **3-Pr**, **3-Nd,** and **3-Sm** via a comproportionation route were unavailable in large quantities our laboratory. Therefore for synthetic ease, the complexes were targeted via the chemical oxidation of the corresponding $(Cp^{Me4})_3Ln$ complex **2-Ln** (Ln = Pr, Nd, Sm) by $PhICl_2$ in THF (Scheme 3.3).[61]

3-Nd was isolated as a turquoise powder by this route, and subsequent recrystallization from THF/hexanes yielded periwinkle-colored blue blocks that were suitable for X-ray diffraction studies. **3-Nd** displays higher solubility in non-polar organic solvents than **3-Ce**, which is only soluble in THF, and is sparingly soluble in toluene and hexanes. Analysis of the solid-state structure of **3-Nd** shows a dimeric structure, with a Nd–Cl bond distance of 2.801 Å and Nd–Nd through-space bond distance of 4.278 Å. The Nd–Cl–Nd bond angle is 99.65°. Bond metrics are consistent with similar chloride bridging cyclopentadienyl complexes reported in the literature.[62,63]

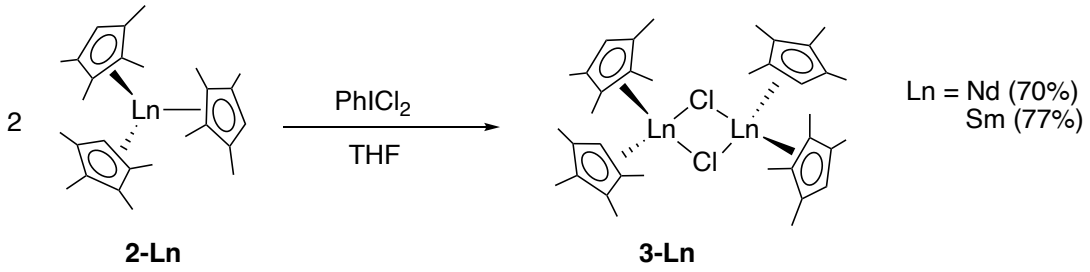

Scheme 3.3. Syntheses of lanthanide complexes **3-Nd** and **3-Sm**.

3-Sm was initially isolated as an orange powder, and recrystallization from THF/hexanes also generated orange blocks that were suitable for X-ray diffraction studies. Like **3-Ce** and **3-Nd**, **3-Sm** is shown to exist as a dimer in the solid state. The Sm–Cl bond distance measures 2.771 Å , the Sm–Sm through-space bond distance is 4.247 Å and the Sm–Cl–Sm bond angle is 99.97°, again similar to related complexes published in the literature.[64–75] **3-Sm** is in turn more

soluble than **3-Nd** and appears to be soluble in hexanes. **3-Pr** could not be characterized by XRD, though given the structures of **3-Ce**, **3-Nd,** and **3-Sm** we anticipate that it also adopts a dimeric structure in the solid-state.

This trend in increasing solubility of **3-Ln** as ionic radii increases could have interesting applications in rare-earth element separations.[76] The separation of neodymium and dysprosium is of particular interest in the reuse of neodymium-iron-boron (NdFeB) permanent magnets.[77] NdFeB magnets are key components in high value electronics and green energy technologies, such as computer hard drives, wind turbines, and hybrid electric vehicles.[78] While neodymium is the main rare-earth element component, 10% by weight of dysprosium is often added to improve magnet heat tolerance.[79] Preliminary investigations into the synthesis of $[(Cp^{Me4})_2DyCl]_2$ (**3-Dy**) through the treatment of $(Cp^{Me4})_3Dy$ (**2-Dy**) with $PhICl_2$ suggests that the resulting product is highly soluble in hexanes, through further characterization and investigation into solubility is needed.

3.3.2.2 General reaction procedure

Using the simple cyclopentadienyl complexes **2-Ln** (Ln = La, Ce, Pr, Nd, Sm, Dy) and **3-Ln** (Ln = Ce,[16] Nd, Sm), we aimed to both probe the catalytic dechlorination of chlorocyclohexane, and also access catalytic C–Cl bond cleavage for other chlorinated substrates including PVC.

First, NaH was again tested as an external reductant, as used in the thermal dechlorination of aromatic chlorohydrocarbons by Penn et. al. Despite the lack of success with this reagent in light-driven dechlorination reactions with **1-Ln**, we anticipated complexes **2-Ln** (Ln = La, Ce, Nd, Sm) and **3-Ln** (Ln = Ce, Nd, Sm), without chelating or encapsulating ligands, would be more susceptible to attack from a nucleophilic hydride to form the proposed active bridging-hydride species. The catalysis procedure consisted of dissolution of the chosen lanthanide complex (20 mol % loading) in THF with five equivalents of chlorohydrocarbon and NaH, internal standard, and exposure to 440 nm light from a low energy Kessil lamp. All reactions were monitored by ^{1}H NMR spectroscopy, with in situ yields determined following 24 hours irradiation. However, only near stoichiometric (Ln = La, Ce) or sub 10% yield (Ln = Nd, Sm) of cyclohexane product was observed in all cases, which is credited to the insolubility of NaH in THF and the lack of stirring during these NMR scale reactions. However, no product generation is observed without light irradiation, and so even stoichiometric yields of cyclohexane implicate light absorption through the Cp^{Me4} ligand in enabling reactivity for Ln = La, Nd, Sm.

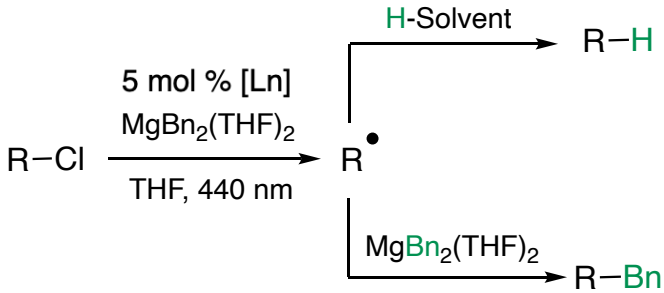

Scheme 3.4. General reaction scheme for C–Cl activation and hydrodechlorination by Ln complexes **1-Ln, 2-Ln** and **3-Ln**. Following C–Cl bond cleavage the hydrocarbyl radical can be quenched either by abstraction of H radical from solvent, or a benzyl radical from turnover reagent $MgBn_2(THF)_2$.

An analogous catalysis procedure instead using THF-soluble $MgBn_2(THF)_2$ as a reductant was then followed, with the dissolution of lanthanide complex (5 mol % loading) in THF with 20 equivalents of chlorohydrocarbon and $MgBn_2(THF)_2$, internal standard, and 24 hours irradiation with 440 nm light. The anticipated reactions are shown in Scheme 3.4. Light absorption occurs first, presumably by the Cp^{Me4} ligand or the cerium cation if present, see later calculations. If this generates an excited state complex that is sufficiently reducing to cleave the R–Cl bond, then the reaction should release the R radical, to be trapped by solvent (R–H, Scheme 3.4, upper) or a Bn group from the $MgBn_2(THF)_2$ co-reagent (R–Bn, Scheme 3.4, lower). While hydrodechlorination is a useful strategy for the dechlorination of organic molecules as previously discussed, the possibility of functionalizing the alkyl radical produced could have significant applications in polymer upcycling.[19,20]

3.3.2.3 Catalytic dechlorination of chlorocyclohexane

Many of the complexes **2-Ln** and **3-Ln** are capable of the hydrodechlorination of chlorocyclohexane; no benzylation of the alkyl radical is observed. For chlorocyclohexane, the radical formed from Cl atom abstraction is short-lived,[80] and the organic product is therefore the hydrocarbon arising from replacement of Cl by H. This was confirmed by ^{1}H NMR spectroscopy. The H atom derives from the THF solvent, (Scheme 3.4, upper), as was seen in the hydrodefluorination chemistry described in **Chapter 2**.[16] This was corroborated by carrying out the dechlorination with **2-Ce** in THF-D_8, where the incorporation of deuterium into cyclohexane following the C–Cl bond activation of chlorocyclohexane can be observed by ^{13}C NMR spectroscopy.[81] The proton resonances of cyclohexane-D_1 coalesce into one broad peak overlapping with the singlet resonance of cyclohexane, so deuterium incorporation could not be observed using ^{1}H NMR spectroscopy.[82] As with our previously reported photocatalytic defluorination chemistry, there is a significant kinetic isotope effect in these reactions.[16]

The yields of cyclohexane using complexes **2-Ln** and **3-Ln** alongside **1-Ce** are summarized in Table 3.2, with the yields of the most efficient catalysts at 5 mol % loading shown Figure 3.6. Of the Ce catalysts, **2-Ce** is best at dechlorination, generating cyclohexane in 93% yield after 24 hours irradiation. Following catalysis, the consumption of **2-Ce** to quantitatively form **3-Ce** is seen, *vide infra*. **3-Ce** is also a very good catalyst for this transformation, producing cyclohexane in 76% yield within the same time frame. Conversely, phenoxy-NHC complex **1-Ce**, a far superior catalyst to **2-Ce** for C–F bond activation,[16] produces cyclohexane in just 37% yield. **2-La** is also capable of the C–Cl bond activation, albeit less effectively, with 29% conversion. Interestingly, the **2-Ln** complexes tested are also more efficient catalysts than the **3-Ln** congeners, though at lower catalyst loadings (1 mol %), the yields of cyclohexane generated by **2-Ce** and **3-Ce** are comparable (*vide infra*.).

All the cerium complexes are better catalysts than the other Ln congeners, in line with the straightforward, allowed excitation of the f^1 to a strongly reducing d^1 centered excited state. Because the Cp^{Me4} ligands can absorb light, all the early lanthanides can be photoexcited and their photocatalytic activity decreases with increasing atomic number. The heaviest lanthanide studied, **2-Dy,** produces negligible dechlorinated product, consistent with the requirement for the chlorinated substrate to bind the Ln, which is increasingly hindered in catalysts with smaller ionic radii.[83] Though rare, molecular complexes of tetravalent praesodymium are known,[84] raising the possibility that a Pr congener could facilitate a Ln(III)/(IV) redox event and be an efficient catalyst. Catalyst **2-Pr** produces cyclohexane in 20% yield, which is in line with the

increased stability of Ce(IV) relative to Pr(IV) and supports the value of the facile $4f \rightarrow 5d$ excitation in the best catalysts.

Table 3.2. Calculated conversion of chlorocyclohexane to cyclohexane following 24 hours irradiation, with product yields determined by ^{1}H NMR spectroscopy. No product formation was seen without irradiation with light.

Entry	Catalyst	Catalyst Loading (mol %)	Product Yield (%)
1	**2-La**	20	52
2	**2-La**	5	29
3	**3-La**	5	28
4	**1-Ce**	20	96
5	**1-Ce**	5	37
6	**2-Ce**	20	89
7	**2-Ce**	5	93
8	**2-Ce**	1	96
9	**3-Ce**	20	63
10	**3-Ce**	5	76
11	**3-Ce**	1	97
12	**2-Pr**	5	19
13	**2-Nd**	20	37
14	**2-Nd**	5	6.6
15	**3-Nd**	20	27
16	**2-Sm**	20	15
17	**2-Sm**	5	2.2
18	**3-Sm**	20	15
19	**2-Dy**	20	0
20	**2-Dy**	5	0

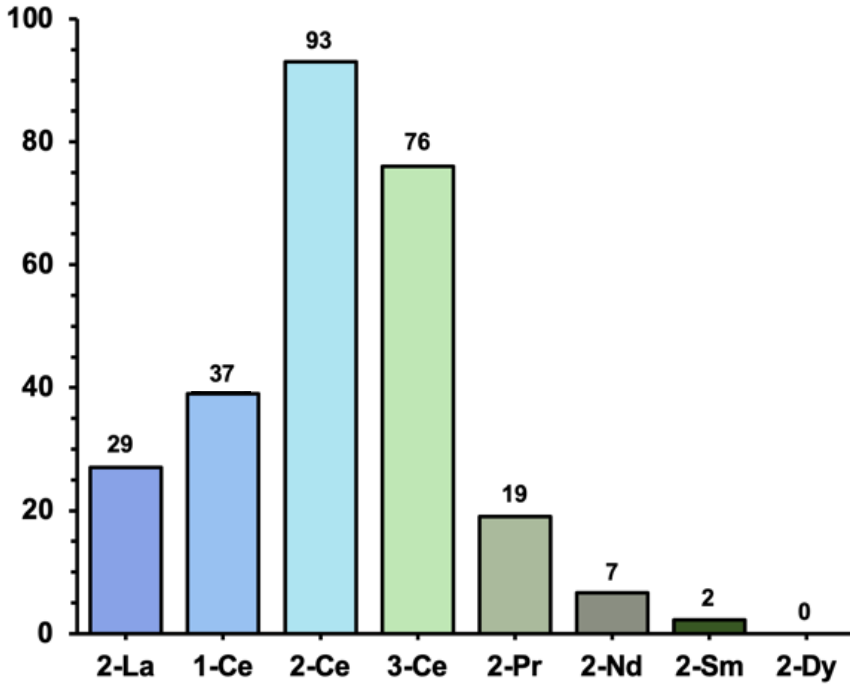

Figure 3.6. Hydrodechlorination of chlorocyclohexane catalyzed by different Ln photocatalysts. Reactions were carried out at RT, in THF-H_8, with 5 mol % catalyst loading, and irradiated with a 40 W Kessil 440 nm lamp. The percentage yield of cyclohexane was determined by ^{1}H NMR spectroscopy relative to an internal standard.

3.3.2.4. Catalytic dechlorination of other C(sp^3)–Cl and C(sp^2)–Cl bonds

A substrate scope for photocatalytic C–Cl activation facilitated by the most effective catalyst, **2-Ce**, was undertaken. The dechlorination reactivity was expanded to include allyl, vinyl, primary and tertiary carbon centers, substituted chloroarenes, and commercial PVC (Table 3.3).

For the products arising from hydrodechlorination, the proton source is again the THF solvent. The incorporation of deuterium into 2-methylpropene following the C–Cl bond activation of 1-chloro-2-methylpropene was observed, this time through both ^{1}H and ^{13}C NMR spectroscopy. In contrast to the dechlorination of chlorocyclohexane, reactions with substrates that produce a more stabilized radical intermediate following dechlorination yield a benzylated product, from reaction with the $MgBn_2(THF)_2$ or benzyl radicals in solution.

For example, the major product generated from dechlorination of 3-chloro-2-methylpropene by **2-Ce** is 3-methyl(but-3-en-1-yl)benzene, arising from the benzylation of the allyl radical. 1,2-bis(4-(trifluoromethyl)phenyl)ethane is formed in 89% yield from the benzylation of the benzyl radical produced by the dechlorination of 1-(chloromethyl)-4-(trifluoromethyl)benzene. Trace defluoroalkylation of the trifluoromethyl group is also observed which can be attributed to the increased activation of the C–F bond through the inductive effect of the chlorine atom. The dechlorination of 2-chloro-2-methylpropane forms 2-methylprop-1-ene, which is the product arising from ^{t}Bu radical generation and subsequent formation of a closed shell molecule.[85]

Table 3.3. Calculated conversion R–Cl to R–H or R–Bn with yields of dechlorinated product determined by ^{1}H NMR spectroscopy. No product formation was seen without irradiation with light.

Entry	Substrate	Major Identified Product	Yield (%)
1	Chlorocyclohexane	Cyclohexane	93
2	Chlorobenzene	Benzene	64
3	Chlorobenzene	Benzene	64[a]
4	1-Chloro-4-fluorobenzene	Fluorobenzene	100
5	(2-chloroethyl)benzene	Ethylbenzene	42
6	1-(chloromethyl)-4-(trifluoromethyl)benzene	1,2-bis(4-(trifluoromethyl)phenyl)ethane	89
7	1-Chloro-2-methylpropene	2-methylprop-1-ene	73
8	3-Chloro-2-methylpropene	(3-methylbut-3-en-1-yl)benzene	79
9	2-chloro-2-methylpropane	2-methylprop-1-ene	20
10	Polyvinyl chloride	Polyethylene[b]	79

[a]100% yield observed after 48 hours irradiation. [b]Characterization techniques suggest PE-like material is generated, *vide infra.*

With an interest in polymer upcycling, preliminary results suggest that under standard conditions, **2-Ce** at 5 mol % loading can photocatalytically cleave 79% of the C–Cl bonds in a commercial sample of PVC over 24 hours (Figure 3.7). As the dechlorination proceeds, the polymer becomes insoluble in THF and can thus be readily isolated. Extending the reaction time to 48 hours or lowering catalyst loadings to 1 mol % result in comparable yields, suggesting that dechlorination progresses until the point at which the polymer becomes insoluble in THF. FT-IR spectroscopy (Figure 3.8) of the sample shows spectral features that correlate with segments of polyethylene, no evidence of polyacetylenic groups,[86] and some level of unsaturation, which is also observed as a natural defect in commercial PVC. However, the insolubility of the polymer in organic solvents at high temperatures support the absence of chain shortening but have precluded characterization by gel permeation chromatography (GPC).[87]

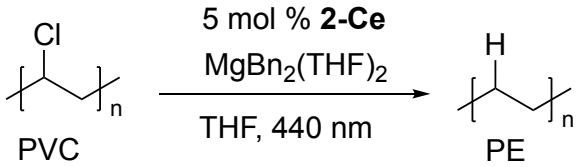

Figure 3.7. Dechlorination of PVC to produce PE using **2-Ce**.

While such results are promising, further optimization of reaction conditions are needed in order to achieve complete dechlorination and potentially extend this chemistry to polymer upcycling through functionalization of the polymer at the site of C–Cl bond cleavage (Scheme 3.5). Such post polymerization modification could impart new chemical properties to the polymer, increasing the value of the material while retaining the beneficial attributes of the parent polymer.[88] For example, recent work by Hartwig et al. demonstrated that the installation of hydroxyl functional groups at the site of C–H bond activation in polyethylene results in enhanced adhesive properties.[89]

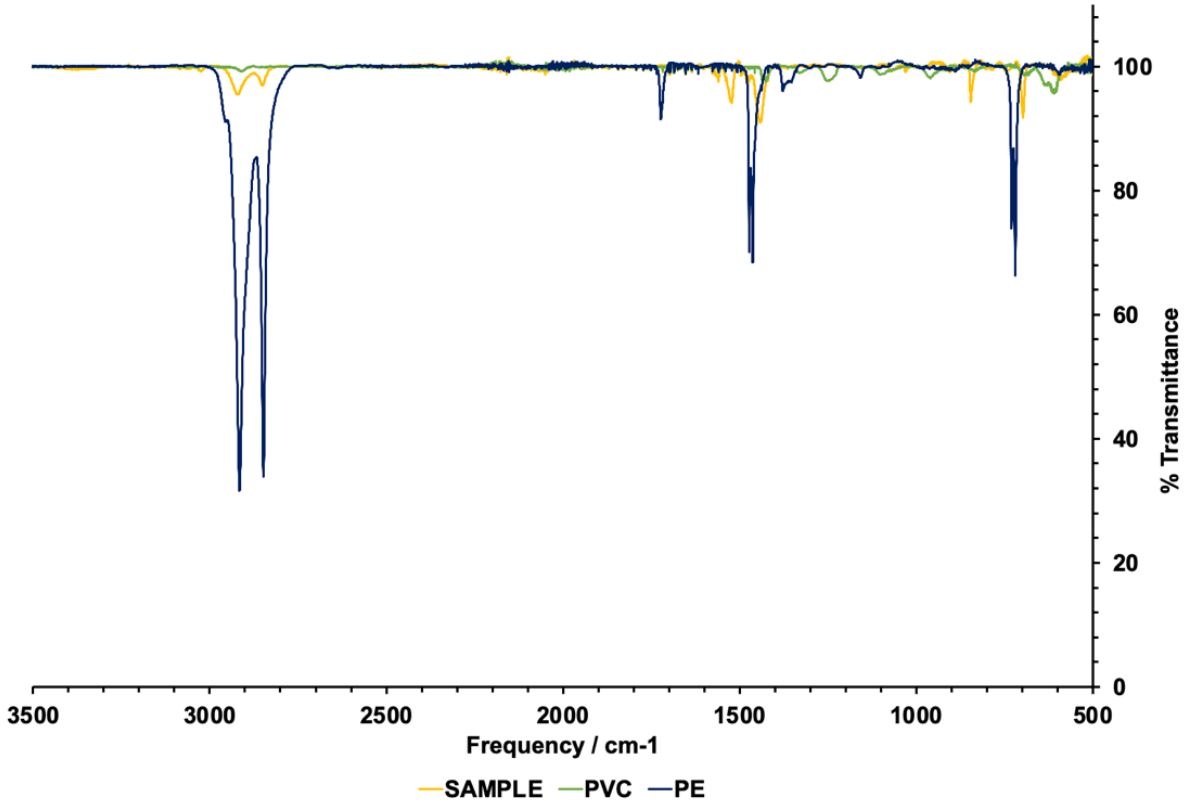

Figure 3.8. FT-IR spectrum of PVC, polyethylene, and the dechlorinated sample. Sample possesses similar features to commercial sample of polyethylene, alongside evidence of unreacted PVC.

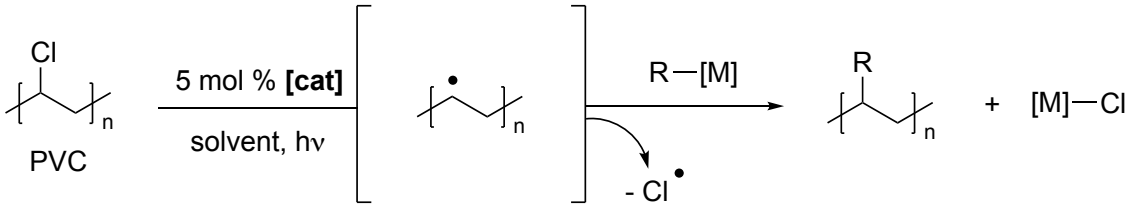

Scheme 3.5. Envisioned reaction scheme for the light-driven dechloroalkylation of PVC.

3.3.3 Mechanistic studies

3.3.3.1 Experimental mechanistic investigation

A series of stoichiometric reactions give more insight into the mechanism of dechlorination by **2-Ce**. Even without irradiation, green THF solutions of **2-Ce** react with $MgBn_2(THF)_2$ turning the solution yellow-green due to the formation of the cerium benzyl species $(Cp^{Me4})_2Ce(Bn)(THF)$ (**6-Ce**), confirmed by ^1H NMR spectroscopy and an independent synthesis.[16] Spectroscopic measurements confirm that the four compounds **2-Ce**, **6-Ce**, $MgBn_2(THF)_2$ and $Mg(Cp^{Me4})_2$ are all present in equilibrium in solution at the start of the reaction.[90] A reaction of **2-Ce** with a 20-fold excess of $MgBn_2(THF)_2$ results in a mixture of these products with a calculated equilibrium constant of 2.5 for the equation in Figure 3.9.

Product yields for both **2-Ce** and **3-Ce** are higher at lower (1 mol %) catalyst loadings, yielding 96% and 97% cyclohexane respectively following 24 hours irradiation. This could be attributed to the greater effective concentration of $MgBn_2(THF)_2$ that pushes the equilibrium towards the active species **6-Ce**. This is not seen for **1-Ce**, as the chelating aryloxy-NHC ligand complex is less susceptible to ligand exchange with benzyl radicals, as shown in our previous study. For the series **2-Ln** other than Ce, the increase in product formation with increasing catalyst loading is as would be anticipated. Control reactions with $Mg(Cp^{Me4})_2$ show negligible product formation, which can be attributed to the high stability of this complex,[91] and highlights the importance of the large, Lewis-acidic lanthanide center.

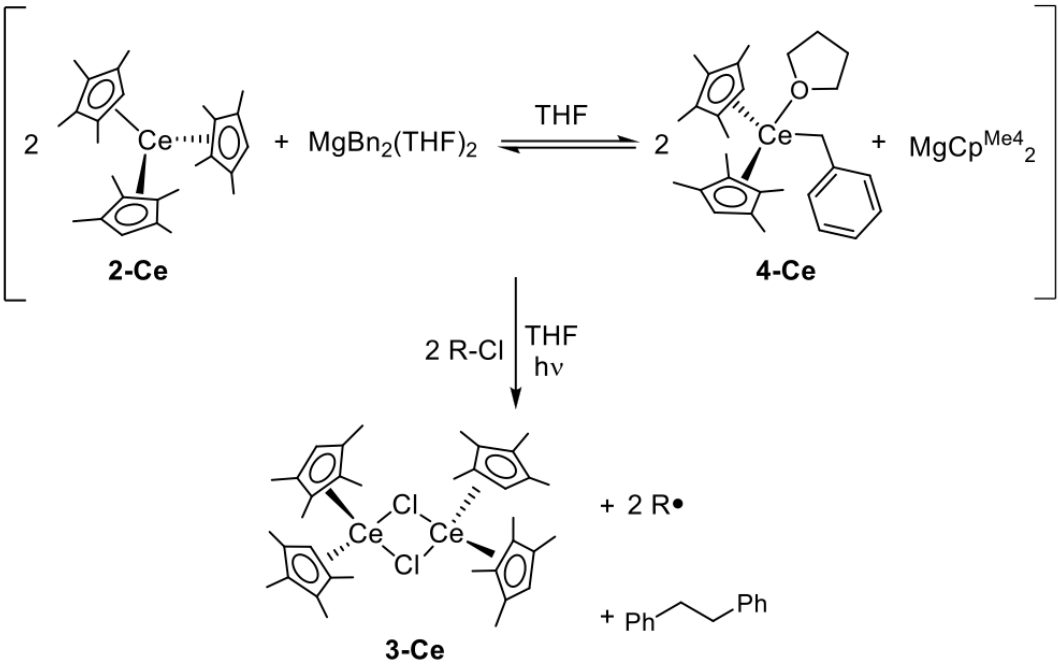

Figure 3.9. Stoichiometric reactions to define the mechanism of C–Cl activation by **2-Ce**.

The addition of chlorohydrocarbon substrate to the mixture containing **2-Ce** and **6-Ce** and irradiation for 24 hours generates a bright yellow solution arising from the complete conversion to the chloride complex **3-Ce** which is identified by ^{1}H NMR spectroscopy (
Figure **3.9**). It was previously experimentally verified that irradiation of a pure sample of **6-Ce** results in the formation of **2-Ce** and bibenzyl (**Chapter 2**) we also determined that the reaction of **3-Ce** and $MgBn_2(THF)_2$ to form the benzyl **6-Ce** does not proceed without irradiation, (Figure 3.10, *vide infra*.) It should be noted that **3-Ce** is able to facilitate stoichiometric dechlorination when irradiated with chlorocyclohexane. This results in its conversion to a white solid which could be cerium trichloride, formed due to the displacement of the Cp^{Me4} ligand by Cl following C–Cl bond activation.

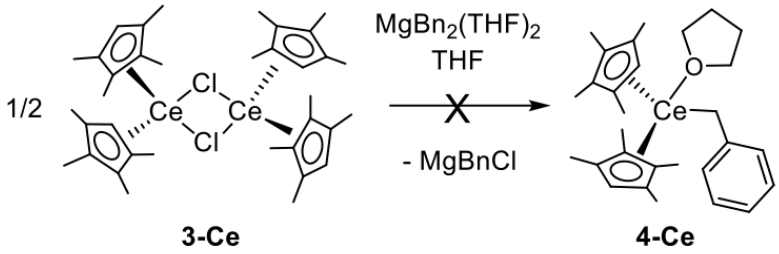

Figure 3.10. Stoichiometric reactions to define the mechanism of C–Cl activation by **2-Ce**. **6-Ce** cannot be formed from **3-Ce** prior to irradiation.

3.3.3.2 Computational studies

Schelter and co-workers showed that Ce(III) amido and guanidinate photocatalysts form an inner-sphere complex with benzyl chloride, which lowers the barrier to halogen atom abstraction, and releases benzyl radical to form products.[83] Here, calculations were performed for the excited states of complexes **2-Ce** and **2-La** and the proposed intermediate in which cyclohexylchloride binds as a Cl–donor ligand to **6-Ce**, recognizing that both the tris(Cp^{Me4}) and benzyl complex can be active in C–X bond activation reactions. Time-dependent DFT (TD-DFT; B3PW91) calculations on both **2-Ce** and **2-La** reveal similar SOMO structures upon photoexcitation (Figure 3.11). Experimentally, both **2-Ce** and **2-La** absorb at 426 nm, calculated as an intense absorption at approximately 380 nm (415nm in solvent).[92] This is assigned as transition from the π-orbital of the Cp^{Me4} ligand to the dz^2 on the metal. For **2-Ce**, this is accompanied by a lower intensity metal-based $4f \rightarrow 5d$ excitation at 410 nm. It is notable that the cerium molecule is pyramidally distorted by 5° away from the ground state pseudo-D_{3h} symmetry, unlike the La congener. This increases access to one end of what was a primarily dz^2-orbital, and may provide greater access to the Cl substrate, or the Bn reagent, which would further contribute to the higher activity of Ce relative to La, despite its smaller ionic radius.

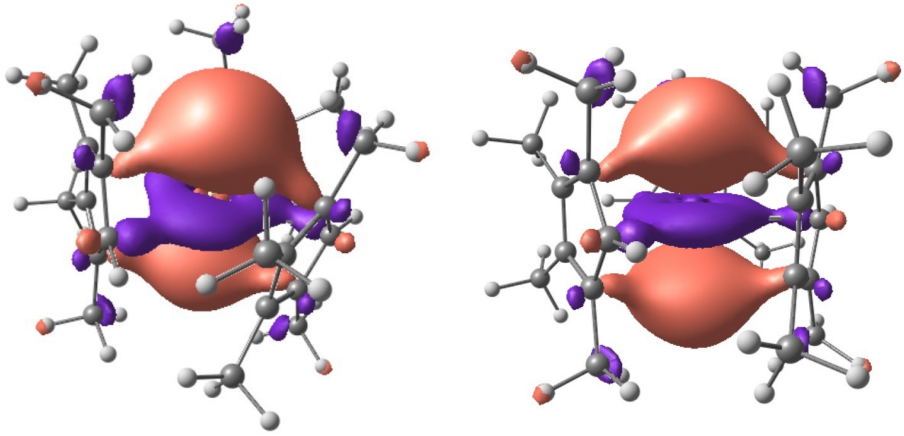

Figure 3.11. Depictions of the calculated SOMO of **2-Ce** (left) and **2-La** (right) after absorption. Color code: gold – Ce; green – Cl; grey – C; white – H.

TD-DFT studies of the Cl–alkyl adduct of **6-Ce** show a low intensity absorption at 425 nm (448 nm calculated with an added solvent correction), experimentally observed at 450 nm, arising from the excitation of the SOMO (4*f* electron) into the LUMO which is primarily bonding for the Ce–Cl bond and antibonding with respect to the C–Cl bond (Figure 3.12). This supports our experimental observation that **6-Ce** cannot be formed from **3-Ce** without irradiation, and could be attributed to the strength of the Ce–Cl bond relative to Ce–C. The excited state populated by irradiation also implies the transition from the HOMO, which is the Ce–Bn bonding interaction, to the LUMO so that the Ce–Bn bond may easily be broken. This early loss of the Bn group is consistent with our observations of the difficulty of trapping it in a product when substrates with short-lived radical products are used.

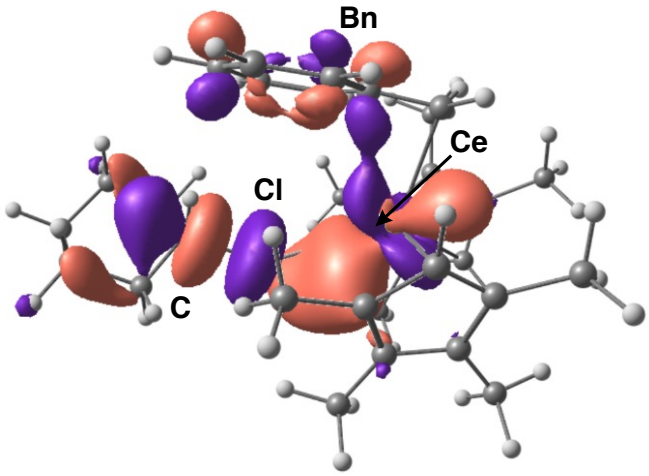

Figure 3.12. Depiction of the TD-DFT-calculated LUMO of the adduct formed during catalysis when chlorocyclohexane binds to **6-Ce**. Color code: gold – Ce; green – Cl; grey – C; white – H.

3.3.3.3 Mechanistic summary

Our proposed mechanism therefore begins with the formation of a mixture of **2-Ce** and **6-Ce** and excess $MgBn_2(THF)_2$. The added chloroalkane will bind as an L–donor, most likely to the less sterically saturated Ln center in **6-Ln**. Photoexcitation results in formation of the Ln–Cl bond as C–Cl bond cleavage occurs, releasing the hydrocarbyl radical R•. The intermediate $(Cp^{Me4})_2Ln(Cl)(Bn)$ will be more stable for Ln = Ce, and to a much lesser extent Ln = Pr, which can form tetravalent complexes, but it was previously shown that the Cp^{Me4} ligand can be oxidized in place of the Ln center, to stabilize the other Ln intermediates for which Ln(IV) is not accessible. The release of the reducing Bn• will still be facile. We had anticipated that the proximity of R• and Ln–Bn in the solvent cage would lead to the alkylated product R–Bn, but in THF, a good H-atom donor, R–H is formed through H atom abstraction from solvent when the resulting alkyl radical is unstabilized and too short-lived to be captured. Longer-lived allyl and benzyl radicals can be benzylated in this system, although it is likely that this does not occur within the local coordination sphere of the lanthanide cation. The resulting chloride **3-Ln** is then photochemically converted back to the benzyl **6-Ln** by the excess $MgBn_2(THF)_2$ present.

This catalytic cycle is consistent with our experimental observations that the activities of precatalysts (Cp^{Me4}_2)CeX (X= Cp^{Me4}, Cl, **L**) are related to the rate at which they can form alkyl species **6-Ce**. Catalyst **2-Ce** is more effective than **1-Ce** and **3-Ce** potentially due to the higher stability of the Ln–(O-NHC) and Ln–Cl bonds respectively relative to Ln–Cp^{Me4}.[16,33,93] While **6-Ce** was shown to be capable of facilitating defluoroalkyation of $PhCF_3$, ultimately it was too unstable to remain active over the longer irradiation times required for efficient, catalytic C–F bond activation. Given the weaker C–Cl bond and consequently shorter required reaction times, **2-Ce** and **6-Ce** can act as efficient dechlorination catalysts.

It should also be noted that the excited state lifetime of **3-Ce** is 175 ns (**Chapter 1**), which is amongst the longest excited state lifetimes reported for a cerium complex.[1] In contrast, the lifetime of **1-Ce** is considerably shorter at 101 ns, though still greater than many other Ce complexes studied.[94] Ultimately, while specialized, light-absorbing ligand **L** is required for cleaving the strong C(sp^3)–F bond, absorption through Cp^{Me4} is satisfactory for activation of the weaker C(sp^3)–Cl bond, providing evidence of the power of ligand-tuning of lanthanide photocatalysis.

3.3.3.4 Preliminary investigations into the dechlorination chemistry of lanthanide cyclooctatetraenyl complexes

Given the light-absorbing capability of the Cp^{Me4} ligand, and the implication of the homolysis of a Ln–Cp^{Me4} bond in both the C–F and C–Cl bond activation chemistry presented in this thesis, we were interested in studying the dechlorination chemistry of lanthanide complexes bearing dianionic cyclooctatetraenyl (COT) ligands.[95–97] A chelating COT ligand on a lanthanide dehalogenation photocatalyst could reduce metal-ligand bond homolysis and work to prevent catalyst degradation, while still allowing for an active site where substrate could interact with the metal center. As discussed in **Chapter 1**, complexes $[(C_8H_8)Ce(\mu–O_3SCF_3)(THF)_2]_2$ and $[(C_8H_8)Ce(\mu–Cl)(THF)_2]_2$, published by Schelter et al. are fluorescent and display lifetimes of 205 ns 145 ns respectively, demonstrating their capability for light absorbance.[94]

Cyclooctatetraene readily reacts with sodium to form Na_2COT, which can be transmetallated through a salt metathesis reaction with lanthanide and actinide halide complexes. The complex $CeI(COT)(THF)_3$ (**12-Ce**) was synthesized according to literature procedure[98,99] and tested in photocatalytic dechlorination of chlorocyclohexane with $MgBn_2(THF)_2$. Upon addition of $MgBn_2(THF)_2$ to **12-Ce** in THF, a brightening of the reaction mixture was observed, attributed to the potential formation of a [Ce(COT)(Bn)] species. Under standard conditions, 19% conversion to cyclohexane was observed following 24 hours irradiation, suggesting catalytic activity less than that of **2-Ce**. Following catalysis, the reaction mixture was fluorescent yellow, and the generation of a white precipitate was observed, which could be insoluble [Mg(COT)] or cerium trichloride. Further mechanistic investigation of this reaction is underway in our laboratory to both explain the observed reactivity and extend photocatalytic studies to other lanthanide COT complexes.

3.4 Conclusions

Expanding on our previously reported photocatalytic defluoroalkylation chemistry, the light-driven cleavage of a variety of C(sp^3)–Cl and C(sp^2)–Cl bonds in chlorohydrocarbons, including the environmentally relevant polymer PVC, can be accessed using simple lanthanide cyclopentadienyl complexes of the form $(Cp^{Me4})_3Ln$ (**2-Ln**) and $[(Cp^{Me4})_2Ln(\mu–Cl)]_2$ (**3-Ln**).

Tris(cyclopentadienyl) complexes in particular are readily synthesized and are widely considered a mainstay of organometallic lanthanide chemistry.[100]

Catalytic C–Cl bond activation is achieved via a reactive lanthanide alkyl intermediate, which was identified through both experiment and computation, and is consistent with previously reported mechanisms for reactions of this type.[17,18] Significantly, photocatalysis is again observed with both cerium and also other typically photo-inactive lanthanides due to absorption of light through ancillary ligands. While specialized, light-absorbing ligand **L** is required for efficient C(sp^3)–F bond activation, light absorption through Cp^{Me4} is satisfactory for activation of the weaker C(sp^3)–Cl bond. The weaker C–Cl bonds relative to C–F bonds also results in shorter required reaction times that reduce the need for a robust catalyst such as **1-Ce**, as described in **Chapter 2**.

The ability of **2-Ce** to cleave the C–Cl bond in PVC could lead to promising applications in polymer upcycling or the purification of polymer waste streams that contain undesirable amounts of PVC. Currently the potential functionalization of an alkyl radical produced via dechlorination with this system appears to depend on the intrinsic stability of the substrate. However, further catalyst tuning such as the addition of bulkier alkyl substituents onto the Cp ligand may allow for the selective alkylation of materials at the site of radical formation, by maintaining proximity of the catalysts and substrates through steric effects or dispersion forces.[101]

3.5 Experimental

General details. All moisture and air sensitive materials were manipulated using standard high-vacuum Schlenk-line techniques and MBraun gloveboxes and stored under an atmosphere of dried and deoxygenated dinitrogen. All glassware items, cannulae and Fisherbrand 1.2 μm retention glass microfiber filters were dried in a 160 °C oven overnight before use.

Solvents and reagents. Hexanes, tetrahydrofuran (THF), diethyl ether (Et_2O) and toluene for use with moisture and air sensitive compounds were dried using an MBraun SPS 800 Manual solvent purification system and stored over activated 3 Å molecular sieves. Benzene-D_6, pyridine-D_5 were purchased from Cambridge Isotope Laboratories and were refluxed over potassium metal for 24 hours, freeze-pump-thaw degassed and purified by trap-to-trap distillation prior to use. THF-D_8 was purchased from Cambridge Isotope Laboratories and dried over sodium/benzophenone before being freeze-pump-thaw degassed and purified by trap-to-trap distillation prior to use. All solvents were purchased from Sigma-Aldrich or Fisher Scientific and stored over 3 Å molecular sieves for 4 hours before being used.

$PhICl_2$ was prepared according to the literature procedure[102] and stored at –30 °C. Dihydrocarbyl magnesium reagents,[103] **HL**, $\mathbf{HL^{Mes}}$ and $\mathbf{HL^{tBu}}$,[104] KC_5Me_4H,[105] lanthanide triiodides (Ln = La, Ce, Nd, Sm),[106,107] and lanthanide tris(tetramethylcyclopentadienyl) complexes (Ln = La, Ce, Pr, Nd, Sm),[107,108] $Mg(Cp^{Me4})_2$[109], Na_2COT,[110] $CeI(COT)(THF)_3$[99] were all prepared using published methods. **1-Ce**, $\mathbf{1\text{-}Ce^tBu}$, **1-Nd**, **1-Sm**, and **3-Ce** were synthesized as previously described in **Chapter 1**. All other chemicals were purchased from commercial suppliers and degassed and/or dried under vacuum or over 3 Å molecular sieves for 12 hours before use.

Characterization. NMR spectra were recorded on Bruker Avance 400, 500 and 600 MHz spectrometers and are referenced to residual protio solvent (3.58 and 1.72 ppm for THF-D_8,

7.16 ppm for C_6D_6) for ^1H NMR spectroscopy. THF was used as solvents for No Deuterium (NoD) NMR experiments,[10] and was referenced to added tetramethylsilane (0.00 ppm for both ^1H and $^{13}C\{^1H\}$ NMR spectroscopic experiments). Quantitative ^1H NMR data were acquired with a minimum of eight scans, with the delay time set to 5x the longest T_1 value present. Chemical shifts are quoted in ppm and coupling constants in Hz. Tetrakis(trimethylsilyl)silane (TMS*) was used as internal standards for quantitative ^1H NMR spectroscopy. NMR spectra were taken at 25°C unless otherwise noted. Structural assignments were performed using HSQC and HMBC NMR spectroscopic experiments when necessary. Elemental analyses were carried out by the microanalytic services in the College of Chemistry at the University of California, Berkeley. ATR-FTIR spectra were recorded on a Shimadzu IRSpirit FTIR spectrometer on neat powders.

Photophysical data. Quartz cells with a 10 mm pathlength equipped with a J-Young valve were used to contain samples prepared under a dinitrogen atmosphere for electronic absorption spectra (UV-Visbile) measurements. UV-Visbile measurements were collected on an Agilent Varian Cary 50 UV-Visbile spectrophotometer.

Crystallography. X-ray diffraction data were collected at beamline 12.2.1 of the Advanced Light Source (ALS) at Lawrence Berkeley National Lab, using a Bruker D8 diffractometer coupled to a Bruker PhotonII CPAD detector with Si(111)-monochromated synchrotron radiation (17 keV radiation). Single crystal X-ray diffraction data of all other compounds were collected using a Rigaku Xtalab Synergy-S diffractometer fitted with a HyPix-6000HE photon counting detector using MoKα (λ = 0.71073 Å) or CuKα (λ = 1.5418Å) radiation. All structures were solved using SHELXT in Olex2 and refined using SHELXL in Olex2.[111,112]Absorption corrections were completed using CrysAlis PRO (Rigaku Oxford Diffraction) software. Analytical numeric absorption corrections used a multifaceted crystal model based on expressions derived by Clark and Reid.[113] Numerical absorption correction was based on a Gaussian integration over a multifaceted crystal model.

Computational details. All DFT and TDDFT calculations were carried out using Gaussian 09[114] software package. Optimizations, frequency calculations and population analysis were performed using the B3PW91[115,116] functional. Ce, La and Cl atoms were treated with a Stuttgart effective core potential and the associated basis set.[117,118] In the case of Cl, a set of polarization functions[119] was added. The 6-31G** basis set[120,121] was employed for C and H atoms. Single point calculations including THF solvent were carried out to correct the TDDFT spectra using the SMD model.

Synthesis of KL. To a cold (-78 °C), magnetically stirred, cream slurry of 2.13 g of [H_2**L**]Br (2.13g, 0.00540, 1.00 equiv.) in THF (50 mL), was added a cold suspension of K(N{$SiMe_3$}$_2$) (2.16 g, 0.0109 mol, 2.00 equiv.) in THF (100 mL) dropwise over ten minutes. The mixture was allowed to warm to room temperature, with stirring, overnight. After this period, the orange solution was isolated from the pale grey powder (KBr) by filtration. Concentration of the solution to 5 mL and the subsequent addition of 10 mL of pentane provided a cream powder. This powder was isolated by filtration and washed with pentane (3 x 20 mL) to afford **KL**. Yield: 1.56 g (82%)

^1H NMR (500 MHz, pyridine-D_5, 300 K): δ 7.49 (d, $J_{H\text{-}H}$ = 2.9, 1H, $CH(5)_{Ph}$), 7.34 (d, $J_{H\text{-}H}$ = 2.9, 1H, $CH(3)_{Ph}$), 7.33 (d, $J_{H\text{-}H}$ = 1.6, 1H, $CH_{Im(Ph)}$), 7.10 (d, $J_{H\text{-}H}$ = 1.6, 1H, $CH_{Im(iPr)}$), 4.51 (sept, $J_{H\text{-}H}$ = 6.7, 1H, CH_{iPr}), 1.69 (s, 9H, CH_{3tBu}), 1.38 (s, 9H, CH_{3tBu}), 1.30 (d, $J_{H\text{-}H}$ = 6.7, 6H, CH_{3iPr}). $^{13}C\{^1H\}$ NMR (125.8 MHz, pyridine-d_5, 300 K): δ 206.3 (s, C-K), 163.4 (s, C-O),

138.6 (s, C_{Ph}), 131.4 (s, C_{Ph}), 127.6 (s, C_{Ph}), 122.7 (s, $CH_{Im(Ph)}$), 122.1 (s, CH_{Ph}), 122.0 (s, CH_{Ph}), 114.6 (s, $CH_{Im(iPr)}$), 51.8 (s, CH_{iPr}), 35.7 (s, C_{tBu}), 33.7 (s, C_{tBu}), 32.2 (s, CH_{3tBu}), 30.0 (s, CH_{3tBu}), 24.0 (s, CH_{3iPr}).

Synthesis of [(Cp^{Me4})$_2$Pr(μ–Cl)]$_2$ (3-Pr). In a glovebox a vial was charged with (Cp^{Me4})$_3$Pr (**2-Pr**) (20.0 mg, 0.0396 mmol, 1.00 equiv.) in THF (5 mL), resulting in a yellow solution. With stirring, a colorless solution of $PhICl_2$ (5.7 mg, 0.0206 mmol, 0.520 equiv.) in THF (1 mL) was added dropwise. After stirring for 16 hours at room temperature, a color change from yellow to pale yellow was seen, and the volatiles were removed under vacuum resulting in a yellow powder which was subsequently washed with cold hexanes (2 x 0.5 mL). Yield: 5.2 mg, 40 %.

^{1}H NMR (500 MHz, THF-H_8) δ δ 24.76 (br. s, 12H, **CH_{3Cp}**), 5.27 (br. s, 2H, **H_{Cp}**), 7.54 (br. s, 12H, **CH_{3Cp}**). Anal. Calcd for: $C_{36}H_{52}Pr_2Cl_2$: C, 54.64; H, 7.20. Found: C,51.53; H,6.99.

Synthesis of [(Cp^{Me4})$_2$Nd(μ–Cl)]$_2$ (3-Nd). In a glovebox a vial was charged with (Cp^{Me4})$_3$Nd (**2-Nd**) (94.5 mg, 0.186 mmol, 1.00 equiv.) in THF (5 mL), resulting in a green solution. With stirring, a colorless solution of $PhICl_2$ (26.6 mg, 0.0968 mmol, 0.520 equiv.) in THF (1 mL) was added dropwise. After stirring for 1 hour at room temperature, a color change to turquoise was seen, and the solution continued to stir overnight. After this time the volatiles were removed under vacuum, resulting in a turquoise powder which was subsequently washed with cold hexanes (2 x 0.5 mL). The powder was redissolved in a minimum of THF (1 mL), layered with hexanes (3 mL) and stored at –30 °C for 3 days to yield periwinkle blue blocks of **[(Cp^{Me4})$_2$Nd(μ–Cl)]$_2$** that were suitable for X-ray diffraction studies (Figure 3.13). 56.0 mg, Yield: 70%.

^{1}H NMR (500 MHz, C_6D_6) δ 17.70 (br. s, 12H, **CH_{3Cp}**), 0.05 (br. s, 12H, **CH_{3Cp}**), -9.86 (br. s, 2H, **H_{Cp}**). Anal. Calcd for: $C_{36}H_{52}Nd_2Cl_2$: C, 51.47; H, 5.76. Found: C,50.78; H, 5.87.

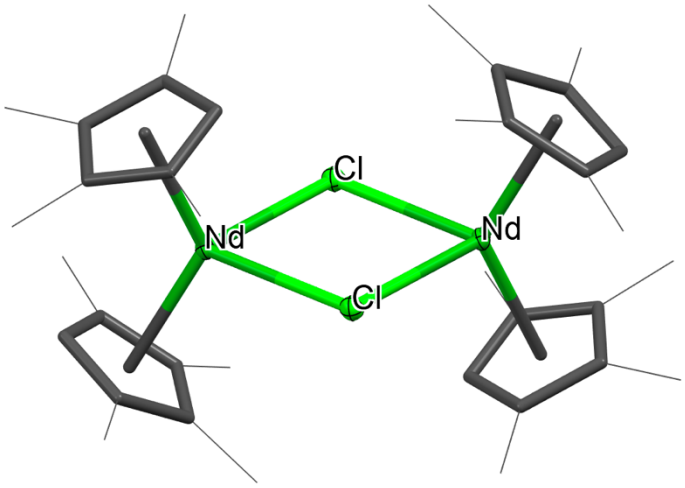

Figure 3.13. Molecular structure of [(Cp^{Me4})$_2$Nd(μ–Cl)]$_2$ (**3-Nd**). Ellipsoids shown at 50% probability, peripheral groups drawn as wireframe, hydrogen atoms and lattice solvent molecules have been omitted for clarity. Color code: green – Nd; grey – C; bright green – Cl.

Synthesis of [(Cp^{Me4})$_2$Sm(μ–Cl)]$_2$ (3-Sm). In a glovebox a vial was charged with (Cp^{Me4})$_3$Sm (**2-Sm**) (95.9 mg, 0.186 mmol, 1.00 equiv.) in THF (5 mL), resulting in a red solution. With stirring, a colorless solution of $PhICl_2$ (26.6 mg, 0.0968 mmol, 0.520 equiv.) in THF (1 mL)

was added dropwise. After stirring for 16 hours at room temperature, a color change to orange was seen, and the volatiles were removed under vacuum resulting in an orange powder which was subsequently washed with cold hexanes (2 x 0.5 mL). The powder was redissolved in a minimum of THF (1 mL), layered with hexanes (3 mL) and stored at –30 °C for 3 days to yield orange blocks that were suitable for X-ray diffraction studie (Figure 3.14). Yield: 60.3 mg, 77%.

^{1}H NMR (500 MHz, THF-D$_8$) δ 11.77 (br. s, 2H, **H$_{Cp}$**), 1.56 (br. s, 12H, **CH$_{3Cp}$**), 0.30 (br. s, 12H, **CH$_{3Cp}$**). Anal. Calcd for: $C_{36}H_{52}Sm_2Cl_2$: C, 50.73; H, 5.68. Found: C,51.03; H,6.03.

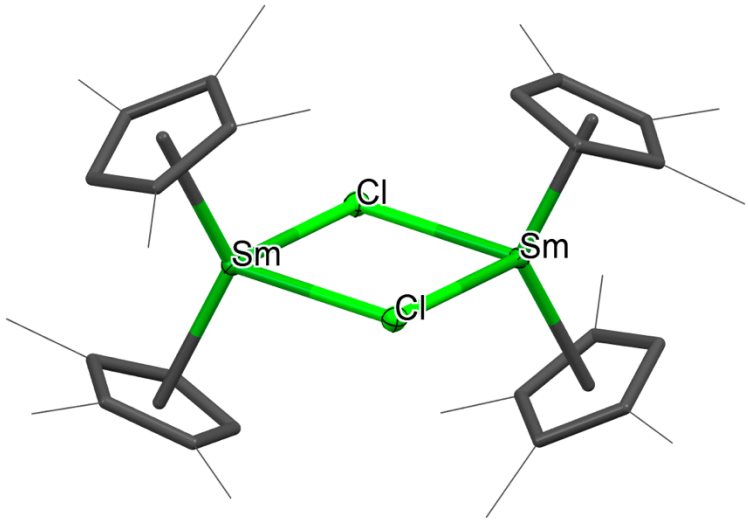

Figure 3.14. Molecular structure of [(Cp^{Me4})$_2$Sm(μ–Cl)]$_2$ (**3-Sm**). Ellipsoids shown at 50% probability, peripheral groups drawn as wireframe, hydrogen atoms and lattice solvent molecules have been omitted for clarity. Color code: green – Sm; grey – C; bright green – Cl.

Targeting the synthesis of [(Cp^{Me4})$_2$DyCl]$_2$ (3-Dy). In a glovebox a vial was charged with (Cp^{Me4})$_3$Dy (**2-Dy**) (9.8 mg, 0.0186 mmol, 1.00 equiv.) in THF (2 mL), resulting in a pale orange solution. With stirring, a colorless solution of PhICl$_2$ (2.7 mg, 0.00967 mmol, 0.520 equiv.) in THF (1 mL) was added dropwise. After stirring for 16 hours at room temperature, a color change from orange to yellow was seen, and the volatiles were removed under vacuum resulting in a yellow oil which was subsequently washed with cold hexanes (2 x 0.1 mL) to give a less than 1 mg of pale-yellow powder. The quantity of product acquired precluded characterization, but preliminary tests suggested that it is soluble in hexanes at room temperature, which is in line with expectation for the targeted product if solubility trends continue through the lanthanide series.

Targeting the synthesis of (L)CeCl$_2$ (11-Ce). In a glovebox a vial was charged with CeCl$_3$ (59.4 mg, 0.242 mmol, 1.00 equiv.) in THF (10 mL), with stirring, resulting in a white slurry. A solution of **KL** (89.3 mg, 0.242 mmol, 1.00 equiv.) in THF (10 mL) was then added dropwise. A rapid color change to orange was observed alongside the formation of a grey precipitate, presumably KCl. After stirring for 16 hours at room temperature, the reaction mixture was filtered, and volatiles from the supernatant were removed under vacuum resulting in a dark yellow powder which was subsequently washed with cold hexanes (2 x 3 mL). The crude product was analyzed by ^{1}H NMR spectroscopy and the resonances were shown to align exactly with the species produced following dechlorination reactions with **1-Ce**. The low thermal, moisture and oxygen stability of the product precluded full characterization.

Catalytic dechlorination of benzyl chloride by 1-Ce. In a glovebox, a vial was charged with **1-Ce** (7.0 mg, 0.01 mmol, 0.100 equiv.), benzyl chloride (11.5 µL, 0.100 mmol, 1.00 equiv.), K(N{SiMe$_3$}$_2$) (19.9 mg, 0.100 mmol, 1.00 equiv.) and C_6D_6 (0.5 mL). The reaction mixture was then transferred to a Young's valve-equipped NMR tube and the sample irradiated with a Kessil Tuna Blue lamp and monitored periodically by ^{1}H NMR spectroscopy. Following 48 hours of irradiation, 80 % yield of bibenzyl was observed.

Targeting the catalytic dechlorination of benzyl chloride by 1-La. In a glovebox, a vial was charged with **1-La** (6.9 mg, 0.0100 mmol, 0.100 equiv.), benzyl chloride (11.5 µL, 0.100 mmol, 1.00 equiv.), K(N{SiMe$_3$}$_2$) (19.9 mg, 0.100 mmol, 1.00 equiv.) and C_6D_6 (0.5 mL). The reaction mixture was then transferred to a Young's valve-equipped NMR tube and the sample irradiated with a Kessil Tuna Blue lamp and monitored periodically by ^{1}H NMR spectroscopy. Following 48 hours of irradiation, 8% yield of bibenzyl was observed.

General procedure for stoichiometric dechlorination of chlorocyclohexane with in THF-H_8. In a glovebox, a vial was charged with metal complex (0.0100 mmol, 0.200 equiv.), chlorocyclohexane (5.90 µL, 0.0500 mmol, 1.00 equiv.) and THF (0.5 mL). The reaction mixture was then transferred to a Young's valve-equipped NMR tube and the sample irradiated with a Kessil Tuna Blue or 440 nm lamp and monitored periodically by ^{1}H NMR spectroscopy, with a time point for all reactions measured after 24 hours.

Dechlorination of chlorocyclohexane by 1-Ce using Ce as a potential turnover reagent. In a glovebox, a vial was charged with **1-Ce** (7.0 mg, 0.01 mmol, 0.200 equiv.) chlorocyclohexane (5.90 µL, 0.05 mmol, 1.00 equiv.) and THF (0.5 mL). The solution was then added to a vial containing freshly shaved cerium metal (7.0 mg, 0.0500 mmol, 1.00 equiv.), and the reaction mixture transferred to a Young's valve-equipped NMR tube. The sample was irradiated with a Kessil 440 nm lamp and monitored periodically by ^{1}H NMR spectroscopy, with a time point measured after 24 hours. Following this time, 23 % yield of cyclohexane was observed.

Dechlorination of chlorocyclohexane by 1-Ce using Zn as a potential turnover reagent. In a glovebox, a vial was charged with **1-Ce** (7.0 mg, 0.0100 mmol, 0.200 equiv.) chlorocyclohexane (5.90 µL, 0.0500 mmol, 1.00 equiv.) and THF (0.5 mL). The solution was then added to a vial containing activated zinc metal (3.0 mg, 0.0500 mmol, 1.00 equiv.), and the reaction mixture transferred to a Young's valve-equipped NMR tube. The sample was irradiated with a Kessil 440 nm lamp and monitored periodically by ^{1}H NMR spectroscopy, with a time point measured after 24 hours. Following this time, 25 % yield of cyclohexane was observed.

Dechlorination of chlorocyclohexane by 1-Ce using trimethyl-(4-trimethylsilylpyrazin-1-yl) silane as a potential turnover reagent. In a glovebox, a vial was charged with **1-Ce** (7.0 mg, 0.0100 mmol, 0.200 equiv.) chlorocyclohexane (5.90 µL, 0.0500 mmol, 1.00 equiv.) and THF (0.5 mL). The solution was then added to a vial containing trimethyl-(4-trimethylsilylpyrazin-1-yl) silane (11.3 mg, 0.0500 mmol, 1.00 equiv.), and the reaction mixture transferred to a Young's valve-equipped NMR tube. The sample was irradiated with a Kessil 440 nm lamp and monitored periodically by ^{1}H NMR spectroscopy, with a time point measured after 24 hours. Following this time, trace cyclohexane was observed alongside 40% yield of trimethylsilyl chloride.

Dechlorination of chlorocyclohexane by 1-Ce using $MgPh_2(THF)_2$ as a potential turnover reagent. In a glovebox, a vial was charged with **1-Ce** (7.0 mg, 0.0100 mmol, 0.200 equiv.) chlorocyclohexane (5.90 µL, 0.0500 mmol, 1.00 equiv.) and THF (0.5 mL). The solution was then added to a vial containing activated $MgPh_2(THF)_2$ (16.1 mg, 0.0500 mmol, 1.00 equiv.), and the reaction mixture transferred to a Young's valve-equipped NMR tube. The sample was irradiated with a Kessil 440 nm lamp and monitored periodically by ^{1}H NMR spectroscopy, with a time point measured after 24 hours. Following this time, 23% yield of cyclohexane was observed.

General procedure for targeting the 20 mol % catalytic dechlorination of chlorocyclohexane with NaH in THF-H_8. In a glovebox, a vial was charged with NaH (1.2 mg, 0.0500 mmol, 1.00 equiv.) chlorocyclohexane (5.90 µL, 0.0500 mmol, 1.00 equiv.) and THF (0.5 mL). The solution was then used to dissolve the metal complex (0.0100 mmol, 0.200 equiv.), and the reaction mixture transferred to a Young's valve-equipped NMR tube. The sample was irradiated with a Kessil 440 nm lamp and monitored periodically by ^{1}H NMR spectroscopy, with a time point for all reactions measured after 24 hours.

General procedure for control reactions in the dark for targeting the 20 mol % catalytic dechlorination of chlorocyclohexane with NaH in THF-H_8. In a glovebox, a vial was charged with NaH (1.2 mg, 0.0500 mmol, 1.00 equiv.) chlorocyclohexane (5.90 µL, 0.0500 mmol, 1.00 equiv.) and THF (0.5 mL). The solution was then used to dissolve the metal complex (0.0100 mmol, 0.200 equiv.), and the reaction mixture transferred to a Young's valve-equipped NMR tube. The sample was wrapped in aluminum foil, stored in the dark and monitored periodically by ^{1}H NMR spectroscopy, with a time point for all reactions measured after 24 hours. No product formation was seen for all reactions.

General procedure for 20 mol % catalytic dechlorination of chlorocyclohexane with $MgBn_2(THF)_2$ in THF-H_8. In a glovebox, a vial was charged with $MgBn_2(THF)_2$, (17.5 mg, 0.0500 mmol, 1.00 equiv.) chlorocyclohexane (5.90 µL, 0.0500 mmol, 1.00 equiv.) and THF (0.5 mL). The solution was then used to dissolve the metal complex (0.0100 mmol, 0.200 equiv.), and the reaction mixture transferred to a Young's valve-equipped NMR tube. The sample was irradiated with a Kessil 440 nm lamp and monitored periodically by ^{1}H NMR spectroscopy, with a time point for all reactions measured after 24 hours.

General procedure for control reactions in the dark for the 20 mol % catalytic dechlorination of chlorocyclohexane with $MgBn_2(THF)_2$ in THF-H_8. In a glovebox, a vial was charged with $MgBn_2(THF)_2$, (17.5 mg, 0.0500 mmol, 1.00 equiv.) chlorocyclohexane (5.90 µL, 0.0500 mmol, 1.00 equiv.) and THF (0.5 mL). The solution was then used to dissolve the metal complex (0.0100 mmol, 0.200 equiv.), and the reaction mixture transferred to a Young's valve-equipped NMR tube. The sample was wrapped in aluminum foil, stored in the dark and monitored periodically by ^{1}H NMR spectroscopy, with a time point for all reactions measured after 24 hours. No product formation was seen for all reactions.

General procedure for 5 mol % catalytic dechlorination of chlorocyclohexane with $MgBn_2(THF)_2$ in THF-H_8. In a glovebox, a vial was charged with $MgBn_2(THF)_2$, (35.0 mg, 0.100 mmol, 1.00 equiv.) chlorocyclohexane (11.8 µL, 0.100 mmol, 1.00 equiv.) and THF (0.5 mL). The solution was then used to dissolve the metal complex (5.00 µmol, 0.0500 equiv.), and the reaction mixture transferred to a Young's valve-equipped NMR tube. The sample was irradiated with a Kessil 440 nm lamp and monitored periodically by ^{1}H NMR spectroscopy, with a time point for all reactions measured after 24 hours.

General procedure for control reactions in the dark for the 5 mol % catalytic dechlorination of chlorocyclohexane with $MgBn_2(THF)_2$ in THF-H_8. In a glovebox, a vial was charged with $MgBn_2(THF)_2$, (35.0 mg, 0.100 mmol, 1.00 equiv.) chlorocyclohexane (11.8 μL, 0.100 mmol, 1.00 equiv.) and THF (0.5 mL). The solution was then used to dissolve the metal complex (5.00 μmol, 0.0500 equiv.), and the reaction mixture transferred to a Young's valve-equipped NMR tube. The sample was wrapped in aluminum foil, stored in the dark and monitored periodically by ^{1}H NMR spectroscopy, with a time point for all reactions measured after 24 hours. No product formation was seen for all reactions.

General procedure for 5 mol % catalytic dechlorination of chlorinated substrates with $MgBn_2(THF)_2$ in THF-H_8. In a glovebox, a vial was charged with $MgBn_2(THF)_2$, (35.0 mg, 0.100 mmol, 1.00 equiv.) chlorinated substrate (0.100 mmol, 1.00 equiv.) and THF (0.5 mL). The solution was then used to dissolve the metal complex (0.005 mmol, 0.05 equiv.), and the reaction mixture transferred to a Young's valve-equipped NMR tube. The sample was irradiated with a Kessil 440 nm lamp and monitored periodically by ^{1}H NMR spectroscopy, with a time point for all reactions measured after 24 hours.

General procedure for control reactions in the dark for 5 mol % catalytic dechlorination of chlorinated substrates with $MgBn_2(THF)_2$ in THF-H_8. In a glovebox, a vial was charged with $MgBn_2(THF)_2$, (35.0 mg, 0.100 mmol, 1.00 equiv.) chlorinated substrate (0.100 mmol, 1.00 equiv.) and THF (0.5 mL). The solution was then used to dissolve the metal complex (0.005 mmol, 0.05 equiv.), and the reaction mixture transferred to a Young's valve-equipped NMR tube. The sample was wrapped in aluminum foil, stored in the dark and monitored periodically by ^{1}H NMR spectroscopy, with a time point for all reactions measured after 24 hours. No product formation was seen for all reactions, except the dechlorination of 1-(chloromethyl)-4-(trifluoromethyl)benzene which showed trace product formation. This can be attributed to the weakening of the C–Cl bond through electron withdrawing inductive effects of the trifluromethyl group on the arene ring.

1 mol % catalytic dechlorination of chlorocylohexane with $MgBn_2(THF)_2$ by 2-Ce in THF-H_8. In a glovebox, a vial was charged with $MgBn_2(THF)_2$, (175 mg, 0.500 mmol, 1.00 equiv.) chlorocyclohexane (59.0 μL, 0.500 mmol, 1.00 equiv.) and THF (0.5 mL). The solution was then used to dissolve **2-Ce** (2.5 mg, 5.00 μmol, 0.0100 equiv.), and the reaction mixture transferred to a Young's valve-equipped NMR tube. The sample was irradiated with a Kessil 440 nm lamp and monitored periodically by ^{1}H NMR spectroscopy, with a time point measured after 24 hours.

1 mol % catalytic dechlorination of chlorocylohexane with $MgBn_2(THF)_2$ by 3-Ce in THF-H_8. In a glovebox, a vial was charged with $MgBn_2(THF)_2$, (175 mg, 0.500 mmol, 1.00 equiv.) chlorocyclohexane (59.0 μL, 0.500 mmol, 1.00 equiv.) and THF (0.5 mL). The solution was then used to dissolve **3-Ce** (2.1 mg, 0.00250 mmol, 0.0100 equiv. (wrt. Ce)), and the reaction mixture transferred to a Young's valve-equipped NMR tube. The sample was irradiated with a Kessil 440 nm lamp and monitored periodically by ^{1}H NMR spectroscopy, with a time point measured after 24 hours.

Incorporation of deuterium into cyclohexane. In a glovebox, a vial was charged with $MgBn_2(THF)_2$, (35.0 mg, 0.100 mmol, 1.00 equiv.) chlorocyclohexane (11.8 μL, 0.100 mmol, 1.00 equiv.) and THF-D_8 (0.5 mL). The solution was then used to dissolve **2-Ce** (2.5 mg, 5.00 μmol, 0.0500 equiv.), and the reaction mixture transferred to a Young's valve-equipped NMR

tube. The sample was irradiated with a Kessil 440 nm lamp and monitored periodically by ^{1}H and ^{13}C NMR spectroscopy, with a time point measured after 24 hours. Following this time coupling arising from the formation of cyclohexane-D_1 was observed by ^{13}C NMR spectroscopy.

Incorporation of deuterium into 2-methylpropene. In a glovebox, a vial was charged with $MgBn_2(THF)_2$, (35.0 mg, 0.100 mmol, 1.00 equiv.) 1-chloro-2-methylpropene (9.84 µL, 0.100 mmol, 1.00 equiv.) and THF-D_8 (0.5 mL). The solution was then used to dissolve **2-Ce** (2.5 mg, 5.00 µmol, 0.0500 equiv.), and the reaction mixture transferred to a Young's valve-equipped NMR tube. The sample was irradiated with a Kessil 440 nm lamp and monitored periodically by ^{1}H and ^{13}C NMR spectroscopy, with a time point measured after 24 hours. 2.4% in situ yield of 2-methylprop-1-ene-1-D was observed by ^{1}H NMR spectroscopy.

Equilibrium between $(Cp^{Me4})_3Ce$ (2-Ce), $(Cp^{Me4})_2(Bn)(THF)$ (6-Ce) and $MgBn_2(THF)_2$ (440 nm). In a glovebox, a Young's valve-equipped NMR tube was charged with **2-Ce** (5.0 mg, 0.010 mmol, 1.00 equiv.), $MgBn_2(THF)_2$ (70.0 mg, 0.200 mmol, 20.0 equiv.), THF (0.5 mL) and an internal standard. The NMR tube was sealed and the mixture characterized by ^{1}H NMR spectroscopy. An equilibrium constant of 2.5 was calculated based on the relative concentrations of **2-Ce**, **6-Ce**, $MgBn_2(THF)_2$ and $Mg(Cp^{Me4})_2$ present in solution.

Reaction to investigate the formation of 3-Ce from dechlorination catalysis mixtures. In a glovebox, a Young's valve-equipped NMR tube was charged with **2-Ce** (5.0 mg, 0.010 mmol, 1.00 equiv.), $MgBn_2(THF)_2$ (70.0 mg, 0.200 mmol, 20.0 equiv.), THF (0.5 mL) and an internal standard. Chlorocyclohexane (23.6 µL, 0.200 mmol, 20.0 equiv.) was then added before the NMR tube was sealed and irradiated for 24 hours under a 440 nm lamp. Following this time, the complete conversion from **2-Ce** to **3-Ce** was observed by ^{1}H NMR spectroscopy.

Reaction of 3-Ce and $MgBn_2(THF)_2$ in the dark. In a glovebox, a Young's valve-equipped NMR tube was charged with **3-Ce** (4.26 mg, 5.00 µmol, 0.5 equiv.), $MgBn_2(THF)_2$ (70.0 mg, 0.200 mmol, 20.0 equiv.), THF (0.5 mL) and an internal standard. The NMR tube was sealed, wrapped in aluminum foil and stored in the dark for 24 hours. Following this time, a color change from bright yellow to darker yellow had occurred but no conversion to **6-Ce** was observed by ^{1}H NMR spectroscopy.

Reaction of 3-Ce and $MgBn_2(THF)_2$ under 440 nm light irradiation. In a glovebox, a Young's valve-equipped NMR tube was charged with **3-Ce** (4.26 mg, 5.00 µmol, 0.500 equiv.), $MgBn_2(THF)_2$ (70.0 mg, 0.200 mmol, 20.0 equiv.), THF (0.5 mL) and an internal standard. the NMR tube was sealed and irradiated for 24 hours under a 440 nm lamp. Following this time a color change from bright yellow to a yellow-green had occurred and 96% conversion to **6-Ce** was observed by ^{1}H NMR spectroscopy.

Dechlorination of chlorocyclohexane using $Mg(Cp^{Me4})_2$ and $MgBn_2(THF)_2$. In a glovebox, a vial was charged with $MgBn_2(THF)_2$, (35.0 mg, 0.100 mmol, 1.00 equiv.) chlorocyclohexane (11.8 µL, 0.100 mmol, 1.00 equiv.) and THF (0.5 mL). The solution was then used to dissolve $MgCp^{Me4}_2$ (1.4 mg, 5.00 µmol, 0.0500 equiv.), and the reaction mixture transferred to a Young's valve-equipped NMR tube. The sample was irradiated with a Kessil 440 nm lamp and monitored periodically by ^{1}H NMR spectroscopy, with a time point measured after 24 hours. Following this time, 1.2% yield of cyclohexane was observed.

Dechlorination of chlorocyclohexane using $MgPh_2(THF)_2$ and $MgBn_2(THF)_2$. In a glovebox, a vial was charged with $MgBn_2(THF)_2$, (35.0 mg, 0.100 mmol, 1.00 equiv.) chlorocyclohexane (11.8 μL, 0.100 mmol, 1.00 equiv.) and THF (0.5 mL). The solution was then used to dissolve $MgPh_2(THF)_2$ (1.6 mg, 5.00 μmol, 0.0500 equiv.), and the reaction mixture transferred to a Young's valve-equipped NMR tube. The sample was irradiated with a Kessil 440 nm lamp and monitored periodically by ^1H NMR spectroscopy, with a time point measured after 24 hours. Following this time, 3.5 % yield of cyclohexane was observed.

Dechlorination of chlorocyclohexane using $MgCl_2$ and $MgBn_2(THF)_2$. In a glovebox, a vial was charged with $MgBn_2(THF)_2$, (35.0 mg, 0.100 mmol, 1.00 equiv.) and chlorocyclohexane (11.8 μL, 0.100 mmol, 1.00 equiv.). 0.5 mL of a stock solution of $MgCl_2$ (4.8 mg, 0.0500 mmol) in THF (10 mL) was then used to dissolve the $MgBn_2(THF)_2$, and the reaction mixture transferred to a Young's valve-equipped NMR tube. The sample was irradiated with a Kessil 440 nm lamp and monitored periodically by ^1H NMR spectroscopy, with a time point measured after 24 hours. Following this time, 2.0 % yield of cyclohexane was observed.

Dechlorination of chlorocyclohexane using KCp^{Me4} and $MgBn_2(THF)_2$. In a glovebox, a vial was charged with $MgBn_2(THF)_2$, (35.0 mg, 0.100 mmol, 1.00 equiv.) and chlorocyclohexane (11.8 μL, 0.100 mmol, 1.00 equiv.). 0.5 mL of a stock solution of KCp^{Me4} (9.0 mg, 0.0500 mmol) in THF (10 mL) was then used to dissolve the $MgBn_2(THF)_2$, and the reaction mixture transferred to a Young's valve-equipped NMR tube. The sample was irradiated with a Kessil 440 nm lamp and monitored periodically by ^1H NMR spectroscopy, with a time point measured after 24 hours. Following this time, 2.0 % yield of cyclohexane was observed.

5 mol % catalytic dechlorination of PVC with $MgBn_2(THF)_2$ in THF-H_8 (24 hours). In a glovebox, a vial was charged with $MgBn_2(THF)_2$, (35.0 mg, 0.100 mmol, 1.00 equiv.) a commercial sample of PVC (6.2 mg, 0.100 mmol, 1.00 equiv. Average $M_w \sim 233{,}000$, average $M_n \sim 99{,}000$) and THF (0.5 mL). The solution was then used to dissolve **2-Ce** (2.5 mg, 5.00 μmol, 0.0500 equiv.), and the reaction mixture transferred to a Young's valve-equipped NMR tube. The sample was irradiated with a Kessil 440 nm lamp and monitored periodically by ^1H NMR spectroscopy. Following 24 hours irradiation, an average 78% dechlorination was determined using Mohr's method. (*vide infra*.)

5 mol % catalytic dechlorination of PVC with $MgBn_2(THF)_2$ in THF-H_8 (48 hours). In a glovebox, a vial was charged with $MgBn_2(THF)_2$, (35.0 mg, 0.100 mmol, 1.00 equiv.) a commercial sample of PVC (6.2 mg, 0.100 mmol, 1.00 equiv. Average $M_w \sim 233{,}000$, average $M_n \sim 99{,}000$) and THF (0.5 mL). The solution was then used to dissolve **2-Ce** (2.5 mg, 5.00 μmol, 0.0500 equiv.), and the reaction mixture transferred to a Young's valve-equipped NMR tube. The sample was irradiated with a Kessil 440 nm lamp and monitored periodically by ^1H NMR spectroscopy. Following 48 hours irradiation, 79% dechlorination was determined using Mohr's method (*vide infra*.)

1 mol % catalytic dechlorination of PVC with $MgBn_2(THF)_2$ in THF-H_8. In a glovebox, a vial was charged with $MgBn_2(THF)_2$, (87.8 mg, 0.250 mmol, 1.00 equiv.) a commercial sample of PVC (15.5 mg, 0.250 mmol, 1.00 equiv. Average $M_w \sim 233{,}000$, average $M_n \sim 99{,}000$) and THF (0.5 mL). The solution was then used to dissolve **2-Ce** (1.3 mg, 5.00 μmol, 0.0500 equiv.), and the reaction mixture transferred to a Young's valve-equipped NMR tube. The sample was irradiated with a Kessil 440 nm lamp and monitored periodically by ^1H NMR

spectroscopy. Following 48 hours irradiation, 78% dechlorination was determined using Mohr's method (vide infra.)

Determination of the extent of dechlorination of PVC. A procedure for the catalytic dechlorination of PVC with $MgBn_2(THF)_2$ in THF-H_8 was followed. Following this, the precipitation of the dechlorinated polymer as a colorless solid (Figure 3.15, left) was observed, alongside generation of a yellow solution shown to contain **3-Ce** by ^1H NMR spectroscopy. Mohr's method was then used to determine the amount of $MgCl_2$ and other chloride-containing species resulting from the dechlorination of polyvinyl chloride. The Young's valve-equipped NMR tube was opened to air, and the white solid manually separated from the solution (Figure 3.15, right). The solution was evaporated to dryness and the resulting solids redissolved in water suitable for trace metal analyses. Potassium chromate indicator was added, and a 25 mM solution of silver nitrate was titrated against the solution until the end point was reached. The extent of dechlorination in the polymer was then determined based on the amount of silver nitrate needed to reach the end point.

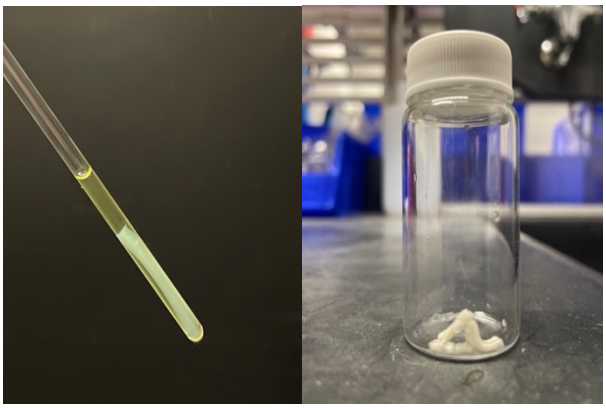

Figure 3.15. Solution and polymer precipitate resulting from the dechlorination of PVC by **2-Ce** (left); isolated dechlorinated polymer (right).

Table 3.4. Crystal data and structure refinement for **3-Nd** and **3-Sm**.

	3-Nd	**3-Sm**
Empirical formula	$C_{36}H_{52}Cl_2Nd_2$	$C_{36}H_{52}Cl_2Sm_2$
Formula weight	844.15	856.37
Temperature/K	100	100
Crystal system	monoclinic	monoclinic
Space group	$P2_1/n$	$P2_1/n$
a/Å	8.504(13)	8.5346(12)
b/Å	10.398(14)	10.3557(14)
c/Å	19.24(3)	19.111(3)
α/°	90	90
β/°	91.801(8)	91.674(5)
γ/°	90	90
Volume/Å^3	1700(4)	1688.4(4)
Z	2	2
ρ_{calc}g/cm^3	1.649	1.684
μ/mm^{-1}	3.395	3.859
F(000)	844.0	852.0
Crystal size/mm^3	0.1 × 0.04 × 0.02	0.2 × 0.1 × 0.1
Radiation	synchrotron (λ = 0.7288)	synchrotron (λ = 0.7288)
2Θ range for data collection/°	4.344 to 52.074	4.588 to 58.288
Index ranges	$-10 \le h \le 10$, $-12 \le k \le 12$, $-23 \le l \le 23$	$-11 \le h \le 11$, $-13 \le k \le 13$, $-25 \le l \le 25$
Reflections collected	21497	25987
Independent reflections	3104 [R_{int} = 0.1314, R_{sigma} = 0.0838]	4208 [R_{int} = 0.0807, R_{sigma} = 0.0554]
Data/restraints/parameters	3104/0/189	4208/0/189
Goodness-of-fit on F^2	0.986	1.037
Final R indexes [I>=2σ (I)]	R_1 = 0.0482, wR_2 = 0.1196	R_1 = 0.0349, wR_2 = 0.0902
Final R indexes [all data]	R_1 = 0.0585, wR_2 = 0.1275	R_1 = 0.0419, wR_2 = 0.0940
Largest diff. peak/hole / e Å^{-3}	0.98/-1.11	0.85/-1.11

3.6 References

(1) Kynman, A. E.; Christodoulou, S.; Ouellette, E. T.; Peterson, A.; Kelly, S.; Maron, L.; Arnold, P. L. Photocatalytic Dechlorination of Unactivated Chlorocarbons Including PVC Using Organolanthanide Complexes. *Chem. Commun.* **2023**, 10.1039.D3CC02906A. https://doi.org/10.1039/D3CC02906A.

(2) Crisenza, G. E. M.; Melchiorre, P. Chemistry Glows Green with Photoredox Catalysis. *Nat. Commun* **2020**, *11* (1), 803. https://doi.org/10.1038/s41467-019-13887-8.

(3) Tucker, J. W.; Stephenson, C. R. J. Shining Light on Photoredox Catalysis: Theory and Synthetic Applications. *J. Org. Chem.* **2012**, *77* (4), 1617–1622. https://doi.org/10.1021/jo202538x.

(4) Twilton, J.; Le, C. C.; Zhang, P.; Shaw, M. H.; Evans, R. W.; MacMillan, D. W. C. The Merger of Transition Metal and Photocatalysis. *Nat. Rev. Chem.* **2017**, *1*.

(5) Cheung, K. P. S.; Sarkar, S.; Gevorgyan, V. Visible Light-Induced Transition Metal Catalysis. *Chem. Rev.* **2022**, *122* (2), 1543–1625. https://doi.org/10.1021/acs.chemrev.1c00403.

(6) Guo, J.-J.; Hu, A.; Chen, Y.; Sun, J.; Tang, H.; Zuo, Z. Photocatalytic C−C Bond Cleavage and Amination of Cycloalkanols by Cerium(III) Chloride Complex. *Angew. Chem. Int. Ed.* **2016**, *128* (49), 15545–15548. https://doi.org/10.1002/ange.201609035.

(7) Cheisson, T.; Schelter, E. J. Rare Earth Elements: Mendeleev's Bane, Modern Marvels. *Science* **2019**, *363* (6426), 489–493. https://doi.org/10.1126/science.aau7628.

(8) Arnold, P. L.; Kerr, R. W. F.; Weetman, C.; Docherty, S. R.; Rieb, J.; Cruickshank, F. L.; Wang, K.; Jandl, C.; McMullon, M. W.; Pöthig, A.; Kühn, F. E.; Smith, A. D. Selective and Catalytic Carbon Dioxide and Heteroallene Activation Mediated by Cerium N-Heterocyclic Carbene Complexes. *Chem. Sci.* **2018**, *9* (42), 8035–8045. https://doi.org/10.1039/c8sc03312a.

(9) Kerr, R. W. F.; Ewing, P. M. D. A.; Raman, S. K.; Smith, A. D.; Williams, C. K.; Arnold, P. L. Ultrarapid Cerium(III)-NHC Catalysts for High Molar Mass Cyclic Polylactide. *ACS Catal.* **2021**, *11* (3), 1563–1569. https://doi.org/10.1021/acscatal.0c04858.

(10) Ogawa, A.; Sumino, Y.; Nanke, T.; Ohya, S.; Sonoda, N.; Hirao, T. Photoinduced Reduction and Carbonylation of Organic Chlorides with Samarium Diiodide. *J. Am. Chem. Soc.* **1997**, *119* (11), 2745–2746. https://doi.org/10.1021/ja963117p.

(11) Jenks, T. C.; Bailey, M. D.; Hovey, J. L.; Fernando, S.; Basnayake, G.; Cross, M. E.; Li, W.; Allen, M. J. First Use of a Divalent Lanthanide for Visible-Light-Promoted Photoredox Catalysis. *Chem. Sci.* **2018**, *9* (5), 1273–1278. https://doi.org/10.1039/c7sc02479g.

(12) Kondo, T.; Akazome, M.; Watanabe, Y. Lanthanide(II) Iodide Catalysed Photochemical Allylation of Aldehydes with Allylic Halides. *J. Chem. Soc. Chem. Commun.* **1991**, No. 11, 757–758. https://doi.org/10.1039/C39910000757.

(13) Ogawa, A.; Ohya, S.; Sumino, Y.; Sonoda, N.; Hirao, T. Novel Enhancement of the Reducing Ability of Ytterbium Diiodide by Irradiation with Near-UV Light. *Tetrahedron Lett.* **1997**, *38* (52), 9017–9018. https://doi.org/10.1016/S0040-4039(97)10409-9.

(14) Qiao, Y.; Schelter, E. J. Lanthanide Photocatalysis. *Acc. Chem. Res.* **2018**, *51* (11), 2926–2936. https://doi.org/10.1021/acs.accounts.8b00336.

(15) Hu, A.; Guo, J. J.; Pan, H.; Zuo, Z. Selective Functionalization of Methane, Ethane, and Higher Alkanes by Cerium Photocatalysis. *Science* **2018**, *361* (6403), 668–672. https://doi.org/10.1126/science.aat9750.

(16) Kynman, A. E.; Elghanayan, L.; Desnoyer, A.; Yang, Y.; Severy, L.; Di Giuseppe, A.; Tilley, T. D.; Maron, L.; Arnold, P. L. Controlled Monodefluorination and Alkylation of C(Sp3)-F Bonds by Lanthanide Photocatalysts: Importance of Metal – Ligand Cooperativity. *Chem. Sci.* **2022**, *13* (47), 14090–14100. https://doi.org/10.1039/D2SC04192H.

(17) Deng, Dao, Li; Qian, Chang Tao; Penn, John H. Catalytic Dechlorination of Aromatic Chlorides by Dicyclopentadienyl Lanthanide Chlorides. *Chin. Chem. Lett.* **1994**, *5* (4), 303–304.
(18) Penn, John H.; Li Deng, Dao; Qian, Chang Tao. Catalytic Dechlorination of Polycyclic Chloroaromatics with Dicyclopentadienyl Yttrium Chloride. *Chin. Chem. Lett.* **1996**, *7* (9), 845–846.
(19) Hou, Q.; Zhen, M.; Qian, H.; Nie, Y.; Bai, X.; Xia, T.; Laiq Ur Rehman, M.; Li, Q.; Ju, M. Upcycling and Catalytic Degradation of Plastic Wastes. *Cell Reports Physical Science* **2021**, *2* (8), 100514. https://doi.org/10.1016/j.xcrp.2021.100514.
(20) Zhao, X.; Boruah, B.; Chin, K. F.; Đokić, M.; Modak, J. M.; Soo, H. S. Upcycling to Sustainably Reuse Plastics. *Adv. Mater.* **2021**.
(21) Geyer, R.; Jambeck, J. R.; Law, K. L. Production, Use, and Fate of All Plastics Ever Made. *Sci. Adv.* **2017**, *3* (7), e1700782. https://doi.org/10.1126/sciadv.1700782.
(22) Ashby, M. F. *Materials and Sustainable Development*, Second edition.; Butterworth-Heinemann: Oxford, 2023.
(23) Hapipi, A. M.; Suda, H.; Uddin, Md. A.; Kato, Y. Dechlorination of Polyvinyl Chloride under Superheated Steam with Catalysts and Adsorbents. *Energy Fuels* **2018**, *32* (7), 7792–7799. https://doi.org/10.1021/acs.energyfuels.8b00838.
(24) Contreras, J. M.; Martínez, G.; Millán, J. Local Chain Configuration Dependence of the Mechanisms of Chemical Reactions of PVC. 8. New Results from the Reductive Dechlorination Reaction. *Polymer* **2001**, *42* (25), 09867–09876. https://doi.org/10.1016/S0032-3861(01)00533-X.
(25) Braun, D.; Mao, W.; Böhringer, B.; Garbella, R. W. Preparation of Vinyl Chloride-Ethylene Copolymers by Partial Reduction of Poly(Vinyl Chloride). *Angew. Makromol. Chemie* **1986**, *141* (1), 113–129. https://doi.org/10.1002/apmc.1986.051410112.
(26) Hjertberg, T.; Wendel, A. Reduction of Poly(Vinyl Chloride) with Tri-n-Butyltin Hydride. *Polymer* **1982**, *23* (11), 1641–1645. https://doi.org/10.1016/0032-3861(82)90186-0.
(27) Starnes, W. H.; Schilling, F. C.; Abbås, K. B.; Plitz, I. M.; Hartless, R. L.; Bovey, F. A. Structural Selectivities in the Reduction of Poly(Vinyl Chloride) with Lithium Aluminum Hydride and Tri-n- Butyltin Hydride. *Macromolecules* **1979**, *12* (1), 13–19. https://doi.org/10.1021/ma60067a004.
(28) Cotman, J. D. Studies on Polyvinyl Chloride. I. Reduction to a Hydrocarbon Polymer. *J. Am. Chem. Soc.* **1955**, *77* (10), 2790–2793. https://doi.org/10.1021/ja01615a035.
(29) Jameison, F. A.; Schilling, F. C.; Tonelli, A. E. Tri-.Eta.-Butyltin Hydride Reduction of Poly(Vinyl Chloride): Kinetics of Dechlorination for 2,4-Dichloropentane and 2,4,6-Trichloroheptane. *Macromolecules* **1986**, *19* (8), 2168–2173. https://doi.org/10.1021/ma00162a011.
(30) Braun, V. D.; Schurek, W. Zum Mechanismus Der Thermischen Abspaltung von Chlorwasserstoff Aus Polyvinylchlorid. 6. Mitt.: Untersuchungen an Reduziertem Polyvinylchlorid. *Angew. Makromol. Chemie* **1969**, *7* (1), 121–133. https://doi.org/10.1002/apmc.1969.050070111.
(31) Bush, N. G.; Assefa, M. K.; Bac, S.; Mallikarjun Sharada, S.; Fieser, M. E. Controlling Selectivity for Dechlorination of Poly(Vinyl Chloride) with (Xantphos)RhCl. *Mater. Horiz.* **2023**, *10* (6), 2047–2052. https://doi.org/10.1039/D2MH01293F.
(32) Assefa, M. K.; Fieser, M. E. Divergent Silylium Catalysis Enables Facile Poly(Vinyl Chloride) Upcycling to Poly(Ethylene- *Co* -Styrene) Derivatives. *J. Mater. Chem. A* **2023**, *11* (5), 2128–2132. https://doi.org/10.1039/D2TA08142C.
(33) Fieser, M. E.; Johnson, C. W.; Bates, J. E.; Ziller, J. W.; Furche, F.; Evans, W. J. Dinitrogen Reduction, Sulfur Reduction, and Isoprene Polymerization via Photochemical

Activation of Trivalent Bis(Cyclopentadienyl) Rare-Earth-Metal Allyl Complexes. *Organometallics* **2015**, *34* (17), 4387–4393. https://doi.org/10.1021/acs.organomet.5b00613.
(34) Yang, Q.; Wang, Y.-H.; Qiao, Y.; Gau, M.; Carroll, P. J.; Walsh, P. J.; Schelter, E. J. Photocatalytic C–H Activation and the Subtle Role of Chlorine Radical Complexation in Reactivity. *Science* **2021**, *372* (6544), 847–852. https://doi.org/10.1126/science.abd8408.
(35) An, Q.; Xing, Y.-Y.; Pu, R.; Jia, M.; Chen, Y.; Hu, A.; Zhang, S.-Q.; Yu, N.; Du, J.; Zhang, Y.; Chen, J.; Liu, W.; Hong, X.; Zuo, Z. Identification of Alkoxy Radicals as Hydrogen Atom Transfer Agents in Ce-Catalyzed C–H Functionalization. *J. Am. Chem. Soc.* **2023**, *145* (1), 359–376. https://doi.org/10.1021/jacs.2c10126.
(36) Fieser, M. E.; Bates, J. E.; Ziller, J. W.; Furche, F.; Evans, W. J. Dinitrogen Reduction via Photochemical Activation of Heteroleptic Tris(Cyclopentadienyl) Rare-Earth Complexes. *J. Am. Chem. Soc.* **2013**, *135* (10), 3804–3807. https://doi.org/10.1021/ja400664s.
(37) Fieser, M. E.; Johnson, C. W.; Bates, J. E.; Ziller, J. W.; Furche, F.; Evans, W. J. Dinitrogen Reduction, Sulfur Reduction, and Isoprene Polymerization via Photochemical Activation of Trivalent Bis(Cyclopentadienyl) Rare-Earth-Metal Allyl Complexes. *Organometallics* **2015**, *34* (17), 4387–4393. https://doi.org/10.1021/acs.organomet.5b00613.
(38) Gilbert, B. C.; Stell, J. K.; Peet, W. J.; Radford, K. J. Generation and Reactions of the Chlorine Atom in Aqueous Solution. *J. Chem. Soc., Faraday Trans. 1* **1988**, *84* (10), 3319. https://doi.org/10.1039/f19888403319.
(39) Troian-Gautier, L.; Turlington, M. D.; Wehlin, S. A. M.; Maurer, A. B.; Brady, M. D.; Swords, W. B.; Meyer, G. J. Halide Photoredox Chemistry. *Chem. Rev.* **2019**, *119* (7), 4628–4683. https://doi.org/10.1021/acs.chemrev.8b00732.
(40) Gonzalez, M. I.; Gygi, D.; Qin, Y.; Zhu, Q.; Johnson, E. J.; Chen, Y.-S.; Nocera, D. G. Taming the Chlorine Radical: Enforcing Steric Control over Chlorine-Radical-Mediated C–H Activation. *J. Am. Chem. Soc.* **2022**, *144* (3), 1464–1472. https://doi.org/10.1021/jacs.1c13333.
(41) Shields, B. J.; Doyle, A. G. Direct C(Sp^3)–H Cross Coupling Enabled by Catalytic Generation of Chlorine Radicals. *J. Am. Chem. Soc.* **2016**, *138* (39), 12719–12722. https://doi.org/10.1021/jacs.6b08397.
(42) McBee, E. T.; Hass, H. B.; Neher, C. M.; Strickland, H. Chlorination of Methane. *Ind. Eng. Chem.* **1942**, *34* (3), 296–300. https://doi.org/10.1021/ie50387a009.
(43) Hass, H. B.; McBee, E. T.; Weber, P. Chlorination of Paraffins [1]. *Ind. Eng. Chem.* **1936**, *28* (3), 333–339. https://doi.org/10.1021/ie50315a017.
(44) Lin, R.; Amrute, A. P.; Pérez-Ramírez, J. Halogen-Mediated Conversion of Hydrocarbons to Commodities. *Chem. Rev.* **2017**, *117* (5), 4182–4247. https://doi.org/10.1021/acs.chemrev.6b00551.
(45) Itabashi, Y.; Asahara, H.; Ohkubo, K. Chlorine-Radical-Mediated C–H Oxygenation Reaction under Light Irradiation. *Chem. Commun.* **2023**, *59* (49), 7506–7517. https://doi.org/10.1039/D3CC01057K.
(46) Vasilopoulos, A.; Golden, D. L.; Buss, J. A.; Stahl, S. S. Copper-Catalyzed C–H Fluorination/Functionalization Sequence Enabling Benzylic C–H Cross Coupling with Diverse Nucleophiles. *Org. Lett.* **2020**, *22* (15), 5753–5757. https://doi.org/10.1021/acs.orglett.0c02238.
(47) Rohe, S.; Morris, A. O.; McCallum, T.; Barriault, L. Hydrogen Atom Transfer Reactions via Photoredox Catalyzed Chlorine Atom Generation. *Angew. Chem. Int. Ed.* **2018**, *57* (48), 15664–15669. https://doi.org/10.1002/anie.201810187.
(48) Kang, Y. C.; Treacy, S. M.; Rovis, T. Iron-Catalyzed Photoinduced LMCT: A 1° C–H Abstraction Enables Skeletal Rearrangements and C(Sp^3)–H Alkylation. *ACS Catal.* **2021**, *11* (12), 7442–7449. https://doi.org/10.1021/acscatal.1c02285.

(49) Zuo, Z.; Ahneman, D. T.; Chu, L.; Terrett, J. A.; Doyle, A. G.; Macmillan, D. W. C. Merging Photoredox with Nickel Catalysis : The Coupling of Sp3-Carbons with Aryl Halides Using Feedstock Chemicals. *Science* **2014**, *345* (6195), 437–440.
(50) Deng, H.-P.; Zhou, Q.; Wu, J. Microtubing-Reactor-Assisted Aliphatic C−H Functionalization with HCl as a Hydrogen-Atom-Transfer Catalyst Precursor in Conjunction with an Organic Photoredox Catalyst. *Angew. Chem. Int. Ed.* **2018**, *57* (39), 12661–12665. https://doi.org/10.1002/anie.201804844.
(51) Deng, H.-P.; Fan, X.-Z.; Chen, Z.-H.; Xu, Q.-H.; Wu, J. Photoinduced Nickel-Catalyzed Chemo- and Regioselective Hydroalkylation of Internal Alkynes with Ether and Amide α-Hetero C(Sp^3)–H Bonds. *J. Am. Chem. Soc.* **2017**, *139* (38), 13579–13584. https://doi.org/10.1021/jacs.7b08158.
(52) Holmberg-Douglas, N.; Nicewicz, D. A. Photoredox-Catalyzed C–H Functionalization Reactions. *Chem. Rev.* **2022**, *122* (2), 1925–2016. https://doi.org/10.1021/acs.chemrev.1c00311.
(53) Zidan, M.; Morris, A. O.; McCallum, T.; Barriault, L. The Alkylation and Reduction of Heteroarenes with Alcohols Using Photoredox Catalyzed Hydrogen Atom Transfer via Chlorine Atom Generation. *Eur J Org Chem* **2020**, *2020* (10), 1453–1458. https://doi.org/10.1002/ejoc.201900786.
(54) Abderrazak, Y.; Bhattacharyya, A.; Reiser, O. Visible-Light-Induced Homolysis of Earth-Abundant Metal-Substrate Complexes: A Complementary Activation Strategy in Photoredox Catalysis. *Angew Chem Int Ed* **2021**, *60* (39), 21100–21115. https://doi.org/10.1002/anie.202100270.
(55) *CRC Handbook of Chemistry and Physics*; CRC Press, 2022.
(56) Yin, H.; Carroll, P. J.; Anna, J. M.; Schelter, E. J. Luminescent Ce(III) Complexes as Stoichiometric and Catalytic Photoreductants for Halogen Atom Abstraction Reactions. *J. Am. Chem. Soc.* **2015**, *137* (29), 9234–9237. https://doi.org/10.1021/jacs.5b05411.
(57) Yin, H.; Carroll, P. J.; Manor, B. C.; Anna, J. M.; Schelter, E. J. Cerium Photosensitizers: Structure-Function Relationships and Applications in Photocatalytic Aryl Coupling Reactions. *Journal of the American Chemical Society* **2016**, *138* (18), 5984–5993. https://doi.org/10.1021/jacs.6b02248.
(58) Tsurugi, H.; Mashima, K. Renaissance of Homogeneous Cerium Catalysts with Unique Ce(IV/III) Couple: Redox-Mediated Organic Transformations Involving Homolysis of Ce(IV)–Ligand Covalent Bonds. *J. Am. Chem. Soc.* **2021**, *143* (21), 7879–7890. https://doi.org/10.1021/jacs.1c02889.
(59) Krasovskiy, A.; Kopp, F.; Knochel, P. Soluble Lanthanide Salts (LnCl3·2 LiCl) for the Improved Addition of Organomagnesium Reagents to Carbonyl Compounds. *Angew. Chem. Int. Ed.* **2006**, *45* (3), 497–500. https://doi.org/10.1002/anie.200502485.
(60) Arnold, P. L.; Liddle, S. T. F-Block N-Heterocyclic Carbene Complexes. *Chem. Commun.* **2006**, No. 38, 3959. https://doi.org/10.1039/b606829d.
(61) Knight, D. W.; Russell, G. A. Phenyliodine(III) Dichloride. In *Encyclopedia of Reagents for Organic Synthesis*; John Wiley & Sons, Ltd, Ed.; John Wiley & Sons, Ltd: Chichester, UK, 2001; p rp071. https://doi.org/10.1002/047084289X.rp071.
(62) Hitchcock, P. B.; Lappert, M. F.; Tian, S. Lanthanocene Chemistry with $[Cp^R]^-$, $[Cp^t]^-$, $[Cp^{tt}]^-$, and $[Cp^{R'}_2SiMe_2]^{2-}$ Ligands: Synthesis and Characterization of Bis(Cyclopentadienyl)Lanthanide(III) Halides and Bis(Cyclopentadienyl)Lanthanide(II) Complexes and Crystal Structures of $[\{NdCp^R_2(\mu\text{-}Cl)\}_2]$, $[\{TmCp^{tt}_2(\mu\text{-}I)\}_2]$, and $[Yb(Cp^{R'}_2SiMe_2)(THF)_2]$ ($Cp^R = \eta^5\text{-}C_5H_4\{CH(SiMe_3)_2\}$, $Cp^t = \eta^5\text{-}C_5H_4(SiMe_2Bu^t)$, $Cp^{tt} = \eta^5\text{-}C_5H_3(SiMe_2Bu^t)_2\text{-}1,3$, and $Cp^{R'} = \eta^5\text{-}C_5H_3\{CH(SiMe_3)_2\}\text{-}3$). *Organometallics* **2000**, *19* (17), 3420–3428. https://doi.org/10.1021/om000305m.

(63) Recknagel, A.; Knösel, F.; Gornitzka, H.; Noltemeyer, M.; Edelmann, F. T.; Behrens, U. Neodym(III)komplexe mit stark raumerfüllenden Cyclopentadienyl- und Benzamidinat-Liganden: Ein Vergleich. *Journal of Organometallic Chemistry* **1991**, *417* (3), 363–375. https://doi.org/10.1016/0022-328X(91)80196-Q.
(64) Spirlet, M.-R.; Goffart, J. Dicyclopentadienyl Complexes of Samarium(III): [Sm(η ^{5} -C $_{5}$ H $_{4}$ SiMe $_{3}$) $_{2}$ (μ-Cl)] $_{2}$. *Acta Crystallogr C Cryst Struct Commun* **1998**, *54* (11), 1624–1626. https://doi.org/10.1107/S0108270198008300.
(65) Evans, W. J.; Forrestal, K. J.; Ziller, J. W. Isopropyltetramethylcyclopentadienyl Samarium Chemistry: Structural Studies of Divalent (C5Me4iPr)2Sm(THF) and Mixed Valent [(C5Me4iPr)2Sm]2(μ-Cl). *Polyhedron* **1998**, *17* (23–24), 4015–4021. https://doi.org/10.1016/S0277-5387(98)00200-9.
(66) Liu, J.; Reta, D.; Cleghorn, J. A.; Yeoh, Y. X.; Ortu, F.; Goodwin, C. A. P.; Chilton, N. F.; Mills, D. P. Light Lanthanide Metallocenium Cations Exhibiting Weak Equatorial Anion Interactions. *Chem. Eur. J.* **2019**, *25* (32), 7749–7758. https://doi.org/10.1002/chem.201901167.
(67) Schumann, H.; Keitsch, M. R.; Mühle, S. H. Metallorganische Verbindungen Der Lanthanoide. 155 [1] Synthese Und Charakterisierung Neuer Lanthanoidocen-Komplexe Mit Silylierten Cyclopentadienylliganden. *Z. anorg. allg. Chem.* **2002**, *628* (6), 1311. https://doi.org/10.1002/1521-3749(200206)628:6<1311::AID-ZAAC1311>3.0.CO;2-2.
(68) Schumann, H.; Heim, A.; Demtschuk, J.; Mühle, S. H. Organometallic Compounds of the Lanthanides. 156. ^{1} ω-Alkenyl-Functionalized Cyclopentadienyl Complexes of Yttrium, Samarium, Ytterbium, and Lutetium. *Organometallics* **2002**, *21* (16), 3323–3334. https://doi.org/10.1021/om020138l.
(69) Evans, W. J.; Drummond, D. K.; Grate, J. W.; Zhang, H.; Atwood, J. L. Structural Diversity of Bis(Pentamethylcyclopentadienyl)Lanthanide Halide Complexes: X-Ray Crystal Structures of [(C5Me5)2SmCl]3 and (C5Me5)10Sm5Cl5[Me(OCH2CH2)4OMe]. *J. Am. Chem. Soc.* **1987**, *109* (13), 3928–3936. https://doi.org/10.1021/ja00247a017.
(70) Satoh, Y.; Ikitake, N.; Nakayama, Y.; Okuno, S.; Yasuda, H. Syntheses of Bis- and Tetra(Trimethylsilyl) Substituted Lanthanocene Methyl Complexes and Their Catalyses for Polymerizations of Methyl Methacrylate, ε-Caprolactone and l-Lactide. *Journal of Organometallic Chemistry* **2003**, *667* (1–2), 42–52. https://doi.org/10.1016/S0022-328X(02)02124-1.
(71) Evans, W. J.; Grate, J. W.; Levan, K. R.; Bloom, I.; Peterson, T. T.; Doedens, R. J.; Zhang, H.; Atwood, J. L. Synthesis and X-Ray Crystal Structure of Di(Pentamethylcyclopentadienyl)Lanthanide and Yttrium Halide Complexes. *Inorg. Chem.* **1986**, *25* (20), 3614–3619. https://doi.org/10.1021/ic00240a017.
(72) Leung, W.-P.; Song, F.-Q.; Xue, F.; Zhang, Z.-Y.; Mak, T. C. W. Synthesis and X-Ray Structures of Trivalent Lanthanide (+)-Neomenthylcyclopentadienyl Complexes. *Journal of Organometallic Chemistry* **1999**, *582* (2), 292–300. https://doi.org/10.1016/S0022-328X(99)00072-8.
(73) Schumann, H.; Zietzke, K.; Weimann, R.; Demtschuk, J.; Kaminsky, W.; Schauwienold, A.-M. Synthesis, Crystal Structure and Catalytic Activity of Some New Chiral Ansa-Metallocenes of Yttrium, Lanthanum, Samarium, Lutetium and of Zirconium. *Journal of Organometallic Chemistry* **1999**, *574* (2), 228–240. https://doi.org/10.1016/S0022-328X(98)00729-3.
(74) Xie, Z.; Chui, K.; Yang, Q.; Mak, T. C. W.; Sun, J. Synthesis, Molecular Structure, and Reactivity of Organolanthanide Fluoride Complexes, [{(Me $_{3}$ Si) $_{2}$ C $_{5}$ H $_{3}$ } $_{2}$ Ln(μ-F)] $_{2}$ (Ln = La, Nd, Sm, Gd) and [(C $_{5}$ H $_{5}$) $_{2}$ Ln(μ-F)(THF)] $_{2}$ (Ln = Y, Yb). *Organometallics* **1998**, *17* (18), 3937–3944. https://doi.org/10.1021/om980162s.

(75) Evans, W. J.; Keyer, R. A.; Ziller, J. W. Tetrahedral versus Square Planar Arrangement of Cyclopentadienyl Ligands in Bimetallic Organosamarium Complexes. X-Ray Crystal Structure of [(C5H4Me)2(THF)Sm(μ-Cl)]2. *Journal of Organometallic Chemistry* **1993**, *450* (1–2), 115–120. https://doi.org/10.1016/0022-328X(93)80146-3.
(76) Xie, F.; Zhang, T. A.; Dreisinger, D.; Doyle, F. A Critical Review on Solvent Extraction of Rare Earths from Aqueous Solutions. *Minerals Engineering* **2014**, *56*, 10–28. https://doi.org/10.1016/j.mineng.2013.10.021.
(77) Binnemans, K.; Jones, P. T.; Blanpain, B.; Van Gerven, T.; Yang, Y.; Walton, A.; Buchert, M. Recycling of Rare Earths: A Critical Review. *Journal of Cleaner Production* **2013**, *51*, 1–22. https://doi.org/10.1016/j.jclepro.2012.12.037.
(78) Gutfleisch, O.; Willard, M. A.; Brück, E.; Chen, C. H.; Sankar, S. G.; Liu, J. P. Magnetic Materials and Devices for the 21st Century: Stronger, Lighter, and More Energy Efficient. *Adv. Mater.* **2011**, *23* (7), 821–842. https://doi.org/10.1002/adma.201002180.
(79) Dewulf, B.; Batchu, N. K.; Binnemans, K. Enhanced Separation of Neodymium and Dysprosium by Nonaqueous Solvent Extraction from a Polyethylene Glycol 200 Phase Using the Neutral Extractant Cyanex 923. *ACS Sustainable Chem. Eng.* **2020**, *8* (51), 19032–19039. https://doi.org/10.1021/acssuschemeng.0c07207.
(80) Griller, D.; Ingold, K. U. Persistent Carbon-Centered Radicals. *Acc. Chem. Res.* **1976**, *9* (1), 13–19. https://doi.org/10.1021/ar50097a003.
(81) Auger, C.; Lesage, A.; Caldarelli, S.; Hodgkinson, P.; Emsley, L. Deuterium−Carbon NMR Correlation Spectroscopy in Oriented Materials. *J. Am. Chem. Soc.* **1997**, *119* (49), 12000–12001. https://doi.org/10.1021/ja972536z.
(82) Ben, H.; Wu, Z.; Han, G.; Jiang, W.; Ragauskas, A. In-Situ Evaluation for Upgrading of Biomass Model Compounds over Noble Metal Catalysts by Isotopic Tracing and NMR Monitoring. *Journal of Analytical and Applied Pyrolysis* **2019**, *142*, 104615. https://doi.org/10.1016/j.jaap.2019.05.004.
(83) Yin, H.; Carroll, P. J.; Manor, B. C.; Anna, J. M.; Schelter, E. J. Cerium Photosensitizers: Structure-Function Relationships and Applications in Photocatalytic Aryl Coupling Reactions. *J. Am. Chem. Soc.* **2016**, *138* (18), 5984–5993. https://doi.org/10.1021/jacs.6b02248.
(84) Willauer, A. R.; Palumbo, C. T.; Fadaei-Tirani, F.; Zivkovic, I.; Douair, I.; Maron, L.; Mazzanti, M. Accessing the +IV Oxidation State in Molecular Complexes of Praseodymium. *J. Am. Chem. Soc.* **2020**, *142* (12), 5538–5542. https://doi.org/10.1021/jacs.0c01204.
(85) Zierhut, M.; Roth, W.; Fischer, I. Photodissociation of the *Tert* -Butyl Radical, C_4H_9. *J. Phys. Chem. A* **2004**, *108* (39), 8125–8130. https://doi.org/10.1021/jp048792x.
(86) Shirakawa, H.; Ikeda, S. Infrared Spectra of Poly(Acetylene). *Polym J* **1971**, *2* (2), 231–244. https://doi.org/10.1295/polymj.2.231.
(87) Glöckner, G. GRADIENT POLYMER CHROMATOGRAPHY: LIQUID CHROMATOGRAPHY. In *Encyclopedia of Separation Science*; Elsevier, 2000; pp 2975–2984. https://doi.org/10.1016/B0-12-226770-2/01851-2.
(88) Jehanno, C.; Alty, J. W.; Roosen, M.; De Meester, S.; Dove, A. P.; Chen, E. Y.-X.; Leibfarth, F. A.; Sardon, H. Critical Advances and Future Opportunities in Upcycling Commodity Polymers. *Nature* **2022**, *603* (7903), 803–814. https://doi.org/10.1038/s41586-021-04350-0.
(89) Chen, L.; Malollari, K. G.; Uliana, A.; Sanchez, D.; Messersmith, P. B.; Hartwig, J. F. Selective, Catalytic Oxidations of C–H Bonds in Polyethylenes Produce Functional Materials with Enhanced Adhesion. *Chem* **2021**, *7* (1), 137–145. https://doi.org/10.1016/j.chempr.2020.11.020.

(90) Yao, Y.; Shen, Q. Organometallic Chemistry of the Lanthanide Metals. In *Rare Earth Coordination Chemistry*; Huang, C., Ed.; John Wiley & Sons, Ltd: Chichester, UK, 2010; pp 309–353. https://doi.org/10.1002/9780470824870.ch8.
(91) Schwarz, R.; Pejic, M.; Fischer, P.; Marinaro, M.; Jörissen, L.; Wachtler, M. Magnesocene-Based Electrolytes: A New Class of Electrolytes for Magnesium Batteries. *Angew. Chem. Int. Ed.* **2016**, *55* (48), 14958–14962. https://doi.org/10.1002/anie.201606448.
(92) Amberger, H.-D.; Reddmann, H. Zur Elektronenstruktur metallorganischer Komplexe der f-Elemente. 67 Erstmalige parametrische Analyse des Absorptionsspektrums einer Molekülverbindung des CeIIIμ: Tris(η5-tetramethylcyclopentadienyl)cer. *Z. anorg. allg. Chem.* **2008**, *634* (1), 173–180. https://doi.org/10.1002/zaac.200700353.
(93) Watson, P. L.; Tulip, T. H.; Williams, I. Defluorination of Perfluoroolefins by Divalent Lanthanoid Reagents: Activating Carbon-Fluorine Bonds. *Organometallics* **1990**, *9* (7), 1999–2009. https://doi.org/10.1021/om00157a006.
(94) Pandey, P.; Yang, Q.; Gau, M. R.; Schelter, E. J. Evaluating the Photophysical and Photochemical Characteristics of Green-Emitting Cerium(III) Mono-Cyclooctatetraenide Complexes. *Dalton Trans.* **2023**, *52* (18), 5909–5917. https://doi.org/10.1039/D3DT00351E.
(95) Lorenz, V.; Liebing, P.; Böhme, M.; Buchholz, A.; Plass, W.; Geue, N.; Hilfert, L.; Busse, S.; Engelhardt, F.; Hrib, C. G.; Edelmann, F. T. Lanthanide(III) Sandwich and Half-Sandwich Complexes with Bulky Cyclooctatetraenyl Ligands: Synthesis, Structures, and Magnetic Properties. *Eur. J. Inorg. Chem.* **2017**, *2017* (41), 4840–4849. https://doi.org/10.1002/ejic.201700878.
(96) Rausch, J.; Apostolidis, C.; Walter, O.; Lorenz, V.; Hrib, C. G.; Hilfert, L.; Kühling, M.; Busse, S.; Edelmann, F. T. One Ligand Fits All: Lanthanide and Actinide Sandwich Complexes Comprising the 1,4-Bis(Trimethylsilyl)Cyclooctatetraenyl (=COT″) Ligand. *New J. Chem.* **2015**, *39* (10), 7656–7666. https://doi.org/10.1039/C5NJ00991J.
(97) Xémard, M.; Zimmer, S.; Cordier, M.; Goudy, V.; Ricard, L.; Clavaguéra, C.; Nocton, G. Lanthanidocenes: Synthesis, Structure, and Bonding of Linear Sandwich Complexes of Lanthanides. *J. Am. Chem. Soc.* **2018**, *140* (43), 14433–14439. https://doi.org/10.1021/jacs.8b09081.
(98) Mashima, K.; Takaya, H. A New Convenient Synthesis of Cyclooctatetraenyllanthanide Complexes: -Ray Crystal Structure of CeI(C8H8)(THF)3. *Tetrahedron Letters* **1989**, *30* (28), 3697–3700. https://doi.org/10.1016/S0040-4039(01)80486-X.
(99) Wayda, A. L. Cyclooctatetraenyllanthanide Complexes. 1. Alkyl- and Arylmonocyclooctatetraenyllutetium Derivatives. *Organometallics* **1983**, *2* (4), 565–566. https://doi.org/10.1021/om00076a022.
(100) Kresinski, R. A. Lanthanides: Cyclopentadienyl Compounds. In *Encyclopedia of Inorganic and Bioinorganic Chemistry*; Scott, R. A., Ed.; John Wiley & Sons, Ltd: Chichester, UK, 2012; p eibc2032. https://doi.org/10.1002/9781119951438.eibc2032.
(101) Ruffoni, A.; Mykura, R. C.; Bietti, M.; Leonori, D. The Interplay of Polar Effects in Controlling the Selectivity of Radical Reactions. *Nat. Synth* **2022**, *1* (9), 682–695. https://doi.org/10.1038/s44160-022-00108-2.
(102) Canestrari, D.; Lancianesi, S.; Badiola, E.; Strinna, C.; Ibrahim, H.; Adamo, M. F. A. Desulfurative Chlorination of Alkyl Phenyl Sulfides. *Org. Lett.* **2017**, *19* (4), 918–921. https://doi.org/10.1021/acs.orglett.7b00077.
(103) Sandoval, J. J.; Palma, P.; Álvarez, E.; Cámpora, J.; Rodríguez-Delgado, A. Mechanism of Alkyl Migration in Diorganomagnesium 2,6-Bis(Imino)Pyridine Complexes: Formation of Grignard-Type Complexes with Square-Planar Mg(II) Centers. *Organometallics* **2016**, *35* (18), 3197–3204. https://doi.org/10.1021/acs.organomet.6b00528.

(104) Kong, Y.; Ren, H.; Xu, S.; Song, H.; Liu, B.; Wang, B. Synthesis, Structures, and Norbornene Polymerization Behavior of Bis(Aryloxide-N-Heterocyclic Carbene) Palladium Complexes. *Organometallics* **2009**, *28* (20), 5934–5940. https://doi.org/10.1021/om900625r.
(105) Evans, W. J.; Kozimor, S. A.; Ziller, J. W.; Fagin, A. A.; Bochkarev, M. N. Facile Syntheses of Unsolvated UI $_3$ and Tetramethylcyclopentadienyl Uranium Halides. *Inorg. Chem.* **2005**, *44* (11), 3993–4000. https://doi.org/10.1021/ic0482685.
(106) Gompa, T. P.; Rice, N. T.; Russo, D. R.; Aguirre Quintana, L. M.; Yik, B. J.; Bacsa, J.; La Pierre, H. S. Diethyl Ether Adducts of Trivalent Lanthanide Iodides. *Dalton Trans.* **2019**, *48* (23), 8030–8033. https://doi.org/10.1039/C9DT00775J.
(107) Windorff, C. J.; Dumas, M. T.; Ziller, J. W.; Gaunt, A. J.; Kozimor, S. A.; Evans, W. J. Small-Scale Metal-Based Syntheses of Lanthanide Iodide, Amide, and Cyclopentadienyl Complexes as Analogues for Transuranic Reactions. *Inorg. Chem.* **2017**, *56* (19), 11981–11989. https://doi.org/10.1021/acs.inorgchem.7b01968.
(108) Scherg, T.; Schneider, S.; Frey, G.; Schwarz, J.; Herdtweck, E.; Herrmann, W. Bridged Imidazolium Salts Used as Precursors for Chelating Carbene Complexes of Palladium in the Mizoroki-Heck Reaction. *Synlett* **2006**, *2006* (18), 2894–2907. https://doi.org/10.1055/s-2006-951539.
(109) Shapiro, P. J.; Vij, A.; Yap, G. P. A.; Rheingold, A. L. The Double Insertion of T-Butyl Isocyanide by Tris(Tetramethylcyclopentadienyl) Aluminum to Form. *Polyhedron* **1995**, *14* (1), 203–209. https://doi.org/10.1016/0277-5387(94)00354-H.
(110) Stevenson, C. D.; Ocasio, I.; Bonilla, A. Heats of Formation of Disodium and Dipotassium Cyclooctatetraenide. *J. Am. Chem. Soc.* **1976**, *98* (18), 5469–5473. https://doi.org/10.1021/ja00434a011.
(111) Dolomanov, O. V.; Bourhis, L. J.; Gildea, R. J.; Howard, J. A. K.; Puschmann, H. *OLEX2* : A Complete Structure Solution, Refinement and Analysis Program. *J. Appl. Crystallogr.* **2009**, *42* (2), 339–341. https://doi.org/10.1107/S0021889808042726.
(112) Sheldrick, G. M. *SHELXT* – Integrated Space-Group and Crystal-Structure Determination. *Acta Crystallogr. A* **2015**, *71* (1), 3–8. https://doi.org/10.1107/S2053273314026370.
(113) Clark, R. C.; Reid, J. S. The Analytical Calculation of Absorption in Multifaceted Crystals. *Acta Crystallographica Section A* **1995**, *51*, 887–897.
(114) M. J. Frisch, G. W. Trucks, H. B. Schlegel, G. E. Scuseria, M. A. Robb, J. R.; Cheeseman, G. Scalmani, V. Barone, B. Mennucci, G. A. Petersson, H. Nakatsuji, M. Caricato, X. Li, H.; P. Hratchian, A. F. Izmaylov, J. Bloino, G. Zheng, J. L. Sonnenberg, M. Hada, M. Ehara, K. Toyota, R.; Fukuda, J. Hasegawa, M. Ishida, T. Nakajima, Y. Honda, O. Kitao, H. Nakai, T. Vreven, J. A.; Montgomery, Jr., J. E. Peralta, F. Ogliaro, M. Bearpark, J. J. Heyd, E. Brothers, K. N. Kudin, V. N.; Staroverov, R. Kobayashi, J. Normand, K. Raghavachari, A. Rendell, J. C. Burant, S. S. Iyengar, J.; Tomasi, M. Cossi, N. Rega, J. M. Millam, M. Klene, J. E. Knox, J. B. Cross, V. Bakken, C. Adamo, J.; Jaramillo, R. Gomperts, R. E. Stratmann, O. Yazyev, A. J. Austin, R. Cammi, C. Pomelli, J. W. Ochterski,; R. L. Martin, K. Morokuma, V. G. Zakrzewski, G. A. Voth, P. Salvador, J. J. Dannenberg, S. Dapprich, A.; D. Daniels, O. Farkas, J. B. Foresman, J. V. Ortiz, J. Cioslowski, D. J. Fox, Gaussian, Inc., Wallingford CT, 2013. Gaussian 09, Revision D.01.
(115) Becke, A. D. Density-functional Thermochemistry. III. The Role of Exact Exchange. *J. Chem. Phys* **1993**, *98* (7), 5648–5652. https://doi.org/10.1063/1.464913.
(116) Dobson, J. F.; Vignale, G.; Das, M. P.; Directions, N. Electronic Density Functional Theory : Recent Progress and New Directions; 1998.
(117) Cao, X.; Dolg, M.; Stoll, H. Valence Basis Sets for Relativistic Energy-Consistent Small-Core Actinide Pseudopotentials. *J. Chem. Phys* **2003**, *118* (2), 487–496. https://doi.org/10.1063/1.1521431.

(118) Küchle, W.; Dolg, M.; Stoll, H.; Preuss, H. Energy-adjusted Pseudopotentials for the Actinides. Parameter Sets and Test Calculations for Thorium and Thorium Monoxide. *J. Chem. Phys* **1994**, *100* (10), 7535–7542. https://doi.org/10.1063/1.466847.
(119) Maron, L.; Teichteil, C. On the Accuracy of Averaged Relativistic Shape-Consistent Pseudopotentials. *Chem. Phys* **1998**, *237* (1–2), 105–122. https://doi.org/10.1016/S0301-0104(98)00243-2.
(120) Hariharan, P. C.; Pople, J. A. The Influence of Polarization Functions on Molecular Orbital Hydrogenation Energies. *Theoret. Chim. Acta* **1973**, *28* (3), 213–222. https://doi.org/10.1007/BF00533485.
(121) Hehre, W. J.; Ditchfield, R.; Pople, J. A. Self—Consistent Molecular Orbital Methods. XII. Further Extensions of Gaussian—Type Basis Sets for Use in Molecular Orbital Studies of Organic Molecules. *J. Chem. Phys* **1972**, *56* (5), 2257–2261. https://doi.org/10.1063/1.1677527.

Concluding Statements and Proposed Future Studies

This dissertation presents a series of new organometallic lanthanide complexes supported by light-absorbing tetramethylcyclopentadienyl and aryloxy-NHC ligands. The synthesis of these complexes and the investigation into their reactivity both furthers the fundamental understanding of lanthanide coordination chemistry and highlights the applications of rare-earth organometallic complexes in photoredox catalysis.

We have presented the synthesis and characterization of several earth-abundant organometallic photocatalysts that can cleave the strong sp^3 C–F bond of $PhCF_3$. To the best of our knowledge, we have demonstrated the first examples of photocatalytic C–F bond activation and functionalization mediated by a rare-earth metal complex.[1] The Lewis acidity of the metal is implicated in binding the substrate, and we learned that light absorption through aromatic ancillary ligands is important for imparting photoreactivity to lanthanides that do not possess a metal-based $4f \rightarrow 5d$ transition like cerium. The reactivity described is significant in that it is not limited to cerium, which has been the focus of lanthanide photocatalysis thus far.[2]

Photophysical measurements suggest that the chelating aryloxy-NHC ligand [2-O-3,5-^{t}Bu$_2$-C_6H_2(1-C{N(CH)$_2$N(^{i}Pr)})] (**L**) is particularly important for light absorption, and the creation of a sufficiently reducing excited state that can activate a C(sp^3)–F bond. We have also shown that the substituent present at the NHC 3-position affects the light absorbing capability of photocatalysts bearing aryloxy-NHC ligands. Noticeably, the intensity of the ligand-based absorption is much greater for (Cp^{Me4})$_2$Ce(**L^{tBu}**) (**1-Ce^{t}Bu**) (**L^{tBu}** = 2-O-3,5-^{t}Bu$_2$-C_6H_2(1-C{N(CH)$_2$N(^{t}Bu)}, Cp^{Me4} = C_5Me_4H) than (Cp^{Me4})$_2$Ce(**L**) (**1-Ce**) or (Cp^{Me4})$_2$Ce(**L^{Mes}**) (**1-CeMes**) (**L^{Mes}** = 2-O-3,5-^{t}Bu$_2$-C_6H_2(1-C{N(CH)$_2$N(Mes)}) and **1-Ce^{t}Bu** demonstrates higher activity than **1-Ce** in stoichiometric C(sp^3)–Cl bond activation reactions. This presents an opportunity to increase catalyst quantum yield and efficiency, and consequent reactivity, by imparting larger, rigid substituents on the complex. Further investigation into the photophysical properties of complexes bearing a variety of substituted aryloxy-NHC ligands (i.e., (Cp^{Me4})$_2$Ce(**L^{Me}**) (**1-CeMe**) (**L^{Me}** = 2-O-3,5-^{t}Bu$_2$-C_6H_2(1-C{N(CH)$_2$N(Me)}) and (Cp^{Me4})$_2$Ce(**L^{Tp}**) (**1-CeTp**) (**L^{Tp}** = 2-O-3,5-^{t}Bu$_2$-C_6H_2(1-C{N(CH)$_2$N(Tp)})) would be of general interest when working to optimize a lanthanide photocatalyst of this type.[3]

It is currently unclear whether tuning of the substituents on the Cp ligands could impart greater reactivity to complexes without **L** that demonstrated relatively poor performance in C(sp^3)–F bond activation reactions.[1] Given the importance of substrate binding in our proposed inner-sphere reaction mechanism, modifying the Cp ligand to decrease steric bulk about the metal center could allow for easier substrate access and improve reactivity for lanthanide tris(cyclopentadienyl) complexes. The synthesis of complexes bearing methylcyclopentadienyl or isopropylcyclopentadienyl ligands, for example, and their subsequent testing in the C(sp^3)–F bond cleavage of $PhCF_3$ would provide insight into this hypothesis.

Our catalytic studies suggested that reactivity towards photocatalytic C(sp^3)–F bond activation decreases along the lanthanide series, consistent with the larger lanthanides providing greater access to an inner sphere mechanism. However, we also hypothesized that reactivity may also be influenced by the extent of orbital overlap between metal and ligand, which could affect the efficiency of the LMCT that is required to impart photoreactivity to metals without an accessible $4f \rightarrow 5d$ transition.[4–7] It would be of great interest to acquire further computational and spectroscopic data, particularly fluorescence measurements, for **1-La**, **1-Sm** and **1-Nd**, to study the excitation energies of each complex. TD-DFT studies could also provide further

insight into the orbitals involved in photoexcitation for the later lanthanides. Further investigation into the synthesis the reactivity of analogous calcium complex would also be of interest, as Ca possesses a similar ionic radius to the lanthanides but *d*-orbitals with higher energy, which may affect the efficiency of LMCT.[8,9]

We targeted the cleavage and functionalization of unactivated sp^2 and sp^3 C–Cl bonds that had been inaccessible to other lanthanide-based visible light photocatalysts.[10] Such reactions are of interest in the context of upcycling chlorinated polymers such as PVC.[11,12] Photocatalytic C–Cl bond activation was achieved using simple tris(cyclopentadienyl) complexes $(Cp^{Me4})_3Ln$ (**2-Ln**, Ln = La, Ce, Pr, Nd, Sm) and $[(Cp^{Me4})_2Ln(\mu\text{–}Cl)]_2$ (**3-Ln**, Ln = Ce, Nd, Sm) via a reactive lanthanide alkyl intermediate $(Cp^{Me4})_2Ln(Bn)(THF)$ (**6-Ln**) formed through reaction with the $MgBn_2(THF)_2$ reductive coupling partner. While C–Cl bond activation by precatalyst $(Cp^{Me4})_3Ce$ (**2-Ce**) was most efficient, reactivity could be extended to typically photo-and redox-inactive lanthanide Cp^{Me4} complexes. These experiments demonstrated that while specialized, light-absorbing ligand **L** is required for efficient C(sp^3)–F bond activation, light absorption through Cp^{Me4} is satisfactory for activation of the weaker C(sp^3)–Cl bond.

In addition, the excited state lifetimes of complexes **1-Ce** and **3-Ce** are amongst the longest of cerium complexes published in the literature (101 ns and 175 ns respectively).[13] Improving the excited state lifetimes of photocatalysts has been shown to enhance photocatalytic activity of even complexes with weak reduction potentials.[14] As such, fluorescence and lifetime measurements of simple tris(cyclopentadienyl) lanthanide complexes and **1-Ce^{t}Bu**, **1-CeMes** would be useful to further investigate the light absorbing capabilities of Cp^{Me4} and aryloxy-NHC ligands and their derivatives both in isolation and when coordinated to a metal center.

Complex **2-Ce** is also capable of cleaving 79% of the C–Cl bonds in PVC. However, the insolubility of the resulting polymer in organic solvents precluded full product characterization. As dechlorination appears to proceed until the product precipitates from the THF, reaction optimization is needed to improve the overall extent of dechlorination of PVC. For example, investigating different types and ratios of reaction solvent, or decreasing the concentration of substrates/reagents may allow complete dechlorination to be achieved. We are also interested in exploring the dechloroalkylation chemistry of PVC and other chlorohydrocarbons, which could allow us to access new polymers with interesting chemical and physical properties.[15] To do so we could invoke larger substituents, such as Ph, Mes, or Tp on the ancillary ligands which could potentially help to maintain proximity of the catalysts, coupling partner and substrates through steric effects or dispersion forces.[16] Controlling secondary interactions on the chosen ligands will be essential for imparting further selectivity into C–X bond activations, particularly when investigating perhalogenated substrates including chlorofluorocarbons, per- and polyfluoroalkyl substances and PVC that can be highly toxic and persistent in the environment.[17]

The homolysis of Ln–Cp^{Me4} bonds was also implicated in the photocatalytic C–X bond activation using complexes of typically photo- and redox-inactive lanthanides. Given the light absorbing capability and rigid bidentate coordination of dianionic cyclooctatetraenyl (COT) ligands,[13] we are interested in investigating photocatalytic reactions using lanthanide COT complexes, which we hypothesized would be less susceptible to metal-ligand bond homolysis and catalyst degradation. Preliminary studies into the dechlorination of chlorocyclohexane by [CeI(COT)] in conjunction with $MgBn_2(THF)_2$ were presented, though greater substrate scope and catalytic and mechanistic investigation is needed. The independent synthesis and characterization of [Ce(Bn)(COT)] and its use in photocatalytic dechlorination and

defluorination reactions would be beneficial here, as would studies of cerocene [Ce(COT)$_2$]. Since the initial synthesis of cerocene in 1976,[18] many spectroscopic and computational studies on its electronic configuration have been carried out, demonstrating the presence of a multiconfigurational ground state (Ce(III)/Ce(IV) character) within this complex.[19–21] Utilizing tethered ansa-Cp ligands in related systems also has the potential for reducing Ln-Cp bond homolysis and prolonging the catalyst lifetime in solution by preventing ligand exchange.[22]

So far, we have only been able to impart catalytic activity to our light-driven C–X bond activation reactions using dialkyl magnesium reagents as both a coupling partner and sacrificial reductant. Investigation into a larger range of potential coupling partners and sacrificial reductants, including α,β-unsaturated carbonyls and inorganic bases such as cesium carbonate respectively,[7,23–25] could allow for a larger scope of catalytic dehaloalkylation and greater mechanistic understanding of such processes. Further investigation into the electrochemical oxidation and reduction of the photocatalysts described here could allow for the photoelectrochemical C–X bond activations to proceed catalytically without large excess of an external chemical reductant.[26] It is also of interest to further develop the substrate scope of these systems and test the capability of our catalysts to cleave other strong bonds, such as the S–F bonds in sulfur hexafluoride (SF_6) or related SF_5 containing compounds which are of environmental significance.[27–29] SF_6 can efficiently absorb infra-red radiation and has a long life-time in the Earth's atmosphere making it a potent greenhouse gas, and its decomposition can produce toxic SF_5 containing compounds.[30]

Finally, during these studies, complexes [(Cp^{Me4})$_2$Ln(μ–Cl)]$_2$ (**3-Ln**, Ln = Ce, Pr, Nd, Sm) were synthesized and characterized. Through working with these complexes, it appeared that the solubility of **3-Ln** in non-polar organic solvents increases as ionic radii increases. These differences in solubility between the lanthanide complexes could be applied to light-driven rare-earth element separations,[31–33] particularly the separation of neodymium and dysprosium which is of relevance to magnetic materials.[34] Preliminary investigations into the synthesis of [(Cp^{Me4})$_2$DyCl]$_2$ (**3-Dy**) were presented, through further characterization and study of the catalytic activity of this complex, and quantitative investigation into the solubility of all relevant complexes at scale is needed. This, and the study of analogous COT complexes, is currently underway in our laboratory.

(1) Kynman, A. E.; Elghanayan, L.; Desnoyer, A.; Yang, Y.; Severy, L.; Di Giuseppe, A.; Tilley, T. D.; Maron, L.; Arnold, P. L. Controlled Monodefluorination and Alkylation of C(Sp3)-F Bonds by Lanthanide Photocatalysts: Importance of Metal – Ligand Cooperativity. *Chem. Sci.* **2022**, *13* (47), 14090–14100. https://doi.org/10.1039/D2SC04192H.
(2) Qiao, Y.; Schelter, E. J. Lanthanide Photocatalysis. *Acc. Chem. Res.* **2018**, *51* (11), 2926–2936. https://doi.org/10.1021/acs.accounts.8b00336.
(3) Qiao, Y.; Cheisson, T.; Manor, B. C.; Carroll, P. J.; Schelter, E. J. A Strategy to Improve the Performance of Cerium(III) Photocatalysts. *Chem. Commun.* **2019**, *55* (28), 4067–4070. https://doi.org/10.1039/C9CC00282K.
(4) Juliá, F. Ligand-to-Metal Charge Transfer (LMCT) Photochemistry at 3d-Metal Complexes: An Emerging Tool for Sustainable Organic Synthesis. *ChemCatChem* **2022**, *14* (19). https://doi.org/10.1002/cctc.202200916.
(5) Miranda, Y. C.; Pereira, L. L. A. L.; Barbosa, J. H. P.; Brito, H. F.; Felinto, M. C. F. C.; Malta, O. L.; Faustino, W. M.; Teotonio, E. E. S. The Role of the Ligand-to-Metal Charge-Transfer State in the Dipivaloylmethanate-Lanthanide Intramolecular Energy Transfer Process. *Eur. J. Inorg. Chem.* **2015**, *2015* (18), 3019–3027. https://doi.org/10.1002/ejic.201500263.

(6) Hasegawa, Y.; Kitagawa, Y.; Nakanishi, T. Effective Photosensitized, Electrosensitized, and Mechanosensitized Luminescence of Lanthanide Complexes. *NPG Asia Mater* **2018**, *10* (4), 52–70. https://doi.org/10.1038/s41427-018-0012-y.
(7) Hu, A.; Guo, J. J.; Pan, H.; Zuo, Z. Selective Functionalization of Methane, Ethane, and Higher Alkanes by Cerium Photocatalysis. *Science* **2018**, *361* (6403), 668–672. https://doi.org/10.1126/science.aat9750.
(8) Hidaka, H.; Tsukamoto, T.; Oyama, T.; Mitsutsuka, Y.; Takamura, T.; Serpone, N. Photoassisted Defluorination of Fluorinated Substrates and Pharmaceuticals by a Wide Bandgap Metal Oxide in Aqueous Media. *Photochem Photobiol Sci* **2013**, *12* (5), 751–759. https://doi.org/10.1039/c2pp25358e.
(9) Friedmann, D.; Caruso, R. A. Indium Oxides and Related Indium-based Photocatalysts for Water Treatment: Materials Studied, Photocatalytic Performance, and Special Highlights. *Solar RRL* **2021**, *5* (7), 2100086. https://doi.org/10.1002/solr.202100086.
(10) Kynman, A. E.; Christodoulou, S.; Ouellette, E. T.; Peterson, A.; Kelly, S.; Maron, L.; Arnold, P. L. Photocatalytic Dechlorination of Unactivated Chlorocarbons Including PVC Using Organolanthanide Complexes. *Chem. Commun.* **2023**, 10.1039.D3CC02906A. https://doi.org/10.1039/D3CC02906A.
(11) Hou, Q.; Zhen, M.; Qian, H.; Nie, Y.; Bai, X.; Xia, T.; Laiq Ur Rehman, M.; Li, Q.; Ju, M. Upcycling and Catalytic Degradation of Plastic Wastes. *Cell Reports Physical Science* **2021**, *2* (8), 100514. https://doi.org/10.1016/j.xcrp.2021.100514.
(12) Zhao, X.; Boruah, B.; Chin, K. F.; Đokić, M.; Modak, J. M.; Soo, H. S. Upcycling to Sustainably Reuse Plastics. *Adv. Mater.* **2021**.
(13) Pandey, P.; Yang, Q.; Gau, M. R.; Schelter, E. J. Evaluating the Photophysical and Photochemical Characteristics of Green-Emitting Cerium(III) Mono-Cyclooctatetraenide Complexes. *Dalton Trans.* **2023**, *52* (18), 5909–5917. https://doi.org/10.1039/D3DT00351E.
(14) Vogt, D. B.; Seath, C. P.; Wang, H.; Jui, N. T. Selective C-F Functionalization of Unactivated Trifluoromethylarenes. *Journal of the American Chemical Society* **2019**, *141* (33), 13203–13211. https://doi.org/10.1021/jacs.9b06004.
(15) Jehanno, C.; Alty, J. W.; Roosen, M.; De Meester, S.; Dove, A. P.; Chen, E. Y.-X.; Leibfarth, F. A.; Sardon, H. Critical Advances and Future Opportunities in Upcycling Commodity Polymers. *Nature* **2022**, *603* (7903), 803–814. https://doi.org/10.1038/s41586-021-04350-0.
(16) Ruffoni, A.; Mykura, R. C.; Bietti, M.; Leonori, D. The Interplay of Polar Effects in Controlling the Selectivity of Radical Reactions. *Nat. Synth* **2022**, *1* (9), 682–695. https://doi.org/10.1038/s44160-022-00108-2.
(17) Hodnebrog, Ø.; Etminan, M.; Fuglestvedt, J. S.; Marston, G.; Myhre, G.; Nielsen, C. J.; Shine, K. P.; Wallington, T. J. Global Warming Potentials and Radiative Efficiencies of Halocarbons and Related Compounds: A Comprehensive Review: HALOCARBON REVIEW. *Rev. Geophys.* **2013**, *51* (2), 300–378. https://doi.org/10.1002/rog.20013.
(18) Greco, A.; Cesca, S.; Bertolini, W. New 7r-Cyclooctate'I'raenyl and IT-Cyclopentadienyl Complexes of Cerium. *Journal of Organometallic Chemistry* **1976**, *113* (4), 321–330. https://doi.org/10.1016/S0022-328X(00)96143-6.
(19) Dolg, M.; Fulde, P.; Stoll, H.; Preuss, H.; Chang, A.; Pitzer, R. M. Formally Tetravalent Cerium and Thorium Compounds: A Configuration Interaction Study of Cerocene Ce(C8H8)2 and Thorocene Th(C8H8)2 Using Energy-Adjusted Quasirelativistic Ab Initio Pseudopotentials. *Chemical Physics* **1995**, *195* (1–3), 71–82. https://doi.org/10.1016/0301-0104(94)00363-F.
(20) Kerridge, A.; Coates, R.; Kaltsoyannis, N. Is Cerocene Really a Ce(III) Compound? All-Electron Spin−Orbit Coupled CASPT2 Calculations on $M(\eta^8\text{-}C_8H_8)_2$ (M = Th, Pa, Ce). *J. Phys. Chem. A* **2009**, *113* (12), 2896–2905. https://doi.org/10.1021/jp807804w.

(21) Walter, M. D.; Booth, C. H.; Lukens, W. W.; Andersen, R. A. Cerocene Revisited: The Electronic Structure of and Interconversion Between $Ce_2(C_8H_8)_3$ and $Ce(C_8H_8)_2$. *Organometallics* **2009**, *28* (3), 698–707. https://doi.org/10.1021/om7012327.
(22) Eppinger, J.; Spiegler, M.; Hieringer, W.; Herrmann, W. A.; Anwander, R. *C_2*-Symmetric *Ansa*-Lanthanidocene Complexes. Synthesis via Silylamine Elimination and β-SiH Agostic Rigidity. *J. Am. Chem. Soc.* **2000**, *122* (13), 3080–3096. https://doi.org/10.1021/ja992786a.
(23) Ruiz Espelt, L.; Wiensch, E. M.; Yoon, T. P. Brønsted Acid Cocatalysts in Photocatalytic Radical Addition of α-Amino C–H Bonds across Michael Acceptors. *J. Org. Chem.* **2013**, *78* (8), 4107–4114. https://doi.org/10.1021/jo400428m.
(24) Rabie, R.; Hammouda, M. M.; Elattar, K. M. Cesium Carbonate as a Mediated Inorganic Base in Some Organic Transformations. *Res Chem Intermed* **2017**, *43* (4), 1979–2015. https://doi.org/10.1007/s11164-016-2744-z.
(25) Connelly, N. G.; Geiger, W. E. Chemical Redox Agents for Organometallic Chemistry. *Chem. Rev.* **1996**, *96* (2), 877–910. https://doi.org/10.1021/cr940053x.
(26) Bessegato, G. G.; Guaraldo, T. T.; De Brito, J. F.; Brugnera, M. F.; Zanoni, M. V. B. Achievements and Trends in Photoelectrocatalysis: From Environmental to Energy Applications. *Electrocatalysis* **2015**, *6* (5), 415–441. https://doi.org/10.1007/s12678-015-0259-9.
(27) Tsai, W.-T. The Decomposition Products of Sulfur Hexafluoride (SF6): Reviews of Environmental and Health Risk Analysis. *Journal of Fluorine Chemistry* **2007**, *128* (11), 1345–1352. https://doi.org/10.1016/j.jfluchem.2007.06.008.
(28) Altomonte, S.; Zanda, M. Synthetic Chemistry and Biological Activity of Pentafluorosulphanyl (SF5) Organic Molecules. *Journal of Fluorine Chemistry* **2012**, *143*, 57–93. https://doi.org/10.1016/j.jfluchem.2012.06.030.
(29) Tomar, P.; Braun, T.; Kemnitz, E. Photochemical Activation of SF_6 by N-Heterocyclic Carbenes to Provide a Deoxyfluorinating Reagent. *Chem. Commun.* **2018**, *54* (70), 9753–9756. https://doi.org/10.1039/C8CC05494K.
(30) Dervos, C. T.; Vassiliou, P. Sulfur Hexafluoride (SF_6): Global Environmental Effects and Toxic Byproduct Formation. *Journal of the Air & Waste Management Association* **2000**, *50* (1), 137–141. https://doi.org/10.1080/10473289.2000.10463996.
(31) Van Den Bogaert, B.; Havaux, D.; Binnemans, K.; Van Gerven, T. Photochemical Recycling of Europium from Eu/Y Mixtures in Red Lamp Phosphor Waste Streams. *Green Chem.* **2015**, *17* (4), 2180–2187. https://doi.org/10.1039/C4GC02140A.
(32) Leblebici, M. E.; Van Den Bogaert, B.; Stefanidis, G. D.; Van Gerven, T. Efficiency vs. Productivity in Photoreactors, a Case Study on Photochemical Separation of Eu. *Chemical Engineering Journal* **2017**, *310*, 240–248. https://doi.org/10.1016/j.cej.2016.10.112.
(33) DiMucci, I. M.; Root, H. D.; Jones, Z. R.; Kozimor, S. A.; MacInnes, M. M.; Miller, J. L.; Mocko, V.; Oldham, W. J.; Stein, B. W. Photochemical Separation of Plutonium from Uranium. *Chem. Commun.* **2022**, *58* (78), 10961–10964. https://doi.org/10.1039/D2CC04225H.
(34) Binnemans, K.; Jones, P. T.; Blanpain, B.; Van Gerven, T.; Yang, Y.; Walton, A.; Buchert, M. Recycling of Rare Earths: A Critical Review. *Journal of Cleaner Production* **2013**, *51*, 1–22. https://doi.org/10.1016/j.jclepro.2012.12.037.

Appendix A

Photophysical Measurements of Organometallic Cerium Complexes

Chapter 1 of this thesis describes the synthesis of a series of cerium complexes which we aimed to use in photocatalytic reactions. As such, photophysical properties of complexes **1-Ce**, **3-Ce** and **4-Ce** were investigated, and their excitation and emission spectra recorded alongside their excited state lifetimes. Measurements were carried out by Drs. Leticia Arnedo-Sanchez and Jennifer Wacker in collaboration with the author at Lawrence Berkeley National Laboratory. The author guided these studies and interpreted the data.

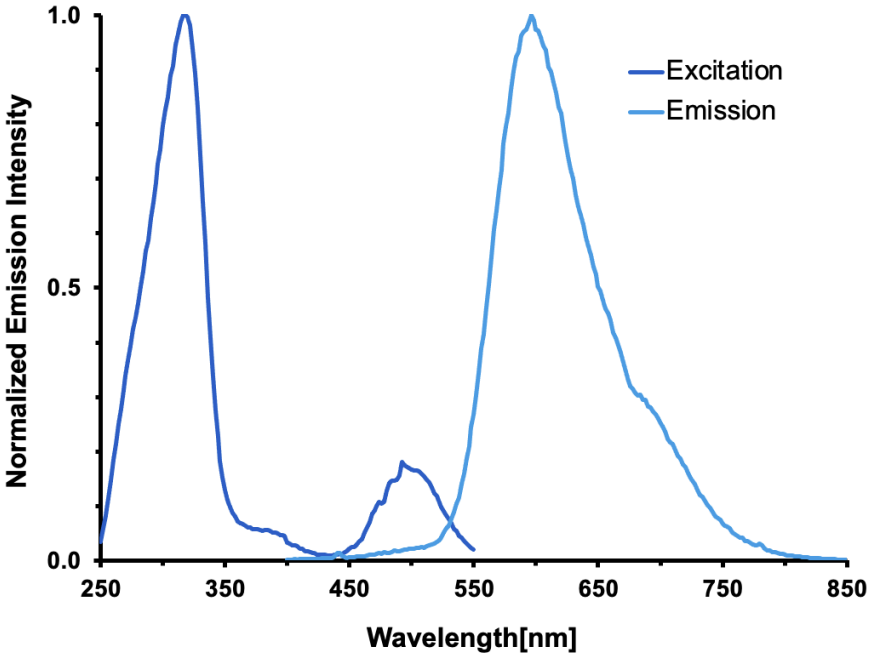

Figure A.1. Emission and excitation spectra of **1-Ce** recorded in THF. The emission spectrum was collected with an excitation wavelength of 390 nm; the excitation was monitored at an emission wavelength of 600 nm. All data were calibrated to the detector efficiency and normalized.

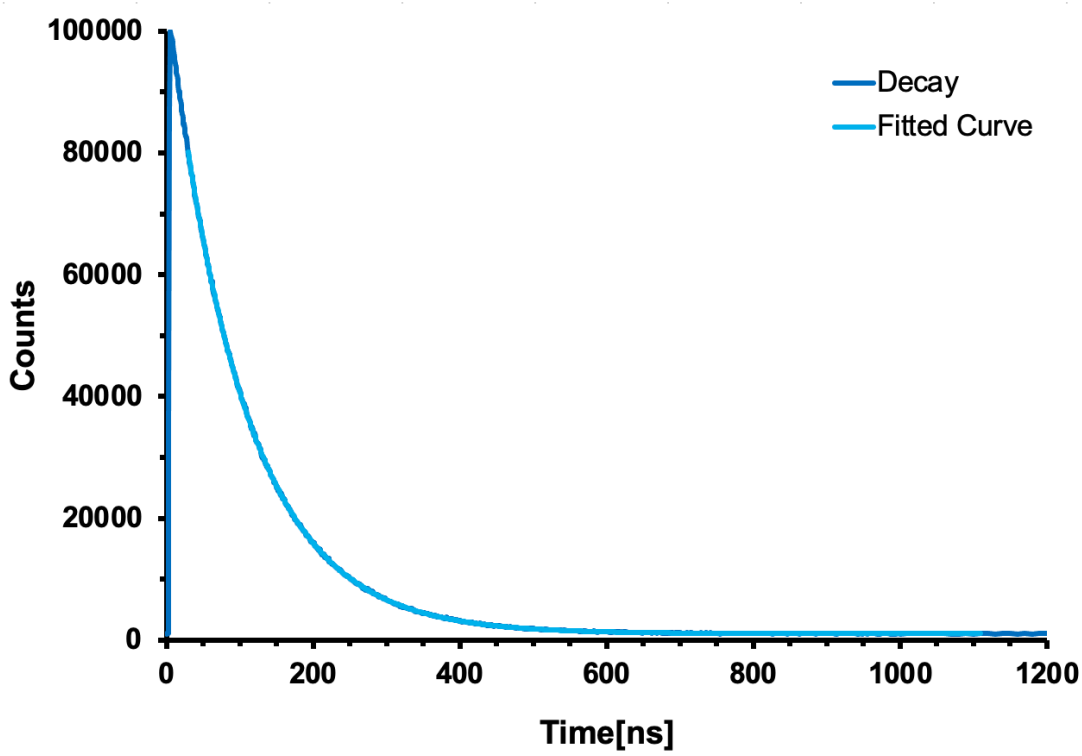

Figure A.2. Lifetime decay of **1-Ce** recorded in toluene. τ1[ns]= 101.941 ±0.039.

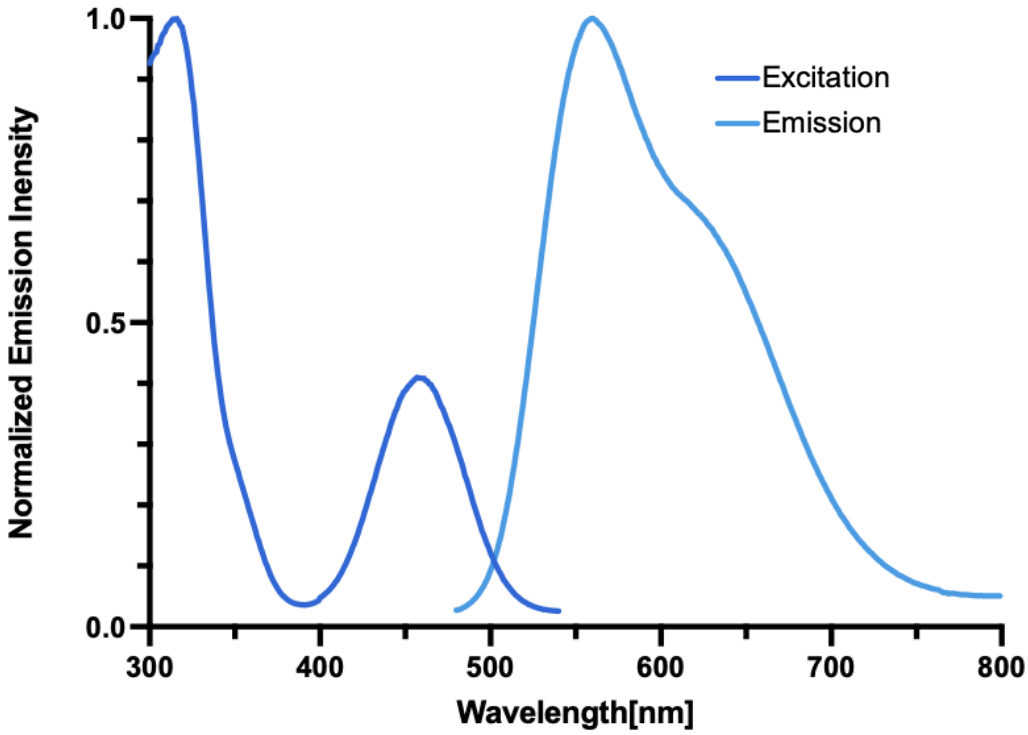

Figure A.3. Emission and excitation spectra of **3-Ce** recorded in THF. The emission spectrum was collected with an excitation wavelength of 300 nm; the excitation was monitored at an emission wavelength of 559 nm. All data were calibrated to the detector efficiency and normalized.

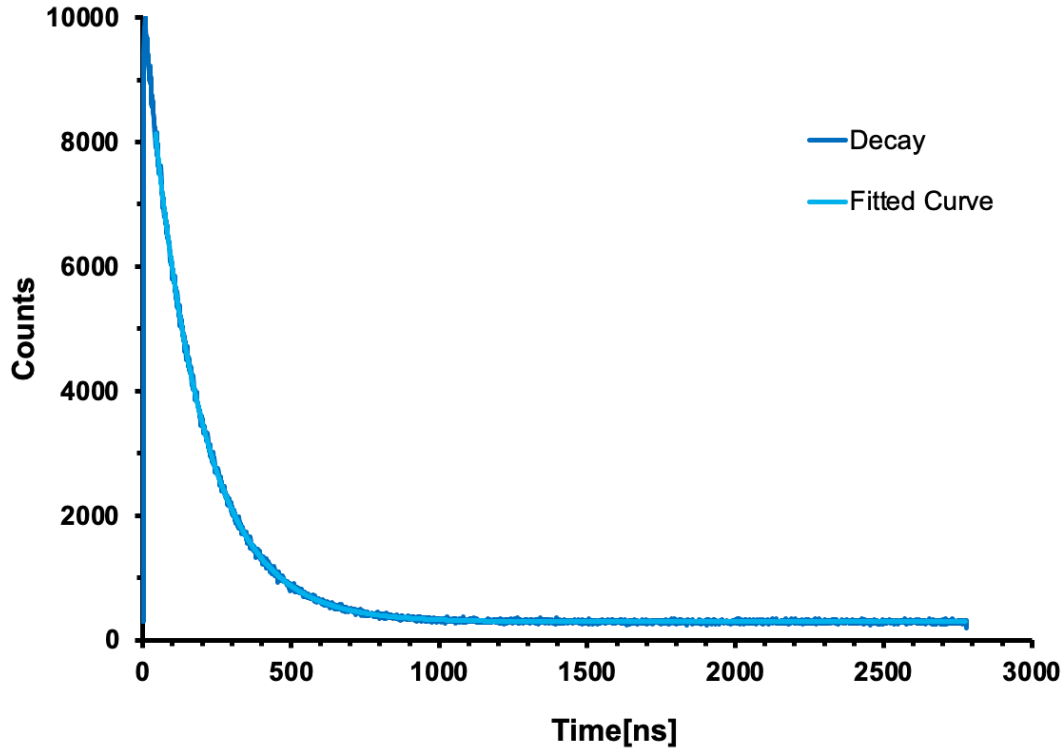

Figure A.4. Lifetime decay of **3-Ce** recorded in THF. τ1[ns]= 175.10 ±0.16.

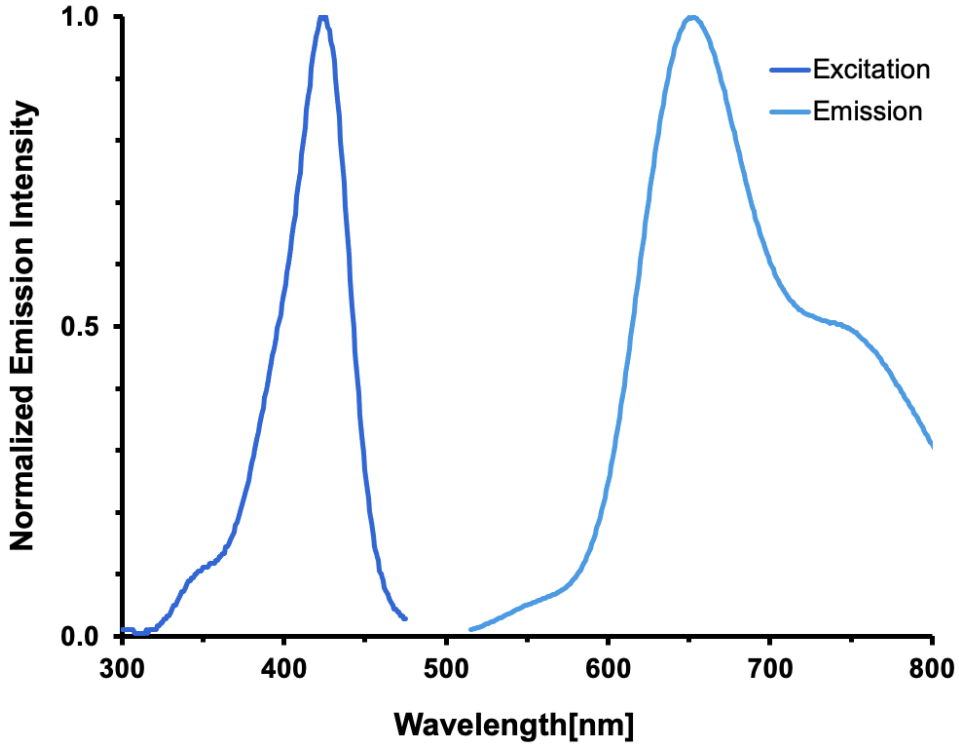

Figure A.5. Emission and excitation spectra of **3-Ce** recorded in THF. The emission spectrum was collected with an excitation wavelength of 494 nm; the excitation was monitored at an emission wavelength of 505 nm. All data were calibrated to the detector efficiency and normalized.

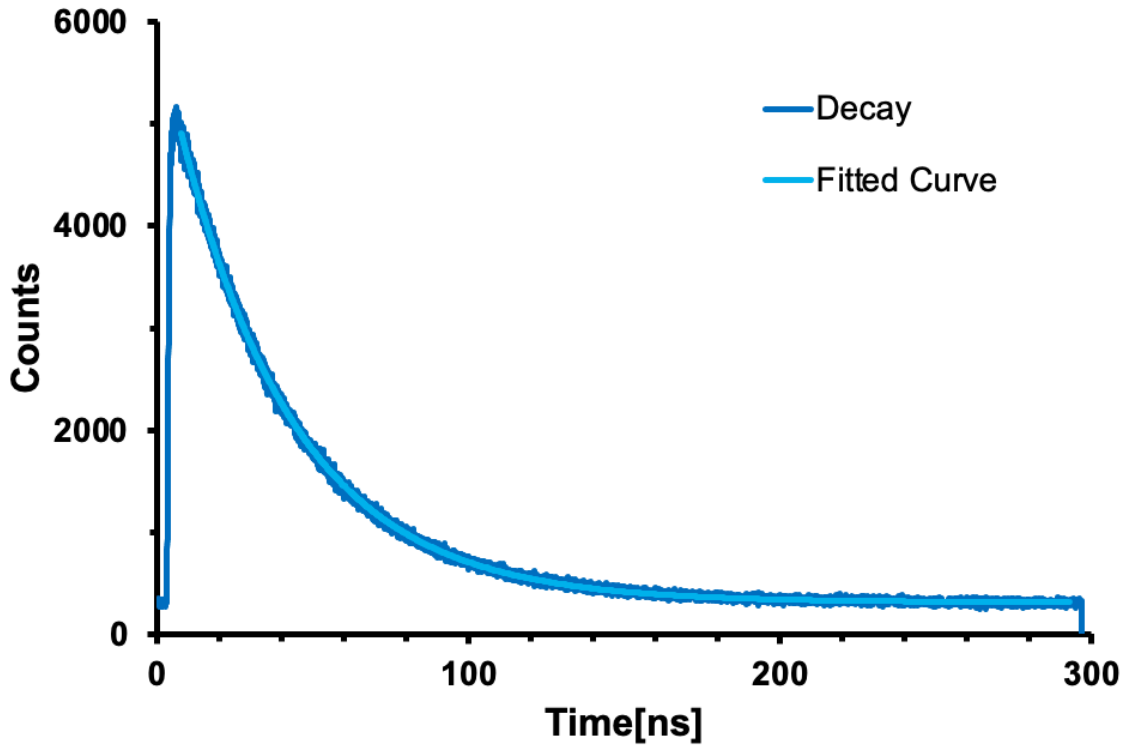

Figure A.6. Lifetime decay of **4-Ce** recorded in THF. τ1[ns]= 78.65 ±0.030. The onset of fluorescence is delayed, indicating that the initial excited state that is populated by the absorption is not the fluorescent excited state. Instead, the populated excited state converts to a radiative state through internal conversion (IC) or intersystem crossing (ISC).

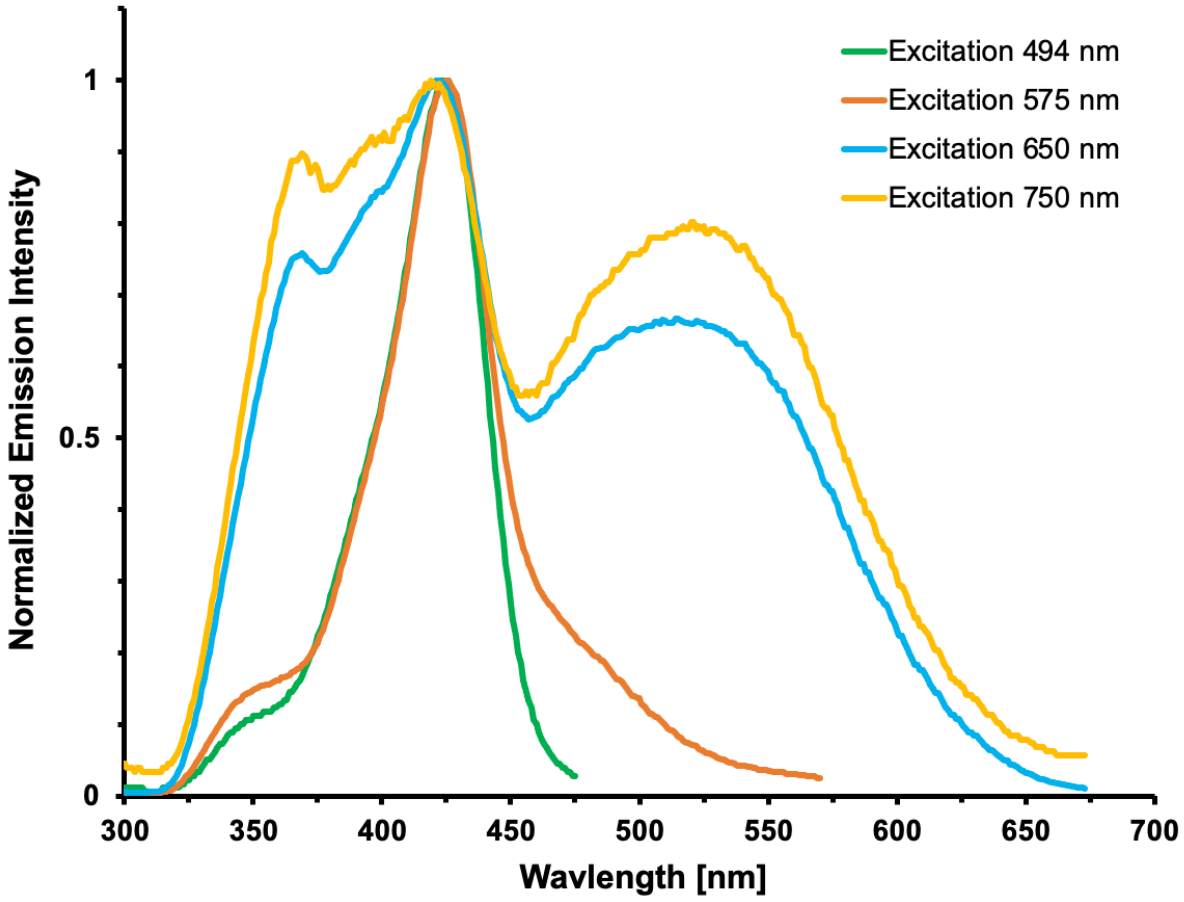

Figure A.7. Excitation measurements of **4-Ce** in THF at a variety of wavelengths. All data were calibrated to the detector efficiency and normalized. The excitation spectrum of **4-Ce** is shown to change depending on excitation wavelength, demonstrating a more complex energy landscape with the potential for multiple populated excited states. This implies that the energies of the excited states in **4-Ce** are relatively close together. Further DFT studies on **4-Ce** would give further insight into the electronic states involved in the photoexcitation of **4-Ce** and their respective energies.

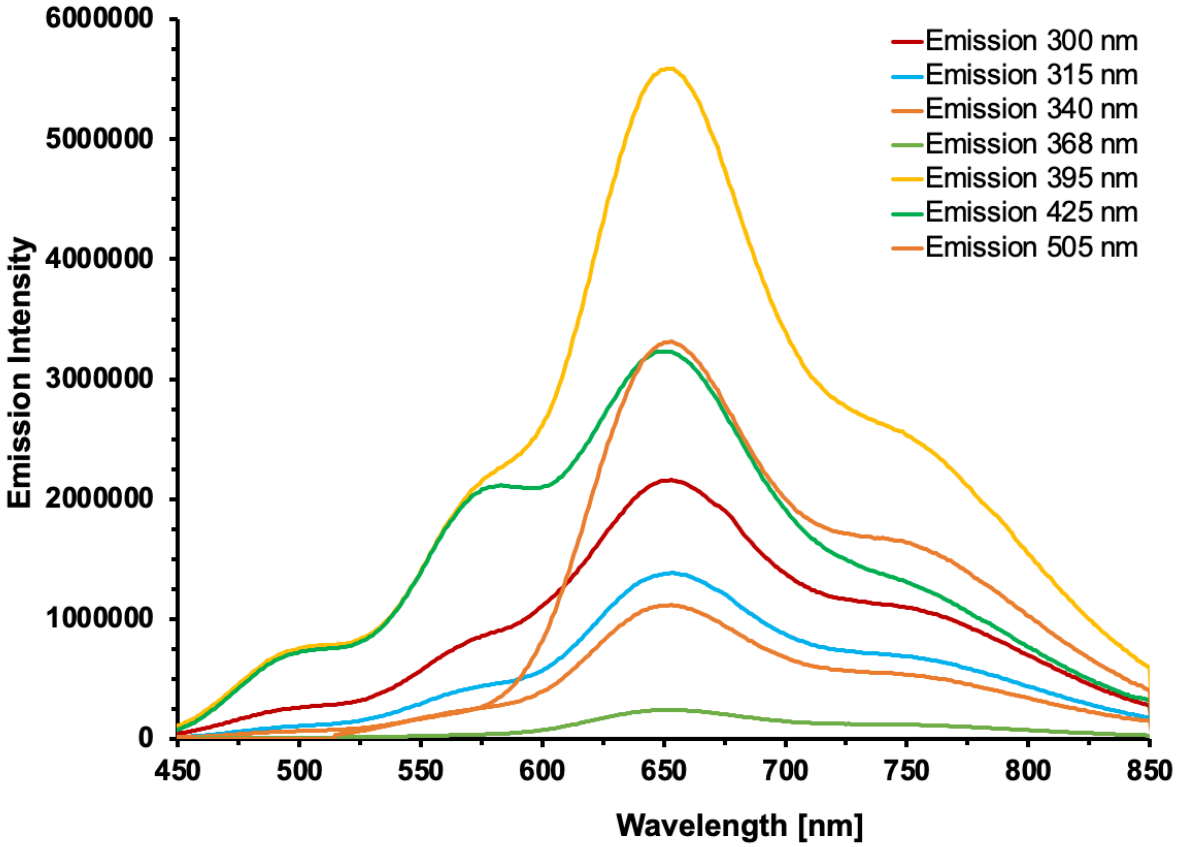

Figure A.8. Emission measurements of **4-Ce** in THF. All data were calibrated to the detector efficiency and normalized.

Appendix B

Cyclic Voltammetry Studies of Organometallic Lanthanide Complexes

Cyclic voltammetry (CV) measurements were carried out to analyze the redox potentials and reversibility of the oxidations of complexes **1-Ce**, **2-Ce**, **1-La** and **2-La** as well as of the ligand **HL**. CV measurements were carried out by Dr. Laurent Sévery at the University of California, Berkeley. The author helped to guide these studies and interpret data.

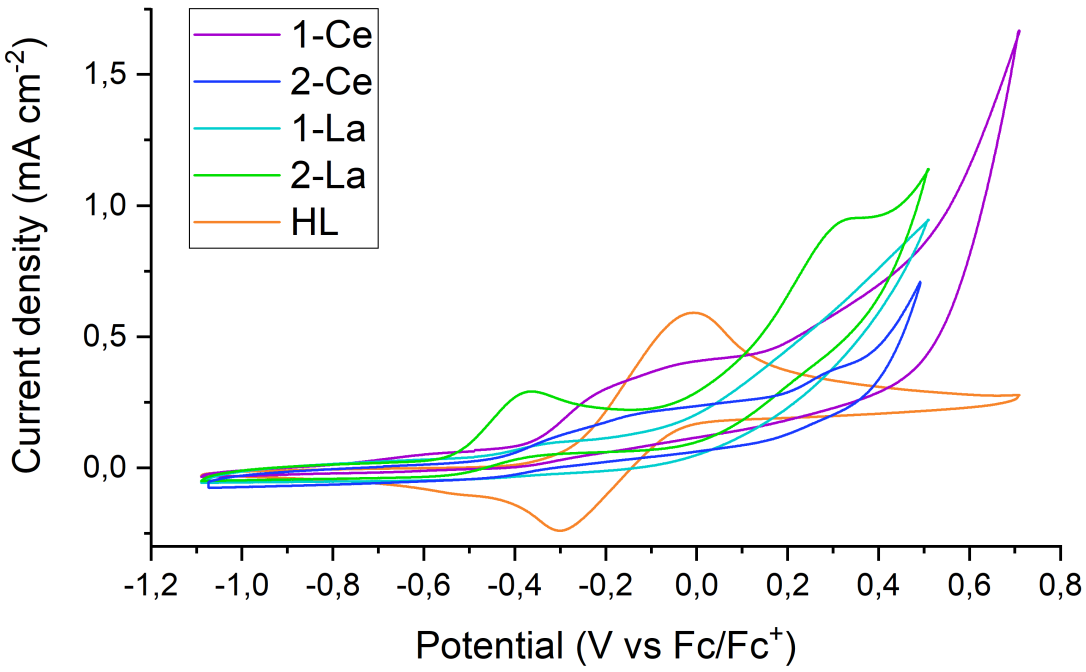

Figure B.1 Cyclic voltammograms of **1-Ce** (purple), **2-Ce** (dark blue), **1-La** (light blue), **2-La** (green) and **HL** (orange) in THF with 0.1 M [^{n}Bu$_4$N][PF$_6$] supporting electrolyte. [analyte] = ca. 5 mM; ν = 0.1 V/sec.

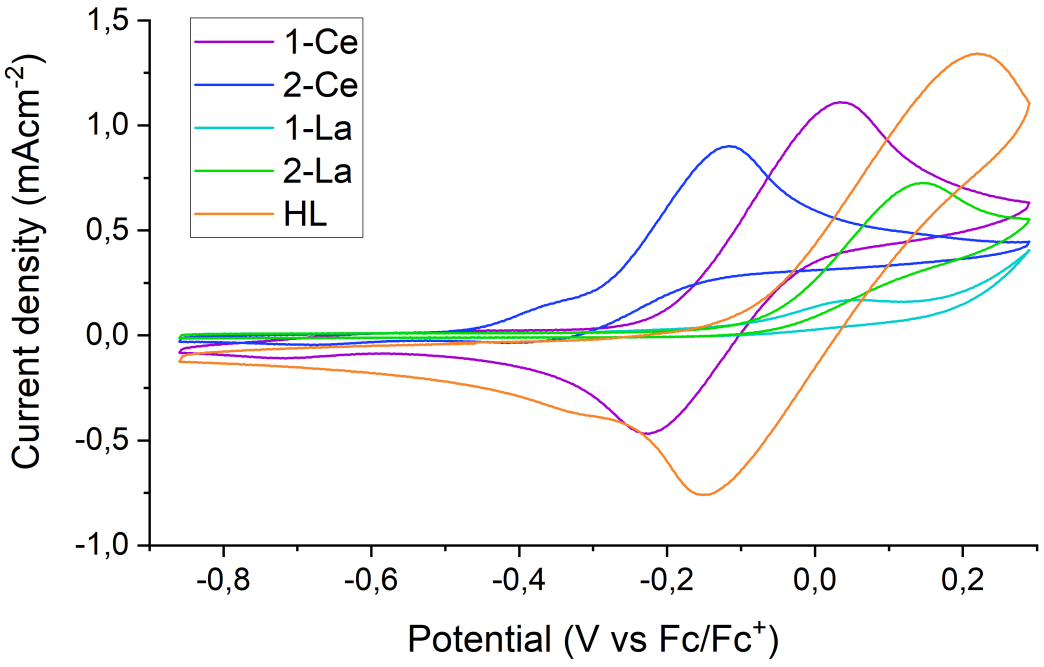

Figure B.2. Cyclic voltammograms of **1-Ce** (purple), **2-Ce** (dark blue), **1-La** (light blue), **2-La** (green) and **HL** (orange) in THF with 0.085 M [^{n}Bu$_4$N][BPh$_4$] supporting electrolyte. [analyte] = ca. 5 mM; ν = 0.5 V/sec.

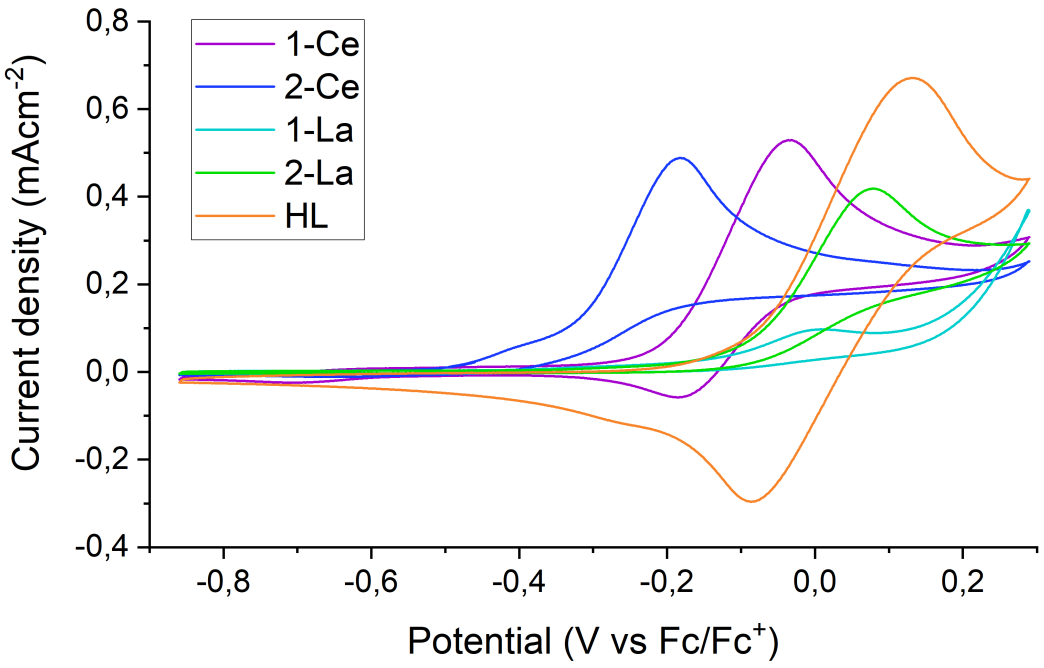

Figure B.3. Cyclic voltammograms of **1-Ce** (purple), **2-Ce** (dark blue), **1-La** (light blue), **2-La** (green) and **HL** (orange) in THF with 0.085 M [^{n}Bu$_4$N][BPh$_4$] supporting electrolyte. [analyte] = ca. 5 mM; ν = 0.1 V/sec.

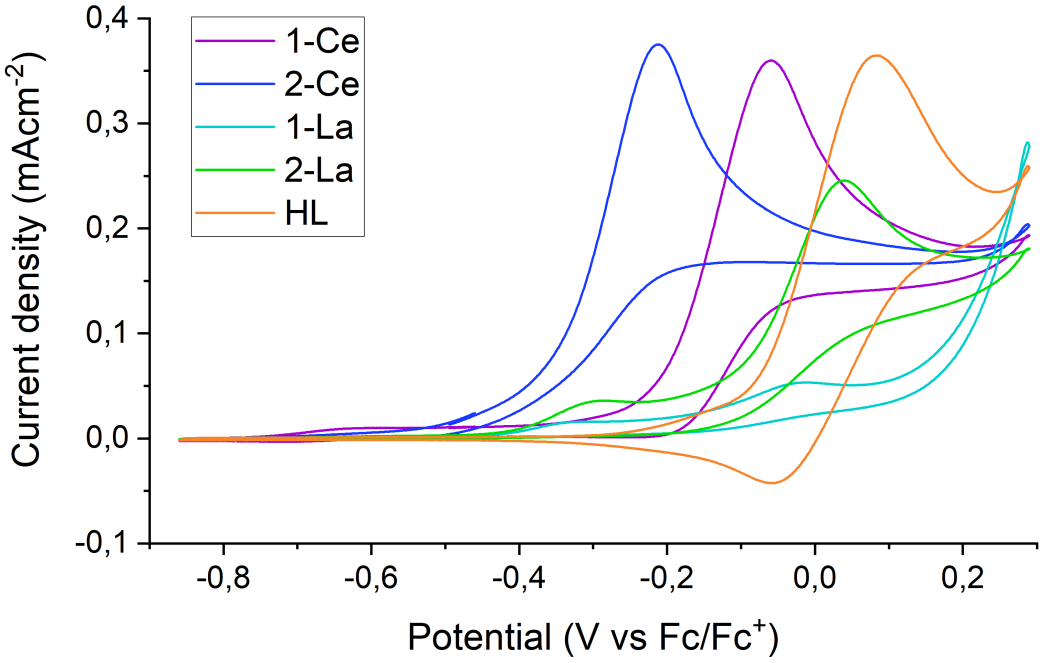

Figure B.4. Cyclic voltammograms of **1-Ce** (purple), **2-Ce** (dark blue), **1-La** (light blue), **2-La** (green) and HL (orange) in THF with 0.085 M [^{n}Bu$_4$N][BPh$_4$] supporting electrolyte. [analyte] = ca. 5 mM; ν = 0.02 V/sec.

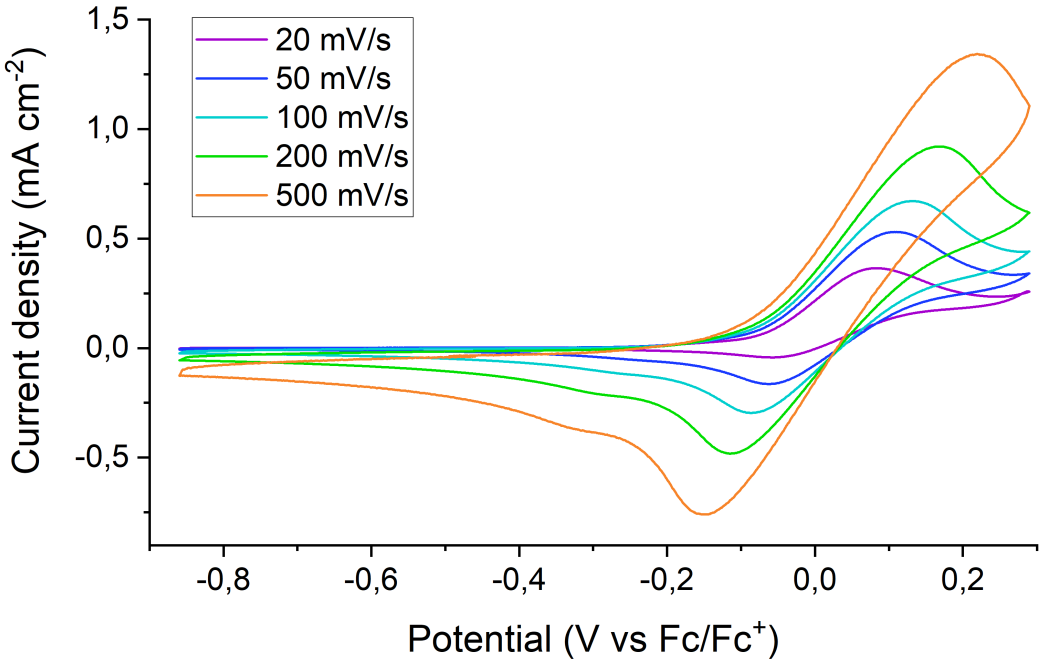

Figure B.5. Cyclic voltammograms **HL** in THF with 0.085 M [^{n}Bu$_4$N][BPh$_4$] supporting electrolyte at different scan speeds between 0.02 and 0.5 V/sec. [analyte] = ca. 5 mM. The $E_{1/2}$ of the partially reversible **HL**/**HL**$^{+\cdot}$ redox couple was determined to be −0.00 V vs. Fc/Fc$^+$. Irreversibility of the redox feature is observed at slow scan speeds, which is attributed to a chemical reaction of the oxidized species.

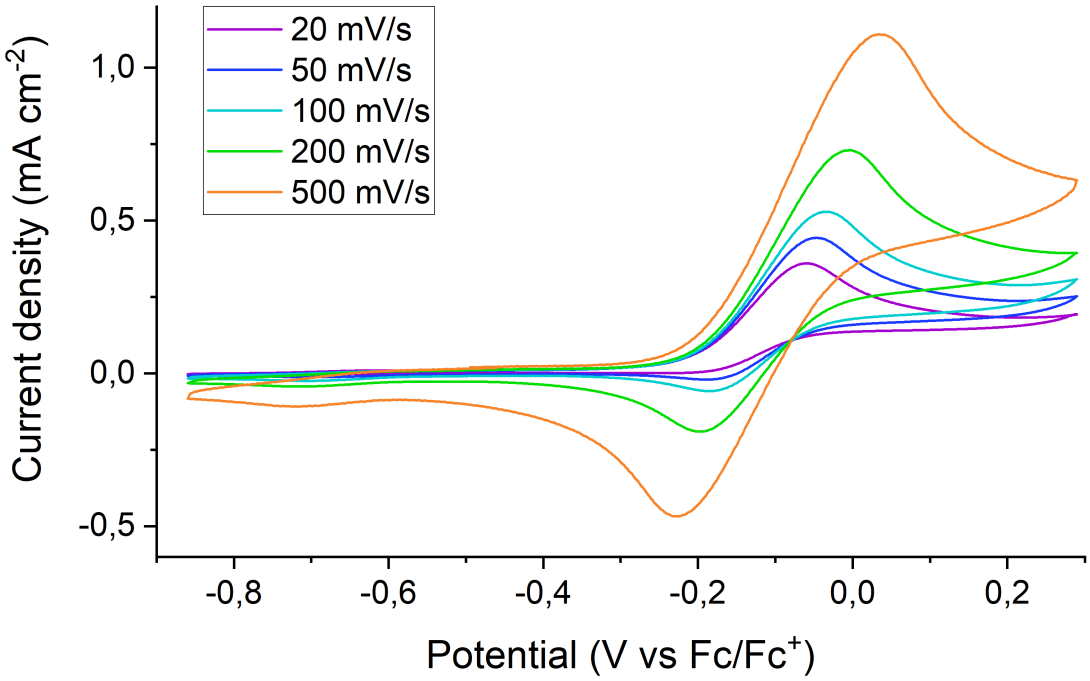

Figure B.6. Cyclic voltammograms **1-Ce** in THF with 0.085 M [^{n}Bu$_4$N][BPh$_4$] supporting electrolyte at different scan speeds between 0.02 and 0.5 V/sec. [analyte] = ca. 5 mM. The $E_{1/2}$ of the partially reversible Ce(III)/Ce(IV) redox couple was determined to be −0.15 V vs. Fc/Fc$^+$. Irreversibility of the redox feature is observed at slow scan speeds, which is attributed to a chemical reaction of the oxidized species similar to the case of **HL**/**HL**$^{+\cdot}$.

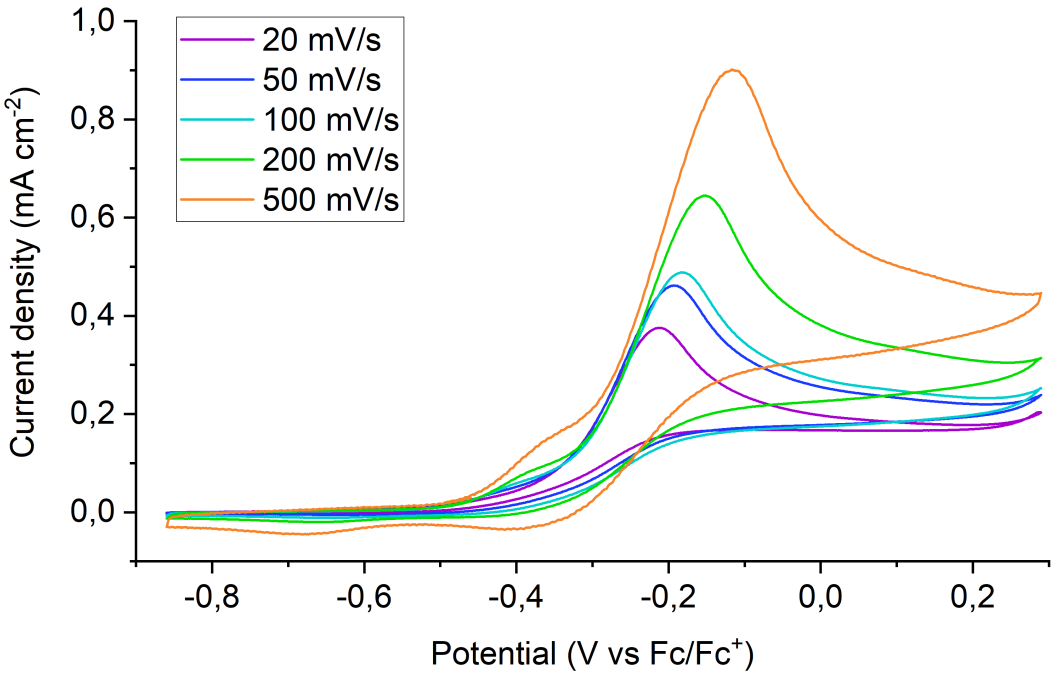

Figure B.7. Cyclic voltammograms **2-Ce** in THF with 0.085 M [^{n}Bu$_4$N][BPh$_4$] supporting electrolyte at different scan speeds between 0.02 and 0.5 V/sec. [analyte] = ca. 5 mM. A fully irreversible oxidation is observed with an onset around -0.3 V vs. Fc/Fc$^+$.

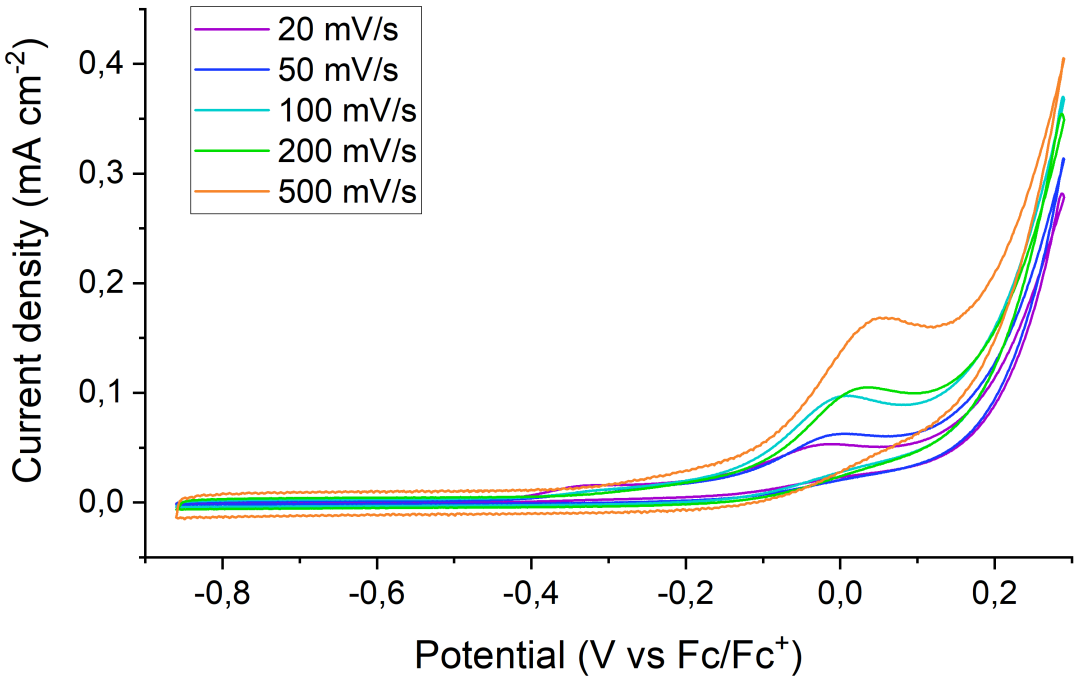

Figure B.8. Cyclic voltammograms **1-La** in THF with 0.085 M [$^{n}Bu_4N$ BPh_4] supporting electrolyte at different scan speeds between 0.02 and 0.5 V/sec. [analyte] = ca. 5 mM. A minor compontent shows an irreversible oxidation with an onset around -0.15 V vs. Fc/Fc^+, followed by a larger increase in oxidative current which is attributed to the main component (**1-La**) with an onset around 0.15 V Fc/Fc^+.

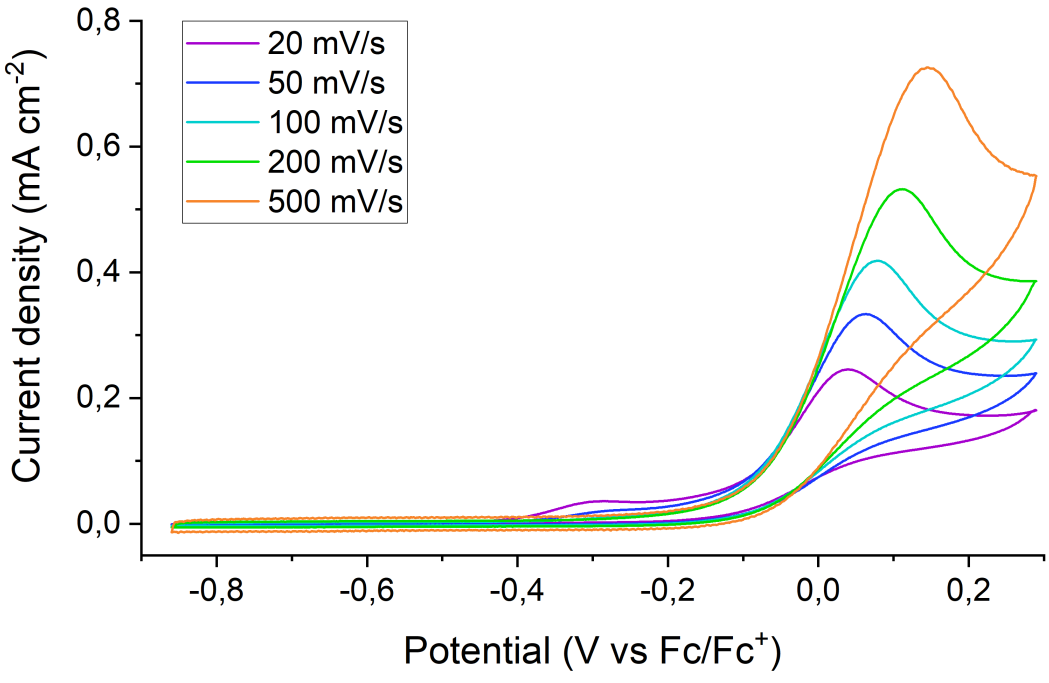

Figure B.9.Cyclic voltammograms **2-La** in THF with 0.085 M [$^{n}Bu_4N$ BPh_4] supporting electrolyte at different scan speeds between 0.02 and 0.5 V/sec. [analyte] = ca. 5 mM. A fully irreversible oxidation is observed with an onset around -0.05 V vs. Fc/Fc^+.